Controls of basin margin tectonics on the Lower Cretaceous sedimentation in the Norwegian Barents Sea

Bereke Kairanov

Thesis submitted in fulfilment of
the requirements for the degree of
PHILOSOPHIAE DOCTOR
(PhD)

University
of Stavanger

Faculty of Science and Technology
Department of Energy Resources

2020

University of Stavanger
NO-4036 Stavanger
NORWAY
www.uis.no

ISBN:978-82-7644-937-2
ISSN:1890-1387
PhD: Thesis UiS No. 530

Preface

This PhD thesis is submitted in fulfilment of the requirements for the degree of *Philosophiae Doctor* (PhD) at the University of Stavanger (UiS), Norway. The research was carried out between June 2014 to June 2018 and it was funded by the LoCrA consortium (https://wp.ux.uis.no/locra). During this period, I worked as a research fellow in the Department of Energy Resources, Faculty of Science and Technology at UiS. My main supervisor is Professor Alejandro Escalona (UiS) and my co-supervisor is Professor Nestor Cardozo (UiS). Industry collaboration was additionally established with Tore Åkermoem and Peter Abrahmson from MultiClient Geophysical, and with Emilie O'Neill from WesternGeco. During my PhD, I helped Professor Alejandro Escalona with the teaching of the introductory bachelor course in *Geology (GEO100)* and contributed to some courses in the Master of *Petroleum Geosciences.*

This research has resulted in five publications. Four of these have been published in different journals, including: *Journal of Geodynamics, Journal of Structural Geology, and Marine and Petroleum geology*. One manuscript has been submitted to *Marine and Petroleum geology* and is currently under review. Besides these publications, I have presented my research in several conferences, seminars, and E&P oil and gas companies. This thesis is structured similarly to a scientific paper and consists of two chapters. The first chapter is an introduction to the thesis, with a description of the general problems, motivation, objectives, results, discussion, and conclusions. The second chapter is a compilation of the five papers forming the main body of the thesis. Supplementary material such as conference abstracts are provided in the appendices.

Acknowledgements

Firstly, I would like to express my sincere gratitude to my supervisor Prof. Alejandro Escalona for his continuous support during my Ph.D., his patience, motivation, and immense knowledge. His guidance helped me during my research, writing of abstracts and papers, and finally the completion of this thesis. I could not imagine a better advisor and mentor for my Ph.D. I also would like to thank my co-supervisor Prof. Nestor Cardozo for his insightful comments and encouragement, but also for his hard questions which motivated me to widen my research from various perspectives.

My sincere thanks go to my colleagues from the D306 office: Dr. Dora, Dr. Sayyid, Dr. Shawn and Luis for all the fun during this journey, the nice discussions and constructive comments which were crucial for this research, but also for being very good friends outside the office.

I would also like to thank all LoCra collaborators: The University Centre in Svalbard (UNIS), Geological Survey of Denmark and Greenland (GEUS) teams: Snorre Olaussen, Sten-Andreas Grundvåg, Kasia K. Sliwinska and Henrik Nøhr-Hansen for their excellent expertise in hard rock geology and biostratigraphy, which helped me pursue my subsurface studies in the Barents Sea. I also thank the Moscow State University team: Alina Mordasova, Anna Suslova and Anatoli Nikishin for sharing their extensive knowledge of the Russian Barents Sea geology and providing support in data gathering. Special thanks to Ian Norton from the University of Texas Institute for Geophysics for teaching me how continents move (plate tectonics) and explaining the essence of potential field data modelling.

I would also like to acknowledge the Norwegian Petroleum Directorate (NPD), WesternGeco Multiclient, and MultiClient Geophysical (MCG) for providing data for this research. Many thanks to Peter Abrahamson (MCG), Tor Åkermoen (MCG) and Emilie O'Neill (WesternGeco) for providing support with data. Thanks to Haliburton, Petroleum Experts and Schlumberger for providing academic licenses of their software’s Decision Space, Move and Petrel, respectively.

I would like to express my sincerest gratitude to my parents, Marat and Tamara, and to my brother Nursultan for their infinite emotional and financial support. My love and gratitude for them can hardly be expressed in words.

And my biggest thanks to my wife Gyuzal and my daughter Aiya, sorry for being grumpy whilst I wrote this thesis. Your love, patience and encouragement helped me a lot in these final steps. You have been amazing, and from now on I will come home earlier as I promised!

Abstract

Structural styles and stratigraphic patterns along North Atlantic margins display a large spectrum of complexity and variability. An extensive amount of subsurface data from the north-central and south-western Barents Sea are used to: (1) at a larger scale understand how various plate tectonics regimes controlled structuring, faulting and sedimentation along the northern and southern margins of the Barents Sea; (2) at a smaller scale understand how the structural evolution of basin bounding faults impacted sedimentation in basins which were affected by one or more phases and multiple directions of extension; and (3) improve the knowledge about the paleogeography of the Barents Sea. In order to fulfil these objectives, this research consists of a systematic analysis which is summarized in five journal articles.

Paper 1 improves the existing knowledge of the Early Cretaceous tectonostratigraphic development of the north-central Barents Sea based on observations from subsurface data, structural and plate tectonic restorations in an area distal from the northern margin of the Barents Sea. As result of this work, compressional tectonics in the Early Cretaceous is suggested to be induced by the opening of the Canada Basin which triggered reactivation of Late Palaeozoic normal faults in reverse mode. Reverse movement along these faults caused the formation of NE oriented structural highs and anticlines, which controlled and routed the progradation of Lower Cretaceous clastic material from the northern to the southern margins of the Barents Sea.

The second paper focuses on understanding the Early Cretaceous structural evolution of the Tromsø Basin (proximal southern margin of the Barents Sea) in the context of the geodynamic processes acting in the southwestern Barents Sea. We propose an Early Cretaceous structural evolution of the Tromsø Basin which explains the formation of compressional features during rifting in the south-western Barents Sea.

2D gravity modelling and 2D structural restoration along a key regional composite seismic section, facilitated the interpretation and assessment of geodynamic constrains for the deeper structures below the Lower Cretaceous. These reveal thinner crust below the Tromsø Basin as compared to the Sørvestnaget and Hammerfest basins, which is suggested as the result of oblique extension in the southwestern margin of the Barents Sea.

In the third paper and at a smaller scale, we integrate stratigraphic and structural observations with throw backstripping and time thickness maps to define the growth processes of a basin-bounding normal fault in the northern Polhem subplatform. During the initial Early Cretaceous rifting, the fault system consisted of at least five en-echelon segments, which were ca. 5–10 km long. Throw backstripping indicates that fault segments were hard-linked after this initial stage to form a single 40 km long fault zone. Cross fault incised valleys provide additional information on the topographic response to fault growth. Major valley incisions at the fault linkage zones outline the extent of the individual fault segments and support early isolated fault growth.

The fourth paper focuses on a genetic correlation of the Lower Cretaceous succession between the north-central and south-western Barents Sea and Svalbard. The structural framework defined in paper 1 is used to locate the main sediment routes and progradation directions. The latest Valanginian to earliest middle Albian sequences in the offshore Barents Sea are correlated with the onshore Rurikfjellet, Helvetiafjellet and Carolinefjellet formations in Svalbard. This results in the reconstruction of four paleogeographic maps that show the progressive evolution and sediment distribution over the Norwegian Barents Sea for: (1) the earliest Valanginian, (2) the latest Hauterivian, (3) the middle to late Barremian and (4) the latest Aptian.

In the fifth paper, three tectonic events are suggested to control the deposition of the diachronous Lower Cretaceous clastic wedges around the Loppa High: 1) the latest Jurassic – earliest Cretaceous uplift of the Loppa High which triggered the deposition of the older wedges progressively eastwards in the northern Hammerfest Basin; 2) the late Barremian–Aptian faulting episode in the western flank of the Loppa High, which resulted in the deposition of shallow and probably deep marine wedges; and 3) the latest Aptian to earliest Albian tilting of the Hammerfest Basin and the Loppa High, which modified the sedimentation patterns in the region.

The results of this research can be applied beyond the Barents Sea, as they provide insights into margins and basins evolution, specifically on how: (1) oblique deformation along margins can control the inversion of pre-existing structures and routing of sediments, as well as modify paleogeography; (2) the growth of basin-bounding normal faults can affect sedimentation, with incised channels reflecting the early stage of fault growth; (3) paleogeographic reconstructions that reflect both the tectonic and stratigraphic setting can be used to understand sand distribution and sediment partitioning.

Table of Contents

Chapter 1

1 Introduction

The Norwegian Barents Sea is part of an epicontinental basin (Fig. 1A) that exhibits a variety of tectonic regimes and structural architectures along its margins. Its tectonic history is mainly attributed to: 1) the Late Palaeozoic initial rifting that formed NE-SW striking rift basins; 2) the Late Jurassic – Early Cretaceous North Atlantic rifting which rejuvenated inherited structures; and 3) the Late Cretaceous – Paleogene strike-slip and extensional tectonics, which dominated the western and northern margins respectively (Breivik et al., 1998; Doré, 1991; Faleide et al., 1993; Gudlaugsson et al., 1998; Minakov et al., 2012; Ritzmann and Faleide, 2007; Ryseth et al., 2003).

The Late Jurassic – Early Cretaceous tectonic processes are related to changes and reorganizations in plate tectonic configurations in the North Atlantic and Arctic regions (Lawver et al., 2002). Plate tectonic models for this time are uncertain due to the lack of constrains (e.g. lack of age control of magnetic anomalies and limited subsurface data; Hosseinpour et al., 2013; Rowley and Lottes, 1988; Seton et al., 2012). Therefore, the Early Cretaceous geodynamic processes related to the propagation of the North Atlantic rifting, the formation of the Canada Basin, and the influence of the High Arctic Large Igneous Province (HALIP) are some of the main tectonic events that modified the entire structural and paleogeographic setting of the Norwegian Barents Sea (Bryn et al.; Glørstad-Clark et al., 2011; Grogan et al., 1998; Grogan et al., 1999; Grundvåg and Olaussen, 2017; Henriksen et al., 2011; Kayukova and Suslova, 2015; Worsley, 2008). Therefore, understanding of these regional tectonic processes in the context of the structural and stratigraphic development of the Norwegian Barents Sea is crucial to better constrain the timing of tectonic events, geodynamic processes and plate kinematics of the North Atlantic and Arctic regions.

This study is a part of larger research project named "Lower Cretaceous Basin studies in the Arctic" (LoCrA; http://locra.ux.uis.no/), which is a consortium between industry and academia with the aim to enhance the knowledge of the tectonic configuration and basin infill in the Arctic during the Early Cretaceous. This study is focused on various scales of observation from margin to sub-basins in order to understand the interaction between tectonics and sedimentation, and involves the following problems:

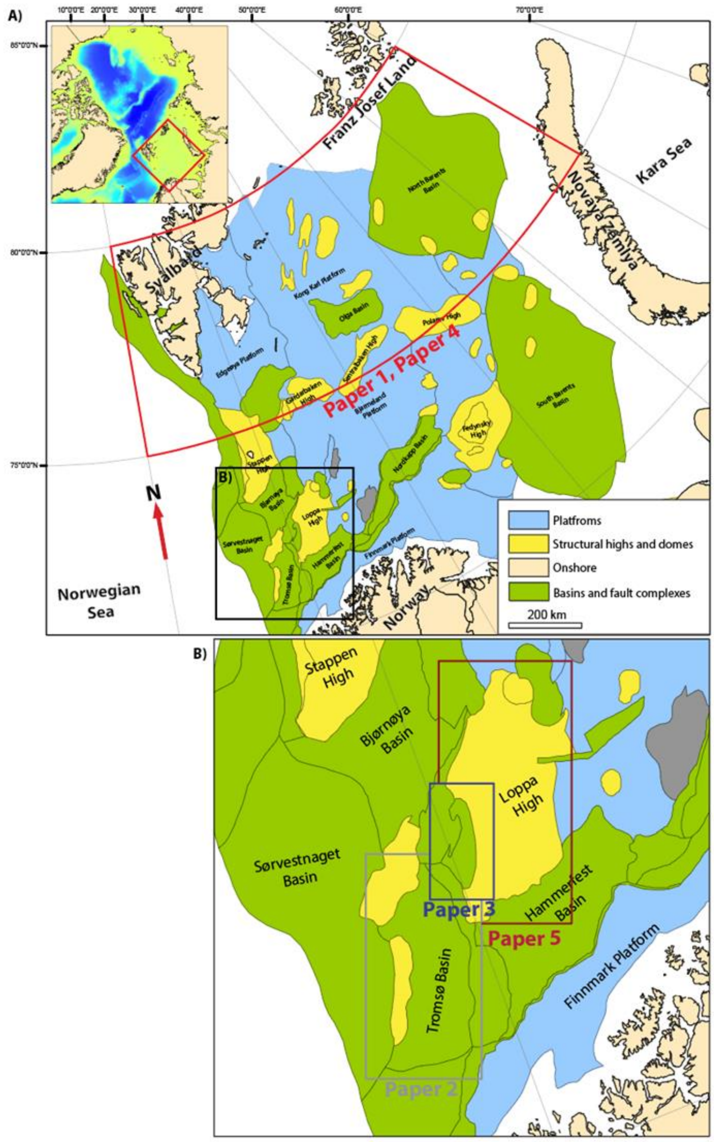

Figure 1A) Main structural elements of the Barents Sea. The polygons highlight the location of the study areas of this research. Papers 1 and 4 (red polygon) are focused on the larger scale of the north-central Barents Sea. B) Papers 2, 3 and 5 (grey, blue and red polygons) are focused on a basin scale in the southwestern Barents Sea.

1.1 Problem 1. Distal impact of margin deformation to an intra-cratonic basin and development of drainage systems

The northern margin of the Barents Sea has been less studied as compared to the other margins (e.g. southwestern Barents Sea; Fig. 1A). This is mainly due to limited data availability and the fact that the area is restricted for any commercial exploration. The structural evolution of the area is a key element for understanding the complex plate tectonic configuration of the Arctic region during the Early Cretaceous (Fig. 2). Most authors agree that during the earliest Cretaceous, the northern margin of the Barents Sea was dominated by compressional tectonics that resulted in the formation of NE oriented structural highs and anticlines due to reverse reactivation of the Late Paleozoic normal faults (Faleide et al., 2008; Grogan et al., 1998; Grogan et al., 1999). This resulted in SW and SE progradation of the Lower Cretaceous clastics today outcropping in Svalbard and Franz Josef Land (Glørstad-Clark et al., 2011; Henriksen et al., 2011; Worsley, 2008). However, this event is poorly described and its link to the tectonic processes in the Arctic region remains unknown.

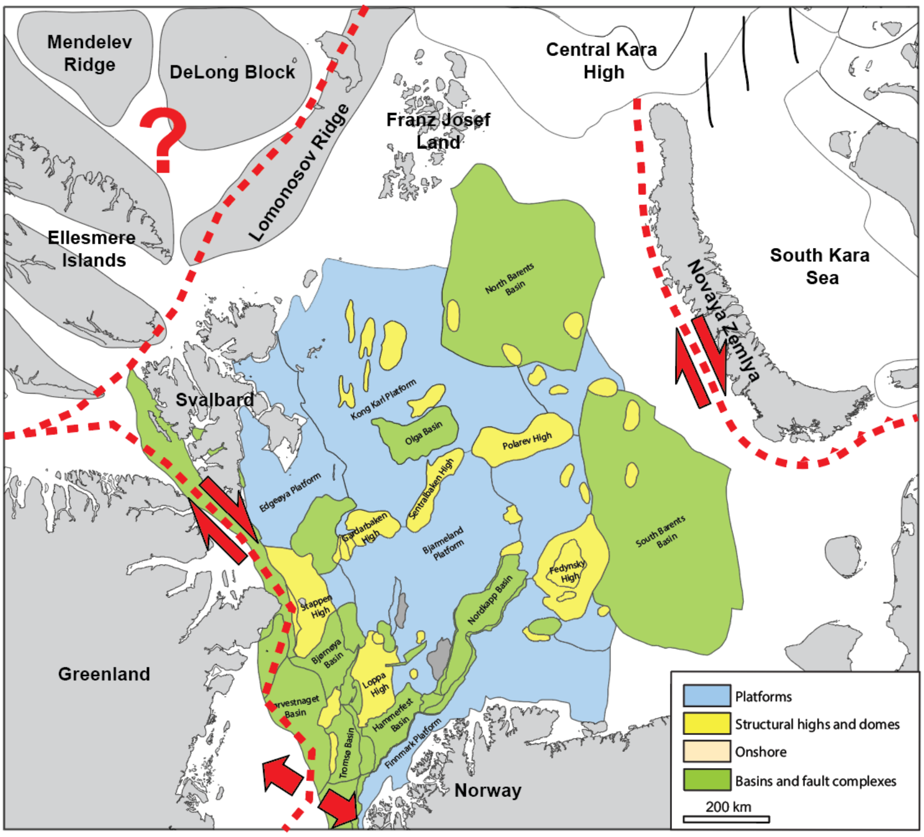

Figure 2 Plate tectonic reconstruction for the Barents Sea during the Hauterivian (130 Ma). From a plate tectonic model provided by the "Plates" project at the Institute for Geophysics, University of Texas. The map shows the major tectonic events during the Early Cretaceous along the Barents Sea margins (red arrows and stippled lines).

1.2 Problem 2. Tectonic basin development and its impact on sedimentation along the basin margin

In the southwestern margin of the Barents Sea, the propagation of the North Atlantic rifting resulted in extensional tectonics with the development of deep basins and highs (Clark et al., 2014; Faleide et al., 2008; Gabrielsen et al., 1990; Indrevær et al., 2016; Rønnevik et al., 1982) (Fig. 1B). The interpreted structural framework of the Tromsø

Basin consists of faults which cannot be entirely explained by a stretching direction perpendicular to the main rift trend, and hence the evolution of some structures involving compression (e.g. Senja Ridge, Loppa and Veslemøy highs, Tromsø Basin) remains controversial (Faleide et al., 1993; Gabrielsen and Færseth, 1988; Indrevær et al., 2013; Riis et al., 1986) (Figs. 3a – 3c). It has also been suggested that the complex structural configuration and sedimentation of the southwestern Barents Sea was influenced by inherited Caledonian or even older Precambrian basement structures (Barrère et al., 2009; Braathen et al., 1999; Doré, 1991; Fichler et al., 1997; Gabrielsen, 1984; Gernigon et al., 2014; Ritzmann and Faleide, 2007; Tsikalas et al., 2012). However, despite the apparent continuity and alignment of these structures with lineaments identified in the gravity or magnetic data (Tsikalas et al., 2012; Gernigon et al., 2014; Indrevær et al., 2013), it is not clear how pre-existing basement faults controlled the evolution, architecture and sedimentation of the Tromsø Basin.

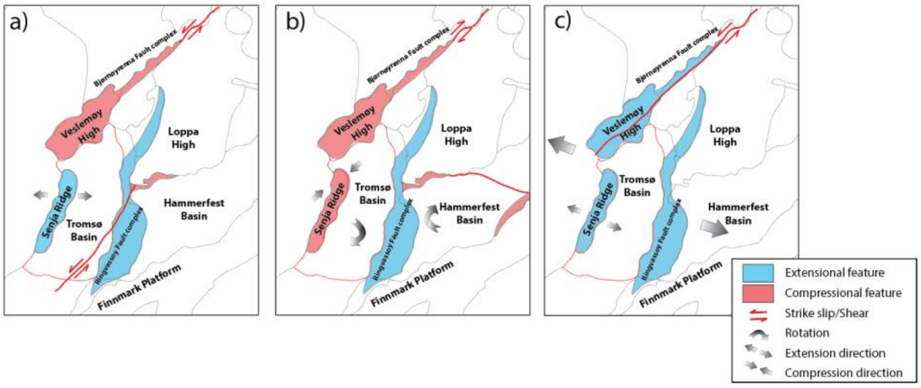

Figure 3. Simplified sketch of previously proposed regional tectonic models for the Late Jurassic - Early Cretaceous tectonic evolution of the Tromsø Basin. Notice the differences in the Senja Ridge and Veslemøy High interpretations, as compressional structural features are formed by either a) sinistral and b) dextral strike-slip faulting along the Bjørnøyrenna and Ringvassoy fault complexes (Riis et al., 1986; Gabrielsen and Færseth, 1988), or c) regional extensional system with sinistral strike-slip movement along the Bjørnøyrenna fault complex (Faleide et al., 1993)

1.3 Problem 3. Impact of basin bounding normal faults evolution on sediment dispersal

During the Early Cretaceous, active and growing normal fault systems in the southwestern Barents Sea controlled the distribution of the Lower Cretaceous clastic wedges along major fault complexes (Glørstad-Clark et al., 2011; Henriksen et al., 2011; Seldal, 2005; Sund et al., 1986; Wood et al., 1989) (Fig.1B). Most of the studies in the southwestern Barents Sea have been focused on the deposition of clastic wedges along major faults or structural highs to infer the timing of fault activity and the stage of rift development (Knutsen et al., 2000; Marín et al., 2018; Prosser, 1993). These studies mainly assess the final fault geometries and displacements, and rarely look at the impact of fault evolution on the topographic and sedimentary response (Cartwright et al., 1995; Mansfield and Cartwright, 2001; Peacock and Sanderson, 1991). At a smaller scale than that of the northern and southern margins (problems 1 and 2), assessing the history of growth of basin bounding normal faults is important to understand changes in basin paleo-topography during fault evolution, as it can provide information about early sedimentary entry points and drainage areas (Gawthorpe and Leeder, 2000).

2 Research aim and objectives

This research focuses on multi-scale observations in the north-central and the southwestern Barents Sea from (1) far field tectonic effects on the Barents Sea margins, to (2) basin scale structural development, and to (3) individual fault segments evolution with implications for sediments dispersal (Figs. 1a and 1b). Considering this, the main objectives are:

1. Document the structural and stratigraphic evolution of the north-central Barents Sea during the Early Cretaceous, including the understanding of the mechanisms that controlled compressional tectonics in the area and its impact on paleogeography. Also improve the understanding of the regional tectonic processes in the Artic region (e.g. opening of the Canada Basin) and how these processes affected the study area.
2. Describe the evolution, geometry and structural style of the major faults of the Tromsø Basin and their influence on deposition of the Lower Cretaceous sedimentary sequences. This contributes to the understanding of the geodynamic processes in the southwestern Barents Sea, and explains the formation of compressional features in this area.
3. Understand the structural mechanisms controlling the sedimentation patterns and variation of depositional environments around the Loppa High. This contributes to a better knowledge of tectonic and sedimentation in complex areas which experienced more than one phase and multiple directions of extension.

This study is multidisciplinary and it integrates seismic, potential field and well data interpretation, sedimentology and biostratigraphy. To achieve the above goals, we use a subsurface dataset of 2D and 3D seismic data and wire line logs, which were provided by the Norwegian Petroleum Directorate, MultiClient Geophysics and WesternGeco.

The study comprises three main articles in which I am the first author, and two additional articles led by Dora Marin and Sten-Andreas Grundvåg, respectively. The main three articles target specific problems related to the structural style and kinematics of basin margins and their bounding faults. The additional two articles are related to the integration of the sequence stratigraphic and tectonic framework of the Barents Sea during the Early Cretaceous. To meet the specific objectives of each paper, the research was performed as follows:

In the first paper, a regional subsurface study of the north-central Barents Sea was performed. Detailed mapping of major faults and structural elements on the Norwegian and the Russian Barents Sea resulted in a holistic understanding of the various regional tectonic processes in the Arctic region, which affected the northern margin of the Barents Sea including its paleogeography.

In the second paper, a basin scale subsurface study was performed in the Tromsø Basin and SW Barents Sea. The main emphasis was given to the interpretation of the fault network and detailed timing of fault movement, and the relation with the Lower Cretaceous sedimentary sequences. Also, gravity modelling along a regional composite seismic section, followed by structural restoration of this section that helped to constrain the basin configuration in the context of the geodynamic processes in the SW Barents Sea.

The third paper is based on a detailed 3D seismic interpretation in the Polhem Sub Platform, SW Barents Sea. Detailed mapping of the footwall and hanging wall stratigraphy helped to describe the sequential growth of a basin bounding normal fault and how it controlled sediment distribution and dispersal patterns during several phases of extension.

In the fourth paper led by Sten-Andreas Grundvåg, the Early Cretaceous structural and stratigraphic framework of the offshore Barents Sea was integrated with that from Svalbard. As a result, a tectonostratigraphic link between the southwestern Barents Sea and Svalbard is discussed.

In the fifth paper led by Dora Marin, a 2D and 3D seismic interpretation was performed around the Loppa High, SW Barents Sea. The tectonic control on sedimentation patterns around the Loppa High is discussed.

3 Study area and geological setting

The research was carried out in two margins of the Barents Sea: (1) the north-central and (2) southwestern margins. These two margins are subdivided into basins, platforms and structural highs (Fig. 1).

3.1 The north-central Barents Sea

The north-central Barents Sea covers the offshore area between Svalbard and the northern part of Novaya Zemlya (Fig. 1a). As mentioned before, this area is poorly studied as compared to the remaining part of the Barents Sea (e.g. southwestern Barents Sea).

Previous work in the region has documented a compressional event that resulted in tectonic inversion during the Late Jurassic – Early Cretaceous (Grogan et al., 1999). This compression resulted in reverse reactivation of Late Palaeozoic, NE-SW and E-W striking normal faults (Fig. 2) (Antonsen et al., 1991; Grogan et al., 1998; Grogan et al., 1999; Nikishin et al., 2014; Nikishin, 2013). Lower Cretaceous clinoforms in the southern Barents Sea reveal clastic source located to the NW and NE which builds the shelf southwards (Grundvåg and Olaussen, 2017; Kayukova and Suslova, 2015; Marin et al., 2017). These northernly to southernly progradation of the Lower Cretaceous clastic materials was related to uplift, formation of structural highs and anticlines in the north-central Barents Sea (Kayukova and Suslova, 2015; Olaussen et al., 2019; Smelror et al., 1998). The north-central Barents Sea was also affected by the formation of the High Arctic Large Igneous Province (125–122 Ma), which resulted in extrusive magmatism and formation of WNW–ESE trending dykes (Corfu et al., 2013; Dibner, 1998; Evenchick et al., 2015; Polteau et al., 2016; Senger et al., 2014).

During the Cenozoic, transpressional and transtensional deformation occurred between NE Greenland and the western Barents Sea. This deformation was responsible for the formation of the Vestbakken provinces and the Svalbard fold and thrust belt (Bergh and Grogan, 2003; Faleide et al., 2008). These events modified the structural configuration of the north-central Barents Sea, by amplifying several structural highs and basins (Anell et al., 2014; Grogan et al., 1999). This was followed by glaciation and a tectonic uplift which caused erosion and exhumation of the northern Barents Sea (Dimakis et al., 1998; Knies and Gaina, 2008).

3.2 The southwestern Barents Sea

The southwestern Barents Sea is located offshore of the north-western corner of the Norwegian mainland (Fig. 1b). Starting from the Late Palaeozoic, regional extension between Greenland and Norway resulted in the formation of NE–SW and E–W trending grabens and half grabens that were covered by Upper Carboniferous to Lower Permian carbonate platforms and thick evaporites (Gudlaugsson et al., 1998; Larssen et al., 2002). The Early Triassic is marked by a rift episode, which has been documented in the North Atlantic region (Tsikalas et al., 2012). This rifting episode may have continued until the Middle Triassic (Smelror et al., 2009). During the Middle Jurassic – Early Cretaceous, northward advance of the Atlantic rifting enhanced a NE–SW and E–W Late Palaeozoic fault system and formed deep basins in the southwestern Barents Sea such as the Harstad, Tromsø, Bjørnøya and Sørvestnaget basins (Fig. 2) (Faleide et al., 2008; Gernigon et al., 2014). The Early Cretaceous rift episode along the NE–SW and E–W trending fault complexes (e.g. Ringvassøy–Loppa, Bjørnøyrenna, Asterias and Troms-Finnmark) led to rapid subsidence and accumulation of the Lower Cretaceous sediments (Clark et al., 2014; Faleide et al., 2008); (Gabrielsen et al., 1990; Indrevær et al., 2016; Rønnevik et al., 1982). The Tromsø, Sørvestnaget and Bjørnøya basins experienced salt related deformation during this rifting event (Gabrielsen et al., 1990; Larssen et al., 2002; Sund, 1984). Three Early Cretaceous rift phases have been interpreted in the southwestern Barents Sea: Berriasian–Valanginian, Hauterivian–Barremian and Aptian–Albian (Faleide et al., 1993). Local compression during the earliest Cretaceous has been identified in the northern part of the Tromsø Basin. This has been suggested to be the result of dextral strike slip movement along the Asterias Fault complex (Berglund et al., 1986; Gabrielsen et al., 1990; Sund, 1984), or localized tectonic inversion due to differential uplift of the Loppa High (Indrevær et al., 2016).

4 State of the art

This section is a short review of previous studies regarding (1) oblique deformation and (2) fault growth styles along basin margins.

4.1 Oblique deformation

Commonly, oblique deformation occurs along margins where the extension direction is not orthogonal to the rift (Dewey et al., 1998; Sanderson and Marchini, 1984). The influence of obliquity on the structural styles of rift systems varies. This is often due to the rift setting, which is mainly controlled by tectonic inheritance (Hodge et al., 2018; Manatschal et al., 2015; Morley, 2017; Phillips et al., 2018), or from changes in crustal composition and configuration (Brune et al., 2017; Molnar et al., 2017; Mondy et al., 2018; Sippel et al., 2017). It is difficult to interpret oblique deformation using 2-D plane strain (Brune et al., 2018). However, there are some key characteristics that can be attributed to this process, for instance segmented en échelon border faults oblique to the rift trend (Agostini et al., 2009; Brune and Autin, 2013; Clifton et al., 2000; Corti, 2008; Withjack and Jamison, 1986), or uncommon crustal thinning (e.g. sharp transitions) along the margin (Montési and Behn, 2007).

In the Norwegian Barents Sea, propagation of the North Atlantic rifting from the southwest towards the north-central margins was aborted during the Cretaceous (Faleide et al., 2008) (Fig. 2). This has been associated with complete reorganization of crustal extension which led to oblique deformation in the southwestern Barents Sea (Faleide et al., 2008; Gernigon et al., 2014). Early Cretaceous oblique deformation in the southwestern parts of the margin is partially evident in the Tromsø and Bjørnøya basins, where the fault trends are oblique to the regional, inherited structural grain (Breivik et al., 1998; Gabrielsen et al., 1990; Gernigon et al., 2014; Henriksen et al., 2011; Ritzmann and Faleide, 2009; Smelror et al., 2009). Most of the plate tectonic reconstructions for the Early Cretaceous place the Canada Basin adjacent to the northern margin of the Barents Sea (Barnett-Moore et al., 2018; Doré et al., 2015; Seton et al., 2012). Opening of the Canada Basin (~145–126 Ma) resulted in large scale crustal up-doming which affected the northern margin of the Barents Sea (Alvey et al., 2008; Grogan et al., 1999). The models for opening of the Canada Basin are still a matter of debate, and they are supported by inconclusive or indirect observations (Cochran et al., 2006; Døssing et al., 2013; Dove et al., 2010; Lawver and Scotese, 1990). Recent studies (Alvey et al., 2008; Hadlari et al., 2016) reveal evidences supporting oblique deformation along the northern margin of the Barents Sea (e.g. northern margin of the Lomonosov Ridge; Evangelatos and Mosher, 2016; Gaina et al. 2014). These studies document Early Cretaceous oblique deformation in the context of regional tectonic processes along the margins of the Norwegian Barents Sea. However, no studies have been conducted to understand the impact of oblique deformation on inherited basins and sedimentation.

4.2 Fault growth and linkage

Observations from outcrop and subsurface datasets, and analogue and numerical models suggests two main ways of fault growth: (1) the isolated fault model, where growth and linkage of individual fault segments occur through displacement and lateral propagation of their tiplines (Cartwright et al., 1995; Dawers and Anders, 1995; Dawers et al., 1993; Walsh and Watterson, 1988; Watterson, 1986) (Fig. 4a), and (2) the constant length fault model, where faults reach their near-final length relatively early in their slip history, and accumulation of displacement occurs without further lateral tipline propagation (Childs et al., 2003; Giba et al., 2012; Jackson and Rotevatn, 2013; Morley, 2002; Nicol et al., 2016; Schlagenhauf et al., 2008; Tvedt et al., 2016; Walsh et al., 2003; Walsh et al., 2002) (Fig. 4b). In the last 30 years, these two models have been a matter of discussion and debate, as the styles of fault growth and rate of tipline propagation impact the tectono-stratigraphic development of sedimentary basins (Gawthorpe and Leeder, 2000; Henstra et al., 2016; Jackson et al., 2017). The character of the initial stage of fault growth remains unclear, since very few studies have been able to capture the earliest (and short lived) stage of fault growth (Schlagenhauf et al., 2008) (Fig. 1c).

In the Norwegian Barents Sea, most of the major fault complexes have been analyzed with the aim of establishing fault geometry, architecture and processes controlling faulting (Braathen et al., 2009; Fisher and Knipe, 2001; Gabrielsen et al., 1990; Gabrielsen et al., 2016). To our knowledge, there are no studies in the Barents Sea documenting how fault growth affects sediment distribution (Fossen and Rotevatn, 2016; Torabi et al., 2019).

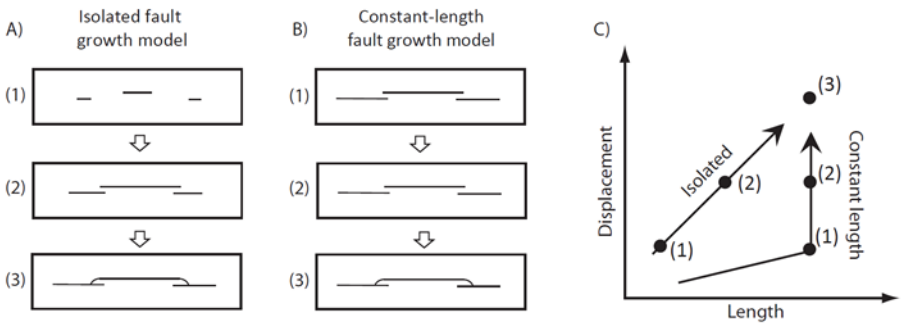

Figure 4 Top views illustrating the (A) isolated and (B) constant length models of fault growth. Numbers represent fault growth stages: (1) initiation, (2) interaction, and (3) linkage. (C) Displacement versus length through time for the two models.

5 Summary of papers

5.1 Paper 1: Early Cretaceous tectonostratigraphic evolution of the north-central Barents Sea

In this paper, we investigate the structural evolution of the north-central Barents Sea during the Early Cretaceous, and the influence of fault activity on sedimentation in the area. This is achieved by integrating 2D seismic data, two exploration wells, and information of shallow cores from the Norwegian and Russian sectors. As result of this work (Fig. 5), three fault families, two Lower Cretaceous seismic sequences, and seven seismic facies, are interpreted in the area. During the Hauterivian–Early Barremian (sequence 1), a syn-tectonic phase is observed, where fault families 1 and 2 of Late Paleozoic age were reactivated as reverse faults and induced the uplift of NE–SW and E–W structural highs on the Kong Karls Land Platform and the North Barents Basin. During the Early Barremian–Early Aptian (sequence 2), the study area experienced a tectonically quiescent period, where the increase of clastic supply from the N–NE was responsible for sediment progradation towards the S–SW Barents Sea. The progradation was controlled and routed by structural highs inherited from the Hauterivian–Early Barremian inversion. Later, a post Early Cretaceous reactivation was responsible for the reactivation of the Late Jurassic – Early Cretaceous inverted faults and structures. Our results suggest that three main regional tectonic events controlled the inversion of the Late Paleozoic faults, resulting in development of structural highs in the north-central Barents Sea (Fig. 5): 1) dextral transpression along Novaya Zemlya, which was responsible for inversion on the ESE flanks of the North Barents Basin; 2) dextral movement along a paleo-boundary of the northern margin of the Lomonosov Ridge during opening of the Amerasia Basin, which controlled the inversion in the Kong Karls Land platform and the Olga Basin; and 3) a compressional event in the present day NE Greenland,

and Ellesmere Islands and the NW Barents Sea (NW Svalbard), which contributed to uplift in Svalbard and inversion in the rest of the study area.

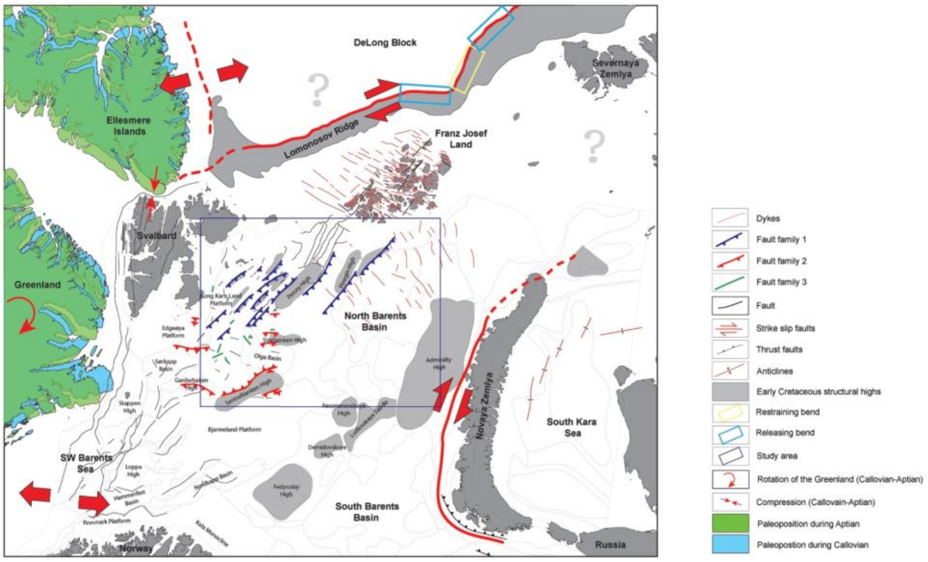

Figure 5 Plate reconstruction map from the "Plates" project (https://ig.utexas.edu/marine-and-tectonics/plates-project/) for the Hauterivian (130 Ma) overlain with the interpreted structural elements in paper 1 and integrated with previous studies.

5.2 Paper 2: The Early Cretaceous evolution of the Tromsø Basin, SW Barents Sea, Norway

Extensional basins developed along oblique or transform margins are less studied as compared to those basins developed along orthogonally extended margins. This study presents an example of a basin developed along an oblique margin, namely the Tromsø Basin, which developed along the southwestern Barents Sea transform margin. Three previous models have been proposed to explain the tectonic evolution and architecture of the basin, but still there is no consensus on the development of individual structures and compressional faults in this basin. In this study, we use fairly new 2D industry seismic reflection data, potential field and well data, as well as previously published information, to understand the Early Cretaceous structural evolution of the Tromsø Basin in the context of the geodynamic processes in the southwestern Barents Sea. Modeled gravity anomalies along a depth converted 2D regional seismic section facilitated the interpretation of crustal structures, which then were structurally restored. We propose a revised Early Cretaceous structural model for the Tromsø Basin, which involves oblique extension and formation of an intra-basinal, transpressional transfer zone (Figs. 6a – 6c). This can explain reverse faulting in the study area. Basement heterogeneity played an important role in focusing and localizing strain. 2D sequential restoration of a regional profile above yields an estimate of ca. 35 km of crustal extension in the SW Barents Sea margin, from the earliest Cretaceous until the present, which is relatively smaller than previous estimations (e.g. 85 km by Breivik et al. 1998). Discrepancies are attributed to the differences in the calculation methods, where our results were based on 2D structural restoration, and Breivik et al., 1998 derived extension from crustal stretching factor. Moreover, from the earliest Cretaceous until Albian (seismic unit 2), the Tromsø and Sørvestnaget basins developed as a single large basin in the SW Barents Sea margin. Crustal thickness along the gravity modeled 2D regional section displayed a thinner crust below the Tromsø Basin as compared to the Sørvestnaget and Hammerfest basins. This is considered as uncommon for orthogonally rifted passive margin models and observations, where crustal thickness typically decreases towards (e.g. Sørvestnaget Basin) the continent – oceanic boundary (Peron-Pinvidic et al., 2013). Therefore, we suggest that the abnormal crustal thickness within the necking zone area is the result of oblique rifting and segmentation in the margin, where increase in obliquity decreases stretching and crustal thinning (Montési and Behn, 2007). This study illustrates the importance of detailed and regionally integrated analysis of rifted basins for reconstructing their evolution, as analysis of oblique rifted basins using two-dimensional plane strain can lead to erroneous assessment of faulting style and deformation.

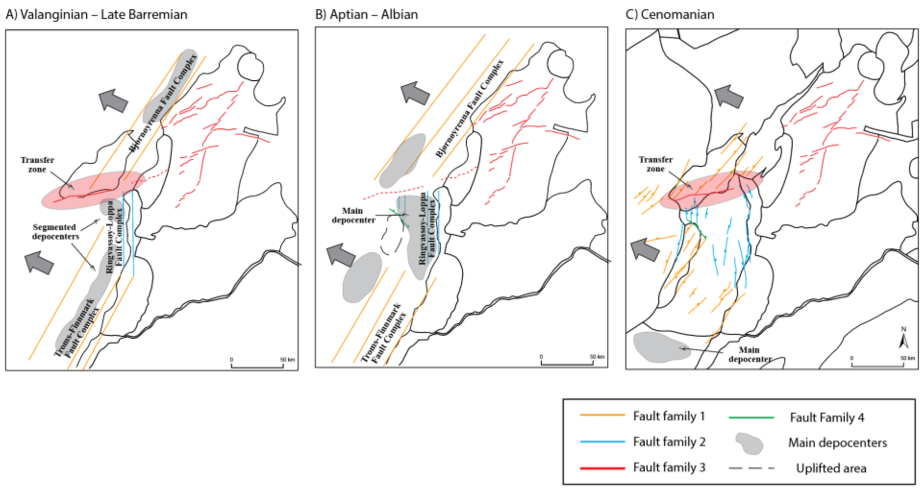

Figure 6. Proposed structural model for the Tromsø Basin and distribution of the main depocenters (grey polygons) during Early Cretaceous: A) Valanginian – Late Barremian extension was accommodated by west dipping boundary faults of FF1 (e.g. fault segments of TFFC and BFC), which resulted in the formation of the internal fault system FF2; B) The Aptian – Albian is marked by a transpressional setting along a transfer zone which is related to the oblique opening of the Tromsø Basin, where basement heterogeneity localized strain; and C) The Cenomanian is considered a tectonically quiescent period, where most of the fault activity occurred in the western and north-western flanks of the Tromsø Basin.

5.3 Paper 3: Growth and linkage of a basin-bounding fault system: Insights from the Early Cretaceous evolution of the northern Polhem Subplatform, SW Barents Sea

Observations from outcrop and subsurface datasets, as well as physical and numerical models suggest two ways of fault growth: (1) growth and linkage of individual fault surfaces through lateral propagation of the tip-lines (isolated model), or (2) near-final fault length formed relatively early in the slip history and displacement accumulation without lateral propagation of the tip-lines (constant-length model). This study integrates stratigraphic and structural observations with throw backstripping and time thickness maps to define the growth of a normal fault in the northern Polhem Subplatform, SW Barents Sea (Figs. 1b and 7a – 7d). During the initial 15 My of Early Cretaceous rifting, the studied fault was comprised of at least five en-echelon segments (ca. 5–10 km long). Throw backstripping indicates that these fault segments were hard-linked after this initial stage to form a single 40 km long fault (Fig. 7d). Major incised valleys coincide with the location of the fault linkage zones and outline the extent of the individual fault segments, supporting early isolated fault growth (Fig. 7c). Based on fault throw backstripping, valley incision was able to keep up with fault slip, such that it remained unaffected by the fault linkage stage. This study highlights the importance of integrating stratigraphic and structural observations during reconstruction of fault growth history, where syn-rift erosional features, sediment thickness variations, sediment distribution, stratal geometries and onlaps/truncations are critical for estimating the growth of these structures.

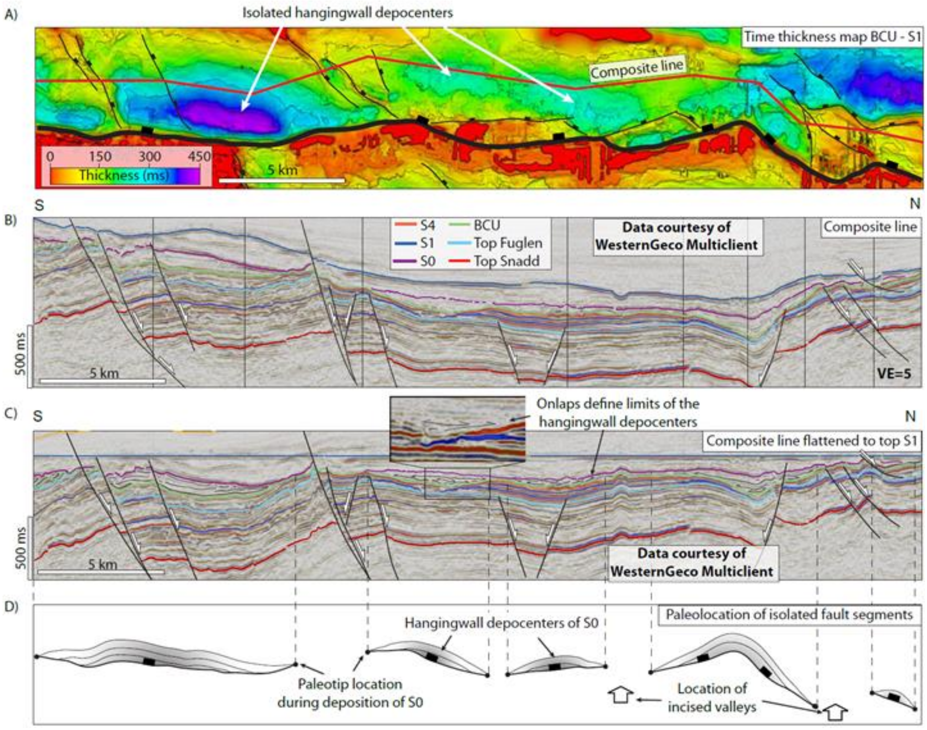

Figure 7 (A) Time thickness map along the studied fault in the Polhem Subplatfrom showing distribution of depocenters. (B) Composite line along the fault (red line in A). (C) Composite line in B flattened to the top S1 horizon, illustrating the distribution of scoop-shaped depocenters in the S0 interval. (D) Interpreted paleo-location of isolated fault segments and hanging wall depocenters.

5.4 Paper 4: The Lower Cretaceous succession of the western Barents Shelf: onshore and offshore correlations

This paper was led by Sten-Andreas Grundvåg. My main contribution was related to the correlation of the Lower Cretaceous sequences and providing examples and descriptions of the clinoforms in the north central Barents Sea. In this paper, we integrate biostratigraphic analysis, outcrop data and seismic and well information of the north-central Barents Sea, with the aim of establishing a genetic link of the Lower Cretaceous successions onshore and offshore. In addition, this study discusses the regional paleogeography, depositional controls, sediment partitioning and sand distribution in the area. This information is key to understand the basin infill and the sedimentary processes that occurred in the western part of the Barents Sea during the Early Cretaceous. We suggest that three sequences defined in the southwestern Barents Sea, with an age of latest Valanginian–earliest middle Albian (S1–S3), correlate with the Rurikfjellet (Valanginian – Hauterivian/early Barremian), Helvetiafjellet (early Barremian – early Aptian) and Carolinefjellet (early Aptian, middle Albian) formations in Svalbard. Based on age control, we propose that the Barremian clinoforms (sequence 1) identified in the western Olga Basin, Fingerdjupet subbasin and western part of the Bjarmeland platform correlate with the upper part of the Rurikfjellet Formation and a Barremian unconformity identified in Svalbard (Figs. 8a and 8b). In addition, the southeastward progradation direction of these offshore clinoforms reflect a similar pattern that the paleocurrents of the Rurikfjellet and Helvetiafjellet formations. This suggests that the offshore and onshore depositional system were under the influence of the same paleo-drainage. The apparent lack of sandstone in the shelf-margin clinoforms is interpreted as a result of the physiographic conditions of the basin, such as storm waves, tidal and alongshore currents. These conditions may have contributed to the sand being trapped in areas such as the inner shelf. Finally, four paleogeographic reconstructions are made: 1) the earliest Valanginian, characterized by a carbonate platform, sediment starvation and the development of clastic wedges in basins such as the Hammerfest Basin; 2) the latest Hauterivian, when Greenland is proposed as the source of the southeastward directed shallow marine wedges in the western part of the study area; 3) the middle to late Barremian, characterized by a fluvio-deltaic system triggered by the uplift of the northern Barents Sea; and 4) the latest Aptian, when the main platform areas were flooded and a seaway connected the Barents Sea and the Canada Basin.

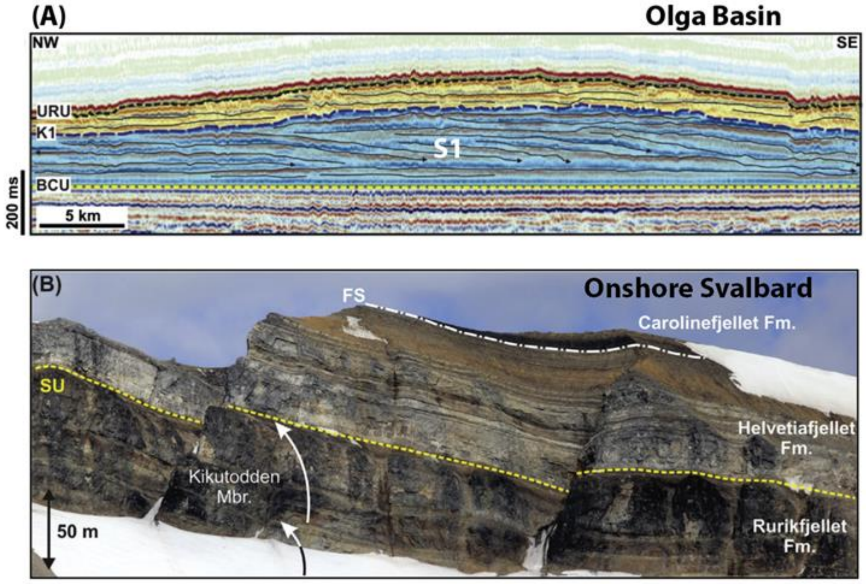

Figure 8 Summary of paper 4 showing the suggested A) offshore and B) onshore genetic link of the Lower Cretaceous sequences (for more information the reader is referred to the full article).

5.5 Paper 5: Effects of adjacent fault systems on drainage patterns and evolution of uplifted rift shoulders: The Lower Cretaceous in the Loppa High, southwestern Barents Sea

This paper was led by Dora Marin. In this study, we integrate the information from the previous papers, in addition to new observations from the western flank of the Loppa High, in order to describe the distribution and timing of diachronous clastic wedges around the Loppa High (Fig. 9). Additionally, this paper aims to understand how multidirectional and diachronous tectonic activity in the area conditioned the Lower Cretaceous sedimentation. Based on detailed mapping of seismic wedges within a chronostratigraphic framework, and palynological analysis, we propose that three events controlled the distribution of the Lower Cretaceous wedges: 1) an uplift event of the Loppa High during the latest Jurassic–earliest Cretaceous (Sund et al., 1986; Berglund et al., 1986; Wood et al., 1989; Glørstad-Clark, 2011; Clark et al., 2014), which deposited progressively younger wedges towards the east of the Hammerfest Basin as result of lateral and vertical fault propagation. This induced eastward switching of the sediment input points. The northernmost part of the Loppa High is interpreted as a local depocenter during the early Barremian, due to the proximity of clinoform progradation. 2) Faulting in the western flank of the Loppa High along the Ringvassøy-Loppa and Bjørnøyrenna fault complexes, which triggered the deposition of syn-rift wedges during the late Barremian–Aptian. The wedges were partially deposited in shallow marine environments, but probably also in deep marine environments. An upper Barremian to lower Aptian syn-rift unconformity is interpreted in the western flank of the Loppa High and in the Fingerdjupet Sub-basin. 3) A renewed uplift and eastwards tilting event of the Loppa High and Hammerfest Basin during the late Aptian–early Albian. This event is supported by: the eastward migration of the depocenter location, a deflection towards the east of submarine fans deposited in the northwestern part of the basin, an unconformity in the western and southwestern flanks of the Loppa High, and progressively deeper environments towards the eastern part of the Hammerfest Basin and the Bjarmeland platform. The last observation is based on the height of the clinoforms (80–200 m in the eastern part of the Hammerfest Basin and > 500 m in the Bjarmeland Platform). This event redirected the drainage system away from the Tromsø Basin towards a gentler slope, where it sourced the clinoforms in the northeastern part of the Hammerfest Basin. Fault activity in the western flank of the Loppa High contributed to the uplift of the northernmost part of the Loppa High.

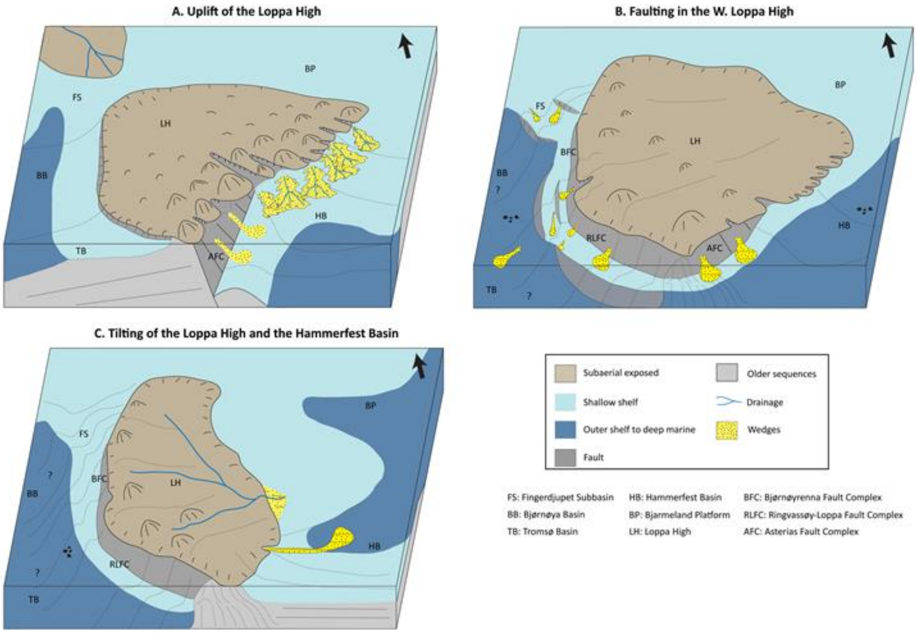

Figure 9. 3D cartoons illustrating the three main events controlling the deposition of the clastic wedges around the Loppa High. For a more detailed explanation of these figures, please see paper 5.

6 Discussion

This section describes the contribution of the thesis to the knowledge of the tectonostratigraphic evolution of the Norwegian Barents Sea margins, as well as the global implications of this study. Specifically, we discuss the implications of both, margins and basin scale deformation on: 1. deposition of the Lower Cretaceous sediments, 2. fault growth and the physiographical and tectonostratigraphic evolution of rift basins, 3. the variables controlling the bypass of coarse-grained sediments into the basin, and 4. regional paleogeography.

6.1 Implications of margin-scale oblique deformation on structural styles

Oblique deformations produce 3D strain which cannot be characterized by simplified 2D plane strain (Brune et al., 2018). In the southwestern and north-central Barents Sea, most of the Early Cretaceous compressional features have been analyzed assuming 2D plane strain, where the analyzed cross section is parallel to the postulated contraction. This leads to a poor explanation of the compressional structures in the context of the overall Late Jurassic – Early Cretaceous tectonic setting of the margins (Antonsen et al., 1991; Grogan et al., 2000; Grogan et al., 1999; Faleide et al., 1993; Gabrielsen et al., 1990; Rønnevik et al., 1982), though several attempts have been made to relate the compression to basement heterogeneity, which could be locally responsible for the change of strain (Barrère et al., 2009; Braathen et al., 1999; Doré, 1991; Fichler et al., 1997; Gabrielsen, 1984; Gernigon et al., 2014; Ritzmann and Faleide, 2007; Tsikalas et al., 2012; Indrevær et al., 2016). In this research, compilation of the regional tectonic events, deformation patterns, mapping of key faults and their associated structures, and mapping of the Lower Cretaceous clastic wedges allowed us to constrain in more detail the tectonic events that operated during this period.

In the north-central Barents Sea (paper 1), the interpreted compression along NE – SW trending faults is caused by the counterclockwise opening of the Canada Basin (Grantz et al., 1998; Lawver et al., 2002; Shephard et al., 2013). This was responsible for the formation of restraining and releasing bends along the paleo-position of the Lomonosov ridge (Evangelatos and Mosher, 2016; Minakov et al., 2012). We suggest that reactivation/inversion of the inherited Late Paleozoic normal faults is the result of transpressional deformation along the northern margin. These processes are very similar to those observed along the present day Dead Sea transform fault (DSTF; Weber et al. 2009). Particularly, in the northern part of the DSTF, transpressional deformation produced restraining bends which resulted in the formation of several anticlines that are oblique to the DSTF (Gomez et al., 2007). This is an analogue of far field strain caused by oblique deformation along margins, which reactivate inherited weak fault zones in reverse mode.

In the southwestern Barents Sea (paper 2), plate tectonic reorganization during the Early Cretaceous resulted in progressive changes in the direction of extension (Lawver et al., 2002; Bernett-Moore et al., 2018; Dore et al., 2016; Seton et al., 2012). The latest plate tectonics models by Barnett-Moore et al., 2018, suggest that from 200 Ma until 80 Ma, the plate tectonics movement between Greenland and Norway had mainly a NW – SE direction, which shifted at 80Ma to an almost N – S direction. Hence, we suggest that before shifting to the N – S direction, the southwestern Barents Sea margins was subjected to oblique deformation that affected the basin evolution. The proposed oblique opening of the Tromsø Basin generated secondary intra-basinal normal faults (Gernigon et al., 2014; Faleide et al., 2008), which are oblique to the inherited fault network (consistent with Bonini et al. 1997 and McClay and White, 1995). Compressional faulting in the northern Tromsø Basin can be explained as an intra-basinal, transpressional transfer zone, which overall fits the oblique opening of the basin (McClay et al., 2002; McClay et al., 2004).

Modeled gravity anomalies along the composite 2D regional seismic section facilitated interpretation of the crustal structures. The distribution of the crustal stretching (β) factor in the southwestern Barents Sea is unlike orthogonally rifted margins (Peron-Pinvidic et al., 2013). The crust below the narrow and confined Tromsø Basin appears to be thinner than in the more distal Sørvestnaget Basin, thus not follow the expected values proposed for extensional margins (consistent with Breivik et al., 2018, Gernigon et al., 2014; Osmundsen and Peron-Pinvidic, 2018). This may suggest that in addition to the expected thinning of the crust during formation of the margin within the necking zone, Early Cretaceous rifting in the southwestern Barents Sea was involved to a certain degree of obliquity where rift parallel deformation most likely decreased crustal thinning (Crosby et al., 2011; Montési and Behn, 2007). Therefore, it is important to integrate the regional tectonic setting in order to understand the basin-scale faulting style and architecture, particularly for complex margins that were subjected to changes in extension direction. This study could serve as a subsurface analogue for basins that developed during oblique extension with inherited basement structures.

6.2 Implications of normal fault growth for the physiographical and tectonostratigraphic evolution of rift basins

The growth history of basin bounding normal faults and interaction with deposition of the Lower Cretaceous clastic wedges are discussed in papers 3 and 5. The two main models of fault growth, isolated versus constant-length, are undistinguishable after the faults have attained their final displacement and length as seen in figure 4 a-b. During the last 30 years, both models have been a matter of discussion and debate (Childs et al., 2017; Jackson et al., 2017). A major difference in these two models is the early growth history of fault displacement versus length (Figs. 4a and 4b), which requires detailed knowledge of fault evolution. In paper 3, a large normal fault (854 m throw) with good record of syn-sedimentary strata in the hanging wall and footwall was chosen to analyze fault growth. Based on fault throw backstripping, we suggest that initially the fault grew in accordance with the isolated model and its near final length was obtained at ~37.5% of its slip history. This is longer than the time suggested by recent compilations by Jackson et al. (2017) and Childs et al. (2017), who suggest that final fault length is established within ~10 – 33% of the fault slip history. Limited vertical seismic resolution (>30 m) and absence of hanging-wall well data introduce additional uncertainties for understanding of the earliest stages of fault growth. Therefore, incised valleys served as key markers for unraveling the growth of the interpreted fault. Thickness map analysis and throw backstripping suggest that fault segments formed earlier than the incised valleys, and hence controlled paleo-drainage, where low areas developed between the fault segments during the early stages of fault growth were exploited by the incised valleys (this is consistent with Gawthorpe and Leeder, 2000). This suggests that the categorical distinction between the isolated versus the constant-length fault growth model may be too simplistic, at least for large basin bounding faults. Detailed interpretation of stratigraphic features, in this case incised valleys, may provide additional information for understating the fault evolution.

6.3 Implications for the regional paleogeography

Most sedimentary processes are related to tectonic processes to some extent (Dickinson, 1974). Their direct or indirect relationship can vary from coarse sediments sourced from uplifted areas or fault scarps to fine sediments deposited in broad sheets away from any direct tectonic influence. In the Barents Sea, structural adjustment in the northern margin (e.g. opening of the Canada Basin, HALIP) triggered southward progradation of Lower Cretaceous clastic material (Marin et al., 2017; Kayukova and Suslova., 2017; Grundvag et al., 2017). Although the main source of the siliciclastics has been suggested to be the area in the N (e.g. North Kara region, Frans Josef Land, etc.) and W-NW (e.g. Greenland), inverted NE – SW striking structural highs in the north-central Barents Sea served as local sediment sources and controlled regional sediment dispersal by funneling fluvio-deltaic systems in a SW direction. This has implications for the paleogeography and tectonic reconstructions of the Arctic. For instance, it implies that during the Early Cretaceous, continental areas were present along the northern edges of the Barents Sea and sourced siliciclastic material to the S and SW Barents Sea.

Previous works in the northern Barents Sea (including the Russian sector) provide general paleogeographic maps for mainly three intervals corresponding to the Valanginian, Barremian and Albian (Smelror et al., 2009 and Worsley, 2008). These maps mainly give information about the location of the continental areas, the shelf and the deep-water environments. In contrast to these previous works, we constructed paleogeographic maps for four time intervals, where mapping of the structurally uplifted and eroded highs, and distribution of clinoforms allowed us to define possible continental areas, deltas and shorelines (papers 1 and 4). The main strength of these paleotectonic and paleo-depositional reconstructions is the integration of several geological observations, such as sequence stratigraphy and seismic facies analysis, sedimentological descriptions of core data and outcrops, and biostratigraphy. These paleogeographic reconstructions help to understand the source of silisiclastics and predict the distribution of potential reservoir sandstones in the study area.

6.4 Limitations

Although this research has significant implications for the understanding the tectonic processes in the Norwegian Barents Sea, it is important to highlight the main limitations related to the data and methods. Highlighting these limitations is essential for future research as it may promote the development of new seismic processing techniques (e.g. de-multiple) and seismic acquisition methods (e.g. shallow water source configurations).

Seismic data

It is well known that acquisition of 2D and 3D seismic data in the Barents Sea is often related to hydrocarbon exploration. The north-central Barents Sea is restricted for any hydrocarbon exploration activities. Consequently, it is covered by a sparse 2D seismic grid with average distance ca. 15 km. This makes difficult the seismic interpretation of key horizons and faults. Poor imaging and abundancy of seafloor multiples due to shallow water depths require better processing techniques. Additionally, the 2D seismic sections are often oblique to the main structural lineaments, which affect the understanding of their true geometries (e.g. faults, clinoforms).

Well data

A limited amount of exploration wells in the north-central and southwestern Barents Sea contribute to the uncertainty in time-to-depth conversion and structural restoration. The lack of exploration wells makes difficult the correlation between gamma-ray logs and seismic facies. We experienced this limitation in papers 1 and 3 where several seismic facies have not been drilled by exploration wells, and the interpretation of depositional environments was based only on seismic reflectivity and internal architectures.

7 Recommendations for future work

Plate tectonic reorganization can often lead to changes in the stress and strain fields along margins (Brune et al., 2018). Most previous works, including our research in paper 2, focus on specific cases of rifted systems, which involve a certain degree of obliquity (Fournier et al., 2004; Lizarralde et al., 2007; Klimke and Franke, 2016; Phethean et al., 2016). Quantification of rift obliquity through time is more difficult since it requires detailed documentation of syn-rift evolution. Further research should be oriented towards validating such quantifications, as it may provide better kinematics constrains for plate tectonics reconstructions.

The detailed fault growth history from paper 3 indicates that the ongoing debate between the two competing fault growth models (isolated versus constant length) may be too categorical. Some authors claim that there is an overall bias in favor of the isolated fault growth model, while the majority of the natural examples of active or extinct fault systems show characteristics of the constant length model (Nicole et al., 2016; Rotevatn et al., 2018; Rotevatn e t al., 2019). Therefore, future research related to the growth of normal faults should be oriented to better document the initial lengthening stages of fault evolution. This might be achieved by integrating high-resolution seismic imaging techniques and well data (e.g. biostratigraphy), which can allow mapping fault structure and associated growth strata (Taylor et al., 2004; Nicol et al., 2005).

8 Conclusions

Based on detailed analysis of subsurface data, this research has improved the geological understanding of the structural elements and depositional patterns of the north-central and southwestern Barents Sea margins. Our main findings are:

1) The inverted pre-existing fault network in the north-central Barents Sea guided the deposition and progradation of the Lower Cretaceous clastics. The interpreted deformation pattern and structural imprint of the area supports a counterclockwise model for the opening of the Canada Basin. This interpretation may contribute to the understanding of how deformation along margins can affect fault evolution and sediment distribution in distal areas.
2) Basins that evolved in an oblique setting (e.g. Tromsø Basin), likely display a complex fault pattern with abnormal crustal thickness and compressional structures that can be easily misinterpreted. Analyzing major basin bounding faults in the context of the overall plate tectonics setting and basin configuration is key to understand the main factors controlling fault distribution.
3) Detailed analysis of a basin bounding normal fault shows that the categorical distinction between isolated versus the constant-length fault growth models may be too simplistic, at least for large basin bounding faults. Analysis of sedimentation or erosional processes (e.g. incised valleys) can provide key information for unraveling the early growth history of these faults.
4) In contrast to previous works, more refined and detailed regional paleogeographic maps for the Norwegian Barents Sea were built. Each time interval reflects the structural and stratigraphic evolution of the area. These paleogeographic maps can help to predict sandstone distribution, and better understand the evolution of the Arctic during the Early Cretaceous.

References

Agostini, A., G. Corti, A. Zeoli, and G. Mulugeta, 2009, Evolution, pattern, and partitioning of deformation during oblique continental rifting: Inferences from lithospheric-scale centrifuge models: Geochemistry, Geophysics, Geosystems, v. 10.

Alvey, A., C. Gaina, N. J. Kusznir, and T. H. Torsvik, 2008, Integrated crustal thickness mapping and plate reconstructions for the high Arctic: Earth and Planetary Science Letters, v. 274, p. 310-321.

Anell, I., A. Braathen, and S. Olaussen, 2014, Regional constraints of the Sørkapp Basin: A Carboniferous relic or a Cretaceous depression?: Marine and Petroleum Geology, v. 54, p. 123-138.

Antonsen, P., A. Elverhoi, H. Dypvik, and A. Solheim, 1991, Shallow Bedrock Geology of the Olga Basin Area, Northwestern Barents Sea American Association of Petroleum Geologists Bulletin, v. 75, p. 1178-1194.

Barnett-Moore, N., D. R. Müller, S. Williams, J. Skogseid, and M. Seton, 2018, A reconstruction of the North Atlantic since the earliest Jurassic: Basin Research, v. 30, p. 160-185.

Barrère, C., J. Ebbing, and L. Gernigon, 2009, Offshore prolongation of Caledonian structures and basement characterisation in the western Barents Sea from geophysical modelling: Tectonophysics, v. 470, p. 71-88.

Bergh, S. G., and P. Grogan, 2003, Tertiary structure of the Sørkapp-Hornsund Region, South Spitsbergen, and implications for the offshore southern extension of the fold-thrust Belt: Norsk Geologisk Tidsskrift, v. 83, p. 43-60.

Berglund, L. T., J. Augustson, R. Faerseth, J. Gjelberg, and H. Ramberg-Moe, 1986, The evolution of the Hammerfest Basin: Habitat of hydrocarbons on the Norwegian continental shelf. Proc. conference, Stavanger, 1985, p. 319-338.

Bonini, M., T. Souriot, M. Boccaletti, and J. P. Brun, 1997, Successive orthogonal and oblique extension episodes in a rift zone: Laboratory experiments with application to the Ethiopian Rift: Tectonics, v. 16, p. 347-362.

Braathen, A., H. D. Maher Jr, T. E. Haabet, S. E. Kristensen, B. O. Tørudbakken, and D. Worsley, 1999, Caledonian thrusting on

Bjornoya: Implications for Palaeozoic and Mesozoic tectonism of the western Barents Shelf: Norsk Geologisk Tidsskrift, v. 79, p. 57-68.

Braathen, A., J. Tveranger, H. Fossen, T. Skar, N. Cardozo, S. E. Semshaug, E. Bastesen, and E. Sverdrup, 2009, Fault facies and its application to sandstone reservoirs: AAPG Bulletin, v. 93, p. 891-917.

Breivik, A. J., J. I. Faleide, and S. T. Gudlaugsson, 1998, Southwestern Barents Sea margin: late Mesozoic sedimentary basins and crustal extension: Tectonophysics, v. 293, p. 21-44.

Brune, S., and J. Autin, 2013, The rift to break-up evolution of the Gulf of Aden: Insights from 3D numerical lithospheric-scale modelling: Tectonophysics, v. 607, p. 65-79.

Brune, S., G. Corti, and G. Ranalli, 2017, Controls of inherited lithospheric heterogeneity on rift linkage: Numerical and analog models of interaction between the Kenyan and Ethiopian rifts across the Turkana depression: Tectonics, v. 36, p. 1767-1786.

Brune, S., S. E. Williams, and R. D. Müller, 2018, Oblique rifting: the rule, not the exception: Solid Earth, v. 9, p. 1187-1206.

Bryn, B. K. L., J. Ahokas, S. Patruno, S. Schjelderup, C. Hinna, C. Lowrey, and A. Escalona, Exploring the reservoir potential of Lower Cretaceous Clinoforms in the Fingerdjupet Subbasin, Norwegian Barents Sea: Basin Research, v. n/a.

Cartwright, J. A., B. D. Trudgill, and C. S. Mansfield, 1995, Fault growth by segment linkage: an explanation for scatter in maximum displacement and trace length data from the Canyonlands Grabens of SE Utah: Journal of Structural Geology, v. 17, p. 1319-1326.

Childs, C., R. E. Holdsworth, C. A.-L. Jackson, T. Manzocchi, J. J. Walsh, and G. Yielding, 2017, Introduction to the geometry and growth of normal faults: Geological Society, London, Special Publications, v. 439.

Childs, C., A. Nicol, J. J. Walsh, and J. Watterson, 2003, The growth and propagation of synsedimentary faults: Journal of Structural Geology, v. 25, p. 633-648.

Clark, S. A., E. Glorstad-Clark, J. I. Faleide, D. Schmid, E. H. Hartz, and W. Fjeldskaar, 2014, Southwest Barents Sea rift basin evolution:

comparing results from backstripping and time-forward modelling: Basin Research, v. 26, p. 550-566.

Clifton, A. E., R. W. Schlische, M. O. Withjack, and R. V. Ackermann, 2000, Influence of rift obliquity on fault-population systematics: Results of experimental clay models: Journal of Structural Geology, v. 22, p. 1491-1509.

Cochran, J. R., M. H. Edwards, and B. J. Coakley, 2006, Morphology and structure of the Lomonosov Ridge, Arctic Ocean: Geochemistry, Geophysics, Geosystems, v. 7, p. 1-26.

Corfu, F., S. Polteau, S. Planke, J. I. Faleide, H. Svensen, A. Zayoncheck, and N. Stolbov, 2013, U-Pb geochronology of Cretaceous magmatism on Svalbard and Franz Josef Land, Barents Sea Large Igneous Province: Geological Magazine, v. 150, p. 1127-1135.

Corti, G., 2008, Control of rift obliquity on the evolution and segmentation of the main Ethiopian rift: Nature Geoscience, v. 1, p. 258-262.

Crosby, A. G., N. J. White, G. R. H. Edwards, M. Thompson, R. Corfield, and L. Mackay, 2011, Evolution of deep-water rifted margins: Testing depth-dependent extensional models: Tectonics, v. 30, p. n/a-n/a.

Dawers, N. H., and M. H. Anders, 1995, Displacement-length scaling and fault linkage: Journal of Structural Geology, v. 17, p. 607-614.

Dawers, N. H., M. H. Anders, and C. H. Scholz, 1993, Growth of normal faults: Displacement-length scaling: Geology, v. 21, p. 1107-1110.

Dewey, J. F., R. E. Holdsworth, and R. A. Strachan, 1998, Transpression and transtension zones, Geological Society Special Publication, p. 1-14.

Dibner, V. D., 1998, The geology of Franz Josef Land - an introduction: Meddelelser, v. 151.

Dickinson, W. R., 1974, Plate Tectonics and Sedimentation, *in* W. R. Dickinson, ed., Tectonics and Sedimentation, Special Publication No. 22: Tulsa, Oklahoma, Society of Economic Paleontologists and Mineralogist, p. 1-27.

Dimakis, P., B. I. Braathen, J. I. Faleide, A. Elverhøi, and S. T. Gudlaugsson, 1998, Cenozoic erosion and the preglacial uplift of the Svalbard-Barents Sea region: Tectonophysics, v. 300, p. 311-327.

Doré, A. G., 1991, The structural foundation and evolution of Mesozoic seaways between Europe and the Arctic: Palaeogeography, Palaeoclimatology, Palaeoecology, v. 87, p. 441-492.

Doré, A. G., E. R. Lundin, A. Gibbons, T. O. Sømme, and B. O. Tørudbakken, 2015, Transform margins of the Arctic: a synthesis and re-evaluation: Geol. Soc. Lond. Spec. Publ., v. 431, p. SP431-SP438.

Døssing, A., H. R. Jackson, J. Matzka, I. Einarsson, T. M. Rasmussen, A. V. Olesen, and J. M. Brozena, 2013, On the origin of the Amerasia Basin and the High Arctic Large Igneous Province—Results of new aeromagnetic data: Earth and Planetary Science Letters, v. 363, p. 219-230.

Dove, D., B. Coakley, J. Hopper, Y. Kristoffersen, and H. L. Y. G. Team, 2010, Bathymetry, controlled source seismic and gravity observations of the Mendeleev ridge; implications for ridge structure, origin, and regional tectonics: Geophysical Journal International, v. 183, p. 481-502.

Evangelatos, J., and D. C. Mosher, 2016, Seismic stratigraphy, structure and morphology of Makarov Basin and surrounding regions: tectonic implications: Marine Geology, v. 374, p. 1-13.

Evenchick, C. A., W. J. Davis, J. H. Bédard, N. Hayward, and R. M. Friedman, 2015, Evidence for protracted High Arctic large igneous province magmatism in the central Sverdrup Basin from stratigraphy, geochronology, and paleodepths of saucer-shaped sills: Bulletin of the Geological Society of America, v. 127, p. 1366-1390.

Faleide, J. I., F. Tsikalas, A. J. Breivik, R. Mjelde, O. Ritzmann, O. Engen, J. Wilson, and O. Eldholm, 2008, Structure and evolution of the continental margin off Norway and Barents Sea: Episodes, v. 31, p. 82-91.

Faleide, J. I., E. Vagnes, and S. T. Gudlaugsson, 1993, Late Mesozoic-Cenozoic Evolution of the South-Western Barents Sea in a Regional Rift Shear Tectonic Setting: Marine and Petroleum Geology, v. 10, p. 186-214.

Fichler, C., E. Rundhovde, S. Johansen, and B. Sæther, 1997, Barents Sea tectonic structures visualized by ERS1 satellite gravity data with indications of an offshore Baikalian trend: First Break, v. 15, p. 355-363.

Fisher, Q. J., and R. J. Knipe, 2001, The permeability of faults within siliciclastic petroleum reservoirs of the North Sea and Norwegian Continental Shelf: Marine and Petroleum Geology, v. 18, p. 1063-1081.

Fossen, H., and A. Rotevatn, 2016, Fault linkage and relay structures in extensional settings-A review: Earth-Science Reviews, v. 154, p. 14-28.

Gabrielsen, R., and R. Færseth, 1988, Cretaceous and Tertiary Reactivation of Master Fault zones of the Barents sea, Oslo, Norks Polarinstitutt, p. 93-97.

Gabrielsen, R. H., 1984, Long-lived fault zones and their influence on the tectonic development of the southwestern Barents Sea: Journal of the Geological Society, v. 141, p. 651-662.

Gabrielsen, R. H., R. B. Faerseth, L. N. Jensen, J. E. Kalheim, and F. Riis, 1990, Structural elements of the Norwegian continental shelf: Part 1. The Barents Sea region Norwegian Petroleum Directorate Bulletin, v. 6, p. 33.

Gabrielsen, R. H., D. Sokoutis, E. Willingshofer, and J. I. Faleide, 2016, Fault linkage across weak layers during extension: an experimental approach with reference to the Hoop Fault Complex of the SW Barents Sea: Petroleum Geoscience, v. 22, p. 123-135.

Gaina, C., S. Medvedev, T. H. Torsvik, I. Koulakov, and S. C. Werner, 2014, 4D Arctic: A Glimpse into the Structure and Evolution of the Arctic in the Light of New Geophysical Maps, Plate Tectonics and Tomographic Models: Surveys in Geophysics, v. 35, p. 1095-1122.

Gawthorpe, R. L., and M. R. Leeder, 2000, Tectono-sedimentary evolution of active extensional basins: Basin Research, v. 12, p. 195-218.

Gernigon, L., M. Brönner, D. Roberts, O. Olesen, A. Nasuti, and T. Yamasaki, 2014, Crustal and basin evolution of the southwestern Barents Sea: From Caledonian orogeny to continental breakup: Tectonics, v. 33, p. 347-373.

Giba, M., J. J. Walsh, and A. Nicol, 2012, Segmentation and growth of an obliquely reactivated normal fault: Journal of Structural Geology, v. 39, p. 253-267.

Glørstad-Clark, E., S. Clark, J. Faleide, S. Bjørkesett, R. Gabrielsen, and J. Nystuen, 2011, Basin dynamics of the Loppa High area, SW Barents Sea: A history of complex vertical movements in an epicontinental basin: Basin analysis in the western Barents Sea area: The interplay between accommodation space and depositional systems. Philosphiae Doctor Series of Dissertation, University of Oslo, p. 111-180.

Gomez, F., T. Nemer, C. Tabet, M. Khawlie, M. Meghraoui, and M. Barazangi, 2007, Strain partitioning of active transpression within the Lebanese restraining bend of the Dead Sea Fault (Lebanon and SW Syria): Geological Society, London, Special Publications, v. 290, p. 285-303.

Grogan, P., K. Nyberg, B. Fotland, R. Myklebust, S. Dahlgren, and F. Riis, 1998, Cretaceous Magmatism South and East of Svalbard: Evidence from Seismic Reflection and Magnetic Data: Polarforschung, v. 68, p. 25 - 34.

Grogan, P., A.-M. Østvedt-Ghazi, G. B. Larssen, B. Fotland, K. Nyberg, S. Dahlgren, and T. Eidvin, 1999, Structural elements and petroleum geology of the Norwegian sector of the northern Barents Sea: Geological Society, London, Petroleum Geology Conference series, v. 5, p. 247-259.

Grundvåg, S.-A., and S. Olaussen, 2017, Sedimentology of the Lower Cretaceous at Kikutodden and Keilhaufjellet, southern Spitsbergen: implications for an onshore–offshore link: Polar Research, v. 36, p. 1302124.

Gudlaugsson, S. T., J. I. Faleide, S. E. Johansen, and A. J. Breivik, 1998, Late Palaeozoic structural developments of the south-western Barents Sea: Marine and Petroleum Geology, v. 15, p. 73-102.

Hadlari, T., D. Midwinter, J. M. Galloway, K. Dewing, and A. M. Durbano, 2016, Mesozoic rift to post-rift tectonostratigraphy of the Sverdrup Basin, Canadian Arctic: Marine and Petroleum Geology, v. 76, p. 148-158.

Henriksen, E., H. M. Bjørnseth, T. K. Hals, T. Heide, T. Kiryukhina, O. S. Kløvjan, G. B. Larssen, A. E. Ryseth, K. Rønning, K. Sollid, and A. Stoupakova, 2011, Chapter 17 Uplift and erosion of the greater Barents Sea: impact on prospectivity and petroleum systems: Geological Society, London, Memoirs, v. 35, p. 271-281.

Henstra, G. A., S.-A. Grundvåg, E. P. Johannessen, T. B. Kristensen, I. Midtkandal, J. P. Nystuen, A. Rotevatn, F. Surlyk, T. Sæther, and J. Windelstad, 2016, Depositional processes and stratigraphic architecture within a coarse-grained rift-margin turbidite system: The Wollaston Forland Group, east Greenland: Marine and Petroleum Geology, v. 76, p. 187-209.

Hodge, M., Å. Fagereng, J. Biggs, and H. Mdala, 2018, Controls on Early-Rift Geometry: New Perspectives From the Bilila-Mtakataka Fault, Malawi: Geophysical Research Letters, v. 45, p. 3896-3905.

Hosseinpour, M., R. D. Müller, S. E. Williams, and J. M. Whittaker, 2013, Full-fit reconstruction of the Labrador Sea and Baffin Bay: Solid Earth, v. 4, p. 461-479.

Indrevær, K., S. G. Bergh, J. B. Koehl, J. A. Hansen, E. R. Schermer, and A. Ingebrigtsen, 2013, Post-Caledonian brittle fault zones on the hyperextended SW Barents Sea margin: New insights into onshore and offshore margin architecture: Norsk Geologisk Tidsskrift, v. 93, p. 167-188.

Indrevær, K., R. H. Gabrielsen, and J. I. Faleide, 2016, Early Cretaceous synrift uplift and tectonic inversion in the Loppa High area, southwestern Barents Sea, Norwegian shelf: Journal of the Geological Society.

Jackson, C. A.-L., R. E. Bell, A. Rotevatn, and A. B. M. Tvedt, 2017, Techniques to determine the kinematics of synsedimentary normal faults and implications for fault growth models: Geological Society, London, Special Publications, v. 439.

Jackson, C. A. L., and A. Rotevatn, 2013, 3D seismic analysis of the structure and evolution of a salt-influenced normal fault zone: A test of competing fault growth models: Journal of Structural Geology, v. 54, p. 215-234.

Kayukova, A. V., and A. A. Suslova, 2015, A seismostratigraphic analysis of the lower cretaceous deposits of the Barents sea to reveal petroleum perspectives: Moscow University Geology Bulletin, v. 70, p. 177-182.

Knies, J., and C. Gaina, 2008, Middle Miocene ice sheet expansion in the Arctic: Views from the Barents Sea: Geochemistry, Geophysics, Geosystems, v. 9, p. n/a-n/a.

Knutsen, S.-M., J. H. Augustson, P. Haremo, K. Ofstad, J. Kittilsen, and P. Alexander-Marrack, 2000, Exploring the Norwegian part of the Barents Sea—Norsk Hydro's lessons from nearly 20 years of experience: Improving the exploration process by learning from the past: Amsterdam, Norwegian Petroleum Society Special Publication, v. 9, p. 99-112.

Larssen, G., G. Elvebakk, L. B. Henriksen, S. Kristensen, I. Nilsson, T. Samuelsberg, T. Svånå, L. Stemmerik, and D. Worsley, 2002, Upper Palaeozoic lithostratigraphy of the Southern Norwegian Barents Sea: Norwegian Petroleum Directorate Bulletin, v. 9, p. 76.

Lawver, L., and C. Scotese, 1990, A review of tectonic models for the evolution of the Canada Basin, *in* A. Grantz, L. Johnson, and J. F. Sweeney, eds., The Geology of North America, v. L: Boulder, Colarado, p. 593-618.

Lawver, L. A., A. Grantz, L. M. Gahagan, E. L. Miller, A. Grantz, and S. L. Klemperer, 2002, Plate kinematic evolution of the present Arctic region since the Ordovician, Tectonic Evolution of the Bering Shelf-Chukchi Sea-Artic Margin and Adjacent Landmasses, v. 360, Geological Society of America, p. 0.

Manatschal, G., L. Lavier, and P. Chenin, 2015, The role of inheritance in structuring hyperextended rift systems: Some considerations based on observations and numerical modeling: Gondwana Research, v. 27, p. 140-164.

Mansfield, C., and J. Cartwright, 2001, Fault growth by linkage: observations and implications from analogue models: Journal of Structural Geology, v. 23, p. 745-763.

Marín, D., A. Escalona, S.-A. Grundvåg, S. Olaussen, S. Sandvik, and K. K. Śliwińska, 2018, Unravelling key controls on the rift climax to post-rift fill of marine rift basins: insights from 3D seismic analysis of the Lower Cretaceous of the Hammerfest Basin, SW Barents Sea: Basin Research, v. 30, p. 587-612.

Marin, D., A. Escalona, K. K. Sliwihska, H. Nøhr-Hansen, and A. Mordasova, 2017, Sequence stratigraphy and lateral variability of Lower Cretaceous clinoforms in the southwestern Barents Sea: AAPG Bulletin, v. 101, p. 1487-1517.

McClay, K. R., T. Dooley, P. Whitehouse, and M. Mills, 2002, 4-D evolution of rift systems: Insights from scaled physical models: AAPG Bulletin, v. 86, p. 935-959.

McClay, K. R., and M. J. White, 1995, Analogue modelling of orthogonal and oblique rifting: Marine and Petroleum Geology, v. 12, p. 137-151.

McClay, K. R., P. S. Whitehouse, T. Dooley, and M. Richards, 2004, 3D evolution of fold and thrust belts formed by oblique convergence: Marine and Petroleum Geology, v. 21, p. 857-877.

Minakov, A., R. Mjelde, J. I. Faleide, E. R. Flueh, A. Dannowski, and H. Keers, 2012, Mafic intrusions east of Svalbard imaged by active-source seismic tomography: Tectonophysics, v. 518-521, p. 106-118.

Molnar, N. E., A. R. Cruden, and P. G. Betts, 2017, Interactions between propagating rotational rifts and linear rheological heterogeneities: Insights from three-dimensional laboratory experiments: Tectonics, v. 36, p. 420-443.

Mondy, L. S., P. F. Rey, G. Duclaux, and L. Moresi, 2018, The role of asthenospheric flow during rift propagation and breakup: Geology, v. 46, p. 103-106.

Montési, L. G. J., and M. D. Behn, 2007, Mantle flow and melting underneath oblique and ultraslow mid-ocean ridges: Geophysical Research Letters, v. 34.

Morley, C. K., 2002, Evolution of Large Normal Faults: Evidence from Seismic Reflection Data: AAPG Bulletin, v. 86, p. 961-978.

Morley, C. K., 2017, The impact of multiple extension events, stress rotation and inherited fabrics on normal fault geometries and evolution in the Cenozoic rift basins of Thailand, Geological Society Special Publication, p. 413-445.

Nicol, A., C. Childs, J. J. Walsh, T. Manzocchi, and M. P. J. Schöpfer, 2016, Interactions and growth of faults in an outcrop-scale system: Geological Society, London, Special Publications, v. 439.

Nikishin, A. M., N. A. Malyshev, and E. I. Petrov, 2014, Geological structure and history of the Arctic Ocean: Netherlands, EAGE Publications bv.

Nikishin, V. A., 2013, Intraplate and marginal deformation of the Kara Sea sedimentary basins, Moscow State University, 21 p.

Olaussen, S., G. B. Larssen, H. Helland, Johannessen, A. Nøttvedt, Riis, Rismyhr, M. Smelror, and D. Worsley, 2019, Mesozoic strata of Kong Karls Land, Svalbard, Norway; a link to the northern Barents Sea basins and platforms.

Osmundsen, P. T., and G. Péron-Pinvidic, 2018. Crustal-scale fault interaction at rifted margins and the formation of domain-bounding breakaway complexes: Insights from offshore Norway. Tectonics, 37, 935– 964.

Peacock, D. C. P., and D. J. Sanderson, 1991, Displacements, segment linkage and relay ramps in normal fault zones: Journal of Structural Geology, v. 13, p. 721-733.

Peron-Pinvidic, G., G. Manatschal, and P. T. Osmundsen, 2013, Structural comparison of archetypal Atlantic rifted margins: A review of observations and concepts: Marine and Petroleum Geology, v. 43, p. 21-47.

Phillips, T. B., C. A. L. Jackson, R. E. Bell, and O. B. Duffy, 2018, Oblique reactivation of lithosphere-scale lineaments controls rift physiography - The upper-crustal expression of the Sorgenfrei-Tornquist Zone, offshore southern Norway: Solid Earth, v. 9, p. 403-429.

Polteau, S., B. W. H. Hendriks, S. Planke, M. Ganerød, F. Corfu, J. I. Faleide, I. Midtkandal, H. S. Svensen, and R. Myklebust, 2016, The Early Cretaceous Barents Sea Sill Complex: Distribution, 40Ar/39Ar geochronology, and implications for carbon gas formation: Palaeogeography, Palaeoclimatology, Palaeoecology, v. 441, p. 83-95.

Prosser, S., 1993, Rift-related linked depositional systems and their seismic expression: Geological Society, London, Special Publications, v. 71, p. 35-66.

Riis, F., J. Vollset, M. Sand, and M. T. Halbouty, 1986, Tectonic Development of the Western Margin of the Barents Sea and Adjacent Areas, Future Petroleum Provinces of the World, v. 40, American Association of Petroleum Geologists, p. 0.

Ritzmann, O., and J. I. Faleide, 2007, Caledonian basement of the western Barents Sea: Tectonics, v. 26, p. n/a-n/a.

Ritzmann, O., and J. I. Faleide, 2009, The crust and mantle lithosphere in the Barents Sea/Kara Sea region: Tectonophysics, v. 470, p. 89-104.

Rønnevik, H., B. Beskow, and H. P. Jacobsen, 1982, Structural and stratigraphic evolution of the Barents Sea: Arctic geology and geophysics, v. 8, Canadian Society of Petroleum Geologists Memoir, 10 p.

Rowley, D. B., and A. L. Lottes, 1988, Plate-kinematic reconstructions of the North Atlantic and Arctic: Late Jurassic to Present: Tectonophysics, v. 155, p. 73-120.

Ryseth, A., J. H. Augustson, M. Charnock, O. Haugerud, S.-M. Knutsen, P. S. Midbøe, J. G. Opsal, and G. Sundsbø, 2003, Cenozoic stratigraphy and evolution of the Sørvestsnaget Basin, southwestern Barents Sea: Norwegian Journal of Geology/Norsk Geologisk Forening, v. 83.

Sanderson, D. J., and W. R. D. Marchini, 1984, Transpression: Journal of Structural Geology, v. 6, p. 449-458.

Schlagenhauf, A., I. Manighetti, J. Malavieille, and S. Dominguez, 2008, Incremental growth of normal faults: Insights from a laser-equipped analog experiment: Earth and Planetary Science Letters, v. 273, p. 299-311.

Seldal, J., 2005, Lower Cretaceous: The next target for oil exploration in the Barents Sea?, Petroleum Geology Conference Proceedings, p. 231-240.

Senger, K., J. Tveranger, K. Ogata, A. Braathen, and S. Planke, 2014, Late Mesozoic magmatism in Svalbard: A review: Earth-Science Reviews, v. 139, p. 123-144.

Seton, M., R. D. Müller, S. Zahirovic, C. Gaina, T. Torsvik, G. Shephard, A. Talsma, M. Gurnis, M. Turner, S. Maus, and M. Chandler, 2012, Global continental and ocean basin reconstructions since 200Ma: Earth-Science Reviews, v. 113, p. 212-270.

Sippel, J., C. Meeßen, M. Cacace, J. Mechie, S. Fishwick, C. Heine, M. Scheck-Wenderoth, and M. R. Strecker, 2017, The Kenya rift revisited: Insights into lithospheric strength through data-driven 3-D gravity and thermal modelling: Solid Earth, v. 8, p. 45-81.

Smelror, M., A. Mørk, E. Monteil, D. Rutledge, and H. Leereveld, 1998, The Klippfisk Formation - a new lithostratigraphic unit of Lower Cretaceous platform carbonates on the Western Barents Shelf: Polar Research, v. 17, p. 181-202.

Smelror, M., O. Petrov, G. B. Larssen, and S. Werner, 2009, Geological history of the Barents Sea: Trondheim, Geological Survey of Norway.

Sund, T., 1984, Tectonic Development and Hydrocarbon Potential Offshore Troms, Northern Norway: AAPG Bulletin, v. 68, p. 1206-1207.

Sund, T., O. Skarpnes, L. N. Jensen, and R. Larsen, 1986, Tectonic development and hydrocarbon potential offshore Troms, northern Norway.

Torabi, A., B. Alaei, and A. Libak, 2019, Normal fault 3D geometry and displacement revisited: Insights from faults in the Norwegian Barents Sea: Marine and Petroleum Geology, v. 99, p. 135-155.

Tsikalas, F., J. I. Faleide, O. Eldholm, and O. Antonio Blaich, 2012, 5 - The NE Atlantic conjugate margins A2 - Roberts, D.G, *in* A. W. Bally, ed., Regional Geology and Tectonics: Phanerozoic Passive Margins, Cratonic Basins and Global Tectonic Maps: Boston, Elsevier, p. 140-201.

Tvedt, A. B. M., A. Rotevatn, and C. A. L. Jackson, 2016, Supra-salt normal fault growth during the rise and fall of a diapir: Perspectives from 3D seismic reflection data, Norwegian North Sea: Journal of Structural Geology, v. 91, p. 1-26.

Walsh, J. J., W. R. Bailey, C. Childs, A. Nicol, and C. G. Bonson, 2003, Formation of segmented normal faults: a 3-D perspective: Journal of Structural Geology, v. 25, p. 1251-1262.

Walsh, J. J., A. Nicol, and C. Childs, 2002, An alternative model for the growth of faults: Journal of Structural Geology, v. 24, p. 1669-1675.

Walsh, J. J., and J. Watterson, 1988, Analysis of the relationship between displacements and dimensions of faults: Journal of Structural Geology, v. 10, p. 239-247.

Watterson, J., 1986, Fault dimensions, displacements and growth: pure and applied geophysics, v. 124, p. 365-373.

Weber, M., K. Abu-Ayyash, A. Abueladas, A. Agnon, Z. Alasonati-Tašárová, H. Al-Zubi, A. Babeyko, Y. Bartov, K. Bauer, and M. Becken, 2009, Anatomy of the Dead Sea Transform from lithospheric to microscopic scale: Reviews of Geophysics, v. 47.

Withjack, M. O., and W. R. Jamison, 1986, Deformation produced by oblique rifting: Tectonophysics, v. 126, p. 25.

Wood, R., S. Edrich, and I. Hutchison, 1989, Influence of North Atlantic tectonics on the large-scale uplift of the stappen high and loppa high, Western barents shelf: Chapter 36: North Sea and barents shelf.

Worsley, D., 2008, The post-Caledonian development of Svalbard and the western Barents Sea: Polar Research, v. 27, p. 298-317.

Chapter 2

Paper 1

Early Cretaceous tectonostratigraphic evolution of the north central Barents Sea

B. Kairanov, A. Escalona, A. Mordasova, K. Śliwińska, A. Suslova.

Journal of Geodynamics, 119, 2018, 183-198, ISSN 0264-3707,
https://doi.org/10.1016/j.jog.2018.02.009

Journal of Geodynamics 119 (2018) 183–198

Contents lists available at ScienceDirect

Journal of Geodynamics

journal homepage: www.elsevier.com/locate/jog

Early Cretaceous tectonostratigraphic evolution of the north central Barents Sea

B. Kairanov[a,*], A. Escalona[a], A. Mordasova[b], K. Śliwińska[c], A. Suslova[b]

[a] *Department of Petroleum Engineering, University of Stavanger, 4036 Stavanger, Norway*
[b] *Lomonosov Moscow State University, Geological Faculty, Moscow, Russia*
[c] *Geological Survey of Denmark and Greenland (GEUS), Øster Voldgade 10 DK-1350 Copenhagen, Denmark*

A B S T R A C T

In this paper we investigate the structural evolution of the northcentral Barents Sea during the Early Cretaceous, and the influence of fault activity on the sedimentation pattern in the area. This is achieved by integrating 2D seismic data, two exploration wells and information of available shallow cores from the Norwegian and Russian sectors. As a result of our work, three fault families, two Lower Cretaceous seismic sequences and seven seismic facies, were interpreted in the area. During the Hauterivian–Early Barremian (sequence 1), a syn-tectonic phase is observed, where fault families 1 and 2 of Late Paleozoic age were reactivated as reverse faults and induced the inversion of NE–SW and E–W structural highs that controlled deposition in the Kong Karls Land Platform, North Barents Basin and the newly formed Olga Basin. During Early Barremian–Early Aptian (sequence 2), the study area was marked by a tectonically quiescent period, where the increase of clastic supply from the N–NE was responsible for progradation of the system towards the S–SW Barents Sea. The progradation was controlled and routed by structural highs inherited from the Hauterivian–Early Barremian inversion.

Our results suggest that three main regional tectonic events controlled the inversion of the Late Paleozoic faults, resulting in development of structural highs in the northcentral Barents Sea: 1) dextral transpression along the Novaya Zemlya; 2) dextral movement along a paleo-boundary of the northern margin of the Lomonosov Ridge during opening of the Amerasia Basin; and 3) a compressional event in the present day North Greenland and Ellesmere Islands with the NW Barents Sea (NW Svalbard).

1. Introduction

The northcentral Barents Sea covers the offshore area between Svalbard and the northern part of Novaya Zemlya (Fig. 1A). The area is not as extensively studied as the remaining part of the Barents Sea (e.g. southwestern Barents Sea), mainly due to limited data availability and the fact that the area is not yet open for any commercial exploration.

Previous work in the region has documented a compressional event that resulted in inversion during the Late Jurassic – Early Cretaceous (Grogan et al., 1999). The inversion resulted in uplift and formation of NE–SW and E–W trending structural highs and anticlines East of Svalbard and Novaya Zemlya (Antonsen et al., 1991; Grogan et al., 2000; Grogan et al., 1999; Nikishin et al., 2014; Nikishin, 2013). The main mechanism responsible for this compression event is not clear, and in the existing literature it has been poorly related to main tectonics events during Late Jurassic – Early Cretaceous, such as: 1) the formation of the High Arctic Large Igneous province (Polteau et al., 2016); 2) the reactivation of Triassic structural lineaments along the Novaya Zemlya (Nikishin et al., 2014; Sobornov et al., 2015); and 3) the opening of the Amerasia Basin to the North (Alvey et al., 2008; Grogan et al., 1999).

The Early Cretaceous development of the Barents Sea is also marked by a major change in the paleogeographic setting. Recent studies of Lower Cretaceous clinoforms complexes in the southern Barents Sea reveal a main clastic source of sedimentation located in the NW and NE that builds the shelf southwards (Grundvåg and Olaussen, 2017; Kayukova and Suslova, 2015; Marin et al., 2017). Overall, northerly to southerly progradation direction of the Lower Cretaceous clastic material is coeval with the formation of structural highs and anticlines in the northcentral Barents Sea indicating a possible relationship between tectonics and depositional processes.

This study integrates previous work and existing subsurface data provided by the Norwegian Petroleum Directorate (NPD) and Marine Arctic Geological Expedition (MAGE), in order to: 1) document the

* Corresponding author.
E-mail addresses: bereke.kairanov@uis.no (B. Kairanov), alejandro.escalona@uis.no (A. Escalona), alenkij_89@inbox.ru (A. Mordasova), kksl@geus.dk (K. Śliwińska), suslovaanna@yandex.ru (A. Suslova).

https://doi.org/10.1016/j.jog.2018.02.009
Received 23 March 2017; Received in revised form 5 February 2018; Accepted 22 February 2018
Available online 05 March 2018
0264-3707/

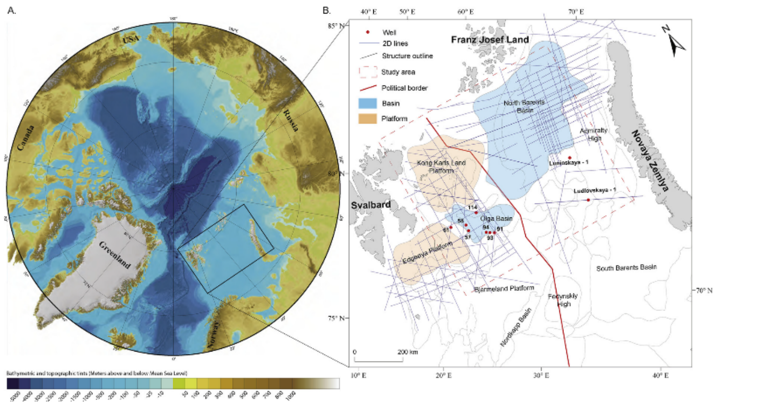

Fig. 1. A) Map of Arctic region showing location of the study area (modified from Jakobsson et al., 2012). B) Location of the well, outcrop and 2D seismic data used in this study.

tectonic development of the northcentral Barents Sea during the Early Cretaceous; 2) understand the mechanisms controlling the Early Cretaceous inversion; and 3) provide a revised paleogeography reconstruction documenting interaction between tectonic and sedimentation processes in the northcentral Barents Sea during Early Cretaceous.

2. Geological background

The study area is comprise by a number of platforms, basins and structural highs, which are spread between offshore Svalbard and the northern tip of the Novaya Zemlya (Fig. 1B). The geological history of the area is characterized by a series of compressional and extensional events (Grogan et al., 1999). Starting from the Paleozoic, the northcentral Barents Sea affected by a two major orogenic events: the Silurian—Devonian Caledonian orogeny and the Late Permian—Triassic Uralian orogeny (Anell et al., 2014; Ritzmann and Faleide, 2009). The Caledonian orogeny caused closing of the Iapetus Ocean, solidifying the basement of the western Barents Sea (Gernigon and Brönner, 2012). The Uralian orogeny was responsible for building and closure of the eastern Barents Sea (Gudlaugsson et al., 1998; Petrov et al., 2008).

Most of the Barents Sea experienced a crustal extension during the Carboniferous – Permian, resulting in a formation of several structural highs and basins (Dengo and Røssland, 1992; Grogan et al., 1999; Gudlaugsson et al., 1998). The sediments of this age generally comprise of shale, interlayered with evaporites in deltaic, shallow marine and carbonate ramp depositional environments (Braathen et al., 2011; Steel and Worsley, 1984). During the Latest Permian—Triassic, the formation of the Ural mountains in the East induced a major SE-NW progradation of the siliciclastic material into the Barents Sea (Glørstad-Clark et al., 2010).

The Late Jurassic–Early Cretaceous structural evolution of the Barents Sea is marked by four major tectonic events (Fig. 2):

1) Rifting in the SW Barents Sea (~157–130 Ma) that formed well defined basins, e.g. Bjørnøya, Tromsø and Hammerfest Basins (Fig. 2A) (Faleide et al., 1993).
2) Reactivation of Triassic structural lineaments as a dextral strike slip fault in the East, along Novaya Zemlya (~152–129 Ma), caused by clockwise rotation of the Siberian platform (Fig. 2A). This event was responsible for inversion and consequently uplift of several highs in the northcentral Barents Sea and South Kara Trough (e.g. Fedynskyi high) (Nikishin et al., 2014; Oxman, 2003; Sobornov et al., 2015).
3) The opening of the Amerasia Basin to the North (~145–126 Ma) resulted in a large scale crustal updoming in the northern Barents Sea (Fig. 2A) (Alvey et al., 2008; Grogan et al., 2000). Opening models of the Amerasia Basin are still a matter of debate. A large number of models have been proposed, and are summarized into three main categories by Døssing et al. (2013): a) the counterclockwise rotational model (Model A; Fig. 2B) (Cochran et al., 2006):, b) the Arctic-Islands strike-slip model (Model B; Fig. 2C) (Lawver and Scotese, 1990), and c) the Alpha–Mendeleev Ridge opening model (Model C; Fig. 2D) (Dove et al., 2010). These models proposed to explain the origin of the Amerasia Basin and are supported by inconclusive or indirect observations. For example, recent studies reveal evidences of a retro-arc extension and intra-continental rifting of the proto-Amerasia Basin (Alvey et al., 2008; Hadlari et al., 2016) supporting the formation of a transform margin along the northern margin of the Lomonosov Ridge (Evangelatos and Mosher, 2016; Gaina et al., 2014). This interpretation is consistent with model A (Fig. 2B) (Cochran et al., 2006). However, a continental origin of the Alpha and Mendeleev Ridges may does not support model A, and rather support the model C (Fig. 2D) (Dove et al., 2010; Kaminsky et al., 2005; Lebedeva-Ivanova et al., 2006).
4) The formation of the High Arctic Large Igneous Province (125–122 Ma) resulted in extrusive magmatism in the northern and northcentral parts of the Barents Sea with formation of WNW–ESE trending dykes in the Franz Josef Land and the North Barents Basin (Fig. 2A) (Corfu et al., 2013; Dibner, 1998; Evenchick et al., 2015; Polteau et al., 2016; Senger et al., 2014).

These Late Jurassic to Early Cretaceous tectonic events were responsible for different degrees of uplift and erosion in the northern Barents Sea, as documented on Svalbard and Franz Josef Land (Dibner, 1998; Embry, 1992; Gavrilov et al., 2010; Gjelberg and Steel, 1995; Grantz et al., 2011; Midtkandal and Nystuen, 2009; Repin et al., 2007).

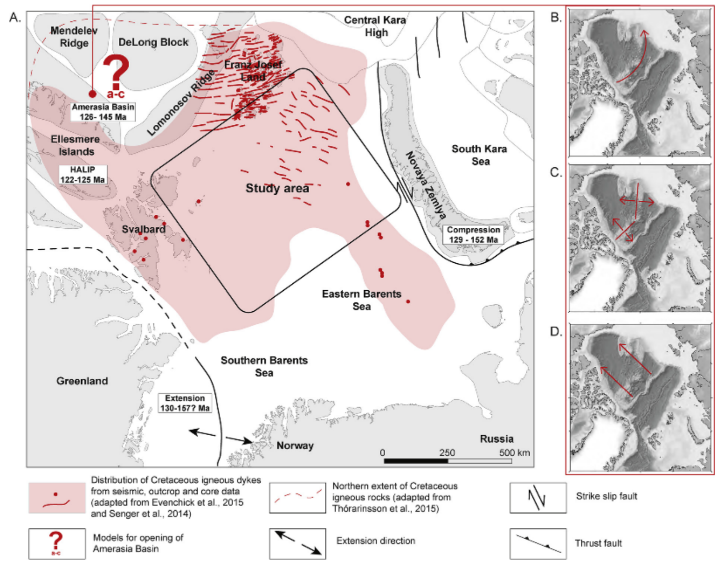

Fig. 2. A) Major tectonic events during Late Jurassic – Early Cretaceous overlain on the reconstruction map for Hauterivian (130 Ma) from plate tectonic model provided by "Plate" project at the Institute for Geophysics, the University of Texas at Austin. Models for the opening of the Amersia Basin as summarized by Døssing et al. (2013): B) Counterclockwise rotational model, C) Arctic-Islands strike-slip model, and D) Alpha–Mendeleev Ridge model.

The uplift of the northern Barents Sea has affected the Lower Cretaceous infilling history of the Greater Barents Sea, where overall NW–SE and NNE–SSW progradation of shallow marine to outer shelf deposits were predominant (Grundvåg et al., 2017; Kayukova and Suslova, 2015; Larssen et al., 2018; Marin et al., 2017).

During the Cenozoic, episodes of transpressional and transtensional deformation occurred between the NE Greenland and the western Barents Sea, and were responsible for formation of the Vestbakken Provinces and Svalbard fold and thrust belt (Bergh and Grogan, 2003; Faleide et al., 2008). These events were responsible for adjusting the structural configuration of the northcentral Barents Sea, by amplifying several structural highs and basins (Anell et al., 2014; Grogan et al., 1999). Later, an extensional episode occurred in the western and northern margins of the Barents Sea. The extension took place between Norway and Greenland (Faleide et al., 2008; Ziegler, 1988), and between the Lomonosov Ridge and the Barents-Kara Sea margin (Minakov et al., 2012). The Cenozoic development of the Barents Sea is also marked by an onset of glaciation and a tectonic uplift that caused exhumation of the northern and western Barents Sea (Dimakis et al., 1998; Knies and Gaina, 2008).

3. Data and methodology

3.1. Seismic and well data

The regional 2D seismic data from the Norwegian and Russian Barents Seas are provided by the Norwegian Petroleum Directorate (NPD) and the Marine Arctic Geological Expedition (MAGE). The 2D seismic data have a record of 6 s two way travel –time (TWT) with 10–30 Hz of dominant frequencies. The seismic data covers an area of ~250 000 km^2 with an average distance between seismic lines of about 100 km (Fig. 1B). The quality of the seismic data is good, except in the northern part of the study area, where shallow water depth, volcanic extrusions and intrusions make seismic imaging very poor to good. Most of the 2D seismic data is publically restricted and limited for publications.

The wells Luninskaya-1 and Ludlovskaya -1 located in the southeastern part of the study area were used to constrain seismic interpretation in the Russian Barents Sea (Fig. 1B). Both wells have a full set of logs, but only the well Luninskaya -1 has five core samples from the Berriasian – Albian interval (Fig. 3). Interpretation in the Norwegian Barents Sea is constrained by information from bed rock samples site 91, 93 and 94 obtained from the Olga Basin published by Antonsen et al. (1991) (Fig. 1B).

3.2. Methodology

In order to improve the age frame for the studied area, five sediment core samples (N1, N3, N4, N5 and N6; Fig. 3) were collected from the well Luninskaya-1 for dinoflagellate cyst (dinocysts) analysis (Evitt, 1985; Head, 1996). The palynological slide preparation followed modified standard methods of Nøhr-Hansen (2012), and dinocysts analysis were carried out at the Geological Survey of Denmark and Greenland (GEUS). The most characteristic dinocysts observed in the

B. Kairanov et al. Journal of Geodynamics 119 (2018) 183–198

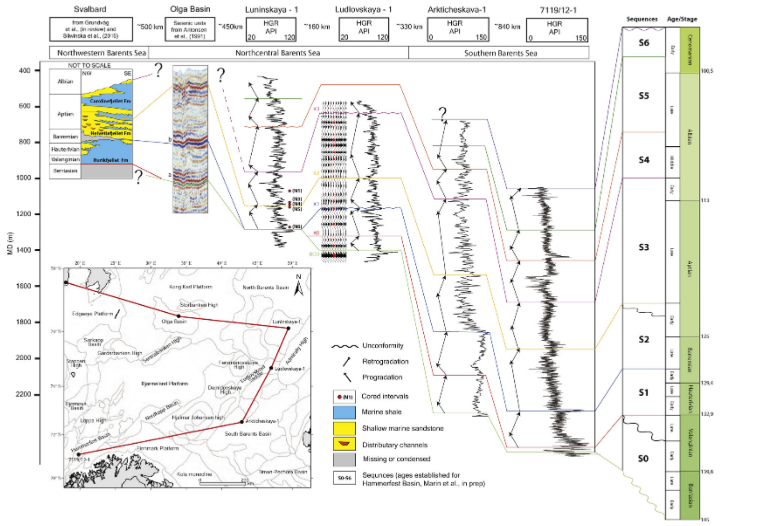

Fig. 3. Well – seismic stratigraphic framework correlation in the northern Barents Sea (adapted from Grundvåg et al., 2017; Marin et al., 2017; and Antonsen et al., 1991). Note that sequence boundaries were correlated to seismic reflectors in the Olga Basin. Positions of samples studied for palynology from the Luninskaya-1 well are marked with red dots. (For interpretation of the references to colour in this figure legend, the reader is referred to the web version of this article.)

well are shown on Fig. 4.

The seismostratigraphic framework used in this work is based on the definition of seven genetic sequences for wells 7119/12-1 and Arkticheskaya-1 (Kayukova and Suslova, 2015; Marin et al., 2017) in the southern Barents Sea (Fig. 3). These are genetic sequences (*S0–S6*) with time span of 1–10 Ma and bounded by flooding surfaces (*K1–K6*) defined from stacking patterns on the gamma ray (GR) well logs and reflector terminations on the seismic data (Galloway, 1989). These sequences were recognized and correlated between the wells Ludlovskaya -1, the well Luninskaya -1 and seismic reflectors of the Olga Basin. The Svalbard lithostratigraphy and its offshore correlation is obtained from Grundvåg et al. (2017), whereas the Olga Basin seismic stratigraphy was adapted from Antonsen et al. (1991) (Fig. 3).

In order to reproduce the paleogeography, internal variations of seismic reflectors of each sequence were characterized and subdivided into seven seismic facies, which were interpreted based on reflectivity configuration and geometry of individual seismic packages. Seismic interpretation was integrated and calibrated with information obtained from the wells Ludlovskaya-1 and Luninskaya-1, shallow cores, the outcrop data from Svalbard, Kong Karls Land and Franz Josef Land. Table 1 shows a summary with the description of these seismic facies and their interpretation. Faults were interpreted and grouped into fault families based on the same structural orientation and relative age. Structural trends and lineaments were guided by a magnetic anomaly map of Marello et al. (2010), where distance between seismic line exceeded 100 km. Regional fault interpretation outside of the study area were compiled from previous publications of Faleide et al. (2008); Grogan et al. (1999); Nikishin et al. (2014); Nikishin (2013); Sobornov et al. (2015); Velichko (2012). Time thickness maps were created and boundaries were described as erosional contact or lap relation. A time-depth conversion was performed using Move Core Application software in order to better determine throw and angle of the faults as well as shortening amount. Interval velocities were obtained from available check shot data of the wells Ludlovskaya-1 and Luninskaya-1. Tectonic reconstruction maps for the Hauterivian were created on PaleoGIS to compare and discuss with the main tectonic events that occurred during the Early Cretaceous. The plate tectonic restoration model was provided by the “Plates” project at the Institute for Geophysics, the University of Texas at Austin, as a part of the “Lower Cretaceous in the Arctic” (LoCrA) consortium.

The paleogeography outside of the study area was compiled from the LoCrA consortium reports, presentations and publications (Grundvåg and Olaussen, 2017; Grundvåg et al., 2017; Kayukova and Suslova, 2015; Marin et al., 2017).

4. Results

4.1. Well, outcrop, seismic and stratigraphic correlation

Fig. 3 shows the well and seismic correlation of stratigraphic sequences from the southern to the northcentral and northwestern Barents Sea.

Sequence 0 (Berriasian – Valanginian) was not observed on Svalbard and well Luninskaya-1, and was indistinguishable in the Olga Basin. Although sequence 0 was observed in the wells Ludlovskaya – 1, Arkticheskaya – 1 and 7119/12-1, it was included as a part of sequence 1 in this study for simplification.

Only sequences 1 and 2 can be correlated and preserved across the

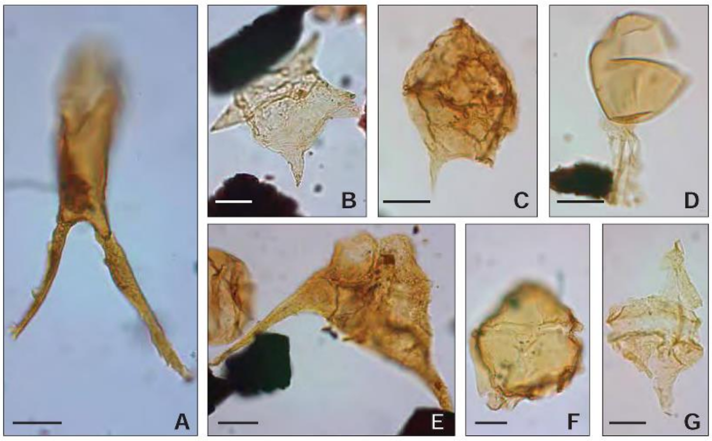

Fig. 4. The most important dinocysts observed in the well Luninskaya-1. Scale bar on all photographs = 20 µm. A) *Batioladinium longicornutum* sample N6, Slide No. 26250-5. B) *Nyktericysta? vitrea* sample N6, Slide No. 26250-5. C) *Palaeoperidinium cretaceum* sample N1, Slide No. 26246-5. D) *Desmocysta plekta* sample N1, Slide No. 26246-5. E) *Pseudoceratium toveae* sample N6, Slide No. 26250-5. F) *Sirmiodinium grossii* sample N4, Slide No. 26248-5. G) (reworked) *Rhaetogonyaulax rhaetica* sample N4, Slide No. 26248-5.

northcentral Barents Sea, which will the focus of this study. T

Furthermore, sequences 3–6 are missing in the Olga Basin and Kong Karls Land Platform, as the result of uplift and glacial erosion. Therefore, these sequences were described briefly and summarized as a single interval where preserved.

In the Olga Basin, it is suggested that the Base Cretaceous Unconformity (BCU) correlates to the seismic reflector “a” sensu Antonsen et al. (1991). The BCU is represented by a well-defined acoustic impedance contrast in seismic data (Figs. 3 and 5).

Horizon K1is interpreted as an “intra Barremian reflector” in the seismic and correlates to the seismic reflector “b” of Antonsen et al. (1991) (Figs. 3 and 5). This reflector constitutes a boundary between sequence 1 and 2, and is represented by dimmed and low amplitude reflectors (Fig. 5).

The K2 is interpreted as the “Early Aptian unconformity” in the seismic data that defines the upper limit of sequence 2 (Fig. 5). This horizon is mapped only in the North Barents Basin, whereas it represents the present day seafloor on the Kong Karls Land Platform and the Olga Basin (Fig. 5B). Sequences 3–6 are combined as a single sequence from the “Early Aptian unconformity” to the seafloor in the North Barents Basin (Fig. 5).

4.2. Seismic sequences

4.2.1. Sequence 1 (S1): Hauterivian – Early Barremian

4.2.1.1. Description. S1 is delimited at its base by the BCU and at the top by the intra-Barremian horizon (Figs. 3 and 5). The sequence is penetrated by the well Ludlovskaya – 1 and vibrocore sample sites 57, 61, 93 and 94 (Antonsen et al., 1991). Palynological analysis of the sample 93 and 94 in the Olga Basin by Antonsen et al. (1991) confined S1 to Hauterivian – Barremian. It is mostly correlative to Rurikfjellet Formation and partially may represent lower part of Helvetiafjellet Formation in Svalbard (Antonsen et al., 1991; Grundvåg et al., 2017) (Fig. 3). In our study area, the GR pattern for S1 is spiky with relatively high values (Fig. 3). S1 was deposited in the entire northcentral Barents Sea, except at the margins towards Svalbard, Franz Josef Land and Novaya Zemlya, where it is either missing or eroded. There are several segmented depocenters reaching thicknesses of 800 ms in the North Barents Basin, along the Persey and Pinegin highs (Fig. 6A). The main three seismic facies types are recognized within S1 (Fig. 6B):

1) Facies A: trough fill with low amplitude discontinuous reflectors bounded by high amplitude parallel reflectors that onlap and pinch out towards the highs flanks (Fig. 7A’). This type of facies was observed on the Kong Karls Land Platform and at the northwestern margin of the North Barents Basin (Fig. 6B). The thickness of these facies commonly increases in the troughs and facies are becoming slightly chaotic towards the top, where they are eroded (Fig. 7B’);
2) Facies B: shingled clinoforms with high amplitude, high frequency, sigmoidal and oblique shape reflectors that downlap the BCU were observed in the western part of the Olga Basin and the trajectory is ascending (Fig. 8B and B’). The clinoforms prograde from NW-SE and SW-NE towards the Olga Basin (Fig. 6B). The clinoforms are of a high-relief (> 100 m), shingled, with a gentle rollover and foreset angle with an average value of 1°. The topsets and bottomset development was not recognized in the seismic lines (Fig. 8B’);
3) Facies C: progradational fill consisting of low amplitude continuous reflectors with a sigmoid pattern are observed along the northwestern margin of the North Barents Basin (Fig. 9A’ and B’). They are typically wedge-like structures that pinch out against the highs and downlapping the BCU. Some internal reflectors are semi-transparent, eroded at the top and becoming chaotic in the thickest part (Fig. 9).

4.2.1.2. Interpretation. Overall, S1 is characterized as a syn-tectonic deposits with growth strata and wedges as common facies for this sequence. Bed rock samples from sites 57, 61, 93 and 94 described by Antonsen et al. (1991) on the Kong Karls Land Platform and the Olga

Table 1
Description and interpretation of the observed seismic facies in the northcentral Barents Sea.

	Facies	Seismic characterization	Interpretation/Environment	Example
Sequence 1	A	Low amplitude, discontinuos reflectors bounded by high amplitude parallel reflectors. Subparallel reflectors wedging to the flanks. Trough, divergent fill. Observed on the Kong Karls Land Platform and at the northwestern margin of the North Barents Basin	early basin fill deposit/ shallow shelf	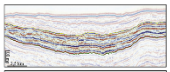
	B	High amplitude, high frequency, continuos to discontinuos reflectors. Low angle (1–2°) prograding clinoforms. Observed in the western part of the Olga Basin	prograding shelf system/ shelf/shallow shelf	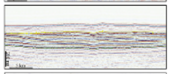
	C	Low amplitude, high frequency, continuos reflectors. Pragrading reflectors with sigmoid pattern. Observed along the northwestern margin of the North Barents Basin	prograding fill/deep marine	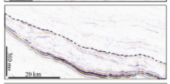
Sequence 1	D	High to low amplitude, high frequency, parallel continuos reflectors. Observed in the Olga Basin and the southern part of Kong Karls Land Platform	shallow shelf/continental depostis	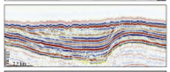
	E	High amplitude, low frequency, chaotic to discontinous reflectors. Observed locally in the central part of the Kong Karls Land Platform	shallow shelf/continental deposits	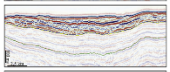
	F	Low amplitude, high frequency, chaotic to subparallel reflectors. Observed in the northwestern margin of the North Barents Basin	continental deposits	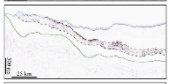
	G	High amplitude, high frequency, continuos to discontinuos reflectors. Prograding low angle divergent facies. Observed in the entire eastern and central part of the North Barents Basin	distal part of prograding slope/wedge	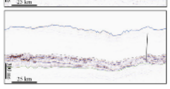

Basin (Fig. 6B) suggest that Facies A and B were deposited in shallow shelf conditions and clinoform interpretation supports paleowater depths of ca. 100–200 m. In contrast, Facies C is interpreted as a prograding slope/wedge that was most likely deposited in a deep marine setting. The observed onlap of Facies A and C on the limbs of the highs and anticlines suggest that the paleotoporaphy was inherited from earlier tectonic stages, most likely from Late Jurassic (Figs. 7A' and 9B'), and growth of these facies suggest a renewed tectonic activity. Downlap directions of Facies B and C indicates that Svalbard, Franz Josef Land, and Pinegin and Persey highs were the main sediment sources for these facies (Fig. 6B).

4.2.2. Sequence 2 (S2): Early Barremian – Early Aptian

4.2.2.1. Description. Similarly to S1, S2 was deposited in the entire northcentral Barents Sea, except towards Svalbard, Franz Josef Land and Novaya Zemlya, where it is eroded. S2 is bounded at its base by the intra-Barremian horizon and at the top by the Early Aptian unconformity (K2) (Figs. 3 and 5). In the Kong Karls Land Platform and Olga Basin, the top of S2 was removed by Cenozoic uplift and a glacial erosion and it truncates the present day seafloor (Figs. 7 and 8). S2 is penetrated by the wells Ludlovskaya − 1 and the Luninskaya − 1, and vibrocore sample sites 58 and 114 (Antonsen et al., 1991) (Fig. 3). The lowermost core sample (N6) in the well Luninskaya – 1 yields *Batioladinium longicornutum, Nyktericysta? vitrea* and *Pseudoceratium tovae* and therefore can be dated to Late Barremian and referred to Subzone I(3) of Nøhr-Hansen (1993) (Fig. 3). It is correlative to the Helvetiafjellet Formation in Svalbard (Grundvåg et al., 2017) (Fig. 3). Sample N5 is barren of dinocysts. The GR pattern for S2 is erratic to spiky with equally coarsening and fining uptrends (Fig. 3). The thickness of S2 is relatively uniform in areas where the top of S2 is preserved (Fig. 10A). There are several scattered depocenters reaching maximum thickness of 450 ms, located in the Olga and the North Barents basins (Fig. 10A). The four main seismic facies recognized in S2 are (Fig. 10B):

1) Facies D: parallel continuous reflectors with high to low amplitude and high frequency observed in the Olga Basin and the southern part of Kong Karls Land Platform (Figs. 7B' and 8A'). They have good parallel continuity that uniformly overly seismic Facies B of S1. This facies is sub-parallel towards its bottom and the top is truncated by the seafloor;
2) Facies E: discontinuous to chaotic with high amplitude, low frequency, reflectors observed locally in the central part of the Kong Karls Land Platform (Fig. 7A'). Usually chaotic reflectors are observed at the base of the S2 and become more continuous towards the top;
3) Facies F: subparallel to chaotic with low amplitude, high frequency reflectors (Fig. 9A') were observed in the northwestern margin of the North Barents Basin (Fig. 10B);
4) Facies G: divergent/stratified reflectors with high amplitude, high frequency, inclined, continuous to discontinuous reflectors (Fig. 9A' and B') covering the entire eastern and central part of the North Barents Basin (Fig. 10B). This facies downlap on top of the Facies C and BCU in the central and eastern part of the North Barents Basin (Figs. 5A, 9A' and B'). The upper boundary of this facies is unclear and seismic reflectors are dimmed towards the top (Fig. 9A).

4.2.2.2. Interpretation. Generally, S2 is deposited in a tectonically

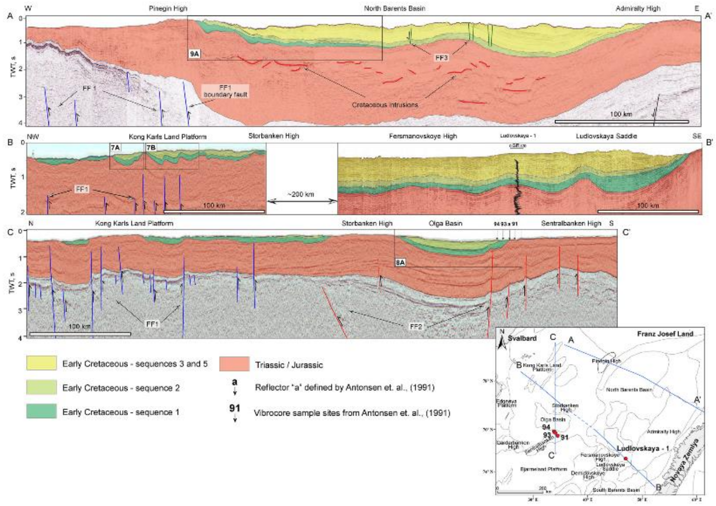

Fig. 5. Regional lines across the study area illustrating interpreted Lower Cretaceous sequences and main fault families. Detailed interpretation of several section highlighted with black boxes on the regional lines. (A) E-W profile through the North Barents Basin; (B) NW-SE profile with tie to the Ludlovskaya − 1 well; and (C) N-S profile crossing the Olga Basin and the Kong Karls Land Platform. Interpretation is calibrated with vibrocore information obtained from Antonsen et al. (1991).

quiescent period, as the absence of growth strata and frequent parallel facies are common for this sequence (Facies D, E and F). Bed rock samples from sites 58 and 114 described by Antonsen et al. (1991) from the Olga Basin suggest that Facies D was deposited in a shallow shelf environment, whereas fluvial systems have been described on Kong Karls Land (Grogan et al., 2000; Larssen et al., 2018). Coeval continental deposits interpreted on the Franz Josef Land (Repin et al., 2007) suggests that Facies E and F were most likely deposited in coastal to continental conditions (Fig. 10B). Observed glauconite/pyrite/siderite and relatively low values of the GR of the well Luninskaya -1 suggest that Facies G were deposited in coastal to marine settings (Fig. 3).

4.2.3. *Sequences 3–6? (S3–S6): Early Aptian – Cenomanian?*

4.2.3.1. Description. S3–S6 is bounded at its base by the Early Aptian Unconformity and at the top by the present day seafloor (Fig. 9). These

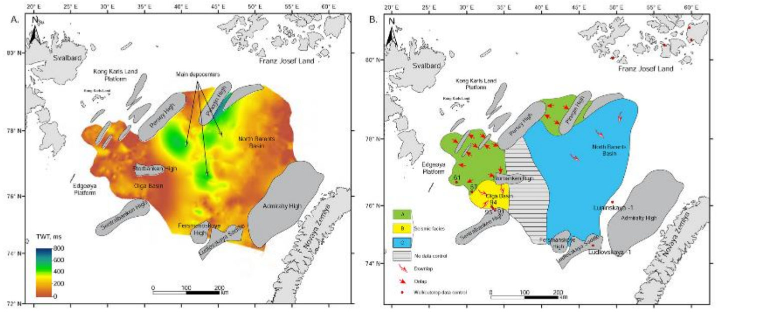

Fig. 6. (A) Time thickness map of sequence 1. (B) Map of distribution of seismic facies A and C in sequence 1. Note the scattered location of the main depocenters associated with inversion of the structural highs.

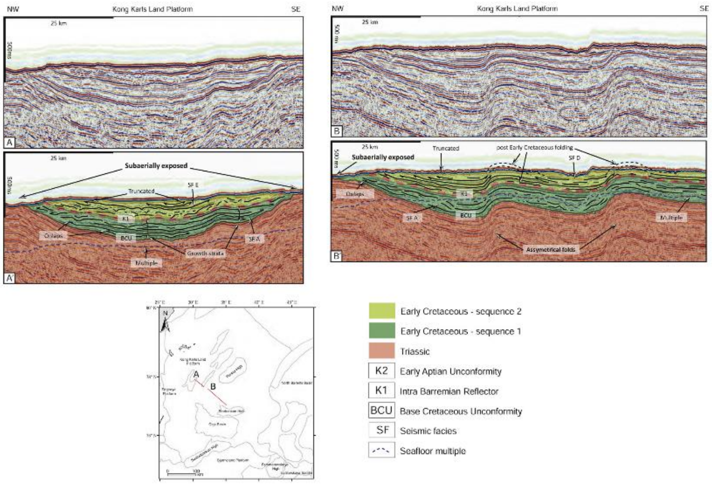

Fig. 7. (A–B) Uninterpreted and (A'–B') interpreted seismic section across the Kong Karls Land Platform. Note (A') increase of thickness of the sequence 1 between highs. (B') Asymmetrical folds resulted from the inversion of the FF 1. Folding of S1 and S2 is interpreted as the result of post Early Cretaceous inversion.

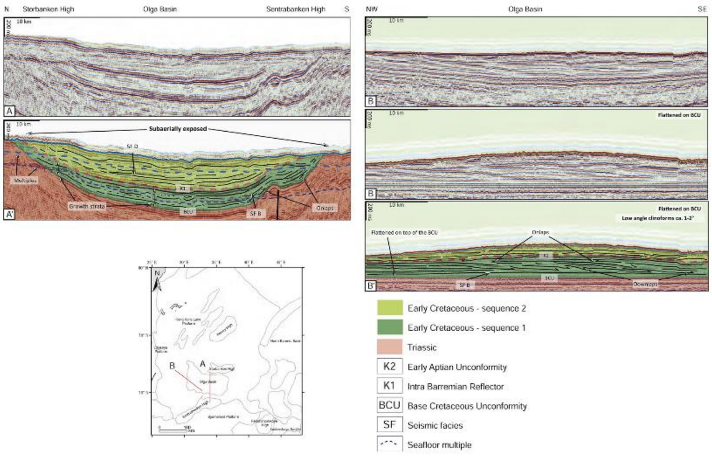

Fig. 8. (A–B) Uninterpreted and (A'–B') interpreted seismic section in the Olga Basin. Note increase of thickness of the sequence 1 in the Olga Basin and NW – SE direction of the clinoforms progradation.

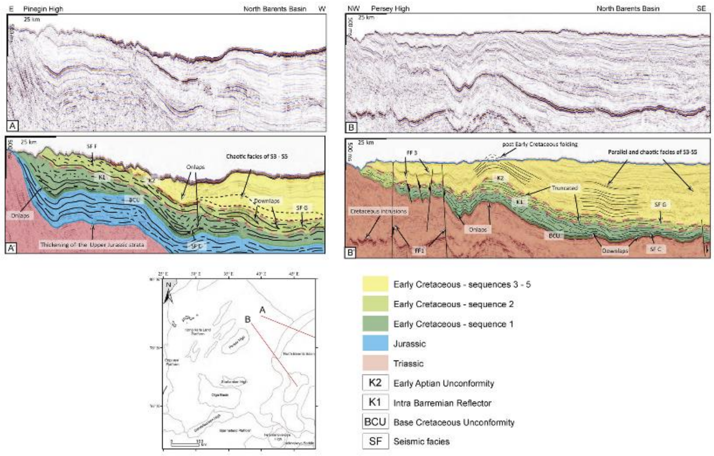

Fig. 9. (A–B) Uninterpreted and (A'–B') interpreted seismic section along the Pinegin High and the Persey High. Note the downlap relation indicating progradation direction from these highs. Similarly to Fig. 7B'; folding of S1–S5 most likely associated with post Early Cretaceous inversion.

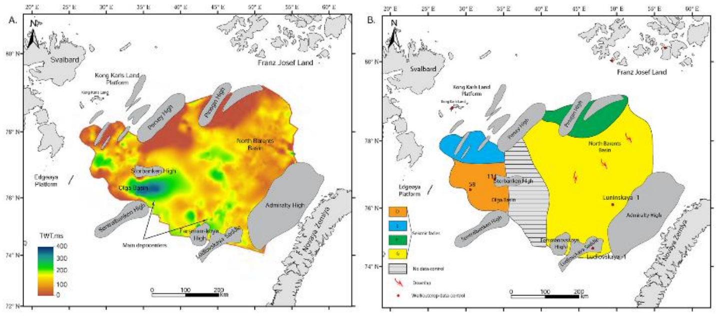

Fig. 10. (A) Time thickness map of sequence 2. (B) Map of distribution of a seismic facies in sequence 2. Note shifting of depocenters S-SW towards the Olga Basin and South Barents Basin.

sequences are only observed in the North Barents Basin and penetrated by the wells Ludlovskaya – 1 and the Luninskaya – 1 (Figs. 3 and 5). Sample N4 from well Luninskaya – 1 yields rare dinocysts and is tentatively dated to Early Aptian (Zone II of Nøhr-Hansen (1993)) based on the presence of *Sirmiodinium grosii* and the absence of Barremian taxa. The sample yields *Rhaetogonyaulax rhaetica* what suggests reworking from Triassic. Samples N1 and N3 yields abundant and well preserved dinocysts, limited however to the dinocysts with long stratigraphic ranges. The assemblage is dominated by *Desmocysta plekta* and *Palaeoperidinium cretaceum* and is characterized by a low diversity. This may suggests coastal, restricted marine settings. The tentative age for the two samples is most likely Aptian or younger. The GR for these sequences is spiky with relatively high values and mainly fining uptrends (Fig. 3). The seismic character of these sequences in the North Barents Basin is represented by high amplitudes, parallel, continuous reflectors with some chaotic or lens-shaped reflections in the central parts of the basin (Fig. 9A' and B').

4.2.3.2. Interpretation. Overall, S3–S6 is deposited in a tectonic quiescent period, as suggested by the absence of growth strata and abundancy of parallel seismic reflectors. The coal fragments observed in the lower part of S3 in the well Luninskaya-1 suggest that this sequence was deposited in a coastal to continental environment. The overall fining upward trend of f S4 and S5, based on the GR log for the well

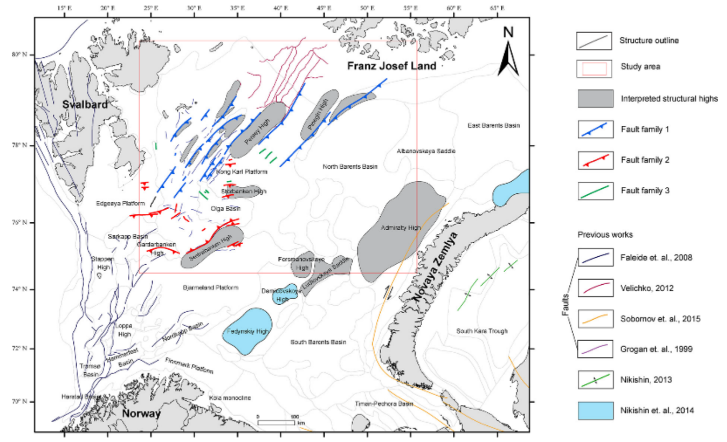

Fig. 11. Map of interpreted fault families and structural elements integrated with previous works (highlighted in the legend) in the study area.

Luninskaya – 1 suggest that these sequences were deposited in a relatively deeper environment, most likely a shallow shelf to coastal.

4.3. *Fault families*

Three main fault families related to the Lower Cretaceous sequences are observed in the study area (Figs. 5 and 11). Fault families 1 and 2 are interpreted as thick-skinned deformation involving reverse faults that tip in the Triassic interval, however due to continuous reactivation some faults propagate to the seafloor (Figs. 5 and 9B). Fault family 3 is interpreted as thin-skinned deformation offsetting strata above the Triassic interval (Figs. 5A and 9B').

Fault family 1 (FF1): a set of NE–SW striking faults, is interpreted from the SW edge of the Kong Karls Land Platform to the Franz Josef Land (Figs. 5C and 11) (Marello et al., 2010). Moreover, faults from the Franz Josef Land (Dibner, 1998) have identical strike as FF1 and most likely represent its onshore continuation. A member of FF1 serves as a main boundary fault that separates the Kong Karls Land Platform from the North Barents Basin (Fig. 5A). FF1 comprises mainly steep (~65–77°) reverse faults that predominantly dip towards the SE (Fig. 12B'). Throw along these faults is typically low, ranging from 0 to 55 m at the base of the Triassic interval (Fig. 12B'). The age of FF1 is interpreted as Late Paleozoic (Faleide et al., 2008; Grogan et al., 2000; Grogan et al., 1999). Based on onlap relationship and the thickening strata, reactivation is evident during Late Jurassic and Early Cretaceous S1 (Figs. 7B' and 9A'). Furthermore, observed folding of the S1 in the seismic section (Figs. 7B' and 9B') indicates younger reactivation, most likely post-Early Cretaceous. Reactivation of FF1 resulted in formation of NE–SW oriented blind folds (anticlines) and structural highs like the Persey and Pinegin (Figs. 7 and 9). Blind folds are interpreted on the Kong Karls Land Platform and are generally asymmetric with steep limbs facing towards the NW and interlimb angles of 160°–170° (Fig. 12B'). Calculated shortening amount for these folds is equivalent to 22 m (~0,1%) and therefore, negligible.

Fault family 2 (FF2): consists of E-W striking faults interpreted along the Olga Basin and on the Edgeøya Platform (Fig. 11) (Marello et al., 2010). These high angle (~52–77°) reverse faults either dip to the S or N and reach a throw of up to 50 m at the base of the Triassic (Fig. 5C). The age is interpreted as Late Paleozoic (Grogan et al., 1999) and similarly to FF1, growth strata and onlap relationship suggest reactivation during Late Jurassic and Lower Cretaceous S1 (Antonsen et al., 1991) (Fig. 8A'). Reactivation of FF2 resulted in the formation of the E-W oriented Olga Basin and structural highs like the Storbanken and Sentralbanken (Fig. 5C). Shortening amount of these folds is also insignificant as they were included in the calculation with folds from the Kong Karls Land Platform.

Fault family 3 (FF3): is generally represented by high angle (~60–77°) normal faults that were interpreted along the Storbanken (Fig. 5A) and Persey highs (Fig. 9B') on the Kong Karls Land Platform. Due to the large distance between seismic lines, the strike direction of these faults cannot be clearly mapped, but most likely it resembles FF1 (NE-SW) and FF2 (E–W). These faults form horst- and graben-like structures with a maximum throw of 80 m (Fig. 9B'). The absence of growth strata suggests the age of these faults as post-Early Cretaceous.

5. Discussion

5.1. *Periods of fault reactivation*

5.1.1. *Post Early Kimmeridgian – pre Valanginian*

This period corresponds to an initial reactivation of the Late Paleozoic FF1 and FF2 as reverse faults. Interpretation is based on observed pinch out of the Upper Jurassic strata towards the Pinegin high (Fig. 9A'). In the rest of the study area, thickness variations of the Upper Jurassic strata were not observed. However onlap of the Lower Cretaceous Facies A and C indicates an established paleotopography prior to its deposition (Figs. 7A' and 9A'). The age is inferred by previous studies in the Olga Basin that documents reactivation/inversion along the flanks during Oxfordian – Hauterivian (Antonsen et al., 1991). However, studies on the Kong Karls Land by Larssen et al. (2018) suggested a post – Early Kimmeridgian – pre Valanginian, because of the observed carbonates of the Klippfisk Formation (Smelror

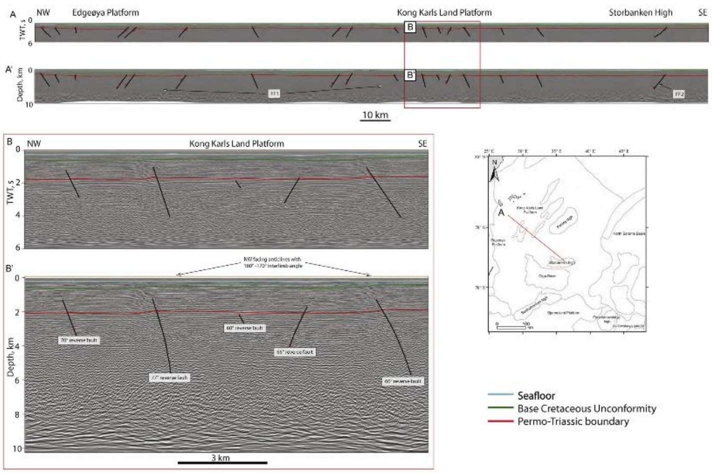

Fig. 12. Regional (A) time and (A') depth section through Kong Karls Land Platform; (B) and (B') enlarged part of the regional section illustrating angles of reverse faults and gentle anticlines.

et al., 1998) which might indicate a tectonically quiescent period during Valanginian.

5.1.2. (Berriasian) Hauterivian – Early Barremian

Further reactivation of FF1 and FF2 is recorded in the Lower Cretaceous during Hauterivian to Early Barremian, and corresponds to S1. Interpretation is based on observed growth strata and wedging of the S1 (Figs. 7–9). Interpretation is consistent with onshore studies on the Kong Karls Land (Larssen et al., 2018) that defines the same period of reactivation. However, along Novaya Zemlya, reactivation was most likely initiated earlier and correspond to the Berriasian – Early Barremian period. This is supported by the absence of pre-Barremian sediments in the well Luninskaya – 1 (Fig. 3) and by the interpretation of the Berriasian – Early Barremian clinoform complexes that infilled South Barents Basin (Kayukova and Suslova, 2015).

5.1.3. Post Early Cretaceous

Reactivation of FF1 and FF2 that led to further inversion was also recognized in the study area (Figs. 7 and 9B'). The age of inversion is uncertain. However, folding of the Lower Cretaceous sequences 1–6 in the Russian Barents Sea suggest that reactivation/inversion took place at least post Cenomanian time (Figs. 7 and 9B'). This inversion was responsible for rejuvenation and enhancing of previously inverted faults and most likely resulted in the present day basins configuration.

5.2. Mechanisms controlling the Late Jurassic – Early Cretaceous inversion

High angle reverse faults (~52–77°) of FF1 and FF2 in the north-central Barents Sea were developed through the reactivation of Late Paleozoic normal faults (Fig. 12). Crustal shortening of 22 m (~0,1%) on the Kong Karls Land Platform is insignificant and suggest that the reactivation was most likely caused by a regional tectonic process outside of the study area. During the Late Jurassic – Early Cretaceous, three suggested major regional tectonic events that might have influenced the study area:

1 Dextral transpression along Novaya Zemlya

Previous work by Nikishin et al. (2014), Malyshev et al. (2013) and Nikishin (2013) documents an inversion of structural highs like the Admiralty, Fersmanovskoye, Ludlovskoye, Demidovskoye and Fedynskyi (Fig. 11). The inversion of these structural highs was suggested to be controlled by pulses of Late Jurassic – Early Cretaceous dextral transpression along Novaya Zemlya (Sobornov et al., 2015) (Fig. 13A). Dextral transpression was related to the rotation of the Siberian Platform due to the collision with the Omolon microcontinent in the Verkhoyansk – Chukotka region that took place in the Tithonian – Barremian (Oxman, 2003). The thinning of S1 towards the Admiralty high and the Ludlovskoye Saddle supports the inversion of these highs at least during Early Cretaceous (S1; Fig. 5A and B).

It also can be speculated whether dextral transpression along Novaya Zemlya could have caused an inversion on the Kong Karls Land Platform and the Olga Basin (Fig. 13A). Numerical models by Buiter and Torsvik (2007) on the orthogonal westward displacement of Novaya Zemlya suggested that the propagation of the deformation is up to 550 km westward during the Late Triassic – Early Jurassic. In comparison to the Late Triassic- Early Jurassic orthogonal compressional event, the dextral transpression during Late Jurassic – Early Cretaceous is considered as a tectonically minor event (Sobornov et al., 2015), hence it is expected that the propagation of deformation is less than 550 km. The northern margin of the Tibetan Plateau is proposed as a possible analogue for comparison (Fig. 14A).

Transpression along Novaya Zemlya was compared to the transpression along the Altyn-Tagh and the Qilian-Haiyuan strike-slip faults that served as boundary faults of the northern Tibetan Plateau (Zheng et al., 2013) (Fig. 14B). Transpression along these faults was caused by India's north directed collision against Asia. Fig. 14B displays the map of the northern margin of the Tibetan Plateau, where the stress/

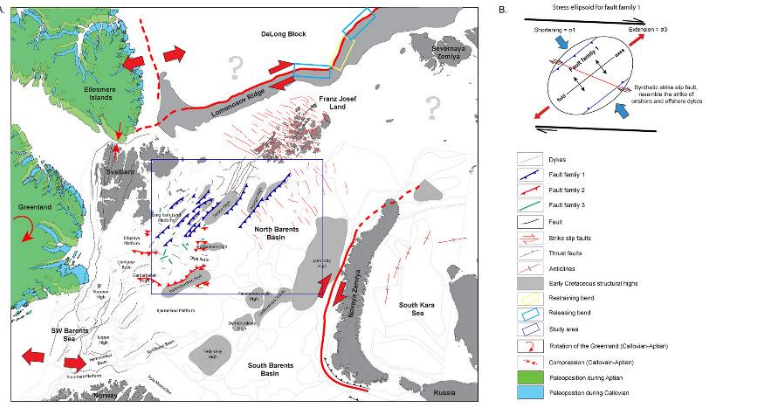

Fig. 13. (A) Plate reconstruction map from "Plates" project for Hauterivian (130 Ma) overlain with interpreted structural elements and integrated with previous studies in the north-central Barents Sea. Thick red lines show main tectonic events during the Callovian – Early Barremian that controlled the tectonic development of the northcentral Barents Sea. Note paleoposition of Greenland and the Ellesmere Islands during Callovian (blue) and Aptian (green). (B) Applied stress ellipsoid for FF1. Riedel shear fault resemble the strike of the onshore and offshore dykes on the Franz Josef Land and North Barents Basin. (For interpretation of the references to colour in this figure legend, the reader is referred to the web version of this article.)

deformation related to the Altyn-Tagh and the Qilian-Haiyuan strike-slip faults propagating to a maximum 400 km to the north of these faults. On Fig. 14C, the Novaya Zemlya was overlain on rotated Fig. 14B to illustrate potential similarities of the structural settings of two margins.

Therefore, considering a distance exceeding ~600 km (between Novaya Zemlya and Kong Karls Land Platform/Olga Bain; Fig. 14B), it is unlikely that the reactivation along Novaya Zemlya controlled the inversion of the NE–SW and E–W oriented structures on the Kong Karls Land Platform and the Olga Basin.

2 Opening of the Amerasia Basin

The stress ellipsoid applied for the faults from FF1 on the Kong Karls Land Platform suggests that the dextral strike-slip motion might have controlled the inversion (Fig. 13B). Previous work by Dibner (1998), Polteau et al. (2016) and Grachev et al. (2001) mapped a significant amount of WNW and NW trending dykes on Franz Josef Land and the North Barents Basin (Figs. 2 and 13A). Dykes are commonly perpendicular to the extension direction or to the minimum horizontal stress σ^3 (Anderson, 1951; Hubbert and Willis, 1972). The orientation of these dykes resemble the direction of the Riedel shear on the stress ellipsoid (Fig. 13B). These dykes were emplaced in this direction mostly due to the structural weaknesses developed during the dextral motion along the northern margin of the Lomonosov Ridge (Fig. 13A). Moreover, Evangelatos and Mosher (2016) characterized the northern margin of

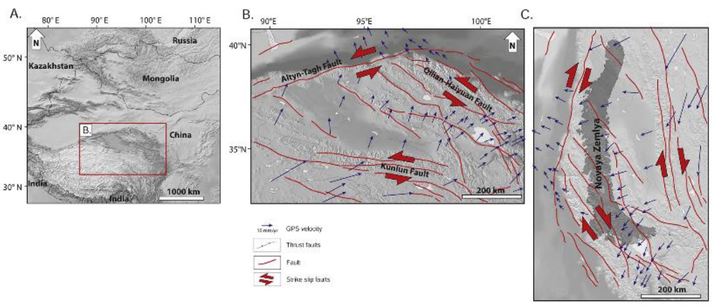

Fig. 14. (A–B) The northern margin of the Tibetan Plateau is used as an analog for dextral strike-slip fault deformation along Novaya Zemlya (adapted from Zheng et al., 2013). (C) The mirrored and rotated image in the context of the northcentral Barents Sea overlaid with contours of Novaya Zemlya (similar scales).

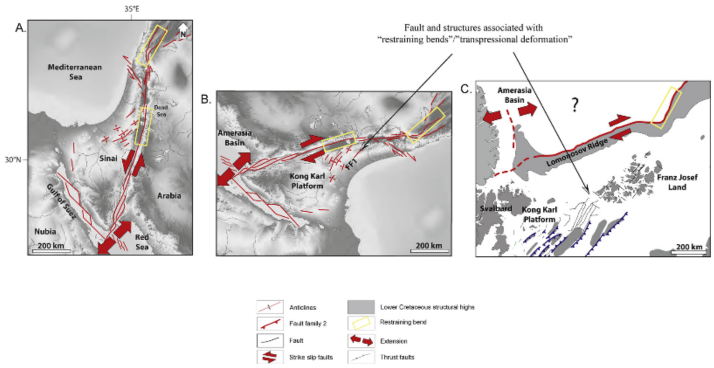

Fig. 15. (A) Proposed Dead Sea transform fault analog for dextral strike slip fault along the Lomonosov Ridge (adapted from; Garfunkel, 1981). (B) The mirrored and rotated image, in the context of (C) northcentral Barents Sea. Note similarities of active anticlines along restraining bends.

the Lomonosov Ridge as a transform margin, suggesting formation of releasing and restraining bends resultant from the "rotational" opening of the Amerasia Basin (Grantz et al., 1998; Lawver et al., 2002; Shephard et al., 2013) (Fig. 13A). Restraining bends along strike-slip faults are usually referred as areas that can accommodate a local contraction due to the transpressional deformation (Christie-Blick and Biddle, 1985; Crowell, 1974). A plate tectonic restoration for the Hauterivian (132.9 Ma), positions the Lomonosov Ridge connected to the northern margin of the Barents – Kara Seas (Minakov et al., 2012) (Fig. 13A). As a result, the paleoposition of the restraining bend along the northern margin of the Lomonosov Ridge occurs to the north of Franz Josef Land during Late Jurassic – Early Cretaceous and shows orientation similar to the strike of FF1 (Fig. 13A). Given that the restraining bend is formed due to a contraction, it is suggested that the reactivation/inversion of FF1 is the result of the transpressional deformation formed along the northern margin of the Lomonosov Ridge. Consequently, the opening of the Amerasia Basin is considered as a main tectonic event that controlled the inversion in the Kong Karls Land Platform (Fig. 13A). An analogue to the strike-slip fault along the Lomonosov Ridge is the Dead Sea transform fault (DSTF, Fig. 15A). The DSTF is a major ~1000 km long sinistral strike-slip fault that separates the Arabia plate and the Sinai subplate (Weber et al., 2009) (Fig. 15A). A restraining bend around the Dead Sea area is associated with a transpressional deformation along the northern part of the DSTF (Gomez et al., 2007) (Fig. 15A). This transpression resulted in the reactivation and consequent formation of several anticlines that are oblique to the main DSTF (Fig. 15B and C). Similarly, a transpressional deformation produced by dextral strike-slip along the northern margin of the Lomonosov Ridge could have caused reactivation, and consequently the inversion of the structural highs and anticlines in the Kong Karls Land Platform and the Olga Basin (Fig. 15B and C).

3 Compression between North Greenland and Ellesmere Islands with NW Barents Sea (NW Svalbard)

The inversion on the Kong Karls Land Platform and the Olga Basin is coeval with the Late Jurassic – Early Cretaceous uplift of Svalbard. The increase in thickness of the Upper Jurassic strata (Steel and Worsley, 1984) overlain by the Early Barremian regional extensive erosional unconformity (Grøsfjeld, 1992; Mørk and Smelror, 2001) might be an important evidence of the tectonic uplift of Svalbard during Late Jurassic – Early Cretaceous. In fact, the Early Barremian unconformity on Svalbard can be considered an equivalent to the interpreted intra Barremian reflector (K1) in the offshore northcentral Barents Sea (Fig. 3). The uplift of Svalbard was suggested to be related to the opening of the Amerasia Basin and a subsequent doming/uplift of the Alpha Ridge (Golonka et al., 2003; Lawver et al., 2002). However, using plate tectonic reconstructions, a substantial amount of crustal shortening (ca. 40 km) is observed between NW Svalbard and NE Greenland/Ellesmere Islands during the Callovian – Aptian (Fig. 13A). In this plate tectonic model, Greenland and Ellesmere Island acted as a single block during Late Jurassic – Early Cretaceous. Observed plate motion in the model is controlled by extension in the North Sea (for more details see Skogseid (2011)). The extension caused a sinistral opening in the SW Barents Sea during Late Jurassic – Early Cretaceous. As a result, a minor clockwise rotation of Greenland and Ellesmere Islands compressed against the NW Barents Sea (Fig. 13A) produced the uplift of Svalbard and the inversion in the Kong Karls Land Platform and the Olga Basin.

5.3. *Paleogeography*

5.3.1. *Sequence 1 (Hauterivian – Early Barremian)*

The deposition of S1 was accompanied by active tectonics (Fig. 16A). The Hauterivian–early Barremian reactivation of Late Jurassic inverted structures and provided an accommodation space for S1 in scattered synclinal structures (Figs. 5 and 7). In contrast to a previous paleogeography map of Smelror et al. (2009) for this period, the Persey, Pingein, Storbanken and Sentralbanken highs, together with several anticlines on the Kong Karls Land Platform, are interpreted to be subaerially exposed during this period (Figs. 11 and 16A). Based on the presence/interpretation of clinoform bottomsets (Facies B) and wedges (Facies C), these structural highs acted as local sediment sources for S1 (Figs. 8 and 9). In agreement with previous work by Antonsen et al. (1991), it is suggested that the Kong Karls Land Platform and the Olga Basin region were dominated by a shallow shelf environment. Based on the height of the interpreted clinoforms (Facies B), the paleowater depth was less than 200 m (Table 1 and Fig. 8B'). In the North Barents Basin, based on interpreted slope deposits of the Facies C (Fig. 9B'), a deep marine setting with paleowater depths of 300 m is suggested. The ESE flank of the North Barents Basin is interpreted as subaerially

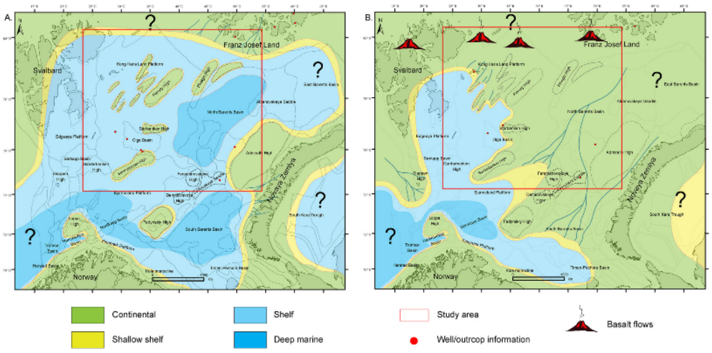

Fig. 16. Proposed paleogeography maps for (A) sequence 1 and (B) sequence 2.Note that interpretation outside of the study area is taken from publications and presentations of the "Lower Cretaceous in the Arctic" (LoCrA) consortium contributors by Marin et al. (2017); Grundvåg et al. (2017); and Kayukova and Suslova, (2015).

exposed, particularly in the area around the Admiralty high. The interpretation is based on the overall thinning and erosion of S1 towards Novaya Zemlya (Fig. 5A) and by the absence of pre-Barremian sediments in the well Luninskaya – 1 (Fig. 3).

5.3.2. *Sequence 2 (Early Barremian – Early Aptian)*

There are a number of previous work suggesting the formation of the High Arctic Igneous Province in the northern edges of the Barents Sea between 125 Ma and 122 Ma (Corfu et al., 2013; Polteau et al., 2016) (Fig. 2) implying that the study area was subjected to overall uplift due to magmatic activity. This interval is equivalent to the time of deposition of S2. However, observations from 2D seismic data suggest that the deposition of S2 occurred during a tectonically quiescent period (Fig. 16B), as advocated by the absence of growth strata and the abundance of parallel seismic facies (Facies D and F). The depositional environment of the Kong Karls Land Platform and the Olga Basin is mainly a shallow shelf to coastal (Facies D and E), while in the North Barents Basin continental environments predominated (Facies F and G) (Fig. 10B). The main source of sediments is interpreted to be located in the N–NE, in Franz Josef Land and the North Kara margin. The shifting of the main depocenters to S–SW, towards the Olga Basin and the Bjarmeland Platform (Fig. 10B) suggest a regional progradation direction from the NNE to SSW (Fig. 16B). This is also supported by the Lower Cretaceous shelf margin clinoforms observed in the southern Barents Sea that indicates a similar NE–SW and NNE–SSW direction of the shelf (Kayukova and Suslova, 2015; Marin et al., 2017). Overall, the NE–SW progradation direction in the study area during S2 is suggested to be controlled by subaerally exposed structural highs inherited from S1 (Fig. 11) (Larssen et al., 2018). These structural highs acted as bounding structures and are responsible for routing the paleodrainage system towards the southern basins of the Barents Sea (e.g. the South Barents Basin and the Bjarmeland Platform; Fig. 16B).

During the deposition of S3–S6, the North Barents Basin was most likely dominated by coastal to continental deposits that were periodically flooded. The distal part of these sequences were recognized as clinoforms complexes in the southern Barents Sea (e.g. the South Barents Basin, the Bjarmeland Platform and the Nordkapp Basin; Kayukova and Suslova, 2015; Marin et al., 2017). The presence of these sequences on the Kong Karls Land Platform and the Olga Basin is uncertain. It is most likely that sequence 3 was deposited on the Kong Karls Land Platform and Olga Basin, as suggested by the presence of the time equivalent deposition of the Carolinefjellet Formation in Svalbard (Fig. 3; Grundvåg et al. (2017)). However, it is still unknown if sequences 4–6 were deposited on the Kong Karls Land Platform and the Olga Basin, as these sediments have not been observed in this area (Fig. 5).

6. Conclusions

Three stages of reactivation are defined in the northcentral Barents Sea: (1) post Early Kimmeridgian – pre Valanginian; (2) (Berriasian) Hauterivian – Early Barremian and (3) post Early Cretaceous. The post Early Kimmeridgian – pre Valanginian and Hauterivian – Early Barremian reactivation were the result of compression that led to inversion of several structural highs such as Sentralbanken, Storbanken, Persey, Pinegin, Admiralty, Fersmanovkoye and Ludlovskaya, and also it resulted in formation of the E-W oriented Olga Basin. The inversion had a significant impact on depositional processes in the northcentral Barents Sea. During the deposition of S1 (Hauterivian – Early Barremian) tectonic activity subdivided the area into scattered depocenters that were filled by sediments sourced from the uplifting structural highs and continental land to the north. During the deposition of S2 (Early Barremian – Early Aptian) the established paleotopography allowed sediments to prograde from NNE to SSW, whereas uplifted and subaerially exposed structural highs acted as bounding structures for controlling and routing the regional NNE–SSW paleodrainage system. Later, a post Early Cretaceous reactivation was responsible for rejuvenation of the Late Jurassic – Early Cretaceous inverted faults and structures.

Three major regional tectonic events are suggested as main mechanisms for controlling the post Early Kimmeridgian – pre Valanginian and (Berriasian) Hauterivian – Early Barremian inversion in the northcentral Barents Sea:

1) the dextral transpression along Novaya Zemlya that was responsible for inversion on the ESE flanks of the North Barents Basin;
2) the opening of the Amerasia Basin which controlled the inversion in the Kong Karls Land Platform and the Olga Basin and;
3) the compression between NE Greenland/Ellesmere Islands and NW Barents Sea considered as event produced the uplift observed in the Svalbard and an inversion in the Kong Karls Land Platform and the Olga Basin.

The paleogeographic maps from this study (S1 and S2) are part of the improved paleogeographic understanding of the northcentral Barents Sea, as it integrates information from the Norwegian and Russian Barents Seas and part of regional maps of LoCrA.

Acknowledgements

This study is part of the industrial sponsored LoCrA consortium. We would like to express our gratitude to Norwegian Petroleum Directorate for providing 2D seismic data and allowing to publish them. In addition, we are thankful to Halliburton-Landmark and Move for providing the software and license. We would also like to show our gratitude to Professor Snorre Olaussen for comments that improved the manuscript and Annette Ryge (GEUS) for preparing palynological slides.

References

Alvey, A., Gaina, C., Kusznir, N.J., Torsvik, T.H., 2008. Integrated crustal thickness mapping and plate reconstructions for the high Arctic. Earth Planet. Sci. Lett. 274, 310–321.

Anderson, E.M., 1951. The Dynamics of Faulting and Dyke Formation with Applications to Britain, Second ed. Oliver and Boyd, Edinburgh.

Anell, I., Braathen, A., Olaussen, S., 2014. Regional constraints of the Sørkapp Basin: a Carboniferous relic or a Cretaceous depression? Mar. Pet. Geol. 54, 123–138.

Antonsen, P., Elverhoi, A., Dypvik, H., Solheim, A., 1991. Shallow bedrock geology of the Olga Basin Area, Northwestern Barents Sea. AAPG Bull. 75, 1178–1194.

Bergh, S., Grogan, P., 2003. Tertiary structure of the Sørkapp-Hornsund Region, South Spitsbergen, and implications for the offshore southern extension of the fold-thrust. Belt. Nor. J. Geol. 83, 43–60.

Braathen, A., Bælum, K., Maher Jr, H., Buckley, S.J., 2011. Growth of extensional faults and folds during deposition of an evaporite-dominated half-graben basin; the Carboniferous Billefjorden Trough, Svalbard. Nor. J. Geol. 91, 137–161.

Buiter, S.J.H., Torsvik, T.H., 2007. Horizontal movements in the eastern Barents Sea constrained by numerical models and plate reconstructions. Geophys. J. Int. 171, 1376–1389.

Christie-Blick, N., Biddle, K.T., 1985. Deformation and basin formation along strike-slip faults. In: Biddle, K.T., Christie-Blick, N. (Eds.), Strike-Slip Deformation, Basin Formation and Sedimentation. SEPM Special publication 37, Houston, pp. 1–34.

Cochran, J.R., Edwards, M.H., Coakley, B.J., 2006. Morphology and structure of the Lomonosov Ridge, Arctic Ocean. G-cubed 7, 1–26.

Corfu, F., Polteau, S., Planke, S., Faleide, J.I., Svensen, H., Zayoncheck, A., Stolbov, N., 2013. U-Pb geochronology of Cretaceous magmatism on Svalbard and Franz Josef Land: Barents Sea Large Igneous Province. Geol. Mag. 150, 1127–1135.

Crowell, J.C., 1974. Origin of Late Cenozoic Basins in Southern California. In: Dickinson, W.R. (Ed.), Tectonics and Sedimentation, Special Publication No. 22. Society of Economic Paleontologists and Mineralogist, Tulsa, Oklahoma, pp. 190–204.

Døssing, A., Jackson, H.R., Matzka, J., Einarsson, I., Rasmussen, T.M., Olesen, A.V., Brozena, J.M., 2013. On the origin of the Amerasia Basin and the High Arctic Large Igneous Province—Results of new aeromagnetic data. Earth Planet. Sci. Lett. 363, 219–230.

Dengo, C.A., Røssland, K.G., 1992. Extensional tectonic history of the western Barents Sea. In: Larsen, R.M., Brekke, H., Larsen, B.T., Talleraas, E. (Eds.), NPF Special Publication 1. Elservier, Amsterdam, pp. 91–107.

Dibner, V., 1998. Geology of Franz Josef Land. In: Solheim, A., Musatov, E., Heintz, N. (Eds.), Geological Aspects of Franz Josef Land and the Northernmost Barents Sea—The Northern Barents Sea Geotraverse 151, Oslo, pp. 10–17.

Dimakis, P., Braathen, B.I., Faleide, J.I., Elverhøi, A., Gudlaugsson, S.T., 1998. Cenozoic erosion and the preglacial uplift of the Svalbard-Barents Sea region. Tectonophysics 300, 311–327.

Dove, D., Coakley, B., Hopper, J., Kristoffersen, Y., Team, H.L.Y.G., 2010. Bathymetry, controlled source seismic and gravity observations of the Mendeleev ridge; implications for ridge structure origin, and regional tectonics. Geophys. J. Int. 183, 481–502.

Embry, A.F., 1992. Mesozoic stratigraphy of Franz Josef Land Archipelago, Arctic Russia—a literature review. Thurston, D.K., Fujita, K. (Eds.), Proceedings, International Conference on Arctic Margins, Anchorage, Alaska, OCS Study MMS 94 15–22.

Evangelatos, J., Mosher, D.C., 2016. Seismic stratigraphy, structure and morphology of Makarov Basin and surrounding regions: tectonic implications. Mar. Geol. 374, 1–13.

Evenchick, C.A., Davis, W.J., Bédard, J.H., Hayward, N., Friedman, R.M., 2015. Evidence for protracted High Arctic large igneous province magmatism in the central Sverdrup Basin from stratigraphy, geochronology, and paleodepths of saucer-shaped sills. GSA Bull. 127, 1366–1390.

Evitt, W.R., 1985. Sporopollenin Dinoflagellate Cysts: Their Morphology and Interpretation. American Association of Stratigraphic, Dallas, Texas.

Faleide, J.I., Vagnes, E., Gudlaugsson, S.T., 1993. Late Mesozoic-Cenozoic evolution of the South-Western Barents Sea in a regional rift shear tectonic setting. Mar. Pet. Geol. 10, 186–214.

Faleide, J.I., Tsikalas, F., Breivik, A.J., Mjelde, R., Ritzmann, O., Engen, O., Wilson, J., Eldholm, O., 2008. Structure and evolution of the continental margin off Norway and Barents Sea. Episodes 31, 82–91.

Gaina, C., Medvedev, S., Torsvik, T.H., Koulakov, I., Werner, S.C., 2014. 4D arctic: a glimpse into the structure and evolution of the arctic in the light of new geophysical maps, plate tectonics and tomographic models. Surv. Geophys. 35, 1095–1122.

Galloway, W.E., 1989. Genetic stratigraphic sequences in basin analysis I: architecture and genesis of flooding-surface bounded depositional units. AAPG Bull. 73, 125–142.

Garfunkel, Z., 1981. Internal structure of the Dead Sea leaky transform (rift) in relation to plate kinematics. Tectonophysics 80, 81–108.

Gavrilov, V.P., Gibshman, N.B., Karnauhov, S.M., Holodilov, V.A., Tsemkalo, M.L., Shamalov, Y.V., 2010. Biostratigraphy and Lithofacies of Petroliferous Sediments of Barents-Kara Region. NEDRA, Moscow.

Gernigon, L., Brönner, M., 2012. Late Palaeozoic architecture and evolution of the southwestern Barents Sea: insights from a new generation of aeromagnetic data. J. Geol. Soc. 169, 449–459.

Gjelberg, J., Steel, R.J., 1995. In: Steel, R.J., Felt, V.L., Johannessen, E.P., Mathieu, C. (Eds.), Helvetiafjellet Formation (Barremian-Aptian), Spitsbergen: Characteristics of a Transgressive Succession. Norwegian Petroleum Society Special Publications. Elsevier, pp. 571–593.

Glørstad-Clark, E., Faleide, J.I., Lundschien, B.A., Nystuen, J.P., 2010. Triassic seismic sequence stratigraphy and paleogeography of the western Barents Sea area. Mar. Pet. Geol. 27, 1448–1475.

Golonka, J., Bocharova, N.Y., Ford, D., Edrich, M.E., Bednarczyk, J., Wildharber, J., 2003. Paleogeographic reconstructions and basins development of the Arctic. Mar. Pet. Geol. 20, 211–248.

Gomez, F., Nemer, T., Tabet, C., Khawlie, M., Meghraoui, M., Barazangi, M., 2007. Strain partitioning of active transpression within the Lebanese restraining bend of the Dead Sea Fault (Lebanon and SW Syria). In: Cunningham, W.D., Mann, P. (Eds.), Tectonics of Strike-Slip Restraining and Releasing Bends. Geological Society of London Special Publication 290, pp. 285–303.

Grøsfjeld, K., 1992. Palynological age constraints on the base of the Helvetiafjellet Formation (Barremian) on Spitsbergen. Polar Res. 11, 11–19.

Grachev, A.F., Arakelyantz, M.M., Lebedev, V.A., Musatov, E.E., Stolbov, N.M., 2001. New K-Ar ages for basalts from Franz Josef Land. Russ. J. Earth Sci. 3 (1), 79–82.

Grantz, A., Clark, D.L., Phillips, R.L., Srivastava, S.P., Blome, C.D., Gray, L.B., Haga, H., Mamet, B.L., McIntyre, D.J., McNeil, D.H., Mickey, M.B., Mullen, M.W., Murchey, B.I., Ross, C.A., Stevens, C.H., Silberling, N.J., Wall, J.H., Willard, D.A., 1998. Phanerozoic stratigraphy of Northwind Ridge, magnetic anomalies in the Canada Basin, and the geometry and timing of rifting in the Amerasia Basin, Arctic Ocean. GSA Bull. 110, 801–820.

Grantz, A., Hart, P.E., Childers, V.A., 2011. Chapter 50: geology and tectonic development of the Amerasia and Canada basins, Arctic Ocean. In: In: Spencer, A.M., Embry, A.F., Gautier, D.L., Stoupakova, A.V., Sørensen, K. (Eds.), Arctic Petroleum Geology: Geol. Soc. London, Memoirs 35. pp. 771–799.

Grogan, P., Østvedt-Ghazi, A.M., Larssen, G.B., Fotland, B., Nyberg, K., Dahlgren, S., Eidvin, T., 1999. Structural elements and petroleum geology of the Norwegian sector of the northern Barents Sea. In: Fleet, A.J., Boldy, S.A.R. (Eds.), Petroleum Geology of Norhwest Europe: Proceedings of the 5th Conference. The Geological Society, London. pp. 247–259.

Grogan, P., Nyberg, K., Fotland, B., Myklebust, R., Dahlgren, S., Riis, F., 2000. Cretaceous magmatism south and east of Svalbard: evidence from seismic reflection and magnetic data. Polarforschung 68, 25–34.

Grundvåg, S.-A., Olaussen, S., 2017. Sedimentology of the Lower Cretaceous at Kikutodden and Keilhaufjellet, southern Spitsbergen: implications for an onshore-offshore link. Polar Res. 36, 1302124.

Grundvåg, S.A., Marin, D., Kairanov, B., Śliwińska, K.K., Nøhr-Hansen, H., Jelby, M.E., Escalona, A., Olaussen, S., 2017. The Lower Cretaceous succession of the northwestern Barents Shelf: onshore and offshore correlations. Mar. Pet. Geol. 86, 834–857.

Gudlaugsson, S.T., Faleide, J.I., Johansen, S.E., Breivik, A.J., 1998. Late Palaeozoic structural development of the south-western Barents Sea. Mar. Pet. Geol. 15, 73–102.

Hadlari, T., Midwinter, D., Galloway, J.M., Dewing, K., Durbano, A.M., 2016. Mesozoic rift to post-rift tectonostratigraphy of the Sverdrup Basin, Canadian Arctic. Mar. Pet. Geol. 76, 148–158.

Head, M., 1996. Modern dinoflagellate cysts and their biological affinities. In: Jansonius, J.J., McGregor, D.C. (Eds.), Palynology: Principles and Applications 3. AASP Foundation, College Station, Texas, pp. 1197–1248.

Hubbert, M.K., Willis, D.G., 1972. Mechanics of hydraulic fracturing. AAPG Bull. 18, 239–257.

Jakobsson, M., Mayer, L., Coakley, B., Dowdeswell, J.A., Forbes, S., Fridman, B., Hodnesdal, H., Noormets, R., Pedersen, R., Rebesco, M., Schenke, H.W., Zarayskaya, Y., Accettella, D., Armstrong, A., Anderson, R.M., Bienhoff, P., Camerlenghi, A., Church, I., Edwards, M., Gardner, J.V., Hall, J.K., Hell, B., Hestvik, O., Kristoffersen, Y., Marcussen, C., Mohammad, R., Mosher, D., Nghiem, S.V., Pedrosa, M.T., Travaglini, P.G., Weatherall, P., 2012. The International Bathymetric Chart of the Arctic Ocean (IBCAO) Version 3.0.Geophys. Res. Lett. 39, L12609.

Kaminsky, V., Poselov, V., Glebovsky, V., Zayonchek, A., Butsenko, V., 2005. Geophysical and geological study of the transition zone between the Mendeleev Rise and the adjacent Siberian Shelf: preliminary results. AGU Fall Meeting Abstract.

Kayukova, A.V., Suslova, A.A., 2015. A seismostratigraphic analysis of the lower cretaceous deposits of the Barents sea to reveal petroleum perspectives. MSU Geol. Bull. 70, 177–182.

Knies, J., Gaina, C., 2008. Middle Miocene ice sheet expansion in the Arctic: views from the Barents Sea. G-cubed 9, 1–8.

Larssen, G.B., Olaussen, S., Helland-Hansen, W., Johannessen, E.P., Nøttvedt, A., Riis, F., Rismyhr, B., Smelror, M., Worsley, D., 2018. Geological evolution of the Kong Karls Land archipelago, High Arctic Norway: a key to the Jurassic and Lower Cretaceous basin development of northern Barents Sea. Norw. J. Geol (in press).

Lawver, L., Scotese, C., 1990. A review of tectonic models for the evolution of the Canada Basin. In: Grantz, A., Johnson, L., Sweeney, J.F. (Eds.), The Geology of North America, Boulder, Colarado, pp. 593–618.

Lawver, L.A., Grantz, A., Gahagan, L.M., 2002. Plate kinematic evolution of the present Arctic region since the Ordovician. In: Miller, E.L., Grantz, A., Klemperer, S.L. (Eds.), Tectonic Evolution of the Bering Shelf-Chukchi Sea-Arctic Margin and Adjacent Landmasses. Geological Society of America, Boulder, Colorado, pp. 337–362.

Lebedeva-Ivanova, N.N., Zamansky, Y.Y., Langinen, A.E., Sorokin, M.Y., 2006. Seismic profiling across the Mendeleev Ridge at 82°N: evidence of continental crust. Geophys. J. Int. 165, 527–544.

Mørk, A., Smelror, M., 2001. Correlation and non-correlation of high order circum-Arctic Mesozoic sequences. Polarforschung 69, 65–72.

Malyshev, N.A., Nikishin, A.M., Obmetko, V.V., Nikishin, V.A., Kleshchina, L.N., Morgunova, E., 2013. Geological structure and history of Western Russian Arctic (Barents-Kara region). In: 3P Arctic Conference. Stavanger.

Marello, L., Ebbing, J., Gernigon, L., 2010. Magnetic basement study in the Barents Sea from inversion and forward modelling. Tectonophysics 493, 153–171.

Marin, D., Escalona, A., Sliwihska, K.K., Nøhr-Hansen, H., Mordasova, A., 2017. Sequence stratigraphy and lateral variability of Lower Cretaceous clinoforms in the southwestern Barents Sea. AAPG Bull. 101, 1487–1517.

Midtkandal, I., Nystuen, J.P., 2009. Depositionalarchitecture of alow-gradient ramp shelf in an epicontinental sea: the lower Cretaceous of Svalbard. Basin Res. 21, 655–675.

Minakov, A., Faleide, J.I., Glebovsky, V.Yu., Mjelde, R., 2012. Structure and evolution of the northern Barents–Kara Sea continental margin from integrated analysis of potential fields, bathymetry and sparse seismic data. Geophys. J. Int. 188, 79–102.

Nøhr-Hansen, H., 1993. Dinoflagellate cyst stratigraphy of the Barremian to Albian, Lower Cretaceous, North-East Greenland. Geol. Greenl. Sur. Bull. 166, 1–171.

Nøhr-Hansen, H., 2012. Palynostratigraphy of the Cretaceous-lower Palaeogene sedimentary succession in the Kangerlussuaq Basin, southern east Greenland. Rev. Palaeobot. Palynol. 178, 59–90.

Nikishin, A., Malyshev, N., Petrov, E., 2014. Geological Structure and History of the Arctic Ocean, first ed. EAGE, Netherlands.

Nikishin, V.A., 2013. Intraplate and Marginal Deformation of the Kara Sea Sedimentary Basins. PhD Thesis. Moscow State University, Moscow.

Oxman, V.S., 2003. Tectonic evolution of the Mesozoic Verkhoyansk-Kolyma belt (NE Asia). Tectonophysics 365, 45–76.

Petrov, O.V., Sobolev, N.N., Koren, T.N., Vasiliev, V.E., Petrov, E.O., Larssen, G.B., Smelror, M., 2008. Palaeozoic and early Mesozoic evolution of the East Barents and Kara seas sedimentary basins. Nor. J. Geol. 88, 227–234.

Polteau, S., Hendriks, B.W.H., Planke, S., Ganerød, M., Corfu, F., Faleide, J.I., Midtkandal, I., Svensen, H.S., Myklebust, R., 2016. The Early Cretaceous Barents Sea Sill Complex: distribution, 40Ar/39Ar geochronology, and implications for carbon gas formation. Palaeogeogr. Palaeoclimatol. Palaeoecol. 441, 83–95.

Repin, Y.S., Polubotko, I.V., Kirichkova, A.I., Kulikova, N.K., 2007. Mesozoic Sediments in The Franz Josef Land Archipelago, First ed. Saint Petersburg State University, Saint Petersburg.

Ritzmann, O., Faleide, J.I., 2009. The crust and mantle lithosphere in the Barents Sea/Kara Sea region. Tectonophysics 470, 89–104.

Senger, K., Tveranger, J., Ogata, K., Braathen, A., Planke, S., 2014. Late Mesozoic magmatism in Svalbard: a review. Earth-Sci. Rev. 139, 123–144.

Shephard, G.E., Müller, R.D., Seton, M., 2013. The tectonic evolution of the Arctic since Pangea breakup: integrating constraints from surface geology and geophysics with mantle structure. Earth-Sci. Rev. 124, 148–183.

Skogseid, J., 2011. The Orphan Basin-a key to understanding the kinematic linkage between North and NE Atlantic Mesozoic rifting. Cent. North Atl. Conjug. Margins Conf. 2, 13–23.

Smelror, M., Mørk, A., Monteil, E., Rutledge, D., Leereveld, H., 1998. The Klippfisk Formation – a new lithostratigraphic unit of Lower Cretaceous platform carbonates on the Western Barents Shelf. Polar Res. 17, 181–202.

Smelror, M., Petrov, O., Larssen, G.B., Werner, S., 2009. Geological History of the Barents Sea. Geological Survey of Norway, Trondheim.

Sobornov, K., Afanasenkov, A., Gogonenkov, G., 2015. Strike-slip faulting in the northern part of the West Siberian Basin and Enisey-Khatanga trough: structural expression, development and implication for petroleum exploration. In: 3P Arctic Conference Search and Discovery Article. Stavanger, Norway.

Steel, R., Worsley, D., 1984. Svalbard's post-Caledonian strat-an atlas of sedimentational patterns and palaeogeographic evolution. In: Spencer, A.M. (Ed.), Petroleum Geology of the North European Margin. Gratham and Trotman, pp. 109–135.

Velichko, B.M., 2012. The results of complex geophysical investigations in the Northwest Barents Sea Shelf (at the junction between the Svalbard Anteclise and East Barents Megatrough). MSU Bull. 67, 58–64.

Weber, M., Abu-Ayyash, K., Abueladas, A., Agnon, A., Alasonati-Tašárová, Z., Al-Zubi, H., Babeyko, A., Bartov, Y., Bauer, K., Becken, M., Bedrosian, P.A., Ben-Avraham, Z., Bock, G., Bohnhoff, M., Bribach, J., Dulski, P., Ebbing, J., El-Kelani, R., Förster, A., Förster, H.J., Frieslander, U., Garfunkel, Z., Goetze, H.J., Haak, V., Haberland, C., Hassouneh, M., Helwig, S., Hofstetter, A., Hoffmann-Rotrie, A., Jäckel, K.H., Janssen, C., Jaser, D., Kesten, D., Khatib, M., Kind, R., Koch, O., Koulakov, I., Laske, G., Maercklin, N., Masarweh, R., Masri, A., Matar, A., Mechie, J., Meqbel, N., Plessen, B., Möller, P., Mohsen, A., Oberhänsli, R., Oreshin, S., Petrunin, A., Qabbani, I., Rabba, I., Ritter, O., Romer, R.L., Rümpker, G., Rybakov, M., Ryberg, T., Saul, J., Scherbaum, F., Schmidt, S., Schulze, A., Sobolev, S.V., Stiller, M., Stromeyer, D., Tarawneh, K., Trela, C., Weckmann, U., Wetzel, U., Wylegalla, K., 2009. Anatomy of the dead sea transform from lithospheric to microscopic scale. Rev. Geophys. 47, 1–44.

Zheng, W.-j., Zhang, P.-z., He, W.-g., Yuan, D.-y., Shao, Y.-x., Zheng, D.-w., Ge, W.-p., Min, W., 2013. Transformation of displacement between strike-slip and crustal shortening in the northern margin of the Tibetan Plateau: evidence from decadal GPS measurements and late Quaternary slip rates on faults. Tectonophysics 584, 267–280.

Ziegler, P.A., 1988. Evolution of the Arctic-North Atlantic and the western Tethys – a visual presentation of a series of paleogeographic – paleotectonic maps. AAPG Memoirs 43, 164–196.

Paper 2

The Early Cretaceous evolution of the Tromsø Basin, SW Barents Sea, Norway

Bereke Kairanov, Alejandro Escalona, Ian Norton and Peter Abrahamson .

Submitted to Marine and Petroleum Geology

ABSTRACT

Extensional basins developed along oblique or transform margins are least studied basins as comparted to those developed along orthogonally extended margins, therefore their evolutionary models are controversial. This study present an example of the basin, namely Tromsø, which developed along the Southwestern Barents Sea transform margin. Three previous models have been proposed to explain the tectonic evolution and architecture of the basin, but still no consensus on how the development of the individual structures is reached. In this study, we use 2D industry seismic reflection data, potential field and wells data, as well as previously published information to understand the Early Cretaceous structural evolution of the Tromsø Basin in the context of the geodynamic processes in the south-western Barents Sea. Modelled gravity anomalies along a composite 2D regional seismic section facilitated the interpretation of crustal structures, which then were used for a 2D structural reconstruction. Unlike any previous models, we propose a new Early Cretaceous structural evolutionary model for the Tromsø Basin, which involves oblique extension and the formation of an intra-basinal transfer zone with transpressional strike slip fault systems. The basement heterogeneity suggested to have played important role in focusing and localizing strain in the area. The 2D sequential restoration of the regional profile yields an estimate of ca. 35 km of crustal extension from the earliest Cretaceous until present. Thinner crust below the Tromsø Basin as compared to Sørvestnaget and Hammerfest basins is suggested to be additional characteristics favoring the oblique rifting of the margin. This study illustrates the importance of integrating regional tectonic settings when reconstructing the evolution of basin-bounding faults.

INTRODUCTION

The structural evolution of orthogonally extended passive margins and basins are well documented through outcrop and subsurface studies (Badley et al., 1988; Bell et al., 2009; Ebinger, 1989; Jackson and Rotevatn, 2013; Lehner and De Ruiter, 1977; Moustafa, 1993; Sharp et al., 2000; Spathopoulos, 1996; Withjack et al., 1998; Ziegler, 1992), as well as numerical and physical analogue modelling (Corti et al., 2003; Huismans et al., 2001; McClay et al., 2002; Naliboff and Buiter, 2015). Due to tectonic inheritance and irregular shapes of the plate boundaries, passive margins and basins include segments where oblique or sheared tectonics is prevailing (Brune et al., 2018; Dewey et al., 1998; Hodge et al., 2018; Manatschal et al., 2015; Morley, 2017; Phillips et al., 2018; Sanderson and Marchini, 1984). Frequently, evolution of such segments are assessed using models assuming an orthogonal alignment of relative plate motion and plate boundary, which may lead to erroneous assessment of the subsidence pattern and faults evolution (Brune, 2014; Brune et al., 2016; Huismans and Beaumont, 2011; Lavier and Manatschal, 2006; McKenzie, 1978; Naliboff et al., 2017; White, 1993). Despite the general knowledge of the extensional basins that involve certain degree of obliquity (Atwater and Stock, 1998; Corti, 2008; Fletcher et al., 2007; Fournier et al., 2004; Klimke and Franke, 2016; Lizarralde et al., 2007; Mart et al., 2005; Phethean et al., 2016), the structuring and kinematics of the past rift basins remains under-researched.

Therefore, in this study, we analysis tectonic evolution of the Tromsø Basin which located along the sheared margin of the SW Barents Sea and has a complex tectonic history that involved both orthogonal and sheared rifting (Faleide et al., 1993). In general, it is accepted that the basin formed in response to Late Jurassic – Early Cretaceous rifting in the SW Barents Sea (Faleide et al., 1993), but there is no clear consensus on basin evolution and tectonic model. Early works proposed at least two models to explain the Late Jurassic – Early Cretaceous evolution and structuring of the Tromsø Basin: 1) Strike-slip model with either (a) sinistral or (b) dextral strike-slip system along the northern basin bounding faults (e.g. Bjørnøyrenna Fault Complex; (Gabrielsen and Færseth, 1988; Riis et al., 1986), and 2) Large scale extensional model with sinistral strike-slip faults (Fig. 2B) (Faleide et al., 1993). Timing and direction of major fault movements in these models are controversial, where for instance, the structural highs along the western margin (e.g. Senja Ridge and Veslemøy High; Fig. 2A) have either an extensional (Faleide et al., 1993; Indrevær et al., 2013; Riis et al., 1986) or a compressional origin that resulted from strike slip tectonics (e.g. along Ringvassøy – Loppa and Bjørnøyrenna fault complexes; (Gabrielsen and Færseth, 1988). Later work, using potential field (magnetic and gravity) data, proposed a new crustal scale "boundinage" model for the SW Barents Sea (Gernigon et al., 2014). Indirect observations from neighboring basin suggested a highly thinned crust and abundancy of low angle fault systems below the Tromsø Basin, which still requires better constrains in terms of basin evolution (Fig. 2C). Disagreements regarding the tectonic models are also attributed to a limited well control and poor imaging of the deep basin by seismic reflection profiles that increases uncertainty in the interpretation (Breivik et al., 1998; Faleide et al., 2008; Faleide et al., 1993; Gabrielsen, 1984; Mosar et al., 2002).

Although all models explain the present-day configuration of the basin, choosing one or another model can lead to an erroneous assessment of the tectonic and geodynamic settings. Therefore, in this paper we aim to: (1) understand the Early Cretaceous tectonic processes in the Tromsø Basin and revise structural evolutionary models; and (2) by restoring 2D regional a crustal profile constrain the development of the area to understand pre-drift configuration of the margin.

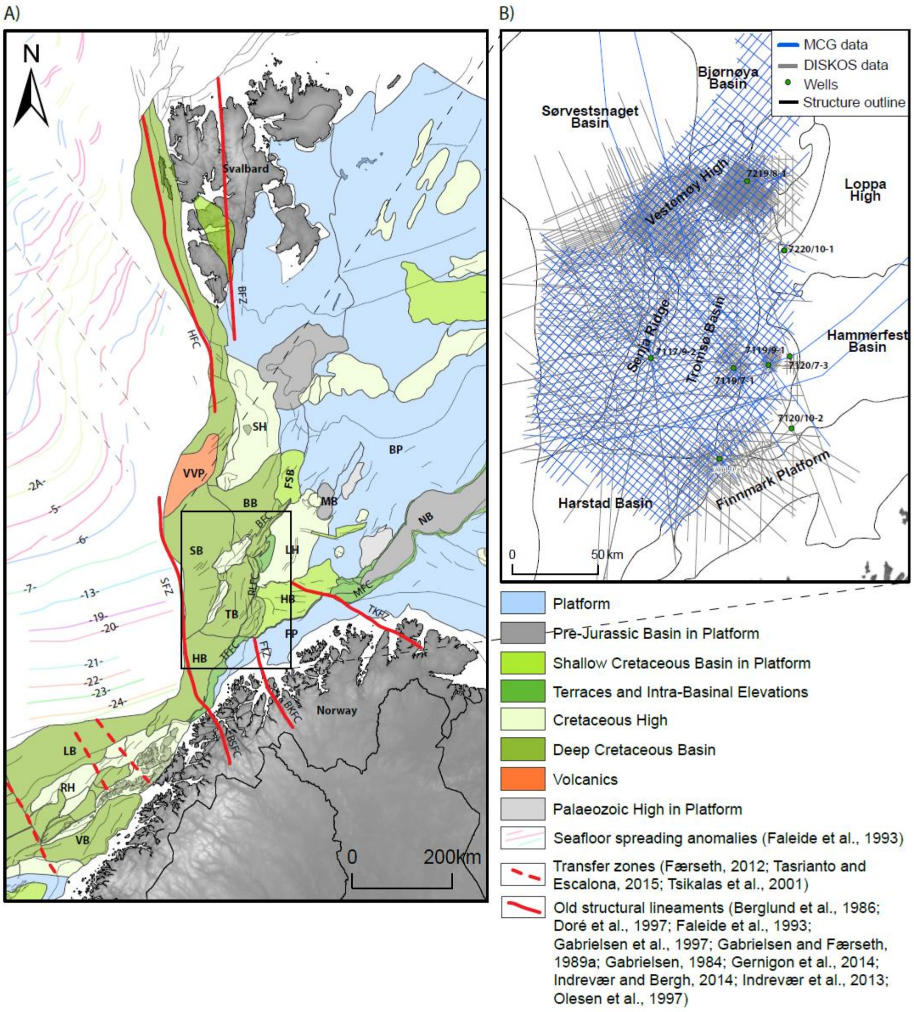

Figure 10 A) Location of the study area with main structural elements of the SW Barents Sea (TB = Tromso Basin; HB = Hammerfest Basin; BB = Bjørnøya Basin; SB = Sørvestnaget Basin; LH = Loppa High; SH = Stappen High; VH =Veslemøy High; SR = Senja Ridge; VVP = Vestbaken Volcanic Province; FP = Finnmark Platform; BKFC = Bothnian Kvænangen Fault Complex; BSFC = Bothnian-Senja Fault Complex; TFFC = Troms-Finnmark Fault Complex; TFFC = Tromsø Finnmark Fault Complex; RFLC =Ringvassøy- Loppa Fault Complex; BFC = Bjørnøyrenna Fault Complex; BFZ = Billefjorden Fault Zone; HFC = Horsund Fault Complex; SFZ = Senja Fracture Zone). B) Location of the 2D seismic profiles and wells.

GEOLOGICAL SETTING

The Tromsø Basin is characterized as an elongated NNE–SSW-striking basin, with a length of 140 km and a width of 60 km (Fig. 1A; (Gabrielsen et al., 1990). The southern boundary is a transition towards the Harstad Basin and termination against the Troms – Finnmark Fault Complex (TFFC) (Fig.1A; (Gabrielsen et al., 1990). The northern boundary is defined by the Veslemøy High and the Bjørnøyrenna Fault Complex (BFC), which separate the Tromsø Basin from the Bjørnøya Basin (Fig.1B). The eastern boundary, towards the Hammerfest Basin, is delineated by the Ringvassøy-Loppa Fault Complex (RLFC), while the western boundary is limited to the Senja Ridge and the Veslemøy High (Fig.1B(Gabrielsen et al., 1990).

The tectonic history of the Tromsø Basin, can be traced back to approximately 400Ma, when the Caledonian orogeny was formed by collision of the Laurentian and Baltic plates with development long lived reversed fault zones with a variety of nappes and thrust sheets over the Fennoscandia Shield (Gabrielsen, 1984; Gasser, 2013; Gee et al., 2006; Gee et al., 2008; Roberts, 2003). Towards the end of the Paleozoic, regional extension caused collapse of thrust sheets resulting in formation of grabens and half grabens that were covered by Upper Carboniferous to Lower Permian carbonate platforms and thick evaporates deposits (Gudlaugsson et al., 1998; Larssen et al., 2002).

The Early Triassic is marked by a rift episode, which has been documented in the North Atlantic region (Tsikalas et al., 2012). It has been suggested that the same Early Triassic rift episode may have continued until the Middle Triassic around the Tromsø Basin (Smelror et al., 2009). The Triassic succession is comprised of prograding and retrograding cycles of marine, deltaic and continental clastic deposits sourced from the ESE (Glørstad-Clark et al., 2010; Klausen et al., 2015).

From the Middle Jurassic to Early Cretaceous, northward advance of the Atlantic rifting formed deep basins in the southwestern Barents Sea such as the Harstad, Tromsø, Bjørnøya and Sørvestnaget basins (Faleide et al., 2008; Gernigon et al., 2014). In the Tromsø Basin, the Early Cretaceous rift episode along the NE – SW trending Ringvassøy–Loppa and Bjørnøyrenna fault complexes led to rapid subsidence and accumulation of thick Cretaceous sediments (Clark et al., 2014; Faleide et al., 2008; Faleide et al., 1993; Gabrielsen et al., 1990; Indrevær et al., 2016; Rønnevik et al., 1982). The central part of the basin experienced salt related deformation during this rift event (Faleide et al., 1993; Gabrielsen et al., 1990; Larssen et al., 2002; Sund, 1984). Three Early Cretaceous rift phases have been interpreted for the Tromsø Basin: Berriasian–Valanginian, Hauterivian–Barremian and Aptian–Albian (Faleide et al., 1993). Local compression during the earliest Cretaceous has been identified in the northern part of the basin. This has been suggested to be the result of dextral strike slip movement along the Asterias Fault complex (Berglund et al., 1986; Gabrielsen et al., 1990; Sund, 1984) or as a localized tectonic inversion due to differential uplift of the Loppa High (Indrevær et al., 2016). In terms of the Lower Cretaceous stratigraphy, a major break in deposition occurred from the Boreal Berriasian/Volgian to Valanginian to Barremian, forming a regional unconformity known as the Base Cretaceous Unconformity (BCU) (Århus et al., 1990; Lundin and Dore, 1997; Marin et al., 2017b; Mork et al., 1999). The BCU is expressed as a high amplitude seismic reflector and its age and stratigraphic significance is complex (Gabrielsen et al., 2001; Nottvedt et al., 1995). In the areas of the southwestern Barents Sea, where basin margins are affected by Late Jurassic to Early Cretaceous tectonism, the BCU represents an unconformity, whereas, in the deeper basins, it is a conformable surface (Marin et al., 2017b). The Lower Cretaceous succession of the SW Barents Sea is divided into four main formations: Knurr, Klippfisk, Kolje and Kolmule, which consist mainly of grey claystone with minor interbedded limestone and sandstone deposited in an open marine environment (Dalland et al., 1988; Mork et al., 1999). More recently, these formations were divided into seven genetic sequences (sequences 0–6; Fig. 3A; Marin et al., 2017b). These sequences are bounded by flooding surfaces, some of which can be correlated on a regional scale (Grundvåg et al., 2017; Marin et al., 2017b).

The Late Cretaceous – Paleocene period is associated with dextral strike-slip movement between the western Barents Sea and northern Greenland (Faleide et al., 1996). This event divided the margin into two shear margins, the Hornsund in the north and Senja in the south (Faleide et al., 2008) (Fig. 1A). The Paleocene – Eocene transition (55 – 54 Ma) is marked by a continental breakup of the North Atlantic margin, followed by separation of the Barents Sea and the eastern Greenland margin, and opening of the Fram Strait (Faleide et al., 1996). During the same period the Barents Sea experienced onset of a tectonic uplift that caused exhumation and erosion of the northern and western margins of the Barents Sea (Dimakis et al., 1998; Henriksen et al., 2011; Knies and Gaina, 2008).

Relationship of onshore basement lineaments and offshore structural trends

It has been suggested that the Early Cretaceous evolution and structural configuration of the SW Barents Sea has been influenced by inherited Caledonian or even older Precambrian basement structures (Barrère et al., 2009; Braathen et al., 1999; Doré, 1991; Fichler et al., 1997; Gabrielsen, 1984; Gernigon et al., 2014; Ritzmann and Faleide, 2007; Tsikalas et al., 2012). There are three well-constrained, long-lived fault complexes identified on the northern mainland of Norway that have affected the structuring of the southern and southwestern Barents Sea:

1) The Trollfjorden-Komagelva Fault Zone (TKFZ), a major Precambrian WNW-ESE striking fault zone that was episodically reactivated during the Paleozoic and Mesozoic (Fig. 1A) (Gabrielsen,

1984; Herrevold et al., 2009; Karpuz et al., 1993; Rice et al., 1989; Roberts, 1972; Roberts et al., 2011; Roberts and Lippard, 2005; Siedlecka and Siedlecki, 1967). The TKFZ is characterized as a transfer fault system that has an increasing component of extension toward the adjacent Hammerfest Basin (Berglund et al., 1986; Gabrielsen and Færseth, 1989; Gabrielsen, 1984). This relationship has been well constrained with magnetic data (Gernigon et al., 2014);

2) The Bothnian-Senja Fault Complex (BSFC) and 3) The Bothnian–Kvænangen Fault Complex (BKFC) are two major Precambrian NNW-SSE striking ductile shear zones that were periodically reactivated during Paleozoic and Mesozoic times (Fig. 1A) (Doré et al., 1997; Indrevær and Bergh, 2014; Indrevær et al., 2013; Olesen et al., 1997). The Senja Shear Zone and Fugløya transfer zone have been proposed as offshore northward extension of the BSFC and BKFC, respectively (Fig. 1A) (Faleide et al., 1993; Gabrielsen et al., 1997; Indrevær et al., 2013). Moreover, the Hornsund Fault Complex (HFC) and Billefjorden Fault Zone (BFZ) identified in Svalbard are suggested to be part of the same NNW – SSE structural trend (Fig. 1A) (Doré et al., 1997). Despite the apparent continuity of onshore and offshore structural expressions, connection of these faults is not supported by direct evidence or reliable documentation.

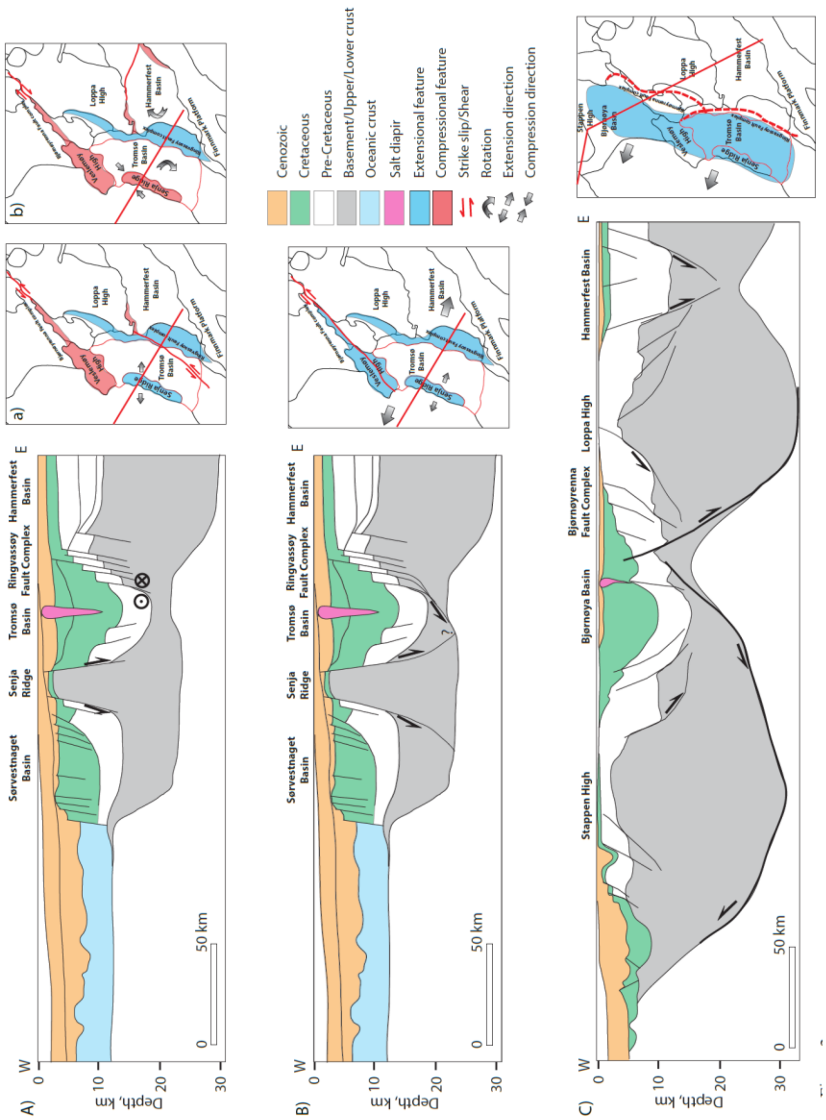

Figure 11 Simplified sketch of previously proposed regional tectonic models for Late Jurassic - Early Cretaceous structuring of the Tromsø Basin. Please note differences in the Senja Ridge and Veslemøy High interpretations as a positive structural feature. A) a) Sinistral and b) dextral strike-slip system along Bjørnøyrenna and Ringvassoy Fault complexes (Riis et al., 1986; Gabrielsen and Færseth, 1988) ; B) Large scale extensional system with sinistral strike-slip along Bjørnøyrenna Fault complex (Faleide et al., 1993) and C) A propagating system of highly thinned crust dominated by reactivated listric fault system (Gernigon et al., 2014)

DATASET

The database for this study comprises a post-stack time migrated, 2D reflection seismic surveys provided by the Norwegian Petroleum Directorate (NPD) and a MultClient Geophysical AS (MCG) (Fig. 1B). It is important to mention that the 2D seismic data acquired by MCG in 2016 have a better quality in imaging and coverage of the study areas. The seismic profiles covers the area of ca. 2500 km2, where the average distance between seismic lines is 2-5 km. The seismic data penetrates depths of 6-9 seconds in two-way-traveltime (TWT) with dominant frequency range between 10-40 Hz. In general, the quality of the seismic data is moderate to good, except the southern part of the study area, where continuity of the seismic reflectors is poor.

The well data used include five exploration wells 7019/1-1, 7119/9-1, 7220/10-1, 7119/7-1 and 7117/9-2 (Fig. 1B). All wells have a full set of logs and biostratigraphic data were obtained from well reports publically available in the NPD web page (http://factpages.npd.no), from the “Lower Cretaceous basins in the high Arctic” consortium project (LoCrA; http://locra.ux.uis.no) and previous publications (e.g. Marin et al., 2017b). Free air gravity map of Sandwell et al. (2014) was used to model anomalies along selected seismic profiles.

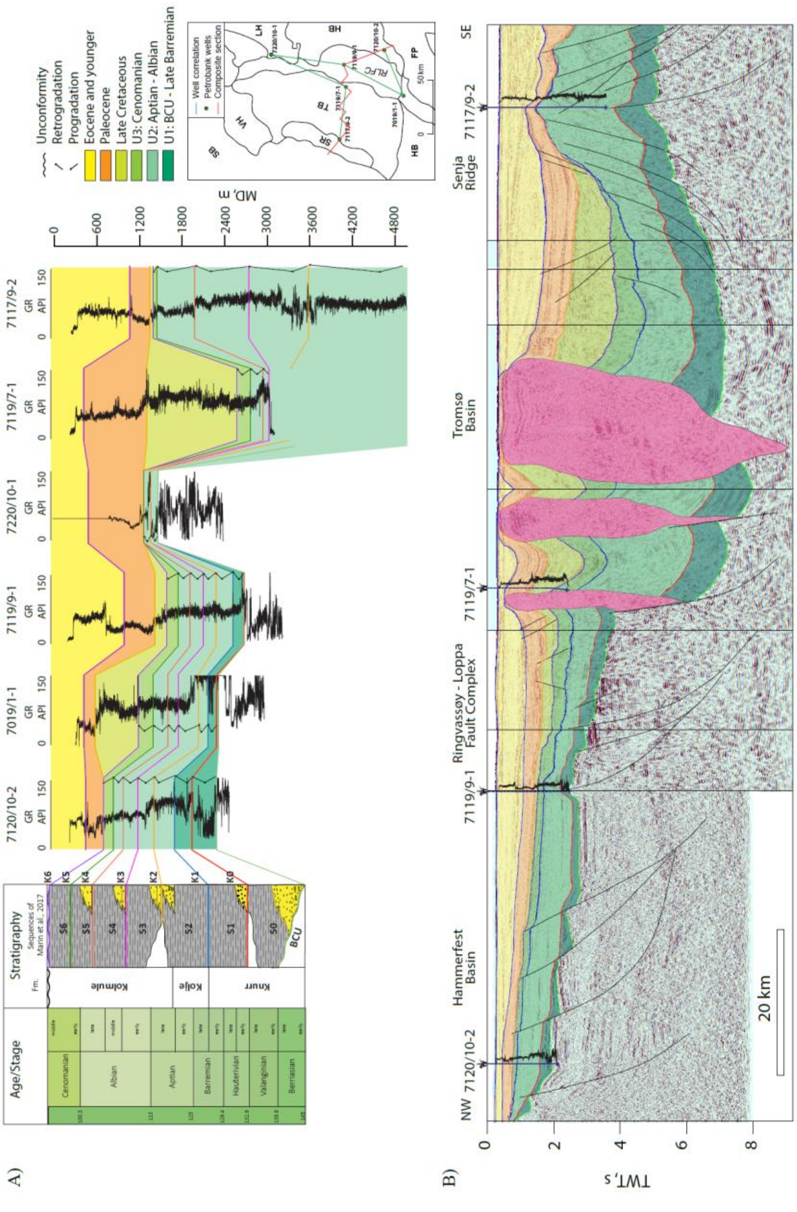

Figure 12 A) Stratigraphic framework based on well correlation of interpreted Lower Cretaceous seismic units with defined sequences of Marin et al., (2017) in the Hammerfest Basin (well 7120/10-2); B) Long distance correlation of the interpreted Lower Cretaceous unit. Please note that wells in the Tromsø Basin do not reach deeper seismic units.

METHODOLOGY

Seismic interpretation:

Based on reflection terminations and regional continuity of the reflectors, four horizons (BCU, K1, K5 and K6) that subdivide three seismic units (U1, U2 and U3) were selected and mapped to constrain the Early Cretaceous evolution of the Tromsø Basin.

In order to establish the regional tectonostratigraphic framework, age of interpreted horizons have been constrained by biostratigraphic data and correlated with flooding surfaces of Marin et al. (2017a) in the Hammerfest Basin (e.g. well 7120/10-2; Figs. 3A and 3B). Seismic horizons and their correlative flooding surfaces are: Base Cretaceous Unconformity (BCU), Late Barremian (K1), Late Albian (K5) and Late Cenomanian (K6) (Fig. 3B). It is important to state that the BCU and K1 have never been penetrated by wells in the Tromsø Basin. Interpretation of these horizons was based on seismic reflector configurations and long distance correlations (Fig. 3B). Consequently, seismic units were also correlated with sequences (S0 – S6) of Marin et al. (2017a), as follow: U1 with S0 – S1; U2 with S2 – S5; and U3 with S6 (Fig. 3A). Stacking patterns and sand/shale indicators from the gamma ray (GR) well logs were used to constrain the depositional setting and to support age determination where biostratigraphic evidence is limited (Galloway, 1989) (Fig. 3A). Internal characteristics of each seismic unit such as growth strata, lap relationships were included in the seismic interpretation to outline main periods of faults activity and quiescence.

Faults were interpreted and grouped into fault families based on the similar structural style, orientation and relative age. Time-thickness maps were created to determine variations in structural styles in the basin, including uplifted areas and main depocenters during the main episodes of fault activity.

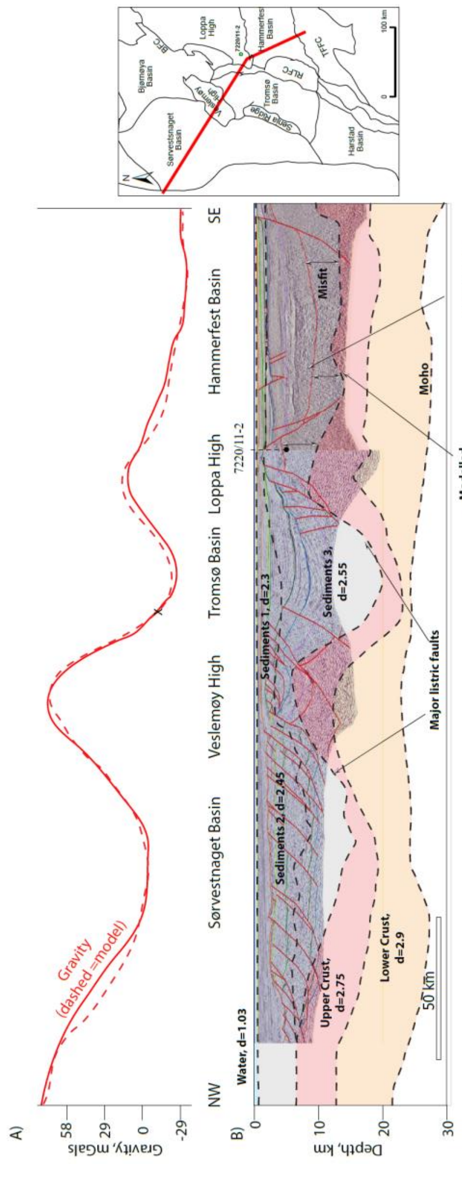

Figure 13 A) Gravity anomalies model along (B) composite regional 2D seismic sections. Coloured polygons represents areas with constant density, and correspond to the main sequence boundaries described in the seismic interpretation (grey, red and orange coloured polygons; Table 1). Note the differences between modelled (dashed line) and interpreted (red line) basement depth below the Loppa High and Hammerfest Basin. Regional profile and gravity modelling:

In order to understand the regional structural configuration around the Tromsø Basin, a composite 2D seismic section has been interpreted through the major structural elements of the SWBS (seismic sections in Fig. 4B). Seismic sections have been selected through areas that were not affected by salt diapirs. Two additional horizons below the Base Cretaceous unconformity have been included into interpretation of the regional section: (1) Top Paleozoic has been interpreted and correlated from the neighboring Hammerfest Basin (purple horizon in Fig. 4B; Indrevaer et al 2016, Gernigon et al., 2014); (2) Top Basement, which has been penetrated by several wells on the Loppa High, and tied to the closest projected (12 km) well 7220/11-2s (red horizon in Fig. 4B). Furthermore, the regional section and interpretations were depth converted using internal velocities obtained from check shot data of wells 7117/9-2 and 7119/7-1 for shallow parts, and from well 7119/9-1 for the deeper parts (Table 1).

In order to facilitate interpretation of deeper structures and delineate its lateral extent, a simple 2D free air gravity anomaly modelling was performed along the depth converted regional section (Fig.4A). Gravity modelling was performed using the GM-SYS Profile Modelling software from Geosoft (https://www.geosoft.com). A 2D model has been divided into constant density polygons corresponding to the main sequence boundaries described in the seismic interpretation (Table 1; grey, red and orange colored polygons on Fig. 4B). The average densities for sedimentary and crustal rocks are derived from the publication of Gernigon et al. (2014). Top-basement and Moho were used as main density contrasts in the lithosphere (Fig. 4B).

The results of the gravity anomalies modelling showed that the Moho depth is consistent with compilation of the crustal depths of Ritzmann et al. (2007) and therefore used as a reference contrast. Discrepancy occurred between modeled and actual (interpreted) basement depth below the Loppa High and Hammerfest Basin (dashed and red horizons in Fig. 4B). Adjustment of modelled basement depth to a shallower level would have resulted in offsetting the Moho depth to a deeper and more unrealistic results. Therefore, it has been decided to use the interpreted basement depth with the key assumption that basement rocks below the Loppa High and Hammerfest Basin are likely to have higher densities than modelled. Despite of the uncertainties in the gravity anomalies modeling, for the purpose of this study, it was much more important to constrain the sizes and geometries of the structures than to constrain the relative densities.

Table 1 Density polygons and stratigraphy for the gravity model, and interval velocities for depth conversion. Densities were obtained from publication of Gernigon e al. (2014). Interval velocities obtained from check shot data of wells 7117/9-2, 7119/7-1, and 7119/9-1.

Sedimentary unit	Stratigraphy	Velocity (m/s)	Density (kg/m3)
Water	Seafloor	1480	1,03
Sediment 1	Eocene and younger	1800	2,30
Sediment 2	Paleocene	1900	2,45
	Upper Cretaceous	2300	
Sediment 3	Lower Cretaceous	2775	2,55
	Jurassic/Triassic	3307	
	Paleozoic	4000	
Upper Crust	Basement	5000	2,75
Lower Crust			2,90

2D structural restoration:

A 2D structural restoration of a regional profile was performed to show the sequential evolution of the Tromsø Basin. 2D Move software (https://www.mve.com) was used to produce a 2D kinematic restoration. The workflow and methods consist of:

1. Erosion estimates, where missing sediments were restored on top of the section. This is important to compensate for isostasy due to sediment unloading. Missing sediments were given properties of the underlying stratigraphy.

2. Compaction and decompaction. The 2D compaction/decompaction tool in the software includes default compaction curves, which define different relationships between porosity and depth. The Sclater-Christie compaction curve were selected, as it is most appropriate for sandstones and mixed sedimentary sequences (Sclater and Christie, 1980). Compaction is only applied for missing sediments (eroded) in order to place removed sediments back and compensate for isostatic load. Decompaction was used sequentially for each restoration step by removing the uppermost sedimentary units. This is applied to correct for the effects of physical compaction in the sedimentary succession and vertically shift this part of the section to simulate an isostatic adjustment for each time-step. Flexural isostasy was applied to consider the isostatic response to sedimentary unloading during decompaction. Average values have been used for sediment (2400 kg/m3; Table 1) and mantle (3300 kg/m3; Robertson (1966)) densities, as well as elastic thickness (15000 m; Roberts et al. (1998)) and Young's modulus (70000 Mpa; Watts et al. (1982));

3. 2D unfolding has been applied extensively during restoration. This option allowed geological horizons to be restored to a pre-deformed stage. The horizons were unfolded using "Simple Shear" and "Flexural Slip" methods (Gibbs, 1983; Verrall, 1981; Withjack and Peterson, 1993). The Simple Shear algorithm is best suited for flattening a regional dip that does not dip too steeply, but the limiting factor with this algorithm is that line length is not preserved. The Flexural Slip algorithm works by rotating the limbs of a fold to a datum or assumed regional geometry. Layer parallel shear is then applied to the rotated fold limbs in order to remove the effects of the flexural slip component of folding. In the study area, Simple Shear and Flexural Slip Unfolding is carried out, following the restoration of the faulted displacement at the surface. Most of the normal faults indicate shear angle ranging between 60° and 90° and the main fold deformation is in the hanging wall side of the main

faults and are associated either with fault propagation folding or fault-ramp-faulting.

4. Fault reconstruction. This method use the "Fault Parallel Flow" algorithm (Egan et al., 1997), where offset horizons on hangingwall and footwall were restored to its pre-faulted levels. The Fault Parallel Flow algorithm subdivide the fault into discrete dip domains and flow lines, along which, hanging wall material moves, maintaining line-length and area.

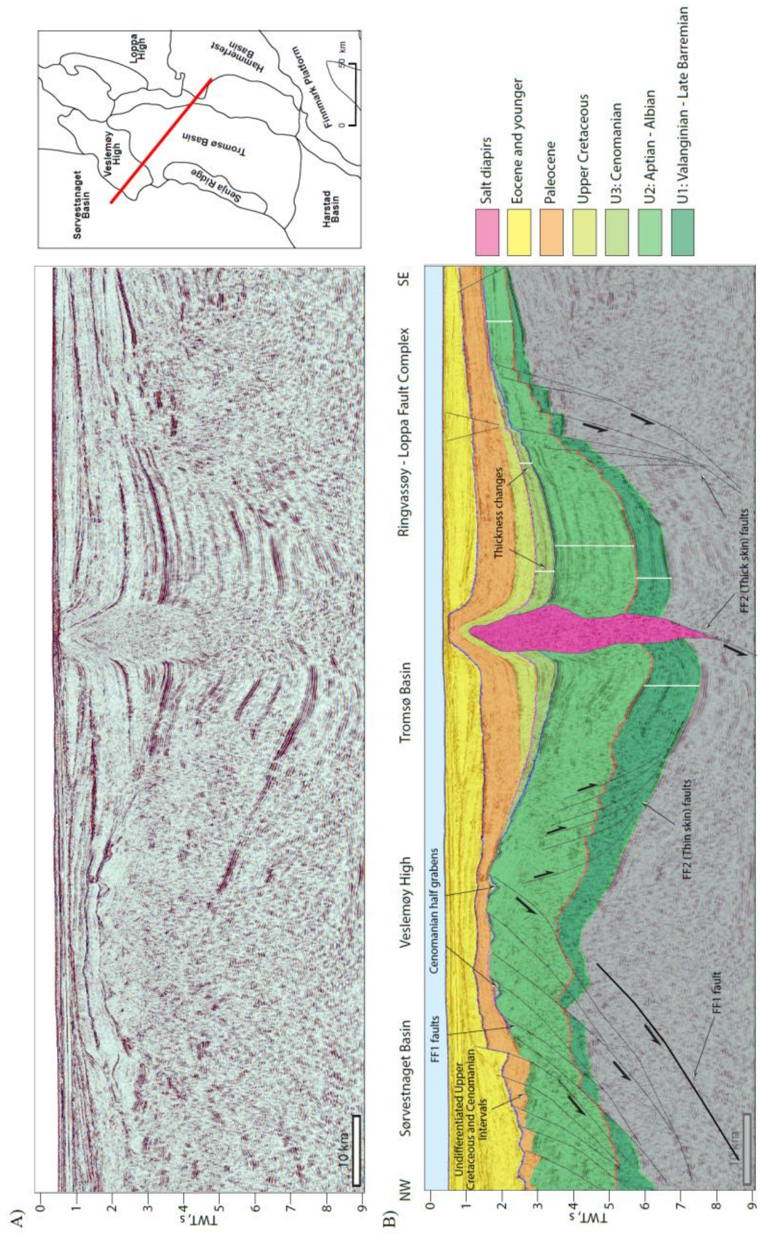

Figure 14 A) Un-interpreted and B) interpreted NW – SE seismic sections though the northern parts of the Tromsø Basin displaying basin configuration. Note distribution of main Lower Cretaceous sequences and interpreted fault families around the Veslemøy High and Ringvassøy-Loppa Fault Complex.

LOWER CRETACEOUS SEISMIC UNITS

Seismic unit 1 (U1): BCU – Late Barremian

Description. U1 has been penetrated by wells 7019/1-1, 7119/9-1 and 7220/10-1 in the eastern flank of the Tromsø Basin, where it is characterized by either very condensed (30 – 50 m) or missing pre – Barremian strata (Fig. 3A). The lower boundary of U1 is delimited by the BCU (green horizon; Figs. 5 – 10), which is represented by a high amplitude and continuous seismic event with an angular relationship to its underlying reflectors (Figs. 5A and 5B). The upper boundary is marked by a prominent continuous seismic event that correspond to the Late Barremian horizon (red horizon; Figs. 5B and 8B). Internally, it is characterized by a discontinuous and sometimes chaotic seismic reflectors in the southern part and by continuous, parallel and divergent reflectors in the northern part of the basin (Figs. 7A and 7B).

This seismic unit was deposited in the central part of the basin and thins out towards the margin (e.g. Veslemøy High and Senja Ridge; Figs. 5B and 6B). Local and segmented depocenters with maximum thickness of up to 2 seconds (TWT) are observed along the axis of the basin (Fig. 11A).

Interpretation. This unit is interpreted as early syn-tectonic deposition as suggested by the presence of growth strata and wedge-like geometry (Figs. 5B and 6B). Condensed and missing pre-Barremian strata along the eastern flank support active tectonic settings (wells 7019/1-1 and 7220/10-1; Fig. 3A). Previous interpretation from wells 7120/10-2, 7019/1-1 and 7220/10-1 in the same interval suggest turbidite and outer shelf deposits distributed along the eastern margin of the basin, in the Hammerfest Basin, Finnmark Platform and Loppa High (Fjeld and Escalona, 2014; Marin et al., 2017a; Marin et al., 2017b; Seldal, 2005). Therefore, distal equivalents of these sediments might have been deposited in depocenters, in the central part of the Tromsø Basin.

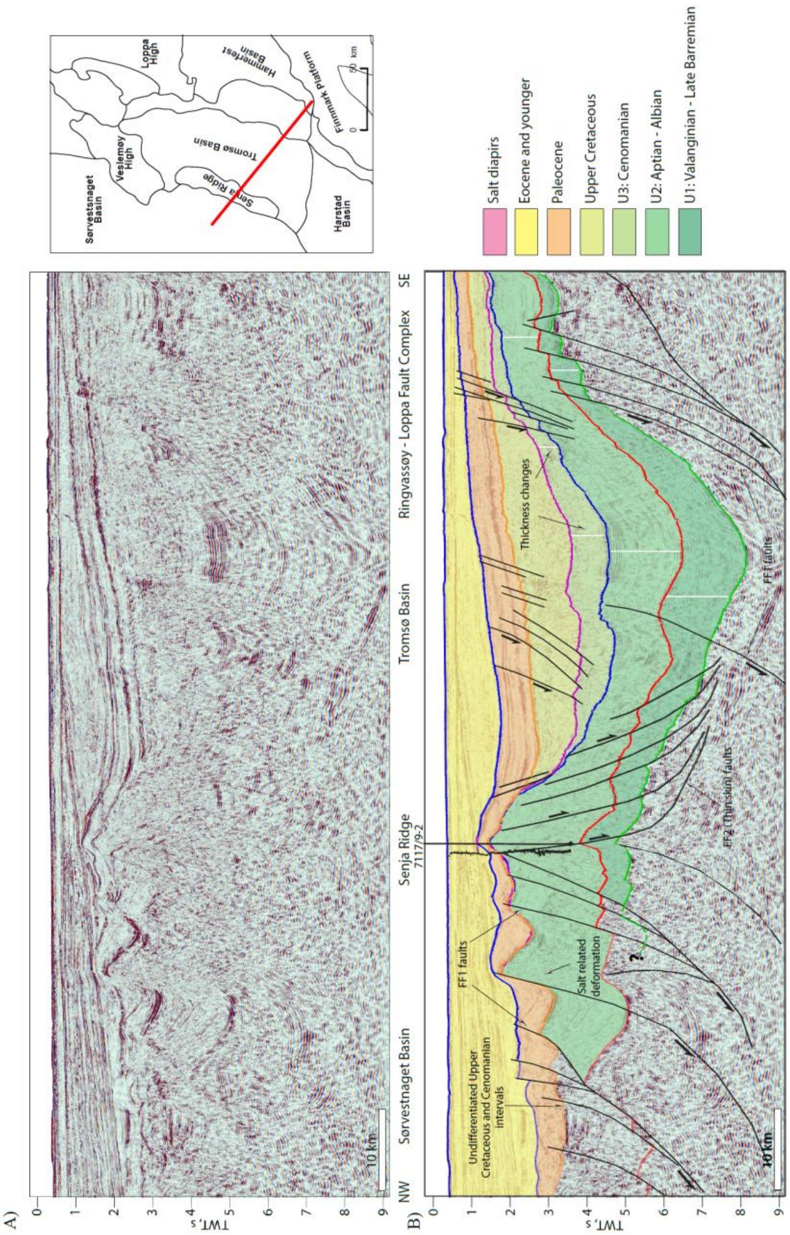

Figure 15 A) Un-interpreted and B) interpreted NW – SE seismic sections though the southern parts of the Tromsø Basin displaying basin configuration. Note distribution of main Lower Cretaceous sequences and interpreted fault families around the Senja Ridge and southern extent of the Ringvassøy-Loppa Fault Complex.

Seismic unit 2 (U2): Aptian – Albian

Description. The GR pattern for this interval is spiky and irregular with relatively higher values than in U1, and well reports and previous publication suggest main lithology consists of siltstone and claystone rocks (Fig. 3A) (Fjeld and Escalona, 2014; Marín et al., 2017a; Marin et al., 2017b; Seldal, 2005).

The lower and upper boundaries of the U2 are limited by Late Barremian and Late Albian horizons, which are characterized by very prominent continuous high amplitude seismic events (red and dark blue horizons; Figs. 5 – 10). Internally, this unit is characterized by discontinuous to chaotic seismic reflectors in the southern part (Fig. 7B); and by relatively continuous, parallel and divergent reflectors in the northern part of the basin (Figs. 5B and 8A). Downlap on the underlying seismic unit U1 (Late Barremian horizon) and growth strata in the lower part of the U2 are locally observed in the northern part of the basin, along the southwestern terraces of the Loppa High (Fig. 8A). Furthermore, in the upper part of the U2, several packages of divergent reflectors that downlap on continuous high amplitude reflectors are observed along salt diapirs in the central part of the basin (Fig. 8B). The external geometry of these packages resemble wedge-like shape that are stacked along salt walls (Fig. 8B). This seismic unit 2 distributed in entire basin and is characterized by a thick, wedge-shape sedimentary package (Figs. 5B and 6B). The northern part of the basin serves as a main depocenter with maximum thickness reaching 3 s (TWT) (Fig. 11B).

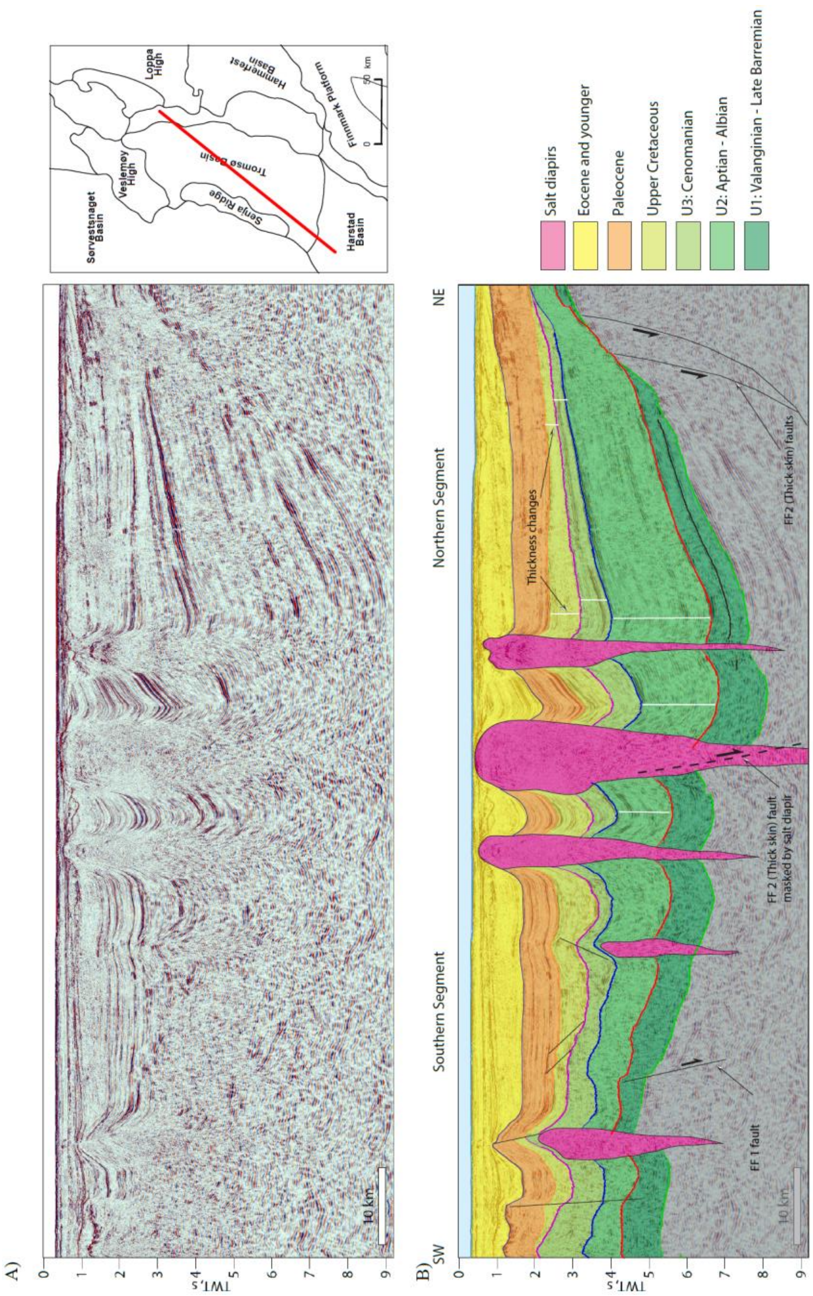

Figure 16 A) Un-interpreted and B) interpreted NE – SW seismic sections though the basin axis of the Tromsø Basin. Note distribution of main Lower Cretaceous sequences and interpreted fault families. Salt diapirs most likely masking some faults of FF2

Interpretation. U2 is interpreted as the main syn-tectonic period, as suggested by the presence of growth strata and thickening of this interval towards the main faults (Figs. 4A and 5B). Abrupt changes in the thickness of U2 along the margins also support active tectonism (Fig. 6B). Divergent reflectors packages along salt diapirs flanks are interpreted as peridiapiric wedges (Rojo and Escalona (2018); Fig 8B). They indicate periods of salt movement towards the end of the U2 (Albian) that may have caused the uplifts along the axis of the basin. Previous interpretations from wells 7120/10-2, 7019/1-1 and 7220/10-1 on the same interval suggest shallow shelf deposits with clastic wedges along downfaulted terraces of the Hammerfest Basin, Finnmark Platform and Loppa High (Fjeld and Escalona, 2014; Marin et al., 2017a; Marin et al., 2017b; Seldal, 2005). Therefore, a deeper or distal depositional environment is suggested for the Tromsø Basin with exposed and isolated domal structures related to upward movement of the salt diapirs.

Seismic unit 3 (U3): Cenomanian

Description. U3 is composed of relatively thin (20 – 70 m) interval that has been penetrated by all wells in the Tromsø Basin. The main lithology consists of siltstone and claystone rocks with occasional dolomite stringers (Fig. 3A). The GR pattern is relatively consistent with lower values compared to U2 (Fig. 3A).

The lower and upper boundaries of U3 are constrained by Late Albian and Cenomanian horizons, which are represented by continuous, high amplitude seismic events (purple and dark blue horizons; Figs. 5 – 10). Internally, this unit is characterized by discontinuous and sometimes chaotic seismic reflectors in the southern part and by continuous, parallel and divergent high amplitude reflectors in the northern part of the basin ((Figs. 7A and 7B). Laterally, U3 thickens towards the central part of the basin and pinches out against the margins (Figs. 5B and 6B). Seismic packages with wedge shape geometries are observed in the small half grabens on the Veslemøy High (Fig. 5B and 10B). This unit is mostly distributed in the central and southern parts of the Tromsø Basin with a southwestward increase in thickness, where it reaches a maximum of 2 seconds (TWT) (Fig. 11C).

Interpretation. The U3 is interpreted as syn-tectonic deposition, as supported by the presence of growth strata and wedges towards the axis of the basin (Figs. 5B and 6B). Based on the abundance of siltstones and dolomites, an outer shelf (open marine) depositional environment is suggested for this period.

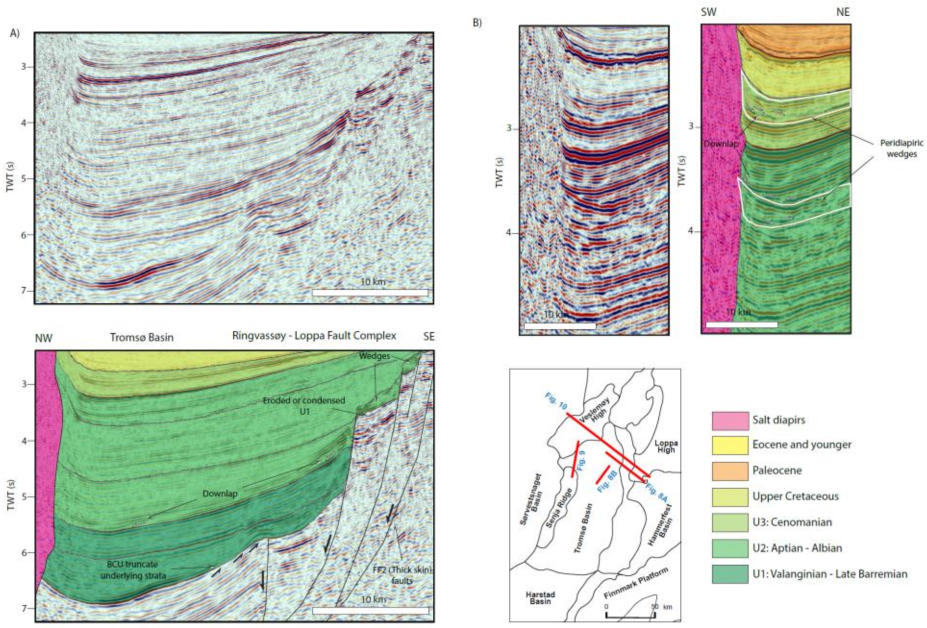

Figure 17 A) Un-interpreted and interpreted NW – SE section along terraces of the Ringvassøy – Loppa Fault complexes illustrating detailed seismic configurations of the interpreted Lower Cretaceous units; B) Un-interpreted and interpreted NE – SW section showing peridiapiric wedges stacked along salt walls.

FAULTS

Three main fault families (i.e. faults with similar structural style, strike and age) affecting the Lower Cretaceous units are interpreted in the study area. Most these faults are interpreted as thick skin basement involved faults, but some thin skin faults were also recognized.

Fault family 1 (FF1) consists of a series of NE–SW striking faults interpreted in the northern and southern parts of the Tromsø Basin (Fig. 12). The lateral extent of these faults is interpreted as a part of the southern segments of the Bjornøyrenna and Troms-Finnamrk fault complexes (Fig.12). These faults are characterized as normal faults, which are interpreted along the Veslemøy High and Senja Ridge, and the southern segments of the Ringvassøy-Loppa Fault Complex (Figs. 5B and 6B). Faults are almost planar for the Paleocene and Cretaceous intervals, but have a listric expression at depth, where they merge into a low-angle plane below 5 - 6 s (TWT) (Fig. 6B). Horizon offset varies from approximately 300 to 500 ms (TWT), with a maximum in the Late Barremian horizon (Fig. 6B). Interpreted growth packages in the Lower Cretaceous U1 and U3, as well as in the Upper Cretaceous and Paleocene indicates fault activity during these periods (Figs. 5B and 6B).

Fault family 2 (FF2) comprises N–S striking normal faults interpreted in the central part and along the eastern flank of the Tromsø Basin (Fig. 12). FF2 consist of (1) thick and (2) thin skin fault systems:

(1) Thick skin faults are interpreted as a normal faults along the eastern boundary of basin (Fig. 8A). These faults are almost planar for the Paleocene and Cretaceous intervals, and become low-angle below 8 - 9 s (TWT) (Figs. 5B). The maximum offset of ca. 400 ms (TWT) observed at the Late Barremian horizon (Fig. 5B). Fault activity is supported by several growth and wedge shape seismic packages observed in the Lower Cretaceous seismic units U1, U2 and U3 (Figs. 5B and 6B). West facing faults of FF1 interpreted as a part of the west-facing Ringvassøy – Loppa

Fault Complex (RFLC) that separates the Tromsø Basin from the Loppa High and the Hammerfest Basin. Laterally, these faults are straight to slightly curved including some en echelon fault segments with various degree of linkage, from soft-links via relay ramps to hard-links (Fig. 12). A few faults are interpreted in the central part of the basin and are masked by salt diapirs, therefore defining their age and amount of displacement is problematic (Figs. 6B and 7B).

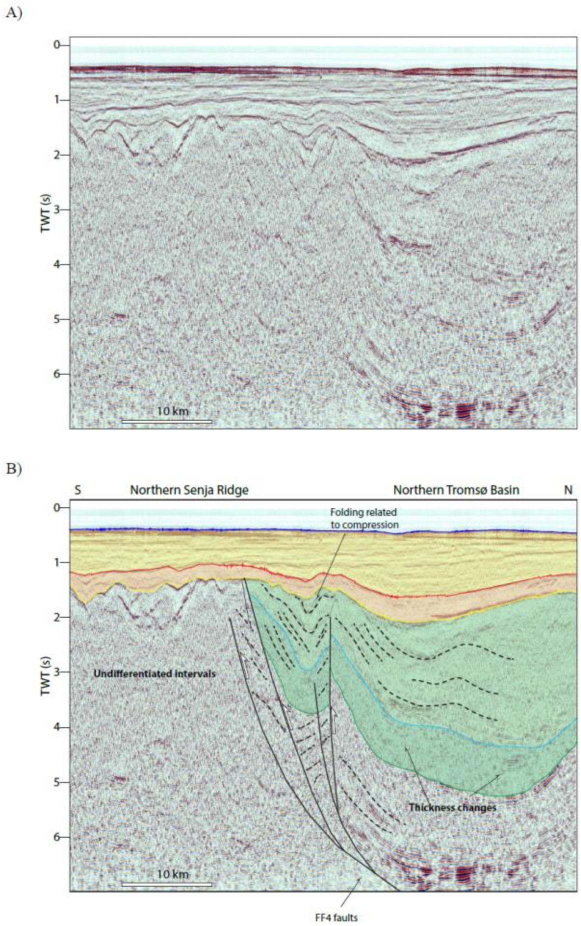

Figure 18 A) Un-interpreted and B) interpreted N – S seismic sections between northern Senja Ridge and Veslemøy High. Interpreted asymmetric folds with a long limb dipping to the south were formed in response to the reverse movement of FF4 faults. Please refer to Figure 8 for colour legend and location.

(2) Thin skin faults of FF2 consist of normal faults observed along the eastern flank of the Veslemøy High and Senja Ridge. These east-facing faults are only developed within the Lower Cretaceous U1 and U2, and detach at the BCU horizon and Upper Jurassic interval (Fig. 5B). The amount of offset at the late Barremian horizon fluctuates between 10 – 25 ms (TWT) (Fig. 5B). Fault activity most likely occurred during the Albian stage, since all these faults are tipping out towards the end of U2.

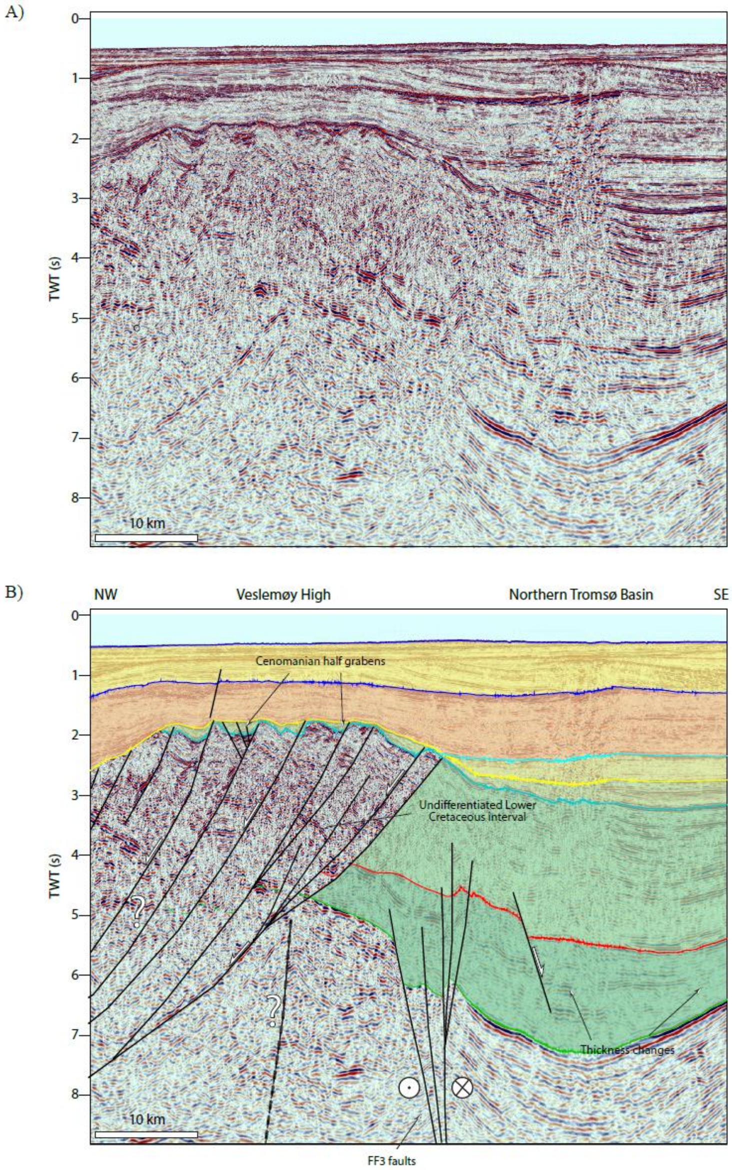

Figure 19 A) Un-interpreted and B) interpreted NW – SE seismic sections along the Veslemøy High. Note interpreted strike slip fault of FF3, left lateral movement is suggested from eastward lateral extension of these faults that coincide with compression and strike slip faults observed on the Polhem Sub Platform and the Loppa High (e.g. Indrevaer et al., 2016; Gabrielsen et al., 2011; Omosanya et al., 2019; Ahlborn et al., 2014). Please refer to Figure 8 for colour legend and location.

Fault family 3 (FF3) consists of several E – W striking faults that were interpreted under the Veslemøy High (Fig. 12). These faults steepened with depth and form positive flower-like structure that tips at the Cretaceous strata (Fig. 10B). Minor growth and wedge shaped seismic packages towards faults were observed in the Lower Cretaceous U1 and U2, suggesting main periods of fault activity (Fig. 10B). These faults are interpreted as strike slip faults, and eastward lateral extension of these faults are coincide with compression and strike slip faults observed on the Polhem Sub Platform and the Loppa High (Ahlborn et al., 2014; Indrevær et al., 2016; Omosanya et al., 2017) (Fig. 12). These strike slip faults have left – lateral movement that support by changed fault polarities east dipping FF2 to west dipping FF1 across the strike of FF3 (Fig. 12), and displaced structural lineaments on the Polhem Sub Platform (e.g. tilt derivative map of Gernigon et al., 2014) and Loppa High (e.g. Swaen Graben; Omosanya et al., 2017).

Fault family 4 (FF4) include WNW-ESE-striking faults that are observed only along the northern tip of the Senja Ridge (Fig. 12). These faults are interpreted as a steep reverse faults that tip or truncated at the Paleocene strata and become listric at depth (Fig. 49B). It is difficult to examine the lateral extent of these faults due to salt diapirs along the axis of the basin (Fig. 12). Interpreted asymmetric folds with a long limb dipping to the south were formed in response to the reverse movement of these faults. The largest offset observed at BCU horizons with ca. 400 ms (TWT). Growth sequences and wedge-shaped packages are interpreted at the Lower Cretaceous seismic units U1 and U3; and Paleocene intervals indicating main faults activity, which may have triggered the uplift of the northern part of the Senja Ridge (Fig. 9B).

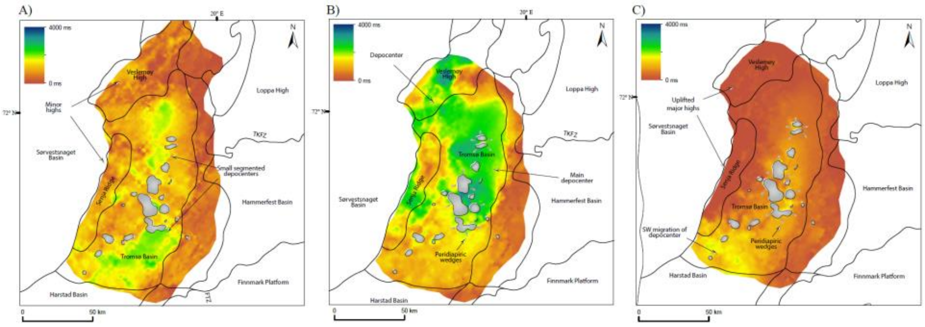

Figure 20 Series of time thickness maps of the Cretaceous units. A) Valanginian – Late Barremian shows early segmentation and isolated depocenters. Note that Veslemøy High and Senja Ridge uplift during this period. B) Aptian - Albian shows segmentation of the basin into a northern and southern segments, where northern segment is a major depocenter. This period is also associated with movement of the salt diapirs (grey arrows). C) Cenomanian shows shift of the depocenter towards southernmost parts of the Tromsø Basin. Note that during this period the Senja Ridge and Veslemøy High experienced major inversion and uplift. Salt movement also affecting this unit.

2D STRUCTURAL RESTORATION

Six restored steps reproduce the geological evolution of the Tromsø Basin from the Early Cretaceous until present (Figs. 13A – 13F). Furthermore, restored sections were grouped into three stages: (1) Pre – Cretaceous basin configuration, (2) Early Cretaceous and (3) post – Early Cretaceous evolution. Emphasis were given to basin geometry; timing of major fault activity; depocenter distribution; and the amount of extension honoring the data and interpretation as much as possible. Although, the pre and post Early Cretaceous history are not the main objective, they were included to highlight important episodes of the margin evolution, which may have implication to the Early Cretaceous evolution.

Stage 1. Pre-Cretaceous basin configuration

The early regional tectonic events during Permian – Carboniferous and Jurassic – Triassic marked the location of the proto Tromsø Basin with up to 15 km thick sediment sequences overlying basement (Fig. 13F). Until the end of the Late Jurassic, Tromsø and Sørvestnaget basins were a formed a single basin dominated by west facing listric faults of FF2 along the Loppa High (Fig. 10F). The SWBS margin was 35 km narrower compared to present day. Main uncertainties with the Late Jurassic – BCU restoration step were related to the poor seismic imaging below 7 seconds (TWT) and absence of well control to the NW of the Loppa High (Fig. 3B). Therefore, interpretation was speculative and primarily based on seismic reflection configuration and gravity modelling (Fig. 4B).

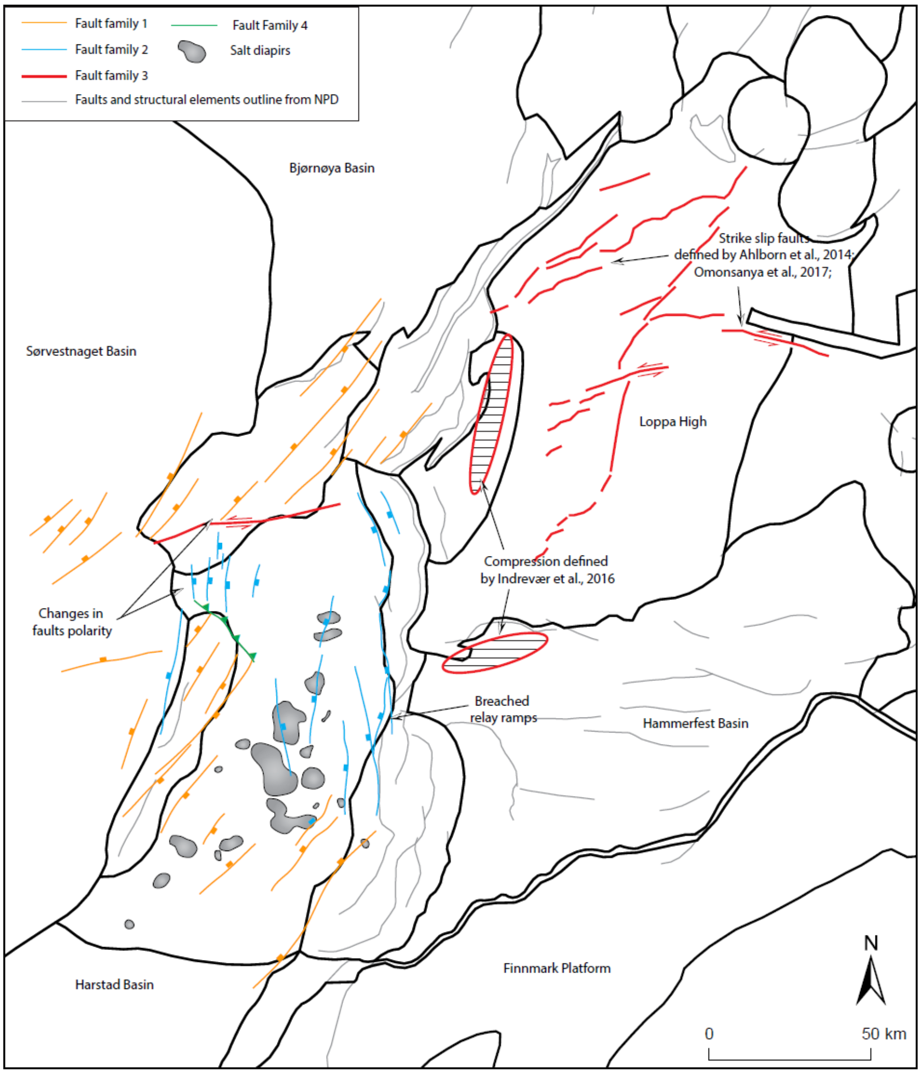

Figure 21 Fault interpretation maps. Location and subdivion of main interpreted fault families. Note interpreted strike slip fault on the Loppa High adapted from previous works of Indrevaer et al., 2016; Gabrielsen et al., 2011; Omosanya et al., 2019; Ahlborn et al., 2014. Location of proposed transfer zones in the North of the Tromsø Basin (red polygon) is coincide with westward lateral extent of the previously defined strike faults.

Stage 2. Early Cretaceous evolution

This stage includes two restoration steps: (1) Late Barremian and (2) Cenomanian (Figs. 13D and 13 E). The Late Barremian step corresponds to the Lower Cretaceous seismic unit U1 (Fig. 13E). The main depocenter observed along the Veslemøy High (Fig. 13E). At this step, the margin extended up to 13 km from Late Jurassic, where most of the displacement of 150 – 200 m was accommodated by faults of FF1 and FF2 along the western boundary of the Tromsø Basin (Fig. 13E). Minor compression might have been accommodated by sinistral strike slip movement along FF3 fault, which triggered the slight uplift of the Veslemøy High and resulted in the division of the Tromsø and Sørvestnaget basins at this time (Figs. 10B and 13E). Continues rifting led to additional extension of the margin by 9km during the Lower Cretaceous U2 and U3 step (Fig. 13D), increase subsidence led to bypass the Veslemøy High, and as the result, the Sørvestnaget and Tromsø basins acted as a single basin capturing up to 7 km of the Lower Cretaceous sediments (Fig. 13D). The main fault activity migrated towards the eastern margin of the Tromsø Basin, where the Ringvassøy – Loppa fault complex accommodated the main displacement of 300 – 400 m (FF2) (Fig. 13D). At this step, the margin extended up to 9 km more from Late Barremian step (Fig. 9D). It is suggested that some of this extension possibly attenuated by the Cenomanian (U3) inversion of FF3 and FF4 (Figs. 9B and 10B), that resulted in uplift of the Veslemøy High and northern Senja Ridge, and consequently reinforced the isolation of the Tromsø from the Sørvestnaget basins (Fig. 4A).

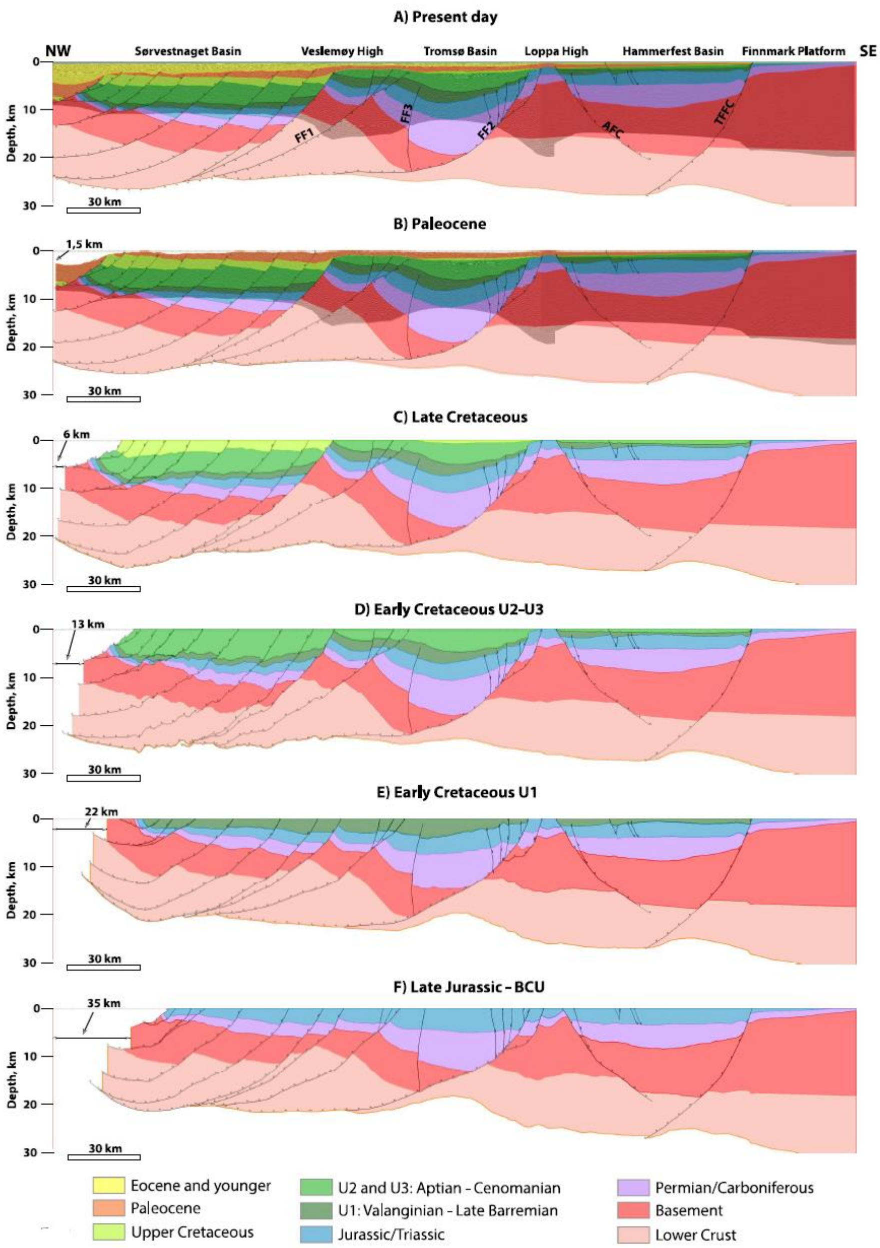

Figure 22 2D structural reconstruction of crustal cross section. Six restoration steps (A – F) are represent the geological evolution of the Tromsø Basin from the Early Cretaceous until present. For location of the line is see Figure 4.

Stage 3. Post Early Cretaceous evolution

This stage contains three restoration steps: (1) Late Cretaceous, (2) Paleocene and (3) Present day (Figs. 13A – 13C).

During the Late Cretaceous, most of the faulting occurred along the western flanks of the Veslemøy High (Fig. 13C). At this time, the margin extended up to 7 km from Cenomanian step, where major displacement of 800 m was accommodated by west facing listric faults of FF1 along the western flank of the Veslemøy High (Figs. 5B and 13C). Footwall uplift of the Veslemøy High resulted in erosion and degradation, as well as separation of the Sørvestnaget and Tromsø basins, where former were considered as main depocenter (Fig. 13C). The Paleocene step is characterized by ongoing faulting of FF1 along the Veslemøy High resulting to additional 4,5 km of extension (Fig. 13B). The Sørvestnaget Basin was still a major depocenter at this time containing up to 5 km of sediments (Fig. 13B). Most of the faulting occurred in the Sørvestnaget Basin, while the Tromsø Basin was relatively passive (Fig. 13B). Onlap and thinning of the Paleocene seismic reflectors suggest that Veslemøy High continued to uplift at least during initial period of this step (Figs. 6B and 10B). At the present day step (Eocene and younger), the margin extended 1,5 km (Fig. 13A). Main deformation at this time occurred to the West of the Sørvestnaget Basin, therefore the study area was only subjected to a minor extension (Fig. 13A). The main depocenter shifted towards the continent oceanic boundary.

DISCUSSION

Proposed evolutionary model

Most of the plate tectonic restorations in the North Atlantic margin from 145 Mya until 55 Mya, suggest that the SW Barents Sea was adjacent to the NE offshore Greenland (Barnett-Moore et al., 2018; Doré et al., 2015; Seton et al., 2012), and NE-SW structural lineaments were predominant in both margins. Latest compilation and comparison of various plate models suggest that main extension directions were orthogonal to the main NE-SW structural lineaments at least during the Early Cretaceous (e.g. plate flowlines of Barnett-Moore et al. (2018); Fig. 14A).

Structural evolution of the Tromsø Basin during the Early Cretaceous was vastly controlled by the NE-SW trending regional TFFC and BFC, which interpreted as FF1 in the study area (Fig. 14A and 14B). In contrast to FF1, the N-S striking FF2 is limited to the extent of the basin (Fig. 12), and most likely represent intra rift fault system (McClay et al., 2004; McClay et al., 2002). Presence of en echelon faults of FF2, which generated breached relay ramps along the western border of the Tromsø Basin, suggest that basin may have evolved in oblique manner (Fig. 12) (Agostini et al., 2009; Brune and Autin, 2013; Clifton et al., 2000; Corti, 2008; Withjack and Jamison, 1986). Oblique opening of the Tromsø Basin is also supported by the interpreted by strike slip faults of FF3 (Fig. 10B), which determine location of the intra basin transfer zone that responsible of changes in faults polarities of FF1 and FF2 (e.g. Corti, 2008; Mc Clay et al., 2002; Fig. 12).

Based on timing of fault activity and kinematics, it is suggested that the Tromsø Basin experienced three major episodes of deformation: (1) Valanginian – Late Barremian; (2) Aptian – Albian; and (3) Cenomanian.

1)Valanginian – Late Barremian (U1): Ongoing rifting

Wells 7220/10-1 and 7019/1-1 located along the eastern margin of the Tromsø Basin indicate a condensed or absent Lower Cretaceous unit U1, suggesting that these areas were uplifted during rifting (Figs. 3A and 3B). Most of the Valanginian – Late Barremian extension was accommodated by west facing boundary faults of FF1 (Figs. 5B; 6B and 14A). Isolated depocenters along the axis of basin suggest on complex interaction between faults of FF1 (e.g. fault segments of TFFC and BFC), which resulted in formation of internal fault system of FF2 (Fig. 12). The N-S strike of FF2 that outline the WSW extent of the Loppa High suggest that basement heterogeneity possibly guided formation of FF2 by localizing strain (Baudon and Cartwright, 2008; Nicol et al., 2005; Richard and Krantz, 1991).

At this stage, the Veslemøy High and Senja Ridge were characterized as minor structural features that separated the Tromsø from Bjørnøya and Sørvestnaget basins (Figs. 6B and 13E). Onset of complex tectonic interaction between the Veslemøy High and northern Senja Ridge occurred through left lateral movement along faults of FF3 resulting in transpressional setting and slight uplift of the Veslemøy High (Figs. 9B and 10B). Previously, based on structural evolution of the neighboring Hammerfest Basin, it has been suggested that this episode comprises two rifting phases, Berriasian – Valanginian and Hauterivian – Barremian (Faleide et al. (1993)). However, considering the poor seismic imaging below 5 seconds (TWT) and the lack of well control in the deeper parts of the Tromsø Basin, these tectonic phases cannot be neither confirmed nor excluded.

2) Aptian – Albian (U2): Rift culmination

Major extension was accommodated by the intra basin faults of FF2 (e.g. RLFC; Figs. 12 and 14B). This is also supported by a large depocenter in the northern part of the Tromsø Basin (Fig. 11B). Towards the end of this stage, possible during Albian – Cenomanian, complex tectonic settings between the Veslemøy High and the northern Senja Ridge resulted in uplift of both (Fig. 14B). Previously, formation of the Senja Ridge and Veslemøy High as positive structural features were attributed to either sinistral or dextral strike-slip movement along Bjørnøyrenna Fault Complex (Figs. 2A and 2B; Gabrielsen and Færseth, 1988; Riis et al., 1986). Our study suggest that uplift is most likely caused by the transpressional settings along FF3, which is also responsible for formation of compressional structures and faults of FF4 (Fig. 9B). One plausible explanation could be that during transpressional conditions, the strike-slip (e.g. FF3; Fig 10B) and dip-slip (e.g. FF4; 9B) components accommodated on separate but relatively parallel structures (e.g. the Veslemøy High and northern Senja Ridge; Fig. 12), whilst decoupling possibly occurred at pre Cretaceous sequences. Transpressional deformation along transfer zone is most likely related to the oblique opening of the Tromsø Basin, where basement heterogeneity localized strain distribution. Furthermore, towards the end of this stage, rapid increase of subsidence and differential loading triggered salt movement that have resulted in diapirism in the central part of the basin and development of the halokinetic sequences (Fig. 8B).

3) Cenomanian (U3): Post rift deformation and inversion

This episode is considered as tectonically quiescent in the central and eastern parts of the basin (Fig. 14C). Most the of the fault activity (FF1) occurred in the western and northwestern flanks of the Tromsø basin (Fig. 13C). Pinching out of the Lower Cretaceous unit U3 against the Veslemøy High and the Senja Ridge suggests that these structures were uplifting (Figs. 5B and 6B). Uplift is suggested to be caused by the same transpressional conditions along FF3 and FF4 (Fig. 9B) (Blaich et al., 2017; Breivik et al., 1998; Brekke and Riis, 1987; Riis et al., 1986). The uplift of Senja Ridge and Veslemøy High caused the isolation of the Tromsø Basin from the Sørvestnaget Basin during this time (Fig. 14C).

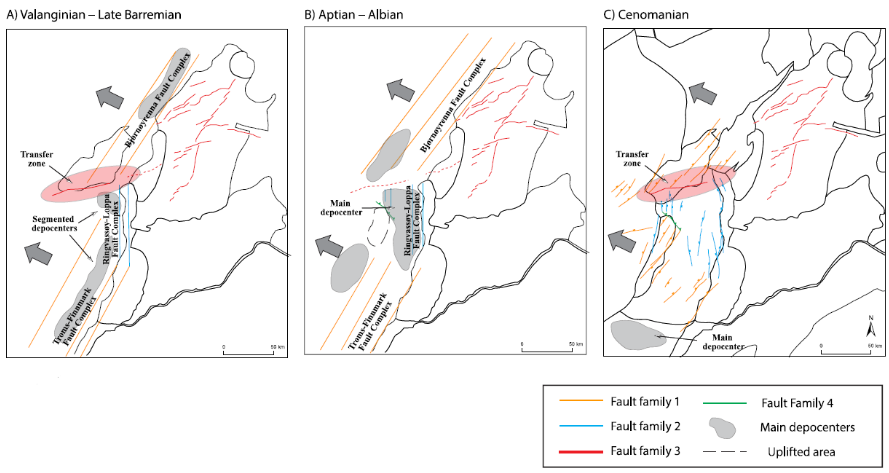

Figure 23 Proposed structural evolutionary model of the Tromsø Basin during Early Cretaceous: A) Valanginian – Late Barremian extension was accommodated by west facing boundary faults of FF1 (e.g. fault segments of TFFC and BFC), which resulted in formation of internal fault system of FF2; B) Aptian – Albian marked by a transpressional settings along transfer zone which is related to the oblique opening of the Tromsø Basin, where basement heterogeneity most likely localized stress and strain distribution; and C) Cenomanian episode is considered as tectonically quiescent, where most the of the fault activity occurred in the western and northwestern flanks of the Tromsø basin.

Margin extension and crustal thinning

The constructed crustal section through the Tromsø Basin is considered to be the most representative of the direction of extension for the SWBS margin. It is almost perpendicular to the major structural elements (Fig. 4B). Constructed and subsequently restored section resembles the "boundinage" model of Gernigon et al., 2014 (Fig. 2C), where the origin of the listric faults (e.g. FF1) is suggested to be the remnants of Caledonian thrust faults that reactivated in response to rifting (Gernigon et al., 2014). The Early Cretaceous reactivation most likely caused backsliding of the Caledonian thrust and triggered upward propagation of fault segment from pre-existing basement faults (Baudon and Cartwright, 2008; Nicol et al., 2005; Richard and Krantz, 1991). The result of sequential restoration suggests that these faults were responsible for 35 km margin extension from the Earliest Cretaceous to the present day (Figs. 13A – 13F). Previous work by Breivik et al. (1998) estimated a post-middle Jurassic extension of 70 – 85 km. Such discrepancies most likely related to calculation methods, where our calculations of 35 km of extension over such time interval seems reasonable and more reliable. Based on the modelled depths of the basement and Moho (Figs. 4 and 13A), post-rift crustal thickness below the Tromsø Basin reaches minimum of 8 km. Assuming that the original pre-rift crustal thickness was 30 – 35 km (Barrère et al., 2009; Clark et al., 2013; Ritzmann and Faleide, 2007), and after dividing pre-rift by post-rift crustal thicknesses we estimated a cumulative crustal thinning (β) factor of 3,7 – 4,4 and 2,9 – 3,1 below the Tromsø and Sørvestnaget basins since the BCU. The calculated β factor is consistent with previous estimation by Breivik et al. (1998) for the Tromsø Basin (β factor of ca.4). Globally, the β factors of rifted margins generally increase towards the continent–oceanic boundary (COB), where the maximum crustal thinning is usually occurs at the location of breakup (Crosby et al., 2011; Montési and Behn, 2007). In case of SWBS, crust is thinner below the Tromsø Basin as compared to a Sørvestnaget Basin, which is relatively closer to a COB. Therefore, common characteristics for rifted margins (Peron-Pinvidic et al. 2013), where crust thins towards the distal domains is not applicable for the SWBS margin. This difference can be attributed to a transform or oblique nature of the Early and post – Early Cretaceous extension in the SWBS, where increase in obliquity of rifting may decrease crustal thinning and stretching towards the continental breakup (Montési and Behn, 2007). This is also advocating to the oblique opening of the Tromsø Basin. Moreover, high crustal thinning (β factor of 3) is observed below the Bjørnøya Basin by Clark et al. (2013) and Gernigon et al. (2014), which suggest that both Tromsø and Bjørnøya basins may have similar origin and were influenced by the same tectonic regimes.

CONCLUSIONS

- The Early Cretaceous evolution of the Tromsø Basin is influenced by the inherited basement structures from the Caledonian orogeny. The presence of west facing low angle detachment faults below the Tromsø Basin supports the idea of post orogenic collapse of Caledonian thrust sheets, that were periodically reactivated or backslided in response to an Early Cretaceous extensional episode.

- The proposed structural model for the Early Cretaceous evolution involve oblique opening of the Tromsø Basin and formation of the intra basinal transfer zone with compressional strike slip faults (Figs. 13A – 13C). This model differs from any previously proposed models and partially resembles both Faleide et al. (1993) and Gernigon et al., (2014) models (Figs. 2B and 2C).

- Extension of 35 km is proposed for the SWBS margin since the Earliest Cretaceous. Among the Cretaceous extensional episodes, the Valanginian – Late Barremian is considered as the period of major crustal extension (13 km) in the SWBS margin (Figs. 13E and 13F). During most of the Early Cretaceous, the Sørvestnaget and Tromsø basins were a single large basin and were separated by activity of FF3 and FF4 faults, resulting in the uplift of the Veslemøy High and northern Senja Ridge.

- Distribution of the crustal thinning (β factor) in the SWBS is unlike for common rifted margins. Crust below narrow and confined Tromsø Basin is suggested to be thinner than in the Sørvestnaget Basin. This supports that the Early Cretaceous rift in the Tromsø Basin involved certain degree of obliquity.

ACKNOWLEDGEMENT

This study is part of the industrial sponsored LoCrA consortium (http://locra.ux.uis.no). We would like to express our gratitude to DISKOS database and MultiClientGeophysical AS for providing 2D seismic data and allowing to publish them. In addition, we are thankful to Halliburton-Landmark and Move for providing the software and license.

REFERENCES

Agostini, A., Corti, G., Zeoli, A., Mulugeta, G., 2009. Evolution, pattern, and partitioning of deformation during oblique continental rifting: Inferences from lithospheric-scale centrifuge models. Geochemistry, Geophysics, Geosystems 10.

Ahlborn, M., Stemmerik, L., Kalstø, T.-K., 2014. 3D seismic analysis of karstified interbedded carbonates and evaporites, Lower Permian Gipsdalen Group, Loppa High, southwestern Barents Sea. Marine and Petroleum Geology 56, 16-33.

Århus, N., Kelly, S.R.A., Collins, J.S.H., Sandy, M.R., 1990. Systematic palaeontology and biostratigraphy of two Early Cretaceous condensed sections from the Barents Sea. Polar Research 8, 165-194.

Atwater, T., Stock, J., 1998. Pacific-north america plate tectonics of the neogene southwestern united states: An update. International Geology Review 40, 375-402.

Badley, M.E., Price, J.D., Dahl, C.R., Agdestein, T., 1988. The structural evolution of the northern Viking Graben and its bearing upon extensional modes of basin formation Journal of the Geological Society (London) 145, 18.

Barnett-Moore, N., Müller, D.R., Williams, S., Skogseid, J., Seton, M., 2018. A reconstruction of the North Atlantic since the earliest Jurassic. Basin Research 30, 160-185.

Barrère, C., Ebbing, J., Gernigon, L., 2009. Offshore prolongation of Caledonian structures and basement characterisation in the western Barents Sea from geophysical modelling. Tectonophysics 470, 71-88.

Baudon, C., Cartwright, J., 2008. The kinematics of reactivation of normal faults using high resolution throw mapping. Journal of Structural Geology 30, 1072-1084.

Bell, R.E., McNeill, L.C., Bull, J.M., Henstock, T.J., Collier, R.E.L., Leeder, M.R., 2009. Fault architecture, basin structure and evolution of the Gulf of Corinth rift, central Greece. Basin Research 21, 824-855.

Berglund, L.T., Augustson, J., Faerseth, R., Gjelberg, J., Ramberg- Moe, H., 1986. The evolution of the Hammerfest Basin. Habitat of hydrocarbons on the Norwegian continental shelf. Proc. conference, Stavanger, 1985, 319-338.

Blaich, O.A., Tsikalas, F., Faleide, J.I., 2017. New insights into the tectono-stratigraphic evolution of the southern Stappen High and its transition to Bjørnøya Basin, SW Barents Sea. Marine and Petroleum Geology 85, 89-105.

Braathen, A., Maher Jr, H.D., Haabet, T.E., Kristensen, S.E., Tørudbakken, B.O., Worsley, D., 1999. Caledonian thrusting on Bjornoya: Implications for Palaeozoic and Mesozoic tectonism of the western Barents Shelf. Norsk Geologisk Tidsskrift 79, 57-68.

Breivik, A.J., Faleide, J.I., Gudlaugsson, S.T., 1998. Southwestern Barents Sea margin: late Mesozoic sedimentary basins and crustal extension. Tectonophysics 293, 21-44.

Brekke, H., Riis, F., 1987. Tectonics and basin evolution of the Norwegian shelf betwwen 62N and 72N. Norks Geologisk Tidsskrift 67, 295-322.

Brune, S., 2014. Evolution of stress and fault patterns in oblique rift systems: 3-D numerical lithospheric-scale experiments from rift to breakup. Geochemistry, Geophysics, Geosystems 15, 3392-3415.

Brune, S., Autin, J., 2013. The rift to break-up evolution of the Gulf of Aden: Insights from 3D numerical lithospheric-scale modelling. Tectonophysics 607, 65-79.

Brune, S., Williams, S.E., Butterworth, N.P., Müller, R.D., 2016. Abrupt plate accelerations shape rifted continental margins. Nature 536, 201-204.

Brune, S., Williams, S.E., Müller, R.D., 2018. Oblique rifting: the rule, not the exception. Solid Earth 9, 1187-1206.

Clark, S.A., Faleide, J.I., Hauser, J., Ritzmann, O., Mjelde, R., Ebbing, J., Thybo, H., Flueh, E.R., 2013. Stochastic velocity inversion of seismic reflection/refraction traveltime data for rift structure of the southwest Barents Sea. Tectonophysics 593, 135-150.

Clark, S.A., Glorstad-Clark, E., Faleide, J.I., Schmid, D., Hartz, E.H., Fjeldskaar, W., 2014. Southwest Barents Sea rift basin evolution: comparing results from backstripping and time-forward modelling. Basin Research 26, 550-566.

Clifton, A.E., Schlische, R.W., Withjack, M.O., Ackermann, R.V., 2000. Influence of rift obliquity on fault-population systematics: Results of experimental clay models. Journal of Structural Geology 22, 1491-1509.

Corti, G., 2008. Control of rift obliquity on the evolution and segmentation of the main Ethiopian rift. Nature Geoscience 1, 258-262.

Corti, G., Van Wijk, J., Bonini, M., Sokoutis, D., Cloetingh, S., Innocenti, F., Manetti, P., 2003. Transition from continental break-up to punctiform seafloor spreading: How fast, symmetric and magmatic. Geophysical Research Letters 30, 6-1 - 6-4.

Crosby, A.G., White, N.J., Edwards, G.R.H., Thompson, M., Corfield, R., Mackay, L., 2011. Evolution of deep-water rifted margins: Testing depth-dependent extensional models. Tectonics 30, n/a-n/a.

Dalland, A., Worsley, D., Ofstad, K., 1988. A Lithostratigraphic Scheme for the Mesozoic and Cenozoic and Succession Offshore Mid-and Northern Norway. Oljedirektoratet.

Dewey, J.F., Holdsworth, R.E., Strachan, R.A., 1998. Transpression and transtension zones, Geological Society Special Publication, pp. 1-14.

Dimakis, P., Braathen, B.I., Faleide, J.I., Elverhøi, A., Gudlaugsson, S.T., 1998. Cenozoic erosion and the preglacial uplift of the Svalbard-Barents Sea region. Tectonophysics 300, 311-327.

Doré, A.G., 1991. The structural foundation and evolution of Mesozoic seaways between Europe and the Arctic. Palaeogeography, Palaeoclimatology, Palaeoecology 87, 441-492.

Doré, A.G., Lundin, E.R., Fichler, C., Olesen, O., 1997. Patterns of basement structure and reactivation along the NE Atlantic margin. Journal of the Geological Society 154, 85-92.

Doré, A.G., Lundin, E.R., Gibbons, A., Sømme, T.O., Tørudbakken, B.O., 2015. Transform margins of the Arctic: a synthesis and re-evaluation. Geol. Soc. Lond. Spec. Publ. 431, SP431-SP438.

Ebinger, C.J., 1989. Geometric and kinematic development of border faults and accommodation zones, Kivu-Rusizi Rift, Africa. Tectonics 8, 117-133.

Egan, S., Buddin, T., Kane, S., Williams, G., 1997. Three-Dimensional Modelling And Visualisation In Structural Geology: New Techniques For The Restoration And Balancing Of Volumes. Electron. Geol. 1.

Faleide, J.I., Solheim, A., Fiedler, A., Hjelstuen, B.O., Andersen, E.S., Vanneste, K., 1996. Late Cenozoic evolution of the western Barents Sea-Svalbard continental margin. Global and Planetary Change 12, 53-74.

Faleide, J.I., Tsikalas, F., Breivik, A.J., Mjelde, R., Ritzmann, O., Engen, O., Wilson, J., Eldholm, O., 2008. Structure and evolution of the continental margin off Norway and Barents Sea. Episodes 31, 82-91.

Faleide, J.I., Vagnes, E., Gudlaugsson, S.T., 1993. Late Mesozoic-Cenozoic Evolution of the South-Western Barents Sea in a Regional Rift Shear Tectonic Setting. Marine and Petroleum Geology 10, 186-214.

Fichler, C., Rundhovde, E., Johansen, S., Sæther, B., 1997. Barents Sea tectonic structures visualized by ERS1 satellite gravity data with indications of an offshore Baikalian trend. First Break 15, 355-363.

Fjeld, T.L., Escalona, A., 2014. Subsurface interpretation of the Lower Cretaceous clastic wedges, Tromsø and Harstad basins, south western Barents Sea, 6th Saint Petersburg International Conference and Exhibition on Geosciences 2014: Investing in the Future, pp. 485-489.

Fletcher, J.M., Grove, M., Kimbrough, D., Lovera, O., Gehrels, G.E., 2007. Ridge-trench interactions and the Neogene tectonic evolution of the Magdalena shelf and southern Gulf of California: Insights from detrital zircon U-Pb ages from the Magdalena fan and adjacent areas. Bulletin of the Geological Society of America 119, 1313-1336.

Fournier, M., Bellahsen, N., Fabbri, O., Gunnell, Y., 2004. Oblique rifting and segmentation of the NE Gulf of Aden passive margin. Geochemistry, Geophysics, Geosystems 5.

Gabrielsen, R., Færseth, R., 1988. Cretaceous and Tertiary Reactivation of Master Fault zones of the Barents sea. Norks Polarinstitutt, Oslo, pp. 93-97.

Gabrielsen, R., Færseth, R., 1989. The off-shore extension of the Trollfjord-Komagelv fault zone-a comment. Norsk Geologisk Tidsskrift 69, 57-62.

Gabrielsen, R.H., 1984. Long-lived fault zones and their influence on the tectonic development of the southwestern Barents Sea. Journal of the Geological Society 141, 651-662.

Gabrielsen, R.H., Faerseth, R.B., Jensen, L.N., Kalheim, J.E., Riis, F., 1990. Structural elements of the Norwegian continental shelf: Part 1. The Barents Sea region Norwegian Petroleum Directorate Bulletin 6, 33.

Gabrielsen, R.H., Grunnaleite, I., Rasmussen, E., 1997. Cretaceous and tertiary inversion in the Bjørnøyrenna Fault Complex, south-western Barents Sea. Marine and Petroleum Geology 14, 165-178.

Gabrielsen, R.H., Kyrkjebø, R., Faleide, J.I., Fjeldskaar, W., Kjennerud, T., 2001. The Cretaceous post-rift basin configuration of the northern North Sea. Petroleum Geoscience 7, 137-154.

Galloway, W.E., 1989. Genetic stratigraphic sequences in basin analysis I: architecture and genesis of flooding-surface bounded depositional units. American Association of Petroleum Geologists Bulletin 73, 125-142.

Gasser, D., 2013. The Caledonides of Greenland, Svalbard and other Arctic areas: status of research and open questions. Geological Society, London, Special Publications 390.

Gee, D.G., Bogolepova, O.K., Lorenz, H., 2006. The Timanide, Caledonide and Uralide orogens in the Eurasian high Arctic, and relationships to the palaeo-continents Laurentia, Baltica and Siberia. Geological Society, London, Memoirs 32, 507-520.

Gee, D.G., Fossen, H., Henriksen, N., Higgins, A.K., 2008. From the early Paleozoic platforms of Baltica and Laurentia to the Caledonide Orogen of Scandinavia and Greenland. Episodes 31, 44-51.

Gernigon, L., Brönner, M., Roberts, D., Olesen, O., Nasuti, A., Yamasaki, T., 2014. Crustal and basin evolution of the southwestern

Barents Sea: From Caledonian orogeny to continental breakup. Tectonics 33, 347-373.

Gibbs, A.D., 1983. Balanced cross-section construction from seismic sections in areas of extensional tectonics. Journal of Structural Geology 5, 153-160.

Glørstad-Clark, E., Faleide, J.I., Lundschien, B.A., Nystuen, J.P., 2010. Triassic seismic sequence stratigraphy and paleogeography of the western Barents Sea area. Marine and Petroleum Geology 27, 27.

Grundvåg, S.A., Marin, D., Kairanov, B., Śliwińska, K.K., Nøhr-Hansen, H., Jelby, M.E., Escalona, A., Olaussen, S., 2017. The Lower Cretaceous succession of the northwestern Barents Shelf: Onshore and offshore correlations. Marine and Petroleum Geology 86, 834-857.

Gudlaugsson, S.T., Faleide, J.I., Johansen, S.E., Breivik, A.J., 1998. Late Palaeozoic structural developments of the south-western Barents Sea. Marine and Petroleum Geology 15, 73-102.

Henriksen, E., Bjørnseth, H.M., Hals, T.K., Heide, T., Kiryukhina, T., Kløvjan, O.S., Larssen, G.B., Ryseth, A.E., Rønning, K., Sollid, K., Stoupakova, A., 2011. Chapter 17 Uplift and erosion of the greater Barents Sea: impact on prospectivity and petroleum systems. Geological Society, London, Memoirs 35, 271-281.

Herrevold, T., Gabrielsen, R.H., Roberts, D., 2009. Structural geology of the southeastern part of the Trollfjorden-Komagelva Fault Zone, Varanger Peninsula, Finnmark, North Norway. Norsk Geologisk Tidsskrift 89, 305-325.

Hodge, M., Fagereng, Å., Biggs, J., Mdala, H., 2018. Controls on Early-Rift Geometry: New Perspectives From the Bilila-Mtakataka Fault, Malawi. Geophysical Research Letters 45, 3896-3905.

Huismans, R., Beaumont, C., 2011. Depth-dependent extension, two-stage breakup and cratonic underplating at rifted margins. Nature 473, 74-78.

Huismans, R.S., Podladchikov, Y.Y., Cloetingh, S., 2001. Dynamic modeling of the transition from passive to active rifting, application to the Pannonian basin. Tectonics 20, 1021-1039.

Indrevær, K., Bergh, S.G., 2014. Linking onshore-offshore basement rock architecture and brittle faults on the submerged strandflat along the SW Barents Sea margin, using high-resolution (5 × 5 m) bathymetry data. Norsk Geologisk Tidsskrift 94, 1-34.

Indrevær, K., Bergh, S.G., Koehl, J.B., Hansen, J.A., Schermer, E.R., Ingebrigtsen, A., 2013. Post-Caledonian brittle fault zones on the hyperextended SW Barents Sea margin: New insights into onshore and offshore margin architecture. Norsk Geologisk Tidsskrift 93, 167-188.

Indrevær, K., Gabrielsen, R.H., Faleide, J.I., 2016. Early Cretaceous synrift uplift and tectonic inversion in the Loppa High area, southwestern Barents Sea, Norwegian shelf. Journal of the Geological Society.

Jackson, C.A.L., Rotevatn, A., 2013. 3D seismic analysis of the structure and evolution of a salt-influenced normal fault zone: A test of competing fault growth models. Journal of Structural Geology 54, 215-234.

Karpuz, M.R., Roberts, D., Olesen, O., Gabrielsen, R.H., Herrevold, T., 1993. Application of multiple data sets to structural studies on Varanger Peninsula, Northern Norway†. International Journal of Remote Sensing 14, 979-1003.

Klausen, T.G., Ryseth, A.E., Helland-Hansen, W., Gawthorpe, R., Laursen, I., 2015. Regional development and sequence stratigraphy of the Middle to Late Triassic Snadd Formation, Norwegian Barents Sea. Marine and Petroleum Geology 62, 102-122.

Klimke, J., Franke, D., 2016. Gondwana breakup: no evidence for a Davie Fracture Zone offshore northern Mozambique, Tanzania and Kenya. Terra Nova 28, 233-244.

Knies, J., Gaina, C., 2008. Middle Miocene ice sheet expansion in the Arctic: Views from the Barents Sea. Geochemistry, Geophysics, Geosystems 9, 1 - 8.

Larssen, G., Elvebakk, G., Henriksen, L.B., Kristensen, S., Nilsson, I., Samuelsberg, T., Svånå, T., Stemmerik, L., Worsley, D., 2002. Upper Palaeozoic lithostratigraphy of the Southern Norwegian Barents Sea. Norwegian Petroleum Directorate Bulletin 9, 76.

Lavier, L.L., Manatschal, G., 2006. A mechanism to thin the continental lithosphere at magma-poor margins. Nature 440, 324-328.

Lehner, P., De Ruiter, P.A.C., 1977. STRUCTURAL HISTORY OF ATLANTIC MARGIN OF AFRICA. AAPG Bulletin (American Association of Petroleum Geologists) 61, 961-981.

Lizarralde, D., Axen, G.J., Brown, H.E., Fletcher, J.M., González-Fernández, A., Harding, A.J., Holbrook, W.S., Kent, G.M., Paramo, P., Sutherland, F., Umhoefer, P.J., 2007. Variation in styles of rifting in the Gulf of California. Nature 448, 466-469.

Lundin, E.R., Dore, A.G., 1997. A tectonic model for the Norwegian passive margin with implications for the NE Atlantic: Early Cretaceous to break-up. Journal of the Geological Society 154, 545-550.

Manatschal, G., Lavier, L., Chenin, P., 2015. The role of inheritance in structuring hyperextended rift systems: Some considerations based on observations and numerical modeling. Gondwana Research 27, 140-164.

Marin, D., Escalona, A., Grundvåg, S.A., Olaussen, S., Sandvik, S., Śliwińska, K.K., 2017a. Unravelling key controls on the rift climax to post-rift fill of marine rift basins: Insights from 3D seismic analysis of the Lower Cretaceous of the Hammerfest Basin, SW Barents Sea. Basin Research.

Marin, D., Escalona, A., Sliwihska, K.K., Nøhr-Hansen, H., Mordasova, A., 2017b. Sequence stratigraphy and lateral variability of Lower Cretaceous clinoforms in the southwestern Barents Sea. AAPG Bulletin 101, 1487-1517.

Mart, Y., Ryan, W.B.F., Lunina, O.V., 2005. Review of the tectonics of the Levant Rift system: The structural significance of oblique continental breakup. Tectonophysics 395, 209-232.

McClay, K., Munoz, J.A., García-Senz, J., 2004. Extensional salt tectonics in a contractional orogen: A newly identified tectonic event in the Spanish Pyrenees. Geology 32, 737-740.

McClay, K.R., Dooley, T., Whitehouse, P., Mills, M., 2002. 4-D evolution of rift systems: Insights from scaled physical models. AAPG Bulletin 86, 935-959.

McKenzie, D., 1978. Some remarks on the development of sedimentary basins. Earth and Planetary Science Letters 40, 25-32.

Montési, L.G.J., Behn, M.D., 2007. Mantle flow and melting underneath oblique and ultraslow mid-ocean ridges. Geophysical Research Letters 34.

Mork, A., Elvebakk, G., Forsberg, A.W., Hounslow, M.W., Nakrem, H.A., Vigran, J.O.S., Weitschat, W., 1999. The type section of the Vikingh0gda Formation: A new lower triassic unit in central and eastern svalbard. Polar Research 18, 51-82.

Morley, C.K., 2017. The impact of multiple extension events, stress rotation and inherited fabrics on normal fault geometries and evolution in the Cenozoic rift basins of Thailand, Geological Society Special Publication, pp. 413-445.

Mosar, J., Lewis, G., Torsvik, T., 2002. North Atlantic sea-floor spreading rates: implications for the Tertiary development of inversion structures of the Norwegian-Greenland Sea. Journal of the Geological Society 159, 503-515.

Moustafa, A.R., 1993. Structural characteristics and tectonic evolution of the east-margin blocks of the Suez rift. Tectonophysics 223, 381-399.

Naliboff, J., Buiter, S.J.H., 2015. Rift reactivation and migration during multiphase extension. Earth and Planetary Science Letters 421, 58-67.

Naliboff, J.B., Buiter, S.J.H., Péron-Pinvidic, G., Osmundsen, P.T., Tetreault, J., 2017. Complex fault interaction controls continental rifting. Nature Communications 8.

Nicol, A., Walsh, J., Berryman, K., Nodder, S., 2005. Growth of a normal fault by the accumulation of slip over millions of years. Journal of Structural Geology 27, 327-342.

Nottvedt, A., Gabrielsen, R.H., Steel, R.J., 1995. Tectonostratigraphy and sedimentary architecture of rift basins, with reference to the northern North Sea. Marine and Petroleum Geology 12, 881-901.

Olesen, O., Gellein, J., Håbrekke, H., Kihle, O., Skilbrei, J.R., Smethurst, M., 1997. Magnetic Anomaly Map Norway ans Adjacent Ocean Areas. Geological Survey of Norway.

Omosanya, K., Zervas, I., Mattos, N., Alves, T., Johansen, S.E., Marfo, G., 2017. Strike-Slip Tectonics in the SW Barents Sea During North Atlantic Rifting (Swaen Graben, Northern Norway). Tectonics 36.

Phethean, J.J.J., Kalnins, L.M., van Hunen, J., Biffi, P.G., Davies, R.J., McCaffrey, K.J.W., 2016. Madagascar's escape from Africa: A high-resolution plate reconstruction for the Western Somali Basin and implications for supercontinent dispersal. Geochemistry, Geophysics, Geosystems 17, 5036-5055.

Phillips, T.B., Jackson, C.A.L., Bell, R.E., Duffy, O.B., 2018. Oblique reactivation of lithosphere-scale lineaments controls rift physiography - The upper-crustal expression of the Sorgenfrei-Tornquist Zone, offshore southern Norway. Solid Earth 9, 403-429.

Rice, A.H.N., Gayer, R.A., Robinson, D., Bevins, R.E., 1989. Strike-slip restoration of the Barents Sea Caledonides Terrane, Finnmark, north Norway. Tectonics 8, 247-264.

Richard, P., Krantz, R.W., 1991. Experiments on fault reactivation in strike-slip mode. Tectonophysics 188, 117-131.

Riis, F., Vollset, J., Sand, M., 1986. Tectonic development of the western margin of the Barents Sea and adjacent areas.

Ritzmann, O., Faleide, J.I., 2007. Caledonian basement of the western Barents Sea. Tectonics 26, n/a-n/a.

Ritzmann, O., Maercklin, N., Faleide, J.I., Bungum, H., Mooney, W., Detweiler, S., 2007. A three-dimensional geophysical model of the crust in the Barents Sea region: model construction and basement characterization. Geophysical Journal International 170, 417-435.

Roberts, A.M., Kusznir, N.J., Yielding, G., Styles, P., 1998. 2D flexural backstripping of extensional basins; the need for a sideways glance. Petroleum Geoscience 4, 327-338.

Roberts, D., 1972. Tectonic deformation in the Barents Sea region of Varanger peninsula, Finnmark. Universitetsforlaget.

Roberts, D., 2003. The Scandinavian Caledonides: event chronology, palaeogeographic settings and likely modern analogues. Tectonophysics 365, 283-299.

Roberts, D., Chand, S., Rise, L., 2011. A half-graben of inferred late palaeozoic age in outer varangerfjorden, finnmark: Evidence from seismic reflection profiles and multibeam bathymetry. Norsk Geologisk Tidsskrift 91, 193-202.

Roberts, D., Lippard, S.J., 2005. Inferred Mesozoic faulting in Finnmark: current status and offshore links. Norges geologiske undersøkelse Bulletin 443.

Robertson, E.C., 1966. The Interior of the Earth: an elementary description. Department of the Interior, US Geological Survey.

Rojo, L.A., Escalona, A., 2018. Controls on minibasin infill in the Nordkapp Basin: Evidence of complex Triassic synsedimentary deposition influenced by salt tectonics. AAPG Bulletin 102, 1239-1272.

Rønnevik, H., Beskow, B., Jacobsen, H.P., 1982. Structural and stratigraphic evolution of the Barents Sea. Canadian Society of Petroleum Geologists Memoir.

Sanderson, D.J., Marchini, W.R.D., 1984. Transpression. Journal of Structural Geology 6, 449-458.

Sandwell, D.T., Müller, R.D., Smith, W.H.F., Garcia, E., Francis, R., 2014. New global marine gravity model from CryoSat-2 and Jason-1 reveals buried tectonic structure. Science 346, 65-67.

Sclater, J.G., Christie, P.A., 1980. Continental stretching: An explanation of the post-Mid-Cretaceous subsidence of the central North Sea Basin. Journal of Geophysical Research: Solid Earth 85, 3711-3739.

Seldal, J., 2005. Lower Cretaceous: The next target for oil exploration in the Barents Sea?, Petroleum Geology Conference Proceedings, pp. 231-240.

Seton, M., Müller, R.D., Zahirovic, S., Gaina, C., Torsvik, T., Shephard, G., Talsma, A., Gurnis, M., Turner, M., Maus, S., Chandler, M., 2012.

Global continental and ocean basin reconstructions since 200Ma. Earth-Science Reviews 113, 212-270.

Sharp, I.R., Gawthorpe, R.L., Underhill, J.R., Gupta, S., 2000. Fault-propagation folding in extensional settings: Examples of structural style and synrift sedimentary response from the Suez rift, Sinai, Egypt. Bulletin of the Geological Society of America 112, 1877-1899.

Siedlecka, A., Siedlecki, S., 1967. Some new aspects of the geology of Varanger Peninsula (Northern Norway). Norges geologiske undersøkelse Bulletin 247, 288-306.

Smelror, M., Petrov, O., Larssen, G.B., Werner, S., 2009. Geological history of the Barents Sea. Norges Geol. undersøkelse, 1-135.

Spathopoulos, F., 1996. An insight on salt tectonics in the Angola Basin, South Atlantic, Geological Society Special Publication, pp. 153-174.

Sund, T., 1984. Tectonic Development and Hydrocarbon Potential Offshore Troms, Northern Norway. AAPG Bulletin 68, 1206-1207.

Tsikalas, F., Faleide, J.I., Eldholm, O., Antonio Blaich, O., 2012. 5 - The NE Atlantic conjugate margins A2 - Roberts, D.G, in: Bally, A.W. (Ed.), Regional Geology and Tectonics: Phanerozoic Passive Margins, Cratonic Basins and Global Tectonic Maps. Elsevier, Boston, pp. 140-201.

Verrall, P., 1981. Structural Interpretation, with Application to North Sea Problems: Course Notes No. 3, 6-10th July, 1981. Joint Association for Petroleum Exploration Courses (UK).

Watts, A.B., Karner, G., Steckler, M.S., Kent, P., Bott, M.H.P., McKenzie, D.P., Williams, C.A., 1982. Lithospheric flexure and the evolution of sedimentary basins. Philosophical Transactions of the Royal Society of London. Series A, Mathematical and Physical Sciences 305, 249-281.

White, N., 1993. Recovery of strain rate variation from inversion of subsidence data. Nature 366, 449-452.

Withjack, M.O., Jamison, W.R., 1986. Deformation produced by oblique rifting. Tectonophysics 126, 99-124.

Withjack, M.O., Peterson, E.T., 1993. Prediction of Normal-Fault Geometries—A Sensitivity Analysis1. AAPG Bulletin 77, 1860-1873.

Withjack, M.O., Schlische, R.W., Olsen, P.E., 1998. Diachronous rifting, drifting, and inversion on the passive margin of central eastern North America: an analog for other passive margins. AAPG Bulletin 82, 817-835.

Ziegler, P.A., 1992. North Sea rift system. Tectonophysics 208, 55-75.

Paper 3

Growth and linkage of a basin-bounding fault system: Insights from the Early Cretaceous evolution of the northern Polhem Subplatform, SW Barents Sea.

Bereke Kairanov, Dora Marín, Alejandro Escalona, Nestor Cardozo

Journal of Structural Geology,124, 2019, 182-196, ISSN 0191-8141, https://doi.org/10.1016/j.jsg.2019.04.014

Journal of Structural Geology 124 (2019) 182–196

Contents lists available at ScienceDirect

Journal of Structural Geology

journal homepage: www.elsevier.com/locate/jsg

Growth and linkage of a basin-bounding fault system: Insights from the Early Cretaceous evolution of the northern Polhem Subplatform, SW Barents Sea

Bereke Kairanov*, Dora Marín, Alejandro Escalona, Nestor Cardozo

Department of Energy Resources, University of Stavanger, NO-4036, Stavanger, Norway

A B S T R A C T

Normal faults grow by either simultaneous increase in displacement and length (isolated model), or by rapid establishment of their final length before accumulating significant displacement (constant-length model), or a combination of these tow end-members. In this study, we integrate stratigraphic and structural observations with throw backstripping and time thickness maps to define the growth processes of a basin-bounding normal fault in the northern Polhem Subplatform, SW Barents Sea. During the initial 15 My of Early Cretaceous rifting, the fault system consisted of at least five en-echelon segments, which were ca. 5–10 km long. Throw backstripping indicates that fault segments were hard-linked after this initial stage to form a single 40 km long fault zone. Fault linkage resulted in displacement redistribution, with the locus of faulting being shifted from the center of each paleo-segment, to the center of the through going fault. Across fault incised valleys provide additional information on the topographic response to fault growth. Major valley incisions at the fault linkage zones outline the extent of the individual fault segments and support early isolated fault growth. Fault backstripping results suggest that valley incision and sedimentation rates kept up with fault slip rate, such that the incised valleys remained unaffected by the uplift of the latter fault linked stage. This study illustrates the importance of integrating stratigraphic and structural observations when reconstructing the evolution of basin-bounding normal faults. In particular, syn-rift erosional features, sediment thickness variations, sediment distribution, stratal geometries and onlap/truncation relationships are critical for estimating the growth of these structures.

1. Introduction

Fault interaction, growth and linkage are important processes in the evolution of major basin-bounding normal fault systems (Gawthorpe and Leeder, 2000; Jackson, 1987; Le Béon et al., 2018; Machette et al., 1991; McLeod et al., 2000; Morley, 1999; Peacock, 2002; Peacock and Xing, 1994; Schlische, 1992; Sharp et al., 2003). Observations from outcrop and subsurface datasets, and analogue and numerical models suggests two ways of fault growth: (1) the isolated fault model, where growth and linkage of individual fault segments occur through displacement and lateral propagation of their tiplines (Cartwright et al., 1995; Dawers and Anders, 1995; Dawers et al., 1993; Walsh and Watterson, 1988; Watterson, 1986) (Fig. 1A); and (2) the constant length fault model, where the faults reach their near-final length relatively early in their slip history, and accumulation of significant displacement occurs without further lateral tipline propagation (Childs et al., 2003; Giba et al., 2012; Jackson and Rotevatn, 2013; Morley, 2002; Nicol et al., 2016; Schlagenhauf et al., 2008; Tvedt et al., 2016; Walsh et al., 2002, 2003) (Fig. 1B). In the last 30 years, these two models have been a matter of discussion and debate, as the style of fault growth differs in both models and has significant impact on predictions regarding the physiographical and tectonostratigraphic evolution of rift basins (Childs et al., 2017; Jackson et al., 2017).

Although fault growth and linkage influence the facies architecture, thickness variations and internal characteristics of syn-rift deposits (Dawers and Underhill, 2000; Jackson et al., 2002; Su et al., 2011), most works on fault growth are focused on the final structural geometry and displacement versus length characteristics (Fig. 1C), and they rarely look at the impact of fault evolution on topographic and sedimentary response (Cartwright et al., 1995; Mansfield and Cartwright, 2001; Peacock and Sanderson, 1991). New studies combining detailed 3D structural observations with sediment dispersal and distribution (e.g. thickness and facies distributions and onlap patterns) are required to further constrain fault zone evolution and associated structures (Corfield and Sharp, 2000; Dawers and Underhill, 2000; McLeod et al., 2000).

In this study, we use high-quality 3D reflection seismic and borehole data from the northern Polhem Subplatform, SW Barents Sea (Fig. 2A) to investigate: (1) the Early Cretaceous syn-rift sediment dispersion and distribution patterns, in order to assess the style of fault growth, and (2) the tectonosedimentary evolution of the area during this period. The northern Polhem Subplatform is characterized by a classical half-graben structure of tilted fault blocks, typically up to 5 km wide (Gabrielsen et al., 1990; Indrevær et al., 2016; Marín et al., 2018) (Fig. 2B). Uplifted

* Corresponding author.
E-mail address: marathekovich@gmail.com (B. Kairanov).

https://doi.org/10.1016/j.jsg.2019.04.014
Received 17 December 2018; Received in revised form 22 April 2019; Accepted 23 April 2019
Available online 28 April 2019
0191-8141/

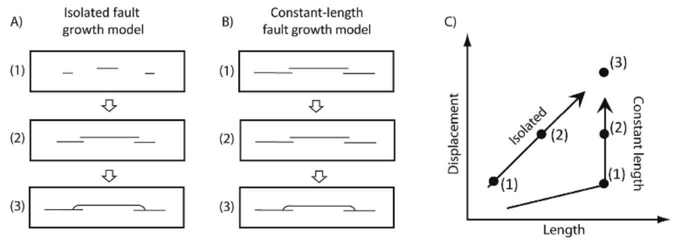

Fig. 1. Top views illustrating the (A) isolated and (B) constant length models of fault growth. Numbers represent fault growth stages: (1) initiation, (2) interaction, and (3) linkage. (C) Displacement versus length through time for the two models. Notice that at the final stage 3, it is not possible to differentiate between the two models from the fault geometry or displacement versus length.

footwall blocks along basin bounding faults have continuous bedrock escarpments and incisions that present an unique opportunity to study the topographic and sedimentary response to the growth of the fault system (Marín et al., 2018).

2. Geological setting

The Polhem Subplatform is a NE – SW trending block-faulted area located on the western part of the Loppa High, in the SW Barents Sea. It is a ~70 km long and ~20 km wide area delineated by an array of down-to-the-west normal faults of the Bjørnøyrenna and Ringvassøy-Loppa fault complexes (BFC and RLFC; Fig. 2A). The subplatform was a tectonically active element of the Loppa High in the Permian, and it was downfaulted relative to the crest of the high in the Early to Mid-Triassic (Blaich et al., 2017; Gabrielsen et al., 1990; Glørstad-Clark et al., 2010). Sedimentary wedges in the hanging walls indicate that the subplatform was tectonically active during the Late Jurassic and Early Cretaceous, Ryazanian – Early Barremian and Late Barremian – Middle Albian (Fig. 3A) (Blaich et al., 2017; Gabrielsen et al., 1990; Indrevær et al., 2016; Serck et al., 2017; Marín et al., 2018). The entire Loppa High was uplifted during the Late Jurassic – earliest Cretaceous (Gabrielsen et al., 1990; Glørstad-Clark et al., 2010; Indrevær et al., 2016; Marín et al., 2018), but the Early Cretaceous fault activity in the RLFC and BFC rejuvenated the topography of the western flank of the Loppa High, establishing high gradient slope systems (Marín et al., 2018). This interpretation is supported by numerous escarpments and incised valleys at the Lower Cretaceous level (Marín et al., 2018).

The Lower Cretaceous succession of the SW Barents Sea is divided into four main formations: Knurr, Klippfisk, Kolje and Kolmule, which consist mainly of grey claystone with minor interbedded limestone and sandstone originally deposited in an open marine environment (Dalland et al., 1988; Mørk et al., 1999). More recently, these formations were divided into seven genetic sequences (sequences 0–6; Marin et al., 2017) (Fig. 3A). Which are bounded by flooding surfaces that could be correlated on a regional scale (Grundvåg et al., 2017; Marín et al., 2017). The lower boundary of the Lower Cretaceous is known as the Base Cretaceous Unconformity (BCU), which is expressed as a high amplitude seismic reflector, but its age and stratigraphic significance is complex (Gabrielsen et al., 2001; Nottvedt et al., 1995). In the areas of the southwestern Barents Sea, where basin margins are affected by Late Jurassic to Early Cretaceous tectonic activity, the BCU represents an unconformity, whereas, in the deeper basins, it is a conformable surface (Fig. 3A). Therefore, the age of the succession immediately above the BCU varies from Boreal Berriasian/Volgian to Valanginian to Barremian (Fig. 3A) (Århus et al., 1990; Marín et al., 2017; Mørk et al., 1999).

3. Dataset

The database for this study comprises a post-stack time migrated, 3D reflection seismic survey (WesternGeco, West Loppa) that is tied to well 7220/5-2 (Fig. 3B). The seismic cube covers an area of 500 km^2 in the north-western part of the Polhem Subplatform (Fig. 1A). The spacing between individual crosslines and inlines is 25 m. The seismic sections are displayed with normal polarity, so that a decrease in acoustic impedance is represented by a trough (blue), while an increase in acoustic impedance is represented by a peak (red-to-yellow) (Brown, 2011) (Fig. 3B). Crosslines are oriented NW-SE and inlines are oriented NE-SW. The vertical seismic resolution in the interval of interest is c. 20–40 m, based on a dominant frequency range of 25–35 Hz and an average P-wave velocity range of 1500–2170 ms^{-1} (Fig. 3B).

Well 7220/5-2 has a full set of logs and biostratigraphic data from well reports in the Norwegian Petroleum Directorate web page (NPD; http://factpages.npd.no), the "Lower Cretaceous basins in the high Arctic" consortium project (LoCrA; http://locra.ux.uis.no), and previous publications (e.g. Marín et al., 2018) (Fig. 3B).

4. Methodology

The stratigraphic framework for the Lower Cretaceous interval analyzed in this study is based on the genetic sequences defined by Marín et al. (2018) (Fig. 3A). Both age and lithology of these sequences (S0 – S6) are constrained by logs and biostratigraphic information in well 7220/5-2, and tied to the seismic data through a synthetic seismogram (Fig. 3). Sequence boundaries are defined by maximum flooding surfaces (Galloway, 1989), which are highlighted by spikes in the gamma ray log (GR) values (Fig. 3B). Some of the maximum flooding surfaces are eroded in well 7220/5-2, therefore unconformities were used as correlative surfaces. The top of sequence 0 represents an unconformity in well 7220/5-2 (red surface, Fig. 3) of Berriasian–Valanginian age (Marin et al., 2017). The top of sequence 1 is also an unconformity (blue surface, Fig. 3), and it is interpreted as of Hauterivian–Early Barremian in age. The top of sequence 2 (yellow surface, Fig. 3) is interpreted as early to late Aptian in age. A flooding surface representing the top of sequence 3 (magenta surface, Fig. 3) is not evident in the well 7220/5-2. Consequently, the top of this sequence is interpreted based on a high amplitude seismic reflector. The lower part of sequence 4 is partially identified, but its upper interval is truncated by an unconformity at the top of the Albian reflector. Sequences 5 and 6 (Late Albian–Mid Cenomanian age) are not observed in the study area, because they are either completely eroded or were not deposited. Additionally, in order to capture the pre-rift configuration, the top Fuglen Formation (Upper Jurassic) and the top Snadd Formation (Upper Triassic) were interpreted in the study area (Fig. 4A). These two

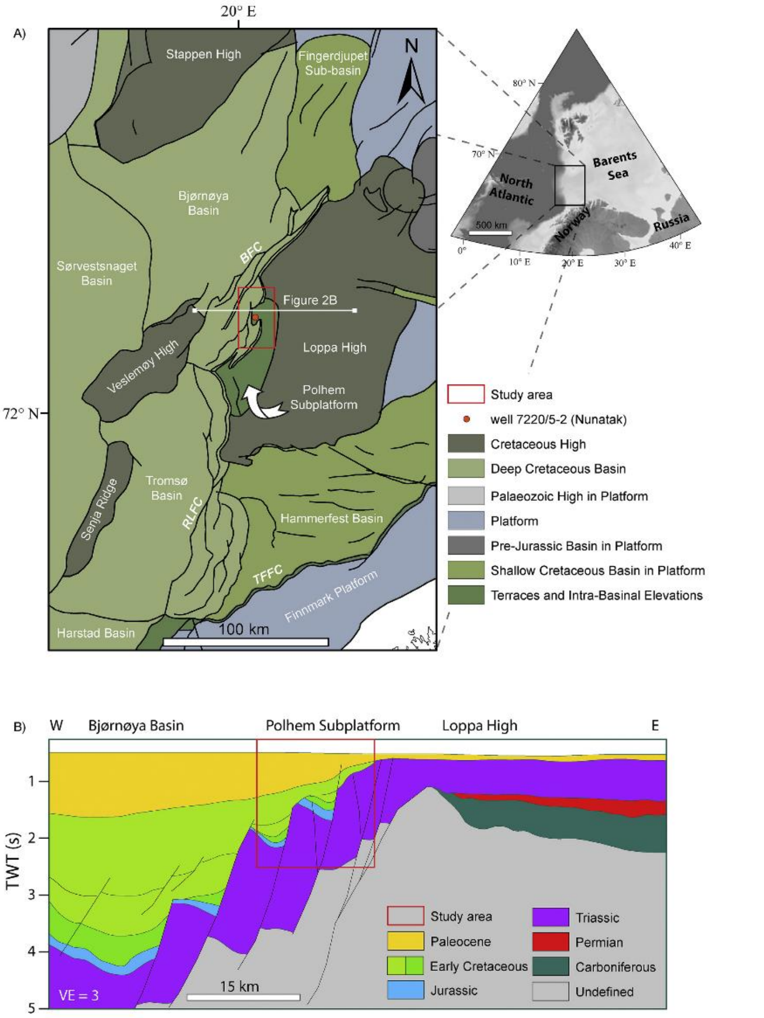

Fig. 2. (A) Location of the study area in the Polhem Subplatform, SW Barents Sea. Geologic map based on data from the Norwegian Petroleum Directorate (RLFC = Ringvassøy-Loppa fault complex; BFC = Bjørnøyrenna fault complex; TFFC = Tromsø Finnmark fault complex). (B) Regional cross section through the major structural elements surrounding the study area (modified from Indrevær et al., 2016). Line of section is shown in A.

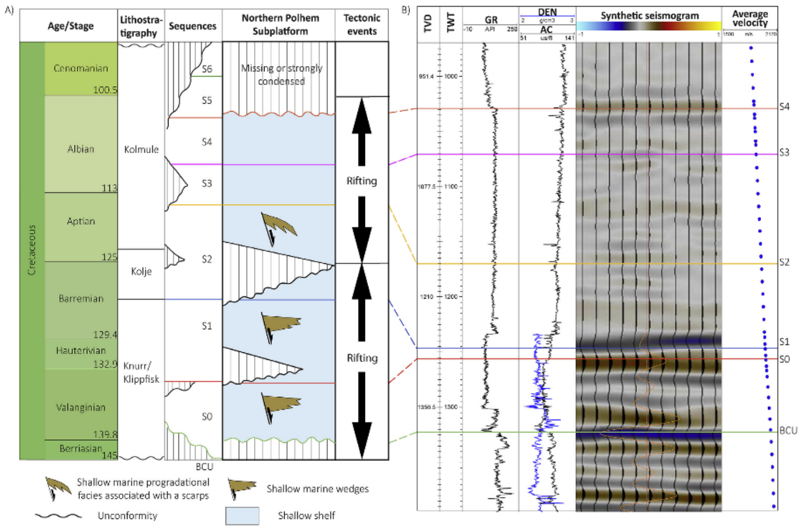

Fig. 3. (A) Stratigraphic framework of the Lower Cretaceous sequences defined by Marin et al. (2018) in the well 7220/5-2 on the northern Polhem Subplatform. Formation names and ages from Dalland et al. (1988) and Mørk et al. (1999). Main tectonic events in the region are compiled from Serck et al. (2017), Indrevær et al. (2016), and Blaich et al. (2017). (B) Synthetic seismogram illustrating the correlation of the Lower Cretaceous sequences with seismic data. Gamma Ray (GR), density (DEN, blue line) and acoustic (AC, black line) logs, as well as average P-wave velocity are included.

formations are silty to sandy (reference, well, etc.?). To enhance the continuity of the reflectors, a structural smoothing technique (Randen et al., 2000) was applied to the 3D seismic cube before interpretation.

Seventeen faults were interpreted in the study area. Only one large fault (fault B, Fig. 4A) was selected for throw analysis, since it has preserved the Lower Cretaceous sequence on both the footwall and hanging wall. Three methods were used to determine the growth history of the fault array: (1) Throw versus length (T – L) plots, which show the distribution of throw along the fault (Childs et al., 1995; Gawthorpe and Leeder, 2000; Walsh and Watterson, 1989); (2) Throw backstripping, which constrains the style of growth of seismic-scale segmented fault arrays (Chapman and Meneilly, 1991; Childs et al., 1993, 2003; Petersen et al., 1992); and (3) Time-thickness maps, which show changes in sediment thickness adjacent to faults, thus revealing the fault growth history (Gawthorpe et al., 2003; Jackson et al., 2002; Jackson and Rotevatn, 2013; Morley, 2002; Schlische, 1995).

Fault throw is defined by vertical (two-way-travel time, TWT) differences between the horizon footwall and hanging wall cutoffs on seismic crosslines perpendicular to the fault strike. The throw was recorded every 100 m along the fault strike direction. The error in throw measurements in the Lower Cretaceous sequences is small, and it is limited to ± 5 ms. All throw-length plots were depth-converted using an average P-wave (checkshot) velocity of 2100 ms $^{-1}$ (Fig. 3B).

Throw backstripping was performed using the "original method" of Chapman and Meneilly (1991). This method calculates the throw of a given horizon by subtracting the measured throw of the shallower horizon at the same along-strike position (Jackson et al., 2017). Throw measurements were performed at present day (compacted) thickness and may include uncertainties related to decompaction. Taylor et al. (2008) pointed out that in sand/shale mixed sequences with low post-faulting burial, the displacement losses due to compaction are typically < 20%. The studied Upper Triassic to Lower Cretaceous succession has < 60% shale and < 0.7 km post-faulting burial, which is similar to the setting discussed by Taylor et al. (2008). Therefore, the impact of differential compaction on the throw of the studied fault is < 20% and hence it does not affect our main observations and conclusions. Fault-propagation-folding was not taken into account in the estimation of fault throw either. This component seems to be important in the analyzed sedimentary succession, particularly in the uppermost sequence S4 where the studied fault (fault B) tips out (Figs. 4A and 5B). Thus, the reported throw measurements, particularly to the top S4, are a minimum estimate.

5. Fault blocks and Lower Cretaceous sequences

Description: The northern Polhem Subplatform is characterized by a series of fault blocks and fault scarps (Fig. 4A and B). The Lower Cretaceous succession was drilled in one of these fault blocks by well 7220/5-2 (Figs. 4A and 5A). The base of the Lower Cretaceous is delimited by the BCU, which is represented by a high amplitude and continuous seismic event with a clear angular relation to its underlying reflectors (Fig. 5B). The top of the Lower Cretaceous is marked by a prominent continuous seismic event corresponding to the top of sequence 4 of middle Albian age (Figs. 4A and 5A). Internally, sequences 0 and 1 are characterized by wedge-shaped geometries thickening towards the faults (Figs. 4A and 5B). Seismic reflectors are continuous to semi-

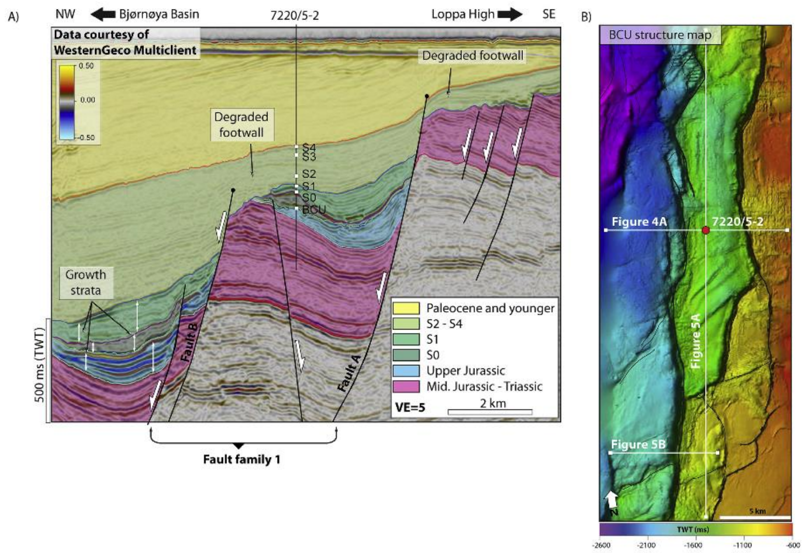

Fig. 4. (A) Crossline intersecting well 7220/5-2 illustrating the Lower Cretaceous sequences and major bounding faults. (B) Location of the cross line overlaid on the Base Cretaceous Unconformity (BCU) structure map. In A, the Upper Jurassic and Lower Cretaceous S0-S1 interval form wedge-shaped packages in the middle and lower fault blocks, while they are either eroded or condensed in the upper fault block towards the Loppa High.

continuous, with downlap relations to the underlying reflectors (Fig. 5B). Sequences 2 to 4 are mostly represented by continuous, low-amplitude, parallel reflectors thickening towards the Bjørnøya Basin (Figs. 4A and 5B). Lower Cretaceous sequences S0 and S1 are only present in the middle and lower fault blocks, while they are either condensed or eroded in the upper fault block (Figs. 4A, 5B and 6A). The main depocenters of S0 and S1 are located along the major bounding faults, and fluctuate in thickness between 350 and 450 ms (TWT) (Fig. 6A). Sequences S2 to S4 are distributed in the entire study area, with a major decrease in thickness in the upper fault block (Figs. 4A and 6B). The main depocenter of S2–S4 is located in the NW part of the area, with a maximum thickness of 1100 ms (TWT) (Fig. 6B).

Interpretation: The Lower Cretaceous sequences were deposited during active faulting, as suggested by the presence of wedge-shaped seismic packages, thickness changes, and onlap relationships towards the footwall crests (Figs. 4A, 5B and 6). Based on the configuration of the seismic reflectors and sedimentological log description by Marin et al. (2018), the depositional setting in the study area is as follows: S0 – S1 wedges were deposited in shallow marine to shelfal environments. This indicates that the sediments were deposited at shallow water depth and proximal to the actual shoreline; S2 – S4 were deposited in a relatively distal environment, outer shelf to open marine setting, as suggested by an overall increase in shale content.

6. Incisions

Description. Four main unconformities are present in the study area: BCU, S0, S1 and S4 (Fig. 5A). These unconformities are characterized by erosional features such as incised valleys (Fig. 5A). At least three main incised valleys across the faults are recognized at the top of S0 and S1 unconformities (Fig. 7). The interpreted incised valleys extend from the E to the W, transverse to the trend of the major basin bounding faults (Fig. 7B). Incised valleys in the middle and northern parts of the middle fault block coincide with synthetic overlapping transfer zones (Fig. 7B; Morley et al., 1990). It is not easy to determine the length of these incisions, particularly in the higher footwalls located to the east (upper fault block), because this area experienced several post Early Cretaceous erosional events (Henriksen et al., 2011; Solheim and Kristoffersen, 1984). The width of the incised valleys fluctuates from 1 to 2 km (Fig. 7B). The incisions at the top of S0 and S1 are partially filled by sequences 1 and 2 in the middle fault block (Fig. 7C–E), and by sequences 3–4 in the higher eastern footwall (Fig. 5A). The incised valley almost in the middle of the study area shows a number of circular, concave (towards the W) embayments (Figs. 7B and 8A).

Interpretation. Consistent with Marín et al. (2018), the presence of the cross-fault incised valleys suggest that the area had a high gradient. Incisions in the middle fault block were most likely formed during the earliest Cretaceous, and persisted until at least the early Aptian as they were filled by the Lower Cretaceous sequences S1 and S2 (Fig. 7C–E). It is not easy to define the age of the incision in the upper fault block, where they were filled by sequences S3 – S4 (SW side in Fig. 5A). However, the continuity of the incisions suggest that they have the same origin, and formed at the same time the incisions in the middle fault block (Fig. 7AandB). The location of the northern and middle

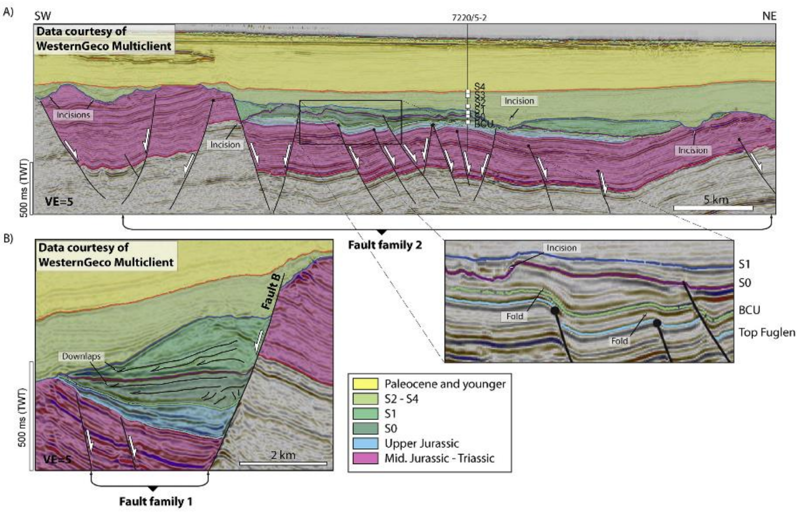

Fig. 5. (A) Inline intersecting well 7220/5-2 illustrating the Lower Cretaceous sequences and faults. Enlarged section shows continuous folds at the BCU level associated with the activity of fault family 2. (B) Southern crossline showing the Lower Cretaceous sequences S0 and S1 and basin bounding fault. Locations of A and B are shown in Fig. 4B.

incised valleys at synthetic overlapping transfer zones suggest that their formation was most likely controlled by fault activity (Fig. 7B). Moreover, circular, concave embayments in one of the incised valleys resemble landslide headwalls making abrupt changes in the gradient, also referred as "knickpoints" (Mitchell, 2006) (Fig. 8AandB). These features are similar to those observed on the present-day New Jersey continental slope, where circular and concave embayments are also interpreted as landslide headwalls forming in response to structurally controlled slope failure (Fig. 8C) (Farre et al., 1983; McAdoo et al., 2000). The formation of several knickpoints along the incision is most likely associated with gradient changes caused by tectonic activity, where knickpoints commonly migrate upstream (e.g. western Niger Delta; Heiniö and Davies, 2007).

7. Fault analysis

7.1. Fault arrays

The interpreted fault arrays consist of various normal fault geometries and styles of linkage. For descriptive purposes, the fault arrays were grouped into two distinct fault families based on their structural trend and timing: (1) NE – SW (family 1) and (2) E – W (family 2, Fig. 9).

Fault family 1 (FF1) consists of a series of major NE–SW trending faults (Fig. 9B). These faults belong to the west-facing Bjørnøyrenna Fault Complex (BFC), which separates the Polhem Subplatform from the Bjørnøya Basin (Figs. 2A and 4A). FF1 is characterized by normal faults, which are almost planar for the Lower Cretaceous interval and tip out upwards in the Lower Cretaceous S3 – S4 and Paleocene strata (Figs. 4A and 5B). The throw of these faults varies from approximately 200 ms–750 ms (200–854 m), with a maximum in the Upper Triassic horizon (Fig. 4A). On map view, these faults are straight to slightly curved including some en-echelon fault segments with hard-links via breached relay ramps (Fig. 9B). FF1 faults were active during deposition of the Upper Jurassic and Lower Cretaceous sequences S0 – S1 (Early Valanginian – early Barremian), as suggested by the growth and wedge-shape packages in these intervals along the hanging walls of FF1 (Figs. 4A and 5B).

Fault family 2 (FF2) comprises minor E–W normal faults (Fig. 9B). FF2 is represented by normal faults, which have higher dip angle than FF1 (Fig. 5A). FF2 faults in general tip out upwards at the BCU horizon, and downwards against major faults of FF1 (Fig. 5A). Fault termination at the BCU horizon resulted in the formation of asymmetric folds with synthetic dips towards the downthrown block (Fig. 5A; Ferrill et al., 2005). The throw of FF2 ranges between 50 and 400 ms (50–550 m) (Fig. 5A), with a maximum observed in the Upper-Triassic horizon. Laterally, FF2 faults terminate against major basin bounding faults of FF1 (Fig. 9B). Faults of FF2 were active during the early Valanginian – early Barremian, based on growth strata in sequences 0 and 1 (Fig. 5A).

7.2. Throw distribution and backstripping

A throw versus length plot was created for a single fault B (Fig. 10A and B) that belongs to FF1 (Fig. 9B). We chose fault B because in comparison to fault A (in Fig. 9B), it has preserved sedimentary record of the Lower Cretaceous sequences in both the hanging wall and footwall (Fig. 4A). Fault B is 40 km long and at the top Snadd Formation, it has a maximum throw of 854 m (Fig. 10A and B, red line). Maximum throw values of 520 m and 340 m are present at the BCU and top S1 horizons, respectively (Fig. 10A, green and blue lines). Based on throw

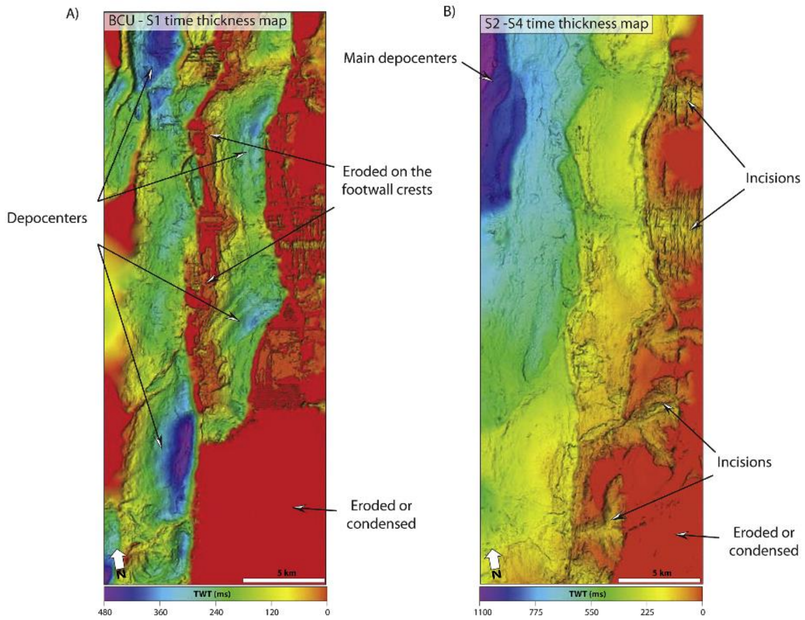

Fig. 6. Time (TWT) thickness maps of (A) BCU – S1 and (B) S2 – S4, illustrating locations of depocenters, eroded footwall crests, and valley incisions.

minima at the top Snadd Formation, fault B can be divided into six fault segments (Fig. 10A). Main fault throw minima in the northern part coincide with the location of hard links via breached relay ramps (Fig. 10C).

Fault throw backstripping (Fig. 10) suggests that during the earliest fault slip increment (Upper Triassic) and deposition of the Upper Jurassic wedges (Fig. 4A), fault B comprised at least 5 major isolated fault segments (Fig. 10F). Throw varied along strike with maxima of 600–650 m on the 4 major faults (Fig. 10F). During the next growth increment and deposition of S0, the fault accumulated in average 60 m of throw (Fig. 10E, green line). Fault segments propagated laterally resulting in the kinematical linkage of the northern and southern segments and the establishment of 3–5 major fault segments, where the longest southern segment was 22 km long (Fig. 10E and F). This growth increment also corresponds to activity of FF2 transverse faults (fault tip folds in Fig. 5A), and suggest that fault B established kinematic linkage with fault A (Fig. 9B). This led to changes in throw gradient in the longest fault segment (at 10 km in Fig. 10E). However, kinematic linkage between fault B and fault A is considered a minor factor controlling throw values because it is confined to the southern part of the study area (between 0 and 10 km in Fig. 10E), whereas the central and northern parts show no evidence of linkage between these two major faults. At the next growth increment and deposition of S1, the fault accumulated considerable average throw of about 120 m (Fig. 10D, blue line). Lateral propagation and linkage of the fault segments established the near final fault length (Fig. 10D). During the final growth increment and deposition of the sequences S2–S4, the fault accumulated a relatively small average throw of 20 m (Fig. 10B, orange line). Further lateral fault propagation is not observed in this period. Thus, fault throw backstripping suggests that fault B grew initially in accordance with the isolated fault model, with the final length being established after ca. 37.5% of the fault slip history.

7.3. Time-thickness map analysis

The time-thickness map of the Lower Cretaceous (BCU – S1) illustrates the distribution of depocenters controlled by the studied fault B (Fig. 11A). Several isolated hanging wall depocenters are present along this fault, where the main depocenter with a maximum thickness of 450 ms (TWT) is located to the south (Fig. 11A). A composite seismic line through the depocenters reveals several minor scoop-shaped depocenters between the BCU and top S0 (Fig. 11B and C). Internally, these depocenters are characterized by tabular seismic reflection packages which onlap the BCU (Figs. 5B and 11C). These scoop-shaped depocenters are most likely associated with the formation of individual fault segments and their slip during the deposition of S0. Furthermore, the location where the onlaps in the scoop-shaped wedges are indicate the lateral extent of the fault segments during deposition of S0 (Fig. 11C and D). Thus, the time-thickness map suggests that at the time of deposition of S0, fault B was formed by at least five kinematically isolated

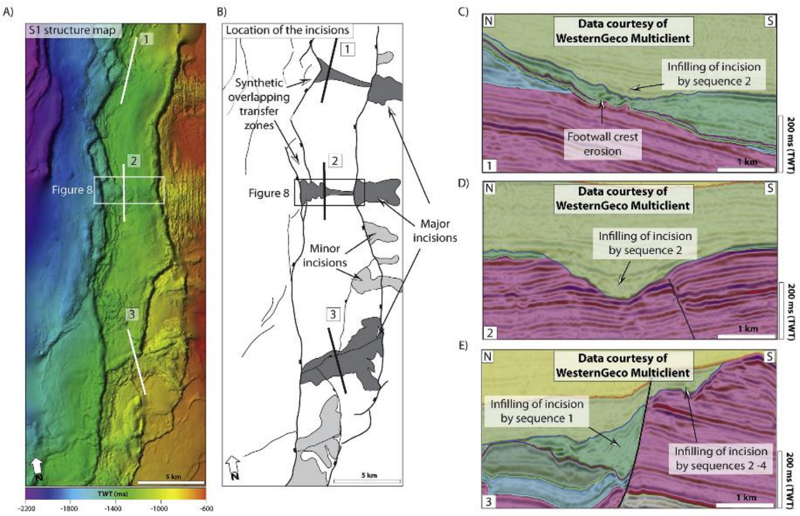

Fig. 7. (A) S1 structure map and (B) interpreted valley incisions. Note that the northern and middle incisions are located at synthetic overlapping transfer zones. (C – E) Cross sections 1 to 3 through major valley incisions showing their infilling patterns. The location of the sections is shown in A and B. Refer to Fig. 5 for color legend.

fault segments (Fig. 11D). This in accordance with the results of throw backstripping at the time of deposition of S0 (Fig. 10E). Therefore, we conclude that during the deposition of sequences S0 and S1, fault growth was dominated by lateral fault propagation and lengthening of the fault segments (isolated model).

8. Discussion

8.1. Style of fault growth and Lower Cretaceous sediment distribution

The two main models of fault growth, isolated versus constant-length, are undistinguishable after the faults have attained their final displacement and length as seen in Fig. 1A–B, stage 3. A key difference between these two models though, is the history of fault displacement versus length (Fig. 1C), which requires knowledge of fault evolution. In this study, a large 854 m throw fault (fault B, Fig. 9B) with good record of syn-sedimentary strata in the hanging wall and footwall was chosen to analyze fault growth. Throw backstripping of this fault suggests that its near final length was obtained at ~37.5% of its slip history and therefore during almost the first half of the fault history, the fault grew in accordance with the isolated fault growth model. This is to some extent in disagreement with recent compilations of case studies by Jackson et al. (2017) and Childs et al. (2017), who suggest the final fault length is established within ~10–33% of the fault slip history. One may argue that this discrepancy is due to the fact that fault B is larger than the faults included in the above compilations, which typically are intra-basinal faults as opposed to basin-bounding faults. In the last case, it is reasonable to expect an initial, longer history of isolated fault growth such as the one observed in fault B.

It can be suggested we only assessed part of the fault without looking at it as a whole fault system, which extends outside of the study area. However, according to several studies, faults have fractal characteristics (Kakimi, 1980; Marrett and Allmendinger, 1992; Walsh et al., 1991; Wojtal, 1994), which means that our observations from a part of the fault are still applicable to the entire fault extent. Nevertheless, estimates of fault slip history have uncertainties, as it is difficult to resolve in detail the early syn-rift stratigraphy and date the earliest stages of fault growth due to relatively low vertical seismic resolution (> 30 m) and absence of hanging-wall well data.

As such, the interpreted incised valleys are key markers in unraveling the growth of fault B, since erosional processes are key indicators of tectonic processes (Kirby and Whipple, 2012; Pritchard et al., 2009; Wobus et al., 2006). The incised valleys' infill sediments consisting of sequences S1 – S2 suggest that the valleys were formed during the Valanginian – Hauterivian (S0) and persisted until the Barremian – Aptian (S2) (Fig. 5A). As suggested by throw backstripping (Fig. 10) and time-thickness maps (Figs. 6 and 11), fault B was comprised of at least four isolated fault segments prior to the Valanginian – Hauterivian (Figs. 10E and 11D), which means that the fault segments formed earlier than the incised valleys. The northern and middle incised valleys coincide with the location of synthetic overlapping transfer zones (Figs. 7B and 11D), which is reasonable because these structures are major sediment input points (Crossley, 1984; Morley et al., 1990; Gawthorpe et al., 1994; Gawthorpe and Hurst, 1993; Jackson et al., 2002; Leeder and Gawthorpe, 1987). This implies that the drainage system exploited topographically low areas that developed between fault segments during the early stages of fault growth (e.g. Late Jurassic rifting; Fig. 12A). Incision along major sediment pathways probably occurred during fault segment linkage and interaction stages (e.g. Early Cretaceous), when erosion and sedimentation were able to

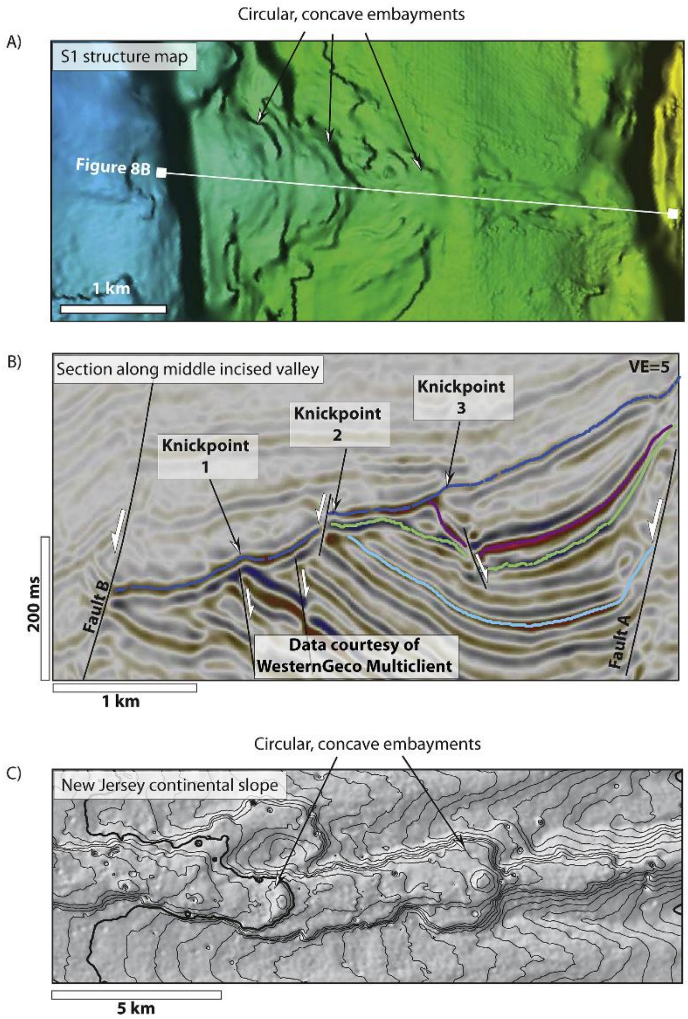

Fig. 8. (A) Enlarged map section from the middle part of Fig. 7A-B showing circular, concave features along incised valley. (B) Cross section along incised valley illustrating the location of paleo-knickpoints associated with changes in slope gradient. (C) Present-day example from the New Jersey continental slope illustrating similar circular and concave features related to structurally controlled slope failure (adapted from Mitchell, 2006). Refer to Fig. 5 for color legend.

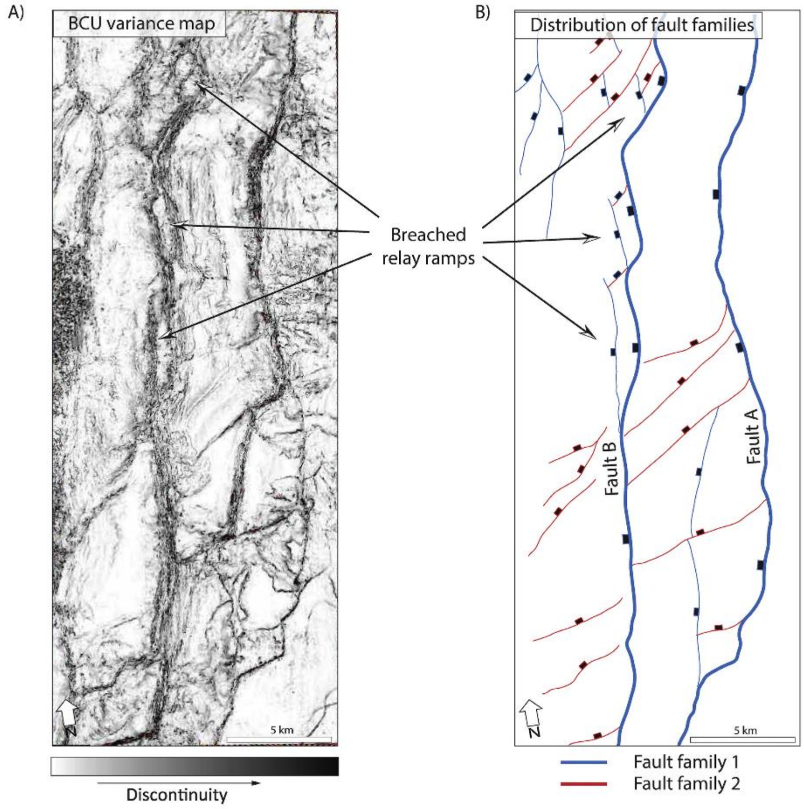

Fig. 9. (A) Seismic variance map along the BCU surface showing seismic reflection discontinuity related to faults. (B) Map view of interpreted fault families and breached relay ramps.

keep up with slip rate on the fault segments (Fig. 12B). Thus, the development of the incised valleys through the uplifted footwall areas of fault B confirms that this fault grew in accordance with the isolated fault growth model.

8.2. *Early Cretaceous evolution of the northern Polhem Subplatform*

Sedimentological and age constrains of the Lower Cretaceous sequences by Marin et al. (2018) for well 7220/5-2 suggest that the process of growth and linkage of the initially isolated fault segments took approximately 15–16 Ma. This is relatively similar to the Jurassic rift system of the northern North Sea, where the evolution of the isolated fault segments lasted 11–15 Ma (Dawers and Underhill, 2000; McLeod et al., 2000; Young et al., 2001). Integration of stratigraphic and structural observations suggest that the tectonic evolution of the study area can be divided into three distinct stages, each characterized by specific fault configurations and basin geometries (Fig. 12A–C):

8.2.1. *Late Jurassic: initiation of isolated fault segments*

Wedge-shaped deposits on the hanging walls of FF1 (Fig. 4A) clearly show the influence of the Late Jurassic rifting in the study area. Throw backstripping of fault B suggests that this fault initially comprised five (5–10 km long) isolated fault segments with throw maxima of 600–650 m (Fig. 10F). Thinning and onlap of the Upper Jurassic strata

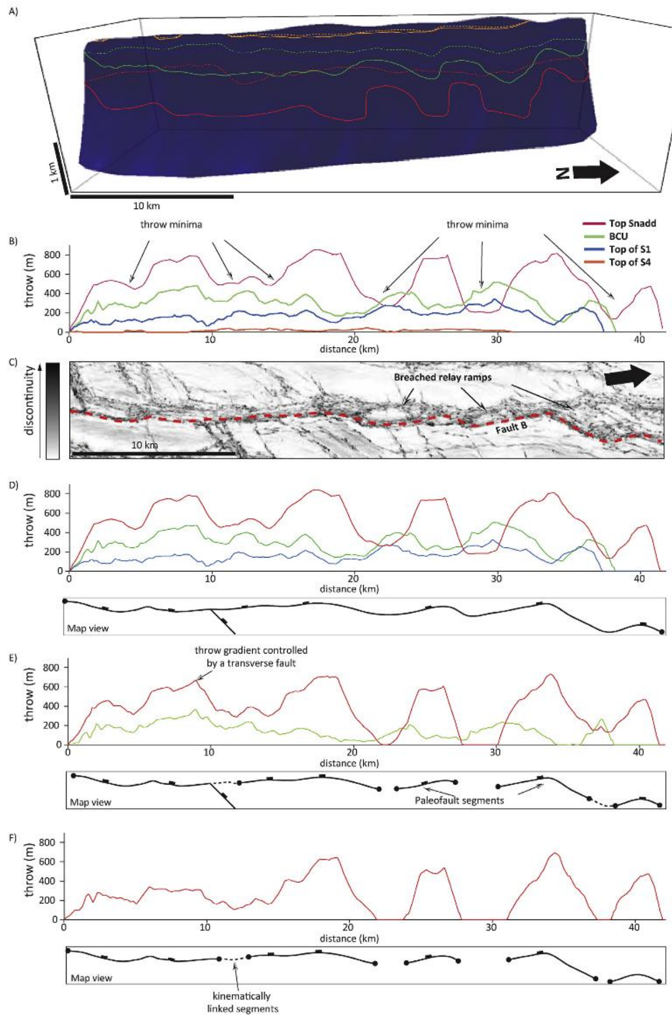

Fig. 10. (A) Allan diagram along fault B. Hanging wall and footwall cutoffs are continuous and dashed lines, respectively. (B) Throw versus length along fault B in Fig. 9B. Top Snadd (Upper Triassic, red line), BCU (green line), top S1 (blue line), and top S4 (orange line) horizons are included. (C) Seismic variance along the BCU surface, showing fault B. The black arrow indicates north. In (B) for the top Snadd, notice the presence of three throw minima to the north associated with the breached relay ramps displayed in (C). (D-F) Throw backstripping of fault B at deposition of (D) S1, (E) S0, and (F) Upper Jurassic.

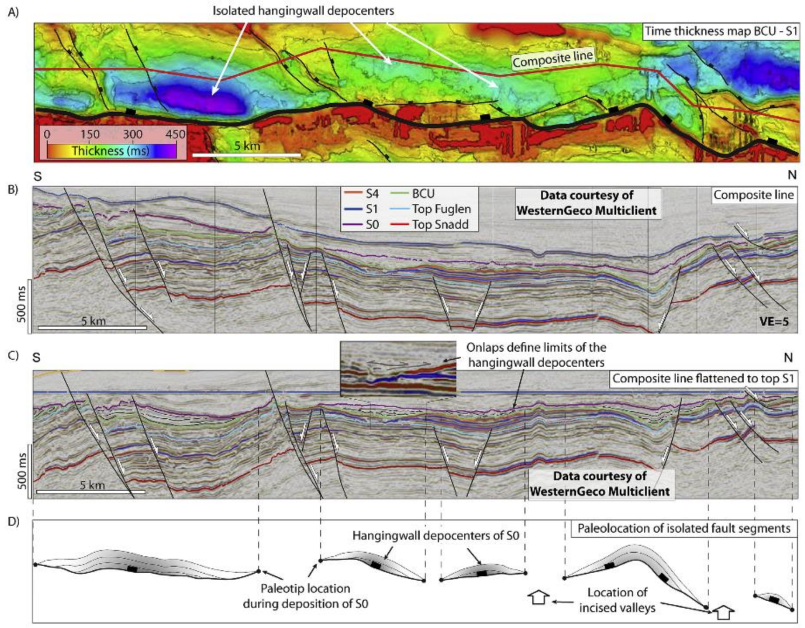

Fig. 11. (A) Time thickness map along fault B showing distribution of depocenters. (B) Composite line along fault B (red line in A). (C) Composite line in B flattened to the top S1 horizon, illustrating the distribution of scoop-shaped depocenters in the S0 interval. (D) Interpreted paleo-location of isolated fault segments and hanging wall depocenters.

towards the crest of the footwalls implies that these were high relief areas during the early syn-rift deposition (Fig. 5B). Erosion of the footwall crests suggest that the uplifted footwalls may have been above sea-level (Figs. 6A and 12A). Low topographic relief areas were most likely developed between the isolated fault segments, which controlled the sediment transport pathways (Figs. 11D and 12A) (Crossley, 1984; Gawthorpe and Hurst, 1993). Shallow to deep marine systems dominated the Upper Jurassic syn-rift fill (e.g. Hekkingen Formation; Dalland et al., 1988).

8.2.2. *Valanginian – Barremian: fault linkage and interaction*

The onset of the Early Cretaceous rifting reactivated faults of FF1 and resulted in the formation of FF2, as suggested by the presence of wedge-shaped geometries and fault tip folds in the Lower Cretaceous sequences S0 and S1 (Figs. 4A and 5). During this period, fault B consisted of 4–5 isolated fault segments that were kinematically linked (Fig. 12B; Gupta and Scholz, 2000). These fault segments accumulated additional 180 m of throw (Fig. 10D and E), where lateral propagation of the faults resulted in various degrees of linkage, from soft-links via relay ramps to hard-links (Fig. 12B).

In the southern part of the study area, fault B segments became hard-linked, which led to the development of a continuous through-going fault segment approximately 22 km long (Figs. 10E and 12B). The deepest depocenters of the combined syn-rift sequences S0 and S1 suggest the locus of fault activity was centered in the southern and northern parts of the study area (Fig. 6A).

Shallow to deep marine settings still prevailed in the area (Marin et al., 2018). Consistent with Marin et al. (2018), the interpreted incised valleys suggest the formation of high gradient, since the area was a transition zone between the uplifted Loppa High and the deep Bjørnøya Basin (Fig. 1A). The topography inherited from the Late Jurassic rifting was enhanced by continued uplift and rotation of the footwall blocks, as suggested by growth strata in S0 and S1 during this stage (Figs. 4A and 5B). Sediment supply through antecedent drainage systems was not influenced by lateral propagation of the fault segments, as incision rate was able to keep up with fault slip rate, by forming incised valleys on the uplifted footwalls (Fig. 12B). In the incised valley of the middle part of the study area, knickpoints reflect changes in the slope gradient due to activity (e.g. linkage) of fault B (Fig. 8A). Headward migration of knickpoints 1 to 3 is probably associated with incremental increase in displacement of fault B (Fig. 8B). This is similar to observations in the slopes of the Niger Delta and Malawi rift basins, where migrating knickpoints are associated with episodes of fault activity (Adeogba et al., 2005; Pirmez et al., 2000; Robinson, 2014). Activity of FF2 resulted in the formation of footwall escarpments and incised valleys. For instance, the formation of the third incised valley in

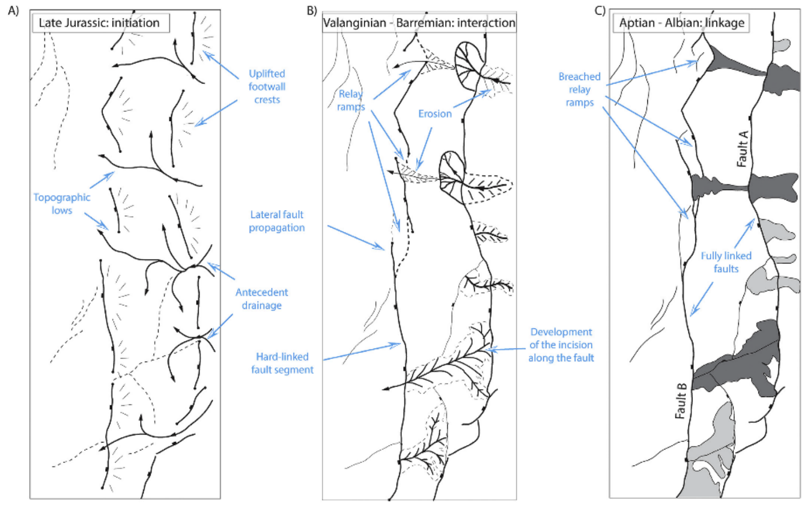

Fig. 12. Evolution of the northern Polhem Subplatform. (A) Late Jurassic: formation of isolated fault segments. (B) Valanginian – Barremian: kinematic interaction and linkage of isolated fault segments, and development of incised valleys. (C) Aptian – Albian: faults established their final length and accumulated minor displacement, while valley incisions and sedimentation rates kept up with fault slip rates.

the southern part of the study area was facilitated by activity of FF2 (Fig. 7B and E).

8.2.3. Aptian – Albian: post – linkage development

Continued rifting in the Polhem Subplatform resulted in the accumulation of additional 20 m of throw along fault B without further lateral propagation of the fault (Fig. 10A). This indicates decrease in tectonic activity, where fault B behaved as a single linked fault system (Fig. 12C). Most of the soft-linked fault segments became hard-linked via breached relay ramps (Fig. 12C). Northward migration of the depocenters of sequences S2 – S4 suggest that the locus of fault activity of FF1 and FF2 shifted from the southern to the northern part of the study area (Fig. 6B). The change in depositional environment from the shallow marine settings of sequences S0 and S1 to the outer shelf – open marine settings of sequences S2 – S4 indicates a marked increase in water depth. The uplifted footwall block in the eastern part of the study area closest to the Loppa High, was a major topographic feature above sea level. Erosional features and in some localities the absence of the Lower Cretaceous sequences S0 - S1 are observed in this eastern high footwall area (Figs. 5A and 6A). Remnant incised valleys were filled with S2. Incised valleys are not observed in younger sequences (Fig. 5A).

9. Conclusions

This study shows that integration of stratigraphic and structural observations is key to determine the style of fault growth. Particularly, analysis of time-thickness maps and interpreted incised valleys provide important details of the basin and fault configuration, as they clearly mark the location of the fault linkage zones and outline individual fault segments.

For the studied fault B, the initial 15 My (Valanginian – Barremian) of rifting were characterized by isolated fault segments 5–10 km long. Tectonic activity resulted in modification of the structural relief that affected the paleo-drainage system. Uplifted footwall blocks diverted sediment pathways towards topographic lows developed between synthetic overlapping fault segments (consistent with Gawthorpe and Leeder, 2000). Erosion and sedimentation were able to keep up with fault slip rates resulting in the formation of cross-fault incised valleys at the locations of fault linkage. Thus, for about half of its initial history, fault B grew in accordance to the isolated model, and although it grew during the second part of its history following the constant-length model, key sedimentary features such as incised valleys still follow preexistent structures (i.e. fault linkage zones) from the initial isolated stage. This suggests that the categorical distinction between isolated versus constant-length fault growth models (Fig. 1) may be too simplistic, at least for large basin bounding faults.

Acknowledgements

This study is part of the industry-sponsored LoCrA consortium. We are grateful with all the sponsors of the consortium for the financial support. Thanks to Schlumberger (WesternGeco) and to the Norwegian DISKOS database for the software and datasets provided.

References

Adeogba, A.A., McHargue, T.R., Graham, S.A., 2005. Transient fan architecture and depositional controls from near-surface 3-D seismic data, Niger Delta continental slope. AAPG Bull. 89, 627–643.

Århus, N., Kelly, S.R.A., Collins, J.S.H., Sandy, M.R., 1990. Systematic palaeontology and biostratigraphy of two Early Cretaceous condensed sections from the Barents Sea. Polar Res. 8, 165–194.

Blaich, O.A., Tsikalas, F., Faleide, J.I., 2017. New insights into the tectono-stratigraphic evolution of the southern Stappen high and its transition to Bjørnøya Basin, SW Barents Sea. Mar. Petrol. Geol. 85, 89–105.

Brown, A.R., 2011. Interpretation of Three-Dimensional Seismic Data. Society of Exploration Geophysicists and American Association of Petroleum Geologists.

Cartwright, J.A., Trudgill, B.D., Mansfield, C.S., 1995. Fault growth by segment linkage: an explanation for scatter in maximum displacement and trace length data from the Canyonlands Grabens of SE Utah. J. Struct. Geol. 17, 1319–1326.

Chapman, T.J., Meneilly, A.W., 1991. The Displacement Patterns Associated with a Reverse-Reactivated, Normal Growth Fault, vol. 56. Special Publications, Geological Society, London, pp. 183–191.

Childs, C., Easton, S.J., Vendeville, B.C., Jackson, M.P.A., Lin, S.T., Walsh, J.J., Watterson, J., 1993. Kinematic analysis of faults in a physical model of growth faulting above a viscous salt analogue. Tectonophysics 228, 313–329.

Childs, C., Watterson, J., Walsh, J.J., 1995. Fault overlap zones within developing normal fault systems. J. Geol. Soc. 152, 535–549.

Childs, C., Nicol, A., Walsh, J.J., Watterson, J., 2003. The growth and propagation of synsedimentary faults. J. Struct. Geol. 25, 633–648.

Childs, C., Holdsworth, R.E., Jackson, C.A.-L., Manzocchi, T., Walsh, J.J., Yielding, G., 2017. Introduction to the Geometry and Growth of Normal Faults, vol. 439 Special Publications, Geological Society, London.

Corfield, S., Sharp, I.R., 2000. Structural style and stratigraphic architecture of fault propagation folding in extensional settings: a seismic example from the Smørbukk area, Halten Terrace, Mid-Norway. Basin Res. 12, 329–341.

Crossley, R., 1984. Controls of sedimentation in the Malawi rift valley, Central Africa. Sediment. Geol. 40, 33–50.

Dalland, A., Worsley, D., Ofstad, K., 1988. A lithostratigraphic scheme for the Mesozoic and Cenozoic succession offshore mid- and northern Norway. Norweg. Petrol. Dir. Bull. 4, 65.

Dawers, N.H., Anders, M.H., 1995. Displacement-length scaling and fault linkage. J. Struct. Geol. 17, 607–614.

Dawers, N.H., Underhill, J.R., 2000. The role of fault interaction and linkage in controlling synrift stratigraphic sequences: late Jurassic, Statfjord east area, northern North sea. AAPG Bull. 84, 45–64.

Dawers, N.H., Anders, M.H., Scholz, C.H., 1993. Growth of normal faults: displacement-length scaling. Geology 21, 1107–1110.

Farre, J.A., McGregor, B.A., Ryan, W.B.F., Robb, J.M., 1983. Breaching the shelfbreak: passage from youthful to mature phase in canyon evolution. In: Stanley, D.J., Moore, G.T. (Eds.), The Shelfbreak: Critical Interface on Continental Margins. Society of Economic Paleontologists and Mineralogists, Tulsa, Oklahoma, pp. 25–40.

Ferrill, D.A., Morris, A.P., Sims, D.W., Waiting, D.J., Hasegawa, S., 2005. Development of Synthetic Layer Dip Adjacent to Normal Faults. AAPG Memoir, pp. 125–138.

Gabrielsen, R.H., Faerseth, R.B., Jensen, L.N., Kalheim, J.E., Riis, F., 1990. Structural elements of the Norwegian continental shelf: Part 1. Barents Sea Region. Norweg. Petrol. Dir. Bull. 6, 33.

Gabrielsen, R.H., Kyrkjebø, R., Faleide, J.I., Fjeldskaar, W., Kjennerud, T., 2001. The Cretaceous post-rift basin configuration of the northern North Sea. Petrol. Geosci. 7, 137–154.

Galloway, W.E., 1989. Genetic stratigraphic sequences in basin analysis I: architecture and genesis of flooding-surface bounded depositional units. Am. Associat. Petrol. Geol. Bull. 73, 125–142.

Gawthorpe, R.L., Hurst, J.M., 1993. Transfer zones in extensional basins: their structural style and influence on drainage development and stratigraphy. J. Geol. Soc. 150, 1137–1152.

Gawthorpe, R.L., Leeder, M.R., 2000. Tectono-sedimentary evolution of active extensional basins. Basin Res. 12, 195–218.

Gawthorpe, R.L., Fraser, A.J., Collier, R.E.L., 1994. Sequence stratigraphy in active extensional basins: implications for the interpretation of ancient basin-fills. Mar. Petrol. Geol. 11, 642–658.

Gawthorpe, R.L., Jackson, C.A.L., Young, M.J., Sharp, I.R., Moustafa, A.R., Leppard, C.W., 2003. Normal fault growth, displacement localisation and the evolution of normal fault populations: the Hammam Faraun fault block, Suez rift, Egypt. J. Struct. Geol. 25, 883–895.

Giba, M., Walsh, J.J., Nicol, A., 2012. Segmentation and growth of an obliquely reactivated normal fault. J. Struct. Geol. 39, 253–267.

Glørstad-Clark, E., Faleide, J.I., Lundschien, B.A., Nystuen, J.P., 2010. Triassic seismic sequence stratigraphy and paleogeography of the western Barents Sea area. Mar. Petrol. Geol. 27, 1448–1475.

Grundvåg, S.A., Marin, D., Kairanov, B., Śliwińska, K.K., Nøhr-Hansen, H., Jelby, M.E., Escalona, A., Olaussen, S., 2017. The lower cretaceous succession of the northwestern Barents shelf: onshore and offshore correlations. Mar. Petrol. Geol. 86, 834–857.

Gupta, A., Scholz, C.H., 2000. A model of normal fault interaction based on observations and theory. J. Struct. Geol. 22, 865–879.

Heiniö, P., Davies, R.J., 2007. Knickpoint migration in submarine channels in response to fold growth, western Niger Delta. Mar. Petrol. Geol. 24, 434–449.

Henriksen, E., Bjørnseth, H.M., Hals, T.K., Heide, T., Kiryukhina, T., Kløvjan, O.S., Larssen, G.B., Ryseth, A.E., Rønning, K., Sollid, K., Stoupakova, A., 2011. Chapter 17 Uplift and Erosion of the Greater Barents Sea: Impact on Prospectivity and Petroleum Systems, vol. 35. Geological Society, London, Memoirs, pp. 271–281.

Indrevær, K., Gabrielsen, R.H., Faleide, J.I., 22 November 2016. Early Cretaceous synrift uplift and tectonic inversion in the Loppa High area, southwestern Barents Sea, Norwegian shelf. J. Geol. Soc. https://doi.org/10.1144/jgs2016-066.

Jackson, J.A., 1987. Active Normal Faulting and Crustal Extension, vol. 28. Special Publications, Geological Society, London, pp. 3–17.

Jackson, C.A.L., Rotevatn, A., 2013. 3D seismic analysis of the structure and evolution of a salt-influenced normal fault zone: a test of competing fault growth models. J. Struct. Geol. 54, 215–234.

Jackson, C.A.L., Gawthorpe, R.L., Sharp, I.R., 2002. Growth and linkage of the East Tanka fault zone, Suez rift: structural style and syn-rift stratigraphic response. J. Geol. Soc. 159, 175–187.

Jackson, C.A.-L., Bell, R.E., Rotevatn, A., Tvedt, A.B.M., 2017. Techniques to Determine the Kinematics of Synsedimentary Normal Faults and Implications for Fault Growth Models. Geological Society, London Special Publications 439.

Kakimi, T., 1980. Magnitude-frequency relation for displacement of minor faults and its significance in crustal deformation. Bull. Geol. Surv. Jpn. 31, 467–487.

Kirby, E., Whipple, K.X., 2012. Expression of active tectonics in erosional landscapes. J. Struct. Geol. 44, 54–75.

Le Béon, M., Tseng, Y.C., Klinger, Y., Elias, A., Kunz, A., Sursock, A., Daëron, M., Tapponnier, P., Jomaa, R., 2018. High-resolution stratigraphy and multiple luminescence dating techniques to reveal the paleoseismic history of the central Dead Sea fault (Yammouneh fault, Lebanon). Tectonophysics 738–739, 1–15.

Leeder, M.R., Gawthorpe, R.L., 1987. Sedimentary models for extensional tilt-block/half-graben basins. 28. Special Publications, Geological Society, London, pp. 139–152.

Machette, M.N., Personius, S.F., Nelson, A.R., Schwartz, D.P., Lund, W.R., 1991. The Wasatch fault zone, Utah—segmentation and history of Holocene earthquakes. J. Struct. Geol. 13, 137–149.

Mansfield, C., Cartwright, J., 2001. Fault growth by linkage: observations and implications from analogue models. J. Struct. Geol. 23, 745–763.

Marin, D., Escalona, A., Sliwihska, K.K., Nøhr-Hansen, H., Mordasova, A., 2017. Sequence stratigraphy and lateral variability of Lower Cretaceous clinoforms in the southwestern Barents Sea. AAPG Bull. 101, 1487–1517.

Marín, D., Escalona, A., Grundvåg, S.-A., Nøhr-Hansen, H., Kairanov, B., 2018. Effects of adjacent fault systems on drainage patterns and evolution of uplifted rift shoulders: the Lower Cretaceous in the Loppa High, southwestern Barents Sea. Mar. Petrol. Geol. 94, 212–229.

Marrett, R., Allmendinger, R.W., 1992. Amount of extension on “small” faults: an example from the Viking graben. Geology 20, 47–50.

McAdoo, B.G., Pratson, L.F., Orange, D.L., 2000. Submarine landslide geomorphology, US continental slope. Mar. Geol. 169, 103–136.

McLeod, A.E., Dawers*, N.H., Underhill, J.R., 2000. The propagation and linkage of normal faults: insights from the Strathspey–Brent–Statfjord fault array, northern North Sea. Basin Res. 12, 263–284.

Mitchell, N.C., 2006. Morphologies of knickpoints in submarine canyons. GSA Bull. 118, 589–605.

Mørk, A., Dallmann, W., Dypvik, H., Johannessen, E., Larssen, G., Nagy, J., Nøttvedt, A., Olaussen, S., Pchelina, T., Worsley, D., 1999. Mesozoic Lithostratigraphy. Lithostratigraphic Lexicon of Svalbard. Upper Palaeozoic to Quaternary Bedrock. Review and Recommendations for Nomenclature Use. pp. 127–214.

Morley, C.K., 1999. Patterns of displacement along large normal faults: implications for basin evolution and fault propagation, based on examples from east Africa. AAPG Bull. (American Association of Petroleum Geologists) 83, 613–634.

Morley, C.K., 2002. Evolution of large normal faults: evidence from seismic reflection data. AAPG Bull. 86, 961–978.

Morley, C.K., Nelson, R.A., Patton, T.L., Munn, S.G., 1990. Transfer zones in the East African rift system and their relevance to hydrocarbon exploration in rifts. Am. Associat. Petrol. Geol. Bull. 74, 1234–1253.

Nicol, A., Childs, C., Walsh, J.J., Manzocchi, T., Schöpfer, M.P.J., 2016. Interactions and Growth of Faults in an Outcrop-Scale System, vol. 439 Special Publications, Geological Society, London.

Nottvedt, A., Gabrielsen, R.H., Steel, R.J., 1995. Tectonostratigraphy and sedimentary architecture of rift basins, with reference to the northern North Sea. Mar. Petrol. Geol. 12, 881–901.

Peacock, D.C.P., 2002. Propagation, interaction and linkage in normal fault systems. Earth Sci. Rev. 58, 121–142.

Peacock, D.C.P., Sanderson, D.J., 1991. Displacements, segment linkage and relay ramps in normal fault zones. J. Struct. Geol. 13, 721–733.

Peacock, D.C.P., Xing, Z., 1994. Field examples and numerical modelling of oversteps and bends along normal faults in cross-section. Tectonophysics 234, 147–167.

Petersen, K., Clausen, O.R., Korstgård, J.A., 1992. Evolution of a salt-related listric growth fault near the d-1 well, block 5605, Danish north sea: displacement history and salt kinematics. J. Struct. Geol. 14, 565–577.

Pirmez, C., Beaubouef, R.T., Friedmann, S.J., Mohrig, D.C., 2000. Equilibrium profile and baselevel in submarine channels: examples from late pleistocene systems and implications for the architecture of deepwater reservoirs. In: Weimer, P. (Ed.), Deep-Water Reservoirs of the World. SEPM Society for Sedimentary Geology.

Pritchard, D., Roberts, G.G., White, N.J., Richardson, C.N., 2009. Uplift histories from river profiles. Geophys. Res. Lett. 36.

Randen, T., Monsen, E., Signer, C., Abrahamsen, A., Hansen, J.O., Sæter, T., Schlaf, J., 2000. Three-Dimensional Texture Attributes for Seismic Data Analysis. SEG Technical Program Expanded Abstracts, pp. 668–671.

Robinson, S.M., 2014. Quantifying the Temporal and Spatial Response of Channel Steepness to Changes in Rift Basin Architecture. Arizona State University.

Schlagenhauf, A., Manighetti, I., Malavieille, J., Dominguez, S., 2008. Incremental growth of normal faults: insights from a laser-equipped analog experiment. Earth Planet. Sci. Lett. 273, 299–311.

Schlische, R.W., 1992. Structural and stratigraphic development of the Newark extensional basin, eastern North America: evidence for the growth of the basin and its bounding structures. GSA Bull. 104, 1246–1263.

Schlische, R.W., 1995. Geometry and origin of fault-related folds in extensional settings. Am. Associat. Petrol. Geol. Bull. 79, 1661–1678.

Serck, C.S., Faleide, J.I., Braathen, A., Kjølhamar, B., Escalona, A., 2017. Jurassic to early Cretaceous basin configuration(s) in the Fingerdjupet Subbasin, SW Barents Sea. Mar. Petrol. Geol. 86, 874–891.

Sharp, I.R., Gawthorpe, R.L., Underhill, J.R., Gupta, S., 2003. Fault-propagation folding in extensional settings: examples of structural style and synrift sedimentary response from the Suez rift, Sinai, Egypt. GSA Bull. 115 640-640.

Solheim, A., Kristoffersen, Y., 1984. Sediments Above the Upper Regional Unconformity: Thickness, Seismic Stratigraphy and Outline of the Glacial History. Norsk Polarinstitutt.

Su, J., Zhu, W., Wei, J., Xu, L., Yang, Y., Wang, Z., Zhang, Z., 2011. fault growth and linkage: implications for tectonosedimentary evolution in the chezhen basin of bohai bay, eastern China. AAPG Bull. 95, 1–26.

Taylor, S.K., Nicol, A., Walsh, J.J., 2008. Displacement loss on growth faults due to sediment compaction. J. Struct. Geol. 30, 394–405.

Tvedt, A.B.M., Rotevatn, A., Jackson, C.A.L., 2016. Supra-salt normal fault growth during the rise and fall of a diapir: perspectives from 3D seismic reflection data, Norwegian North Sea. J. Struct. Geol. 91, 1–26.

Walsh, J.J., Watterson, J., 1988. Analysis of the relationship between displacements and dimensions of faults. J. Struct. Geol. 10, 239–247.

Walsh, J.J., Watterson, J., 1989. Displacement gradients on fault surfaces. J. Struct. Geol. 11, 307–316.

Walsh, J., Watterson, J., Yielding, G., 1991. The importance of small-scale faulting in regional extension. Nature 351, 391.

Walsh, J.J., Nicol, A., Childs, C., 2002. An alternative model for the growth of faults. J. Struct. Geol. 24, 1669–1675.

Walsh, J.J., Bailey, W.R., Childs, C., Nicol, A., Bonson, C.G., 2003. Formation of segmented normal faults: a 3-D perspective. J. Struct. Geol. 25, 1251–1262.

Watterson, J., 1986. Fault dimensions, displacements and growth. Pure Appl. Geophys. 124, 365–373.

Wobus, C., Whipple, K.X., Kirby, E., Snyder, N., Johnson, J., Spyropolou, K., Crosby, B., Sheehan, D., 2006. Tectonics from topography: procedures, promise, and pitfalls. In: Willett, S.D., Hovius, N., Brandon, M.T., Fisher, D.M. (Eds.), Tectonics, Climate, and Landscape Evolution. Geological Society of America.

Wojtal, S.F., 1994. Fault scaling laws and the temporal evolution of fault systems. J. Struct. Geol. 16, 603–612.

Young, M.J., Gawthorpe, R.L., Hardy, S., 2001. Growth and linkage of a segmented normal fault zone; the late Jurassic Murchison–Statfjord north fault, northern North sea. J. Struct. Geol. 23, 1933–1952.

Paper 4

The Lower Cretaceous succession of the western Barents Shelf: onshore and offshore correlations

Grundvåg, S.-A., Marin, D., Kairanov, B., Nøhr-Hansen, H., Śliwińska, K.K., Escalona A., & Olaussen S.

Marine and Petroleum Geology, 86, 2017, 834-857, ISSN 0264-8172,

https://doi.org/10.1016/j.marpetgeo.2017.06.036

Marine and Petroleum Geology 86 (2017) 834–857

Contents lists available at ScienceDirect

Marine and Petroleum Geology

journal homepage: www.elsevier.com/locate/marpetgeo

Research paper

The Lower Cretaceous succession of the northwestern Barents Shelf: Onshore and offshore correlations

S.-A. Grundvåg [a,*], D. Marin [b], B. Kairanov [b], K.K. Śliwińska [c], H. Nøhr-Hansen [c], M.E. Jelby [e], A. Escalona [b], S. Olaussen [d]

[a] *Department of Geosciences, UiT – The Arctic University of Norway, PO Box 6050 Langnes, 9037 Tromsø, Norway*
[b] *Department of Petroleum Engineering, University of Stavanger, 4036 Stavanger, Norway*
[c] *Geological Survey of Denmark and Greenland (GEUS), Øster Voldgade 10, DK-1350 Copenhagen K Denmark*
[d] *Department of Arctic Geology, University Centre in Svalbard, PO Box 156, 9171 Longyearbyen, Norway*
[e] *Natural History Museum of Denmark, University of Copenhagen, Øster Voldgade 5-7, DK-1350 Copenhagen K, Denmark*

A R T I C L E I N F O

Article history:
Received 17 February 2017
Received in revised form
19 June 2017
Accepted 23 June 2017
Available online 24 June 2017

Keywords:
Early cretaceous
Clinoforms
Barents sea geology
Dinoflagellate biostratigraphy

A B S T R A C T

The Lower Cretaceous succession in the Barents Sea is listed as a potential play model by the Norwegian Petroleum Directorate. Reservoirs may occur in deep to shallow marine clastic wedges located in proximity to palaeo-highs and along basin margins. In addition, shelf-prism-scale clinoforms with high amplitude anomalies in their top- and bottomsets have been reported from reflection seismic but they have never been drilled. In Svalbard, the exposed northwestern corner of the Barents Shelf, Lower Cretaceous strata of shelfal to paralic origin occur, and includes the Rurikfjellet (Valanginian–Hauterivian/lowermost Barremian), Helvetiafjellet (lower Barremian–lower Aptian) and Carolinefjellet formations (lower Aptian–middle Albian). By combining sedimentological outcrop studies and dinocyst analyses with offshore seismic and well ties, this study investigate the link between the onshore strata and the offshore clinoforms. Age-vise, only three (S1–S3) of the seismic sequences defined in the offshore areas correlate to the onshore strata; S1 correspond to the Rurikfjellet Formation, S2 to the Helvetiafjellet Formation and the lower Carolinefjellet Formation, and S3 to the upper Carolinefjellet Formation. Offshore, all three sequences contain generally southward prograding shelf-prism-scale clinoforms. A lower Barremian subaerial unconformity defines the base of the Helvetiafjellet Formation, and its extent indicates that most of the Svalbard platform was exposed and acted as a bypass zone in the early Barremian. Onshore palaeo-current directions is generally towards the SE, roughly consistent with the clinoform accretion-direction towards the S. The local occurrence of a 150 m thick succession of gravity flow deposits transitionally overlain by prodelta slope to delta front deposits in the Rurikfjellet Formation, may indicate that shelf-edges also developed in Svalbard. The late Hauterivian age of theses deposits potentially highlights the inferred offlapping nature of the Lower Cretaceous strata as they predate the lower Barremian unconformity, and thus record a hitherto unknown regression in Svalbard. The presence of the lower Barremian subaerial unconformity in Svalbard, the general southeastward palaeo-current directions, and the age-equivalent clinoform-packages south of Svalbard, suggests that the onshore and offshore strata is genetically linked and was part of the same palaeo-drainage system.

1. Introduction

After several technical discoveries in clastic wedges of deep to shallow marine origin (e.g. Stewart et al., 1995; Seldal, 2005; Sattar et al., 2017), the Lower Cretaceous have been listed as one of several play models on the Barents Shelf by the Norwegian Petroleum Directorate. Lower Cretaceous shelf-margin-scale clinoforms containing prolific hydrocarbon-reservoirs in their shelf top-sets and base-of-slope toe-sets occur in the West Siberian Basin (Pinous et al., 1999, 2001; Ulmishek, 2003) and the Alaskan North Slope (Houseknecht et al., 2009). The Lower Cretaceous palaeogeography and basin development on the Barents Shelf are not yet fully understood. Lower Cretaceous clinoforms have been reported from

* Corresponding author.
E-mail address: sten-andreas.grundvag@uit.no (S.-A. Grundvåg).

http://dx.doi.org/10.1016/j.marpetgeo.2017.06.036

seismic reflection data on the Bjarmeland Platform and in the Fingerdjupet Subbasin (Henriksen et al., 2011; Marin and Escalona, 2014; Marin et al., 2016a, 2016b). Several studies have discussed the stratigraphic and lateral development of the Lower Cretaceous in Svalbard (e.g. Steel et al., 1978; Nemec et al., 1988; Nemec, 1992; Gjelberg and Steel, 1995, 2013; Midtkandal et al., 2007, 2008), and some have invoked a genetic link between the onshore and the offshore depositional systems (Århus et al., 1990; Steel et al., 2000; Midtkandal and Nystuen, 2009; Grundvåg and Olaussen, 2017). However, to date no studies have documented such a link due to a combination of limited data, long-distance correlations, poor age constrains and the lack of preserved Lower Cretaceous strata in parts of the northern Barents Sea.

This paper aims to shed new light on the onshore–offshore correlation of the Lower Cretaceous mainly in the northwestern part of the Barents Shelf (Fig. 1) by combining new biostratigraphic data, conventional outcrop data from Svalbard, and an offshore dataset consisting of seismic and geophysical well data. This study is part of the industry funded LoCrA (Lower Cretaceous basin studies in the Arctic, for more details see http://locra.ux.uis.no) consortium, and this paper summarizes some of our preliminary geological results and argue for a genetic link between the onshore and offshore depositional systems.

2. Geological framework

2.1. Study area and tectonic setting

Svalbard is an Arctic archipelago which represents the uplifted and exposed northwest corner of the Barents Shelf (Fig. 1). The shelf is bounded to the west by a sheared margin, to the north by a rifted (now passive) continental margin, and to the south and east by the Baltic Shield and Novaya Zemlya, respectively (Fig. 1). The latter separates it from the prolific Kara Sea region. Mesozoic strata are well preserved in Svalbard and occur in several basins and platform areas offshore, providing a unique opportunity to correlate onshore and offshore strata (e.g. Nøttvedt et al., 1992; Henriksen et al., 2011).

The Lower Cretaceous in the northern Barents Shelf, including Svalbard, was deposited in a subsiding epicontinental sag basin (e.g. Faleide et al., 2008; Henriksen et al., 2011, Fig. 2). Some minor fault activity is indicated on the Svalbard platform by stratal thickness variations across regional lineaments and syn-sedimentary collapse features in proximity to these (Steel and Worsley, 1984; Nemec et al., 1988; Onderdonk and Midtkandal, 2010). A shelf-edge setting have also been invoked to explain the presence of the collapse features on the east coast of Spitsbergen (Steel et al., 2000; Gjelberg and Steel, 2013). The region was heavily influenced by differential uplift and magmatism related to the opening of the Canada Basin in Late Jurassic to Early Cretaceous times (Maher, 2001; Grantz et al., 2011). In Svalbard, Franz Josef Land, and nearby shelf areas, the magmatic activity peaked in the Barremian to early Aptian (Corfu et al., 2013; Polteau et al., 2015) with the development of circum-Arctic dyke swarms and local volcanism (Grogan et al., 2000; Senger et al., 2014, Fig. 2). Some workers have also suggested a hot spot origin for the Canada Basin as the Iceland hot spot transited the Polar region in the latest part of the Early Cretaceous to Late Cretaceous (Lawver and Muller, 1994; Lawver et al., 2002). In Svalbard, early Barremian uplift and southward tilting of the shelf created a regionally-extensive sub-aerial unconformity (Gjelberg and Steel, 1995, 2013; Maher, 2001).

The southwestern Barents Shelf is characterized by several N–S to NE–SW-trending rift basins and structural highs belonging to the Mesozoic North Atlantic rift system (e.g. Dalland, 1981; Doré et al., 1999; Torsvik et al., 2002; Faleide et al., 1993, 2008, Fig. 2). Although some minor fault displacement is evident in the middle Jurassic, the main phase of extensional faulting took place in the Early Cretaceous with a rift climax in the Hauterivian (Faleide et al., 1993; Doré et al., 1999). In this period the rift basins experienced significant subsidence resulting in thick successions of Lower Cretaceous deposits (e.g. Faleide et al., 1993). The submerged structural highs experienced sediment starvation, and condensed carbonate successions developed locally (Smelror et al., 1998). Compressional tectonics leading to inversion and vertical movement of some structural elements also influenced the basin development in the Early Cretaceous (Faleide et al., 1993; Gabrielsen et al., 1997; Grogan et al., 1999; Indrevær et al., 2016), particularly in the northeastern Barents Shelf, including Kong Karls Land, where a series of SW–NE-trending anticlines formed and locally controlled the palaeo-drainage (Grogan et al., 2000; Kairanov et al., 2015).

2.2. Onshore lithostratigraphy and depositional system

In Svalbard, the Adventdalen Group (Parker, 1967, Fig. 3) is subdivided into the Upper Jurassic Agardhfjellet Formation (not considered herein), and the Lower Cretaceous Rurikfjellet, Helvetiafjellet and Carolinefjellet formations, which together form an up to 2 km thick siliciclastic succession (Figs. 3 and 4; Mørk et al., 1999). The lower Rurikfjellet Formation (Valanginian–Hauterivian/early Barremian) is shale-dominated and represents deposition on an open marine shelf (Wimanfjellet Member in Figs. 3 and 5). Thick successions of gravity flow deposits occur locally in the Rurikfjellet Formation (Braathen et al., 2012; informally referred to as the Advenpynten member in Fig. 3, Fig. 5b and Fig. 6). The base of the formation is defined by a condensed glauconitic clay unit, the Myklegardfjellet Bed, which formed during maximum flooding of the shelf (Dypvik et al., 1992, Fig. 3). Recent studies have dated the Myklegardfjellet Bed to be of earliest Valanginian age indicating the presence of an uppermost Volgian to lower Ryazanian hiatus in the immediate underlying strata (Wierzbowski et al., 2011; Koevoets et al., 2016, Fig. 3). This unconformity may be the onshore equivalent to the similar-aged Base Cretaceous Unconformity (BCU in Fig. 3; Lundin and Doré, 1997; Osmundsen and Ebbing, 2008) recorded in several offshore basins on the Norwegian Continental Shelf. The amount of siltstone and sandstone increases upwards in the Rurikfjellet Formation (the Kikutodden Member in Fig. 3, Fig. 4b and Fig. 5d), recording a gradual change from outer shelf to inner shelf and shoreface environments possibly in response to uplift in the north (Dypvik et al., 1991; Gjelberg and Steel, 1995). The base of the unconformably overlying Helvetiafjellet Formation (Barremian–early Aptian) is a regionally extensive subaerial unconformity of early Barremian age which formed during peak uplift in the north (Gjelberg and Steel, 1995, 2013; Maher, 2001, Figs. 3–6). The uplift, which is linked to the opening of the Canada Basin, resulted in a forced regression with sediment dispersal towards the SE (Gjelberg and Steel, 1995; Midtkandal and Nystuen, 2009). Above the basal boundary, the Helvetiafjellet Formation shows an overall transgressive development, and consists of a lower sandstone-dominated sheet-like unit deposited in a fluvial braidplain setting (the Festningen Member in Fig. 3, Fig. 4c and Fig. 6), and an upper heterolithic unit rich in thin coals and carbonaceous shales deposited in paralic environments (the Glitrefjellet Member in Figs. 3 and 6; Gjelberg and Steel, 1995; Midtkandal and Nystuen, 2009). At Kvalvågen, eastern Spitsbergen, the Glitrefjellet Member includes three regressively stacked deltas immediately above the fluvial sandstone sheet (Fig. 5e). The conformably overlying Carolinefjellet Formation (early Aptian–Albian) was grossly deposited in an open marine, storm-dominated shelf setting and consists of alternating inner shelf sandstones and offshore

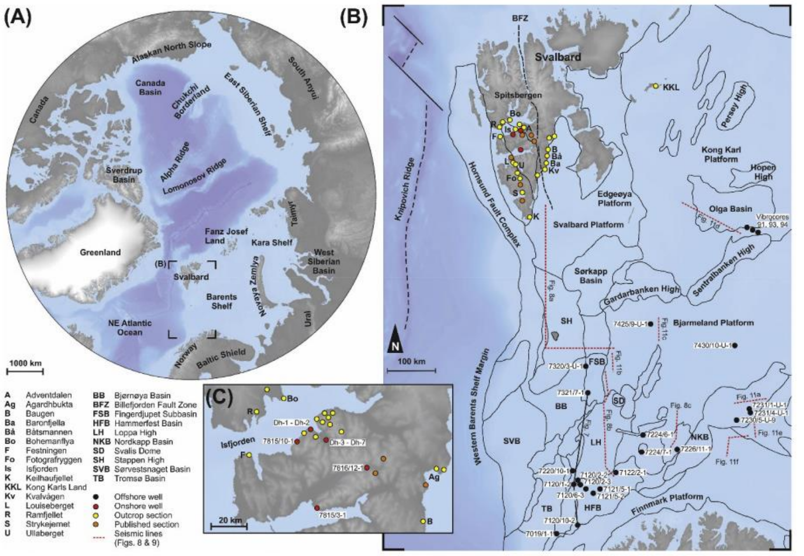

Fig. 1. (A) Circum-Arctic map showing the location of the study area on the Barents Shelf (dashed rectangle) and some of the main tectonic features of the Arctic Basin. (B) Map of the study area showing the main structural elements (based on Grogan et al., 1999; Henriksen et al., 2011) and location of the investigated outcrops, and onshore and offshore well data used in this study. The position of the seismic lines used in the study are shown in inset maps accompanying the seismic cross-sections. (C) Map of Nordenskiöld Land in Central Spitsbergen showing the location of some outcrop sections and onshore wells used in this study. Bathymetry data is from IBCAO (http://www.ngdc.noaa.gov/mgg/bathymetry/arctic/downloads.html).

mudstones (Nagy, 1970; Hurum et al., 2016, Figs. 3–6). The boundary between the Helvetiafjellet and Carolinefjellet formations has traditionally been described as interfingering (Gjelberg and Steel, 1995). However, the present study have demonstrated that in most outcrop sections in Spitsbergen, a c. 10–30 m thick black shale unit separate the two formations (FS in Figs. 4–6). The shale is dated to be of an early Aptian age and interpreted as a regional flooding event marking a return from paralic to open marine shelf environments (Figs. 4–6). Recent carbon isotope (δ13C) studies have also identified the early Aptian oceanic anoxic event (OAE1a) within the shale unit (Midtkandal et al., 2016; Vickers et al., 2016).

2.3. *Offshore lithostratigraphy and depositional system*

In the offshore basins, the Adventdalen Group encompass Valanginian to Cenomanian deposits (Fig. 3). For convenience, it will, age-vise, be referred to as Lower Cretaceous for the remaining part of this paper. The group shows major lateral changes in facies and thickness, and in combination with poor data resolution, long distance correlations across basins that formed under various tectonic regimes, and the lack of detailed age constraints, this has led to a confusing lithostratigraphic nomenclature (Figs. 3 and 7). Although the existing lithostratigraphic framework provides a good basis for mapping at local basin scale, it does not facilitate a detailed understanding of the regional depositional history and palaeogeography. A more genetic approach is necessary, particularly when it comes to correlation of the onshore and offshore depositional systems.

Offshore, the Adventdalen Group are generally confined by the Base Cretaceous Unconformity (BCU) and the Upper Regional Unconformity (URU; Fig. 3). In some places though, depending on degree of preservation, the Lower Cretaceous is overlain by thick Upper Cretaceous (the Nygrunnen Group) and Paleogene (the Sotbakken Group) strata (Worsley et al., 1988). The base of the Upper Cretaceous Nygrunnen Group is characterized by a Turonian–Santonian unconformity which separates it from the underlying Adventdalen Group. In some basins, the URU therefore truncates Upper Cretaceous or Paleogene rather than Lower Cretaceous strata (e.g. in the Hammerfest Basin; Solheim and Kristoffersen, 1984; Worsley et al., 1988). Within the Lower Cretaceous of the Barents Sea, seven sequences (S0–S6) each separated by flooding surfaces (K0–K5) have been identified by combining well data, biostratigraphy and seismic data (Marin and Escalona, 2014; Marin et al., 2016a, Figs. 3 and 7). Each sequence has a duration of 5–10 Ma, conforming to third-order sequences. A regional well correlation of the sequences are shown in Fig. 7 (7120/10-2, 7120/1-2 and 7321/7-1), and regional well-tied, two-

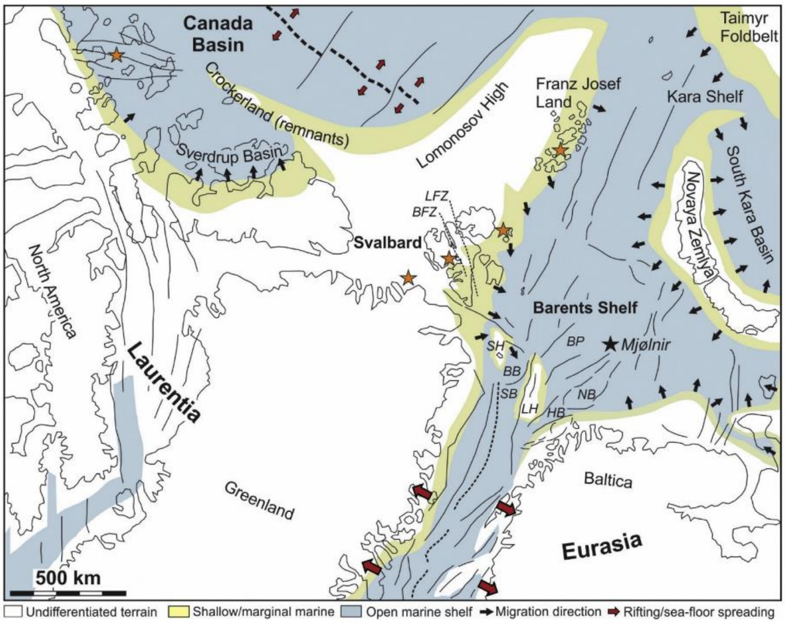

Fig. 2. Palaeogeographic map showing the regional tectonic setting and palaeo-drainage in the Early Cretaceous. The reconstruction represents the end of the Hauterivian and beginning of the Barremian when the initial rifting in the Canada Basin had been replaced by rapid sea-floor spreading. Note that the Barents Shelf acted as the final sink for many of its bordering and uplifted terrains. Based on Torsvik et al. (2002), Golonka et al. (2003), and Basov et al. (2009). Red stars indicate areas influenced by igneous activity in the Early Cretaceous. The black star indicates the position of the Mjølnir Impact Crater (see text for more details) BB: Bjørnøya Basin, BP: Bjarmeland Platform, FP: Finnmark Platform, FSB: Fingerdjupet Subbasin, HB: Hammerfest Basin, LH: Loppa High, NB: Nordkapp Basin, SB: Sørvestsnaget Basin, SH: Stappen High, BFZ: Billefjorden Fault Zone, LFZ: Lomfjorden Fault Zone. (For interpretation of the references to colour in this figure legend, the reader is referred to the web version of this article.)

dimensional seismic lines are shown in Fig. 8. This study only focus on S1–S3 (Figs. 3, 7 and 8), as S0 only occur as sedimentary wedges along the margin of the Hammerfest Basin (Marin et al., 2016a; Sattar et al., 2017), and the younger sequences S4–S6 typically show progradation from the NE towards the SW, the latter suggesting a regional change in source area and palaeo-drainage (Bugge et al., 2002; Marin et al., 2016a). The investigated sequences are roughly correlated to the lithostratigraphic units in Fig. 3, but for historical context a short review of the offshore lithostratigraphy follows.

Offshore, the Adventdalen Group is subdivided into the Klippfisk (late Berriasian–Hauterivian, locally early Barremian), Knurr (Valanginian–early Barremian), Kolje (early Barremian–early Aptian), and Kolmule formations (Aptian–middle Cennomanian, Worsley et al., 1988; Smelror et al., 1998, Fig. 3). Most of the offshore strata are shale-dominated and was apparently deposited in open-marine shelf environments (e.g. the Kolje Formation; Fig. 3). However, sandstones of shallow marine and fan delta origin occur locally in the Kolmule Formation in proximity to the Loppa High (e.g. the 7120/6-3S Juksa, 7220/10-1 Salina and 7120/2-3S Skalle wells; Fig. 1 for location). In addition, sandstone-dominated gravity-flow deposits are known from the Knurr Formation, typically occurring along basin-bounding faults (Seldal, 2005; Henriksen et al., 2011; Marin et al., 2016a; Sattar et al., 2017, Fig. 3). Condensed carbonates (i.e. glauconitic limestones and marls) deposited during a regional transgression occur locally on the platforms and highs, and is referred to as the Klippfisk Formation (Smelror et al., 1998, Fig. 3). The unit is in part equivalent to the Myklegardfjellet Bed on Spitsbergen (Dypvik et al., 1992, Fig. 3). In some areas, like the Bjarmeland Platform, the clinoforms described in this study downlap onto the top surface of the Klippfisk Formation (Århus et al., 1990, Fig. 3). The basal boundary of the formation is defined by the BCU (Århus et al., 1990; Lundin and Doré, 1997; Osmundsen and Ebbing, 2008). The unconformity which spans from latest Volgian to earliest Valanginian in age is characterized by an abrupt decrease in gamma ray response and increased velocity upward from the underlying shale-dominated Upper Jurassic Hekkingen Formation (Fig. 3). Its formation mechanisms is poorly understood, but it may have formed in relation to regional uplift resulting in a relative sea-level lowstand (Faleide et al., 1993).

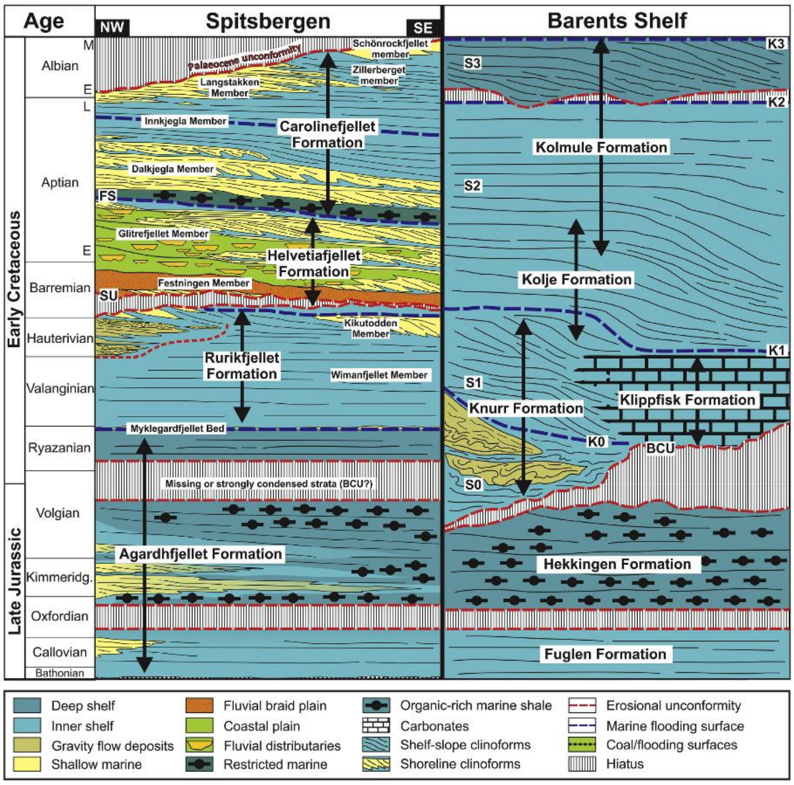

Fig. 3. Stratigraphic cross-section showing the regional development of the Upper Jurassic to Lower Cretaceous Adventdalen Group on Spitsbergen and the Barents Shelf. Onshore, the Myklegardfjellet Bed separates the Upper Jurassic from the Lower Cretaceous and corresponds to a maximum flooding surface. The underlying Berriasian hiatus probably corresponds to the Base Cretaceous Unconformity (BCU) in the offshore basins. To facilitate discussion, the third-order sequences on the Barents Shelf (S0–S3) have roughly been correlated to the lithostratigraphic units. The sequences are bounded by flooding surfaces (K0–K3) of regional extent. The cross-section integrates data compiled from Parker (1967), Nagy (1970), Steel and Worsley (1984), Dypvik et al. (1991), Gjelberg and Steel (1995, 2013), Midtkandal et al. (2007, 2008), Marín and Escalona (2014), Koevoets et al. (2016), Midtkandal et al. (2016), Vickers et al. (2016), and Grundvåg and Olaussen (2017) No vertical scale intended. BCU: Base Cretaceous Unconformity, URU: Upper Regional Unconformity, SU: lower Barremian subaerial unconformity, FS: lower Aptian flooding surface.

or alternatively as the result of a tsunami triggered during formation of the Mjølnir Impact crater (Rokoengen et al., 2005; see Fig. 2 for crater location).

3. Data and methods

3.1. Onshore data

The onshore data include logged sections from onshore wells (collective thickness of c. 2000 m; Fig. 6) and several outcrops (collective thickness >3500 m) together covering the entire extent of the Lower Cretaceous outcrop belt, including the southernmost outcrop section in Sørkapp Land (Keilhaufjellet section in Fig. 1b) and the inferred most proximal and northernmost section north of Isfjorden (Bohemanflya and Ramfjellet sections in Fig. 1c). Palaeocurrent data were obtained in all the visited outcrops and from previous publications (e.g. Gjelberg and Steel, 1995; Midtkandal and Nystuen, 2009). In addition, the gamma-ray log from three

S.-A. Grundvåg et al. / Marine and Petroleum Geology 86 (2017) 834–857

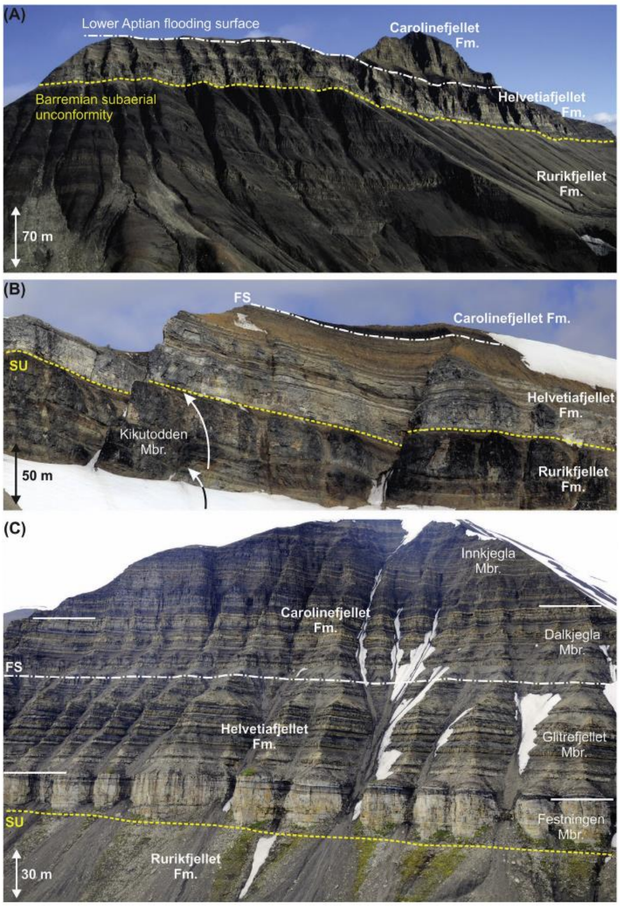

Fig. 4. (A) Picture showing the lithostratigraphic development at Louiseberget in south central Spitsbergen. A lower Barremian subaerial unconformity (annotated SU in the following pictures) and a lower Aptian flooding surface (annotated FS in the following pictures) separates the paralic Helvetifjellet Formation from the open marine shelf deposits of the Rurikfjellet and Carolinefjellet formations, respectively. Note that the Rurikfjellet Formation is shale-dominated. (B) Picture showing the Lower Cretaceous succession at Keilhaufjellet in the southernmost part of Spitsbergen. The upper Rurikfjellet Formation (Kikutodden Member) consists of sandstone-dominated, coarsening-upward parasequences (white arrows) at this location (see also Fig. 5d). (C) The Lower Cretaceous succession at Båtsmannen, eastern Spitsbergen. The member subdivision is easy to recognize. Note that both the Barremian subaerial unconformity and the lower Aptian flooding surface is present in all the outcrops and thus represent regional events. For location see Fig. 1b.

840 S.-A. Grundvåg et al. / Marine and Petroleum Geology 86 (2017) 834–857

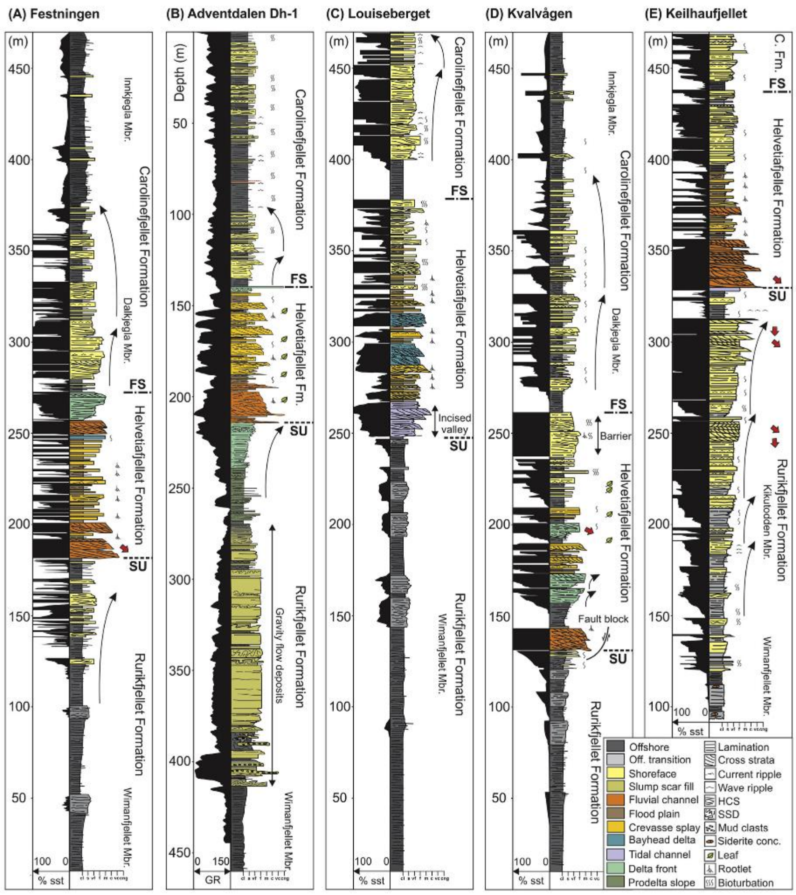

Fig. 5. Five vertical sections from Spitsbergen showing the lateral development of the Valanginian to lower Aptian depositional system from north to southeast. The sections are not stratigraphically correlated. Red arrows indicate general palaeo-flow directions measured on dune-scale cross-stratification. SU: lower Barremian subaerial unconformity, FS: lower Aptian flooding surface, HCS: Hummocky cross-stratification, SSD: Soft-sediment deformation, GR: Gamma ray, Sst: Sandstone. Grain sizes: cl: clay, s: silt, vf: very fine sand, f: fine sand, m: medium sand, c: coarse sand, vc: very coarse sand, cng: conglomerate (granule and pebble size). For section location see Fig. 1b and c. (For interpretation of the references to colour in this figure legend, the reader is referred to the web version of this article.)

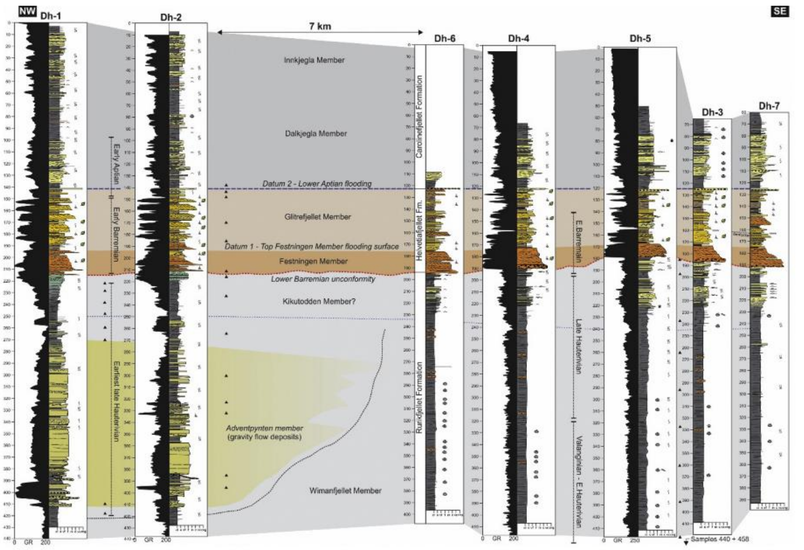

Fig. 6. Correlation panel linking the seven onshore wells in central Spitsbergen. The panel is corrected for structural dip and is flattened on the lower Aptian flooding surface separating the Helvetiafjellet and Carolinefjellet formations. The panel is oriented in a NW–SE direction and is therefore oriented parallel to the inferred SE-directed palaeo-shoreline migration direction. Gamma ray logs are included for wells Dh-1, Dh-2, Dh-4 and Dh-5. Note the presence of a thick succession of gravity flow deposits in wells Dh-1 and Dh-2, here informally referred to as the Adventpynten member. Note also the local thickness variation of the Festningen Member, indicating variable degrees of incision and possibly the presence of incised valleys.

exploration wells (7815/10-1 Colesbukta, 7816/12-1 Reindalspasset, and 7815/3-1 Ishøgda) have aided in regional correlations between areas lacking good outcrops (Fig. 1c for location).

3.2. Offshore data

Two- and three-dimensional seismic and well data were provided by the Norwegian Petrobank database. The seismic data covers an area of 100,000 km^2 (Fig. 1c). The quality of the seismic is variable with general frequencies between 10 and 50 Hz; multiples occur in some areas (Fig. 8). Vertical seismic resolution is in the order of 20–30 m. The seismic quality and resolution restrict interpretation in some areas, and low-relief clinoforms (<100 m), for example, can only be identified in the frequency range of 27–50 Hz. The third-order sequence-bounding flooding surfaces were defined on the basis of the gamma-ray well logs (Fig. 7) in combination with reflector terminations (Fig. 8) according to the nomenclature of Mitchum et al. (1977). The trajectory analysis followed the principles outlined by Helland-Hansen and Hampson (2009) and was performed on flattened seismic cross-sections oriented close to the perpendicular direction of clinoform progradation. The lines used for this purpose were flattened on the BCU, or on regional flooding surfaces in the topset or bottomset segment of the investigated clinforms (Fig. 9). The BCU is considered here to lack any significant relief on the platform areas because a parallel continuous reflector interpreted to be a flooding surface (Surface K0; Fig. 3) is generally observed to occur immediately above it. An exception is along the margin of the Hammerfest Basin were the sedimentary wedges of S0 occur and separate the BCU from the overlying K0 flooding surface.

Only the three most representative wells used for the definition and correlation of the seismic sequences are shown herein (7120/10-2, 7120/1-2 and 7321/7-1; Fig. 7), see Marin and Escalona (2014) and Marin et al. (2016a) for a complete well list. Because most of the exploration wells with Lower Cretaceous core data specifically targeted submarine fans of the Knurr Formation (e.g. 7019/1-1, 7120/1-2, 7120/10-2, 7122/2-1 and 7321/7-1), no exploration wells have to date have fully cored any of the clinoform packages. However, some shallow stratigraphic wells penetrate parts of the clinoform sequences; well 7231/1-U-1 penetrate what is inferred to be the toeset of S2 in the Nordkapp Basin, whereas well 7231/4-U-1 penetrate parts of the topset of the same sequence. In the northernmost part of the Bjørnøya Basin, well 7320/3-U-1 probably penetrates S1 where a 30 m thick coarsening upwards mudstone-dominated unit of early Barremian age sharply overlies condensed carbonates of the Klippfisk Formation (Århus et al., 1990). Core descriptions of the published shallow stratigraphic wells 7230/5-U-9, 7231/1-U-1, 7320/3-U-1, 7430/10-U-1, and 7425/

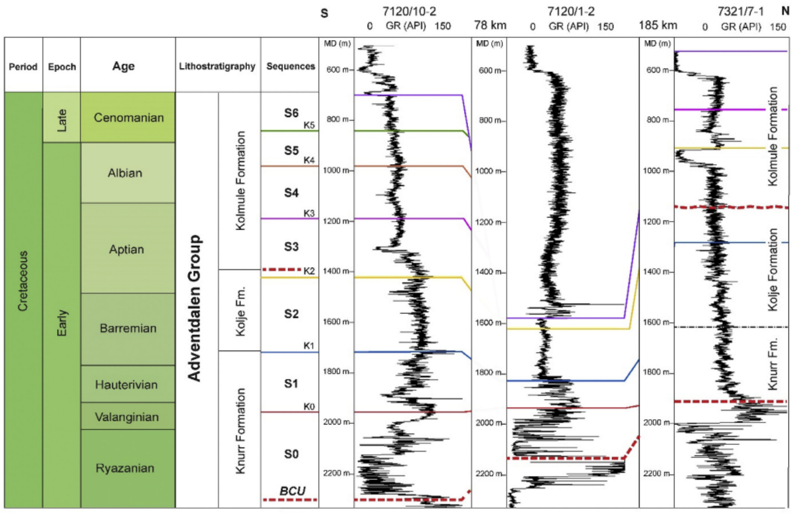

Fig. 7. North to south-oriented well panel from the Fingerdjupet Subbasin southward to the Hammerfest Basin showing the lateral correlation and distribution of the Lower Cretaceous seismic sequences. This study focus particularly on the S1–S3 interval. The sequence division is based on the recognition of regionally extensive flooding surfaces and biostratigraphic analyses. For location of the well transect, see Fig. 1b. BCU: Base Cretaceous Unconformity.

9-U-1 have been integrated in this study (Århus et al., 1990; Århus, 1991a; Smelror et al., 1998; Bugge et al., 2002; Langrock et al., 2003).

3.3. Biostratigraphic data

Palynological analysis (dinoflagellate cysts; dinocyst) were carried out on altogether 101 sediment samples. From Svalbard, 72 samples were collected in both outcrops sections (Bohemanflya, Keilhaufjellet, Baugen, Båtsmannen, Louiseberget, Ullaberget and Schönrockfjellet; Fig. 1b for location) and drill cores (wells Dh-1: eight samples; Dh-2: 14 samples; Dh-5: 11 samples). From the Barents Sea samples for palynological analysis were collected from cored intervals of five wells (7019/1-1, 7120/1-2, 7120/2-2, 7121/5-1 and 7121/5-2; Fig. 1c for location; Fig. 7 for well correlation of the three first wells). Palynological slides were prepared at the Geological Survey of Denmark and Greenland (GEUS) by conventional processing techniques used for palynological preparation as described by Nøhr-Hansen (2012).

Additionally, 20 palynological slides from wells 7121/5-1 and 7121/5-2 were analyzed. These slides were prepared from ditch cutting (DC) and sidewall core (SWC) samples. The slides from these two wells were prepared by Statoil and were borrowed from the Norwegian Petroleum Directorate (NPD). Slides have been scanned in order to identify key species. For the uppermost Hauterivian to Albian strata, we have applied the dinocyst zonation of Nøhr-Hansen (1993) established for North-East Greenland. Most of the analyzed samples contained age-diagnostic dinocysts.

In the Olga Basin, shallow vibrocores containing Lower Cretaceous deposits have been described and biostratigraphically dated by Antonsen et al. (1991). This data have been used for a preliminary age assignment of the sequences in the northeastern part of the study area.

4. Onshore depositional trends

The facies types in the onshore succession are thoroughly documented in previous papers (e.g. Edwards, 1976; Mørk, 1978; Nemec et al., 1988; Dypvik et al., 1991; Nemec, 1992; Gjelberg and Steel, 1995; Midtkandal et al., 2007; Midtkandal and Nystuen, 2009; Grundvåg and Olaussen, 2017) and will not be reiterated in detail here. However, the facies development and the spatial distribution of individual depositional elements going vertically from the base of the Rurikfjellet Formation and upwards through the Helvetiafjellet and Carolinefjellet formations are briefly summarized as basis for a regional synthesis of the basin fill history and its controls. The vertical facies development at three different locations are summarized in Fig. 4, and generalized sedimentary logs is shown in Figs. 5 and 6.

4.1. Depositional trends of the Rurikfjellet Formation

The basal unit of the Rurikfjellet Formation, the Myklegardfjellet Bed, consists of an up to 10 m thick plastic clay unit rich in glauconite deposited during maximum flooding of the shelf. Recent stratigraphic investigations indicate the presence of a significant

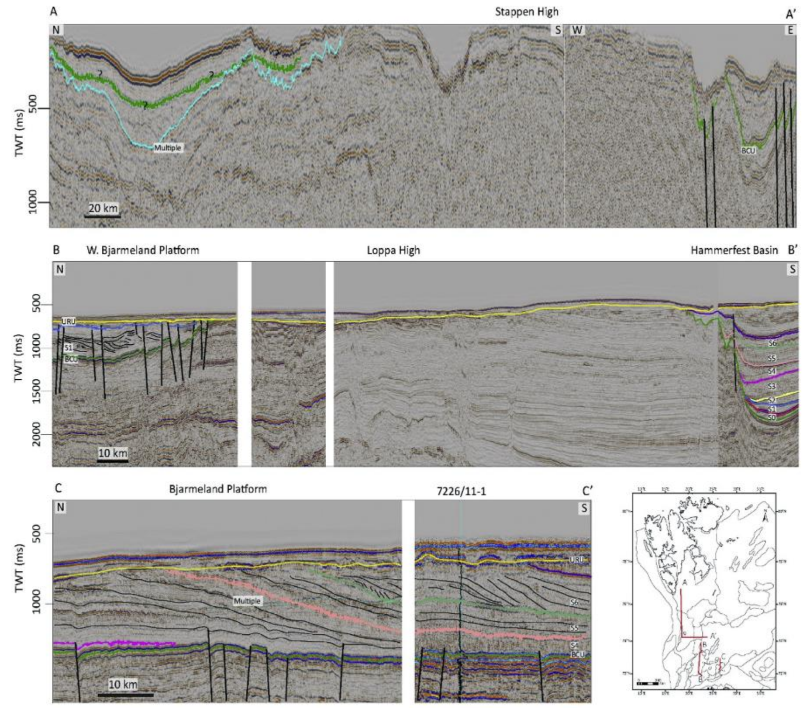

Fig. 8. Two-dimensional regional seismic profiles showing the interpreted sequence division and correlation. A–A' is a composite profile going from the Edgeøya Platform south of Spitsbergen southward to the Stappen High turning east to the Hopenbanken Arch. The sequences are difficult to recognize in these northern areas due to the poor data quality and Cenozoic uplift and erosion. B–B' is an N–S-oriented profile going from the western Bjarmeland Platform southward across the Loppa High into the Hammerfest Basin where all the sequences are well preserved. Clinoforms occur in S2 and S3 on the Bjarmeland Platform. C–C' is a profile dip-oriented profile going from the Bjarmeland Platform southeastward into the Nordkapp Basin. The final shelf-break for the sequences investigated in this study (S1–S3) is located in the northern part of the Nordkapp Basin. The inset map shows the location of the profiles, including the three shorter profiles shown in Fig. 9. BCU: Base Cretaceous Unconformity, URU: Upper Regional Unconformity.

hiatus in the strata immediately below the Myklegardfjellet Bed (Wierzbowski et al., 2011; Koevoets et al., 2016). A similar setting is seen offshore where the base of the age- and lateral-equivalent to the Myklegardfjellet Bed, the Klippfisk Formation, is defined by the BCU (Århus et al., 1990). Although some Upper Jurassic sandstone wedges may have a northern source terrane, the Myklegardfjellet marks the onset of a tectonically controlled regional regression with sediments being derived from uplifted terranes north of Svalbard. The lower Rurikfjellet Formation, the Wimanfjellet Member, consists of mudstones deposited in an outer shelf setting (Figs. 3–5 and Fig. 9a). The mudstones grade upwards into siltstones and very-fine grained sandstones deposited in an offshore transition to lower shoreface setting (Fig. 3; Dypvik et al., 1991). In the north central part of Spitsbergen the siltstones and sandstones form shallowing upwards parasequences (*sensu* Van Wagoner et al., 1990, Figs. 3, 5a and Fig. 6 and 9b). Individual parasequences are 10–50 m thick, and stacked units are separated by flooding surfaces. The source area for this system must have been located N–NW of the present day outcrop belt as the parasequences are not that well-developed in eastern, south-central, or southeastern Spitsbergen (Figs. 3 and 5), reflecting proximal–distal trends and a south to mainly southeastward prograding shoreline. In southernmost Spitsbergen, coarser-grained and more quartz-rich parasequences which generally show progradation towards the S–SE occur (the Kikutodden Member; Figs. 3–5). Individual units are up to 50 m thick and stack to form a 150 m thick sandstone-dominated package (Edwards, 1976; Mørk, 1978; Grundvåg and Olaussen, 2017.; Fig. 4b and Fig. 5e). The parasequences are interpreted to

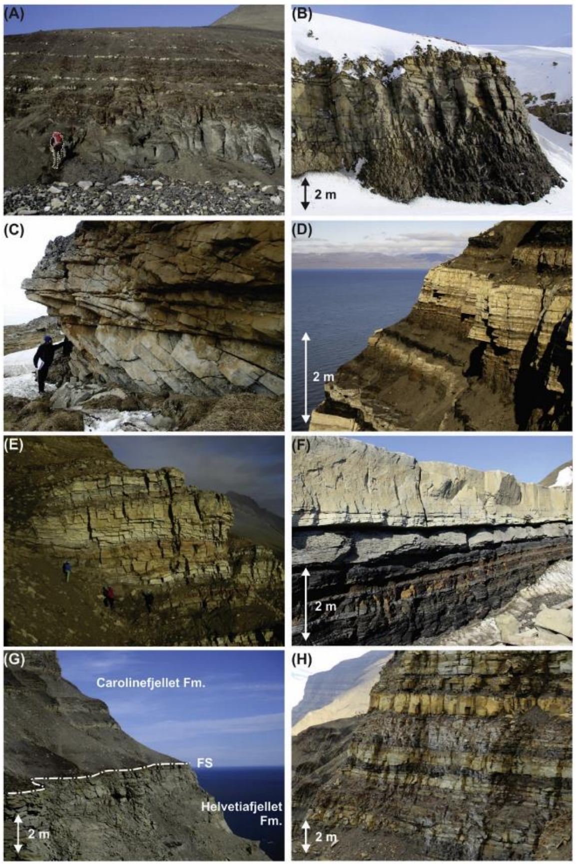

Fig. 9. (A) Typical expression of the shale-dominated Wimanfjellet Member of the Rurikfjellet Formation (location Ba, Fig. 1b). Person for scale (180 cm) (B) Coarsening- and shoaling upward lower shoreface parasequence in the Kikutodden Member of the Rurikfjellet Formation (location A, Fig. 1b). (C) Meter-scale stratification in fluvial braidplain deposits in the Festningen Member of the lower Helvetiafjellet Formation (person for scale: c. 185 cm, location A, Fig. 1b). The upper Helvetiafjellet Formation consists of various paralic deposits and include (D) flood plain and crevasse splay (location Is, Fig. 1b), (E) tidal channel (persons for scale: c. 170 cm, location U, Fig. 1b), and (F) mouth bar deposits (location Kv, Fig. 1b). (G) The formation is capped by a lower Aptian flooding surface (annotated FS) marking a return from paralic to open marine shelf deposition in the Carolinefjellet Formation (location Ba, Fig. 1b). (H) The sandstone-dominated part of the Dalkjegla Member in the lower Carolinfjellet Formation consists of various storm deposits that accumulated in an offshore transition to lower shoreface setting on a shallow, open-marine shelf (location Bå, Fig. 1b).

represent successively southward-progradig shoreline tongues. The lack of backshore and coastal plain deposits in any of the parasequences indicate high rates of sediment accumulation relative to the rates of relative sea-level change. The rapid basinward accretion resulted in low-angle facies lines and limited accommodation space for such deposits to accumulate. Alternatively, all backshore deposits got eroded during the intervening transgressions, or the sea level at all times were too deep. In this regard, each parasequence may represent an infralittoral prograding wedge (*sensu* Hernández-Molina et al., 2000) that formed a subaqueous platform in front of the actual shoreline. It is suggested here that these parasequences had their source area to the west as similar units are not present north of Fotografryggen in Wedel Jarlsberg Land (the Fo section in Fig. 1). A potential source area could be Greenland, which was located much closer to the western margin of the Barents Shelf and Svalbard in the Early Cretaceous than at present (Fig. 2). In most studied outcrops, a 5–30 m thick marine shale unit occur on top of the uppermost sand-rich parasequence. This suggests an early Barremian regional flooding event (possibly corresponding to surface K1 offshore; Fig. 3) prior to the formation of the subaerial unconformity at the base of the overlying Helvetiafjellet Formation (Fig. 3).

4.2. Age of the Rurikfjellet Formation

Foraminiferal fauna reported from the basal Myklegardfjellet Bed suggest predominantly an early Valanginian age for this unit, but may also include the uppermost Ryazanian (Dypvik et al., 1992; Koevoets et al., 2016). The depositional break reported in the Upper Jurassic Agardhfjellet Formation underlying the Myklegardfjellet Bed spans the uppermost Volgian and lower Ryazanian (Wierzbowski et al., 2011; Koevoets et al., 2016), and may thus correlate to the BCU offshore (Fig. 3).

The dinocyst from the Rurikfjellet Formation were analysed in three onshore wells (Dh-1, Dh-2 and Dh-5; Fig. 6) and in samples from the Bohemanflya and Ullaberget outcrop sections. The preservation of dinocysts in the Rurikfjellet Formation is moderate to poor and the assemblages are of low diversity. Based on the presence of the two most common dinocyst markers *Endoscrinium hauterivianum* and *Nelchinopsis kostromiensis* the Rurikfjellet Formation is dated as late Valanginian to late Hauterivian (Fig. 10). Our result confirms the previous age assessment of Århus (1992). Based on the presence of *Pseudoceratium anaphrissum* specimens in the Dh-5 well and in the Bohemanflya outcrop section, as well as *Dingodinium cerviculum*, *Muderongia tetracantha*, *Oligosphaeridium complex*, questionable *Pseudoceratium anaphrissum* and *Subtilisphaera perlucida* specimens in the Ullaberget outcrop section, the uppermost part of the Rurikfjellet Formation is tentatively assigned an early Barremian age (Subzone I (2); Figs. 3 and 10). A Barremian age for the uppermost few meters of the formation have previously been suggested by Grøsfjeld (1992).

4.3. Depositional trends of the Helvetiafjellet Formation

The base of the overall transgressive Helvetiafjellet Formation is defined by a regionally-extensive subaerial unconformity that by variable amounts cut down into the underlying strata (Nemec, 1992; Gjelberg and Steel, 1995, 2013; Midtkandal et al., 2008, Figs. 3–6). For large parts of the outcrop belt, the unconformity separates underlying marine shales from fluvial sandstones, and its presence is a spectacular proof of forced regression as it represent a major sediment bypass surface (Steel et al., 2000). The lower Helvetiafjellet Formation, the Festningen Member (Figs. 3 and 6), consists of fine-to very coarse-grained pebbly sandstones and conglomerates with abundant cross-stratification indicating deposition in a low-gradient braid-plain setting (Nemec, 1992; Gjelberg and Steel, 1995, Figs. 5, 6 and Fig. 9c). The rivers were generally transporting sediments in a southeastward direction (Gjelberg and Steel, 1995; Midtkandal and Nystuen, 2009). However, in Kong Karls Land, eastern Svalbard, the fluvial system are confined to topographic lows between SW–NE-trending anticlines and a southwestward palaeo-drainage is evident. Local and abrupt thickness-variations indicate that the lower part of the Festningen Member was deposited in wide, and partly coalescing river valleys that formed during shelf exposure in the early Barremian (Nemec, 1992; Midtkandal and Nystuen, 2009, Fig. 6). In some of the incised river valleys, higher frequency relative sea-level fluctuations driven by multiple episodes and variable rates of uplift, promoted intra-valley incisions and the development of bay head deltas and estuaries as evident at the Louiseberget and Ullaberget localities (Gjelberg and Steel, 1995; Midtkandal et al., 2008, Fig. 5c). The top of the braid-plain unit represent an expansion surface which marks the change from a low-accommodation setting controlled by the incised valley topography to a high-accommodation setting characterized by both increasing lateral and vertical accommodation (Figs. 3 and 6). In many areas, particularly in eastern Spitsbergen, this surface also represent a marine flooding surface where overlying deltas downlap onto it (Nemec et al., 1988; Steel et al., 2000; Onderdonk and Midtkandal, 2010, Fig. 5d). The upper Helvetiafjellet Formation, the Glitrefjellet Member, consists of variable amounts of alternating mudstones, sandstones and thin coals deposited in continental to paralic settings, including flood plain, crevasse splay, tidally influenced distributary channels, and mouth bar to interdistributary bay environments (Nemec, 1992; Gjelberg and Steel, 1995; Midtkandal et al., 2007, Figs. 5, 6 and Fig. 9d–f). In areas that was still affected by the incised valley-topography, typically in central Spitsbergen, large tidal-dominated estuaries formed (e.g. Gjelberg and Steel, 1995; Midtkandal and Nystuen, 2009, Fig. 5c and Fig. 9e). The marine influence generally increases upwards, and the upper part of the unit include sediments deposited in wave-influenced delta front and barrier environments (Nemec et al., 1988; Nemec, 1992, Fig. 5d). The boundary to the overlying Carolinefjellet Formation is marked by an abrupt upward-deepening of facies from delta front or barrier sandstones to offshore shale (Fig. 9g). The shale is typically 10–30 m thick and represent a marine flooding surface of regional extent (Figs. 3–6). Locally, a transgressive lag formed by wave-ravinement is also present at the boundary (Fig. 6).

4.4. Age of the Helvetiafjellet Formation

Within the Helvetiafjellet Formation, biostratigraphical analysis were carried out on five samples from well Dh-2 and on 12 samples from the Ullaberget outcrop section. The dinocyst preservation is very poor and the diversity is low, and the samples are dominated by terrestrially-derived particles (i.e. wood, pollen, spores and plant membranes), in line with the continental to paralic and restricted marine depositional setting of the formation (Grøsfjeld, 1992; Midtkandal et al., 2016). In well Dh-2, the presence of *Odontochitina nuda* and *P. anaphrissum* in the lower and middle part of the formation indicates a possible early Barremian age (Subzone I (2); Fig. 10). In the samples from the Ullaberget outcrops section, the co-occurrence of *Circulodinium aff. attadalicum* sensu Nøhr-Hansen 1993 (ranges from early Barremian to early Aptian, Nøhr-Hansen, 1993), *Muderongia australis* (ranges from Hauterivian to early Barremian; Århus et al., 1990), *Pseudoceratium anaphrissum* and *Stanfordella fastigiata* (ranges from early Hauterivian to earliest late Barremian; Nøhr-Hansen, 1993) supports an early Barremian age for the Helvetiafjellet Formation. Our data confirms dinocyst-derived age estimates by previous studies (Grøsfjeld, 1992) and

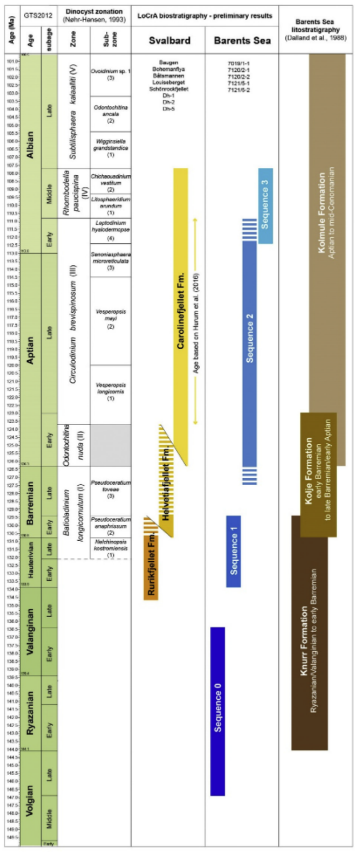

Fig. 10. Ages for the Lower Cretaceous succession of Spitsbergen and four of the sequences (S0–S3) *sensu* Marin et al. (2016a) of the SW Barents Shelf referred to the dinocyst zonation of Nøhr-Hansen (1993). Dashed columns represent tentative ages. Note that ages for Subzones I 1 and I 2 are updated. Ages for the upper part of the Carolinefjellet Formation is based on Hurum et al. (2016), and ages for the lithostratigraphic units of the Barents Sea is based on Dalland et al. (1988).

those recently provided by Midtkandal et al. (2016) and Śliwińska et al. (2016). The age is however slightly older than the U-Pb dating (123.3 ± 0.2 Ma) performed on a bentonite in the middle of the formation in central Spitsbergen by Corfu et al. (2013). However, an early Aptian age may be suggested for the uppermost part of the formation based on the presence of *Odontochitina nuda* and *Pseudoceratium cf. retusum* (Nøhr-Hansen, 1993, Fig. 10). .

The dinocyst assemblage from the Helvetiafjellet Formation also yields a significant amount of taxa characterized by a variety of older ranges: *Endoscrinium hauterivianum* (range: early to earliest late Hauterivian), *Nelchinopsis kostromiensis* (range: Valanginian to Hauterivian or earliest Barremian), *Tubotuberella* sp. (resembles Jurassic species) and *Tubotuberella apatela* (range: Kimmeridgian to earliest Valanginian). The presence of these species indicates major reworking of older strata and is consistent with uplift and erosion of the northwestern margin of the Barents Shelf in the Barremian.

4.5. Depositional trends of the Carolinefjellet Formation

The lowermost part of the Carolinefjellet Formation, the Dalkjegla Member (Fig. 3), consists of the above-mentioned 10–30 m thick shale package deposited in a restricted to open marine shelf setting during marine flooding of the coastal plain of the underlying Helvetiafjellet Formation (Figs. 4–6; Midtkandal et al., 2016; Vickers et al., 2016). The shale grade upwards into siltstones and very fine-grained sandstones arranged into a heterolithic coarsening and shoaling upwards unit up to 15 m thick (Figs. 5 and 6). The succeeding part of the Dalkjegla Member forms an up to 100 m sandstone-dominated succession that can be traced all across the outcrop belt (Nagy, 1970, Figs. 4–6). Internally, this succession contains vertically stacked and commonly amalgamated coarsening-upward parasequences (*sensu* Van Wagoner et al., 1990) representing offshore transition to lower shoreface environments of shoreline tongues that successively built out on to the shallow shelf (Fig. 5). The predominance of hummocky cross-stratified sandstones (Fig. 9h) and the marine trace-fossil assemblage (mixed *Skolithos* and *Cruziana* Ichnofacies) suggests an open-marine storm-dominated shelf (Fig. 5; Nagy, 1970; Maher et al., 2004). Locally, in west and north central Spitsbergen (the Festningen and Ramfjellet outcrop sections, Fig. 1c), medium to coarse-grained trough cross-stratified sandstones occur. These deposits represent upper shoreface environments and thus indicate proximal–distal trends and the possible presence of a shoreline N–NW of the present day outcrop belt (Maher et al., 2004). In the upper half of the Dalkjegla Member there is an overall retrogradational stacking trend; parasequences gradually thins and becomes more heterolithic upwards toward the overlying shale-dominated Innkjegla Member (Figs. 3, 5a and Fig. 5d, and Fig. 6; Nagy, 1970). The latter unit, which is several hundreds of meters thick, represent deposition in a slightly deeper shelf setting (Fig. 5).

4.6. Age of the Carolinefjellet Formation

The regionally-extensive shale package at the base of the Carolinefjellet Formation (biostratigraphically studied at the Baugen, Båtsmannen, Keilhaufjellet and Louiseberget outcrop sections and the Dh-2 well, Fig. 1c) is of earliest Aptian age (dinocyst Zone II of Nøhr-Hansen, 1993, Fig. 10). Samples from the Keilhaufjellet outcrop section (Fig. 1c for location) yielded no datable palynomorphs due to its proximity to the Paleogene fold-and-thrust belt. The two most characteristic dinocysts in the other investigated outcrop sections are *Pseudoceratium* cf. *retusum* (*sensu* Nøhr-Hansen, 1993) and *Odontochitina nuda*. In the Dh-2 well, the dinocyst assemblage yields additionally *Subtilisphaera perlucida* and *Muderongia pariata*. Based on ammonites, the Dalkjegla Member has previously been dated to Aptian, whereas the transitionally overlying Innkjegla Member was dated late Aptian to early Albian (Nagy, 1970).

The two youngest units of the Carolinefjellet Formation, the Zillerberget and Schönrockfjellet members (Fig. 3), are of middle Albian age (Fig. 10). The dinocyst analysis of the Zillerberget member performed by Århus (1991b) were recently revised in Hurum et al. (2016) who referred the unit to the dinocyst Zone IV of Nøhr-Hansen (1993). The dinocyst assemblage of the Schönrockfjellet member suggest also a middle Albian age, confirming the previous age assignment of Århus (1991b). This age is inferred from the presence of *Chichaouadinium vestitum*, *Pseudoceratium polymorphum*, *Litosphaeridium arundum*, *Pseudoceratium expolitum* and *Odontochitina singhii*. Furthermore, the upper part of the Schönrockfjellet member belongs to Subzone IV (2) (Fig. 10), as suggested by the common presence of *Chichaouadinium vestitum*.

5. Offshore seismic sequences

Sequences 1–3 (S1–S3; Figs. 3 and 7) occur in the Hammerfest Basin, the Fingerdjupet Subbasin (of the Bjørnøya Basin), parts of the Nordkapp Basin, and on the Bjarmeland Platform (Marin and Escalona, 2014; Marin et al., 2016a). Interpreted clinoforms generally show progradational trends towards the south (varies from SE to SW). In the Fingerdjupet Subbasin, a more SE-directed progradational trend dominates. Note that S1–S2 are not present in the southwestern part of the Nordkapp Basin, suggesting that they never reached that far south. In the Nordkapp Basin, which is known for its many salt diapirs, the constant thickness of S1 and S2 on both sides of most salt diapirs indicate that the salt was not moving at this time and did not form a barrier that prevented clinoform progradation (cf. Nilsen et al., 1995; Rojo et al., 2015). A short characterization of S1–S3 follows, and seismic lines showing details of the clinoforms in these sequences are shown in Figs. 11 and 12. For more details, see Marin and Escalona (2014) and Marin et al. (2016a, 2016b).

5.1. Sequence 1 (S1)

Sequence 1 display continuous parallel reflections of high to medium amplitudes. In the Hammerfest Basin, thickness variations in S1 are clearly controlled by normal faults as it is thicker in the graben areas and thinner against the basin margins (Fig. 8b). The top surface of S1 (Surface K1) has high amplitude and is interpreted to be a flooding surface (Figs. 7 and 12). In S1, clinoforms occur in the eastern part of the Nordkapp Basin, and southeastward prograding clinoforms occur in the Fingerdjupet Subbasin and in the western part of the Bjarmeland Platform (Figs. 11 and 12). In the Nordkapp Basin, they have sigmoidal geometries with average foreset angles of 1° (Figs. 11 and 12), reliefs increasing basinward from 130 m to 400 m, and progradational direction towards the SW. The clinoforms downlap either against the BCU or Surface K0. Low seismic resolution in combination with the limited thickness of the Knurr Formation on the Bjarmeland Platform and the Norsel High (e.g. 7224/7-1: 30 m, 7224/6-1: 16 m, and 7226/11-1: 6 m), occasionally makes it difficult to distinguish whether the clinoforms downlap onto the BCU or Surface K0. On the Bjarmeland Platform, the latter surface is represented by a condensed carbonate horizon inferred to be the top of the Klippfisk Formation, which here, is considered to be a lateral equivalent to S0 in the Hammerfest Basin (Fig. 3). The shelf-edge trajectory is ascending and topset developments are common, whereas bottomsets are poorly developed. The clinoforms in S1 are interpreted to be of a shelf-slope-basin type, recording a shelf-margin that successively built into deeper water. The sigmoidal clinoform geometries may point to mudstone-prone foresets with thin sandstones only occurring in the shelf topsets. The lack of bottomsets may indicate strong bottom currents parallel to base-of-slope (e.g. Cattaneo et al., 2007).

Clinoforms in the western part of the Bjarmeland Platform are oblique parallel with reliefs of 35–60 m and steep foreset angles with an average of 5–8° (Figs. 11 and 12). The clinoforms have high seismic amplitude and descending trajectories, indicating sand-prone foresets and high rates of accretion, respectively. It is suggested that they represent a sand-dominated deltaic shoreline that prograded rapidly to an outer shelf position (Figs. 11 and 12). Progradational wedges characterized by similarly steep and sand-prone clinoforms occasionally form in front of high-supply, storm-dominated shorelines (Hernández-Molina et al., 2000). In the southwestern part of the Fingerdjupet Subbasin, the clinoforms are oblique to sigmoidal and their relief increase to 125–220 m whereas their foreset angles are reduced to 1.5–5°. They typically show flat to descending or low-angle ascending trajectories, and a general basinward increase in seismic amplitude. These clinoforms are therefore interpreted as a shelf-margin system that built basinward aided by a relative sea-level fall. The clinoform geometries suggests generally mudstone-prone foresets. However, steep foresets, descending trajectories, and the local occurrence of bottomsets, suggests that sediments periodically was bypassed downslope from the shelf and onto the basin floor.

Along the strike to the NE, the foreset angles of the clinoforms gradually decrease, and in the western part of Bjarmeland Platform, sigmoidal clinoforms with reliefs of 85–110 m and foreset angles around 1° dominate. It is suggested that they formed laterally away from to the main sediment source and may thus be dominated by mudstone.

5.2. Age of S1

The distribution and the relative abundance of dinocysts within S1 was studied in four wells 7120/1-2, 7120/2-2, 7121/5-1 and 7121/5-2. The presence of only sparse dinocyst assemblages in the wells 7120/1-2 and 7120/2-2 gave a very broad age range, (i.e. a latest Ryazanian/Valanginian or younger, see Marin et al., 2016a). The presence of *Systematophora palmula* and *Lagenorhytis delicatula* indicate reworking of Ryazanian strata whereas the record of *Gonyaulacysta dualis* and *Paragonyaulacysta* suggest reworking of Kimmeridgian to Ryazanian strata. Moderately good preservation and diversity of dinocyst in wells 7121/5-1 and 7121/5-2 narrow the age of S1 significantly. The most characteristic dinocysts within S1 are: *Batioladinium longicornutum*, *Stanfordella fastigiata* and *Muderongia simplex* subsp. *microperforata* sensu Nøhr-Hansen (1993). The presence of *Oligosphaeridium abaculum* in the lower part of the sequence suggests a Hauterivian age for this interval. The middle and upper part of the sequence is referred to the lower Barremian (Subzone I (2)), based on the occurrence of rare *P. anaphrissum*. Therefore, S1 is suggested to be of a latest Valanginian/earliest Hauterivian to early Barremian age (Fig. 10).

5.3. Sequence 2 (S2)

Reflections in S2 vary from parallel continuous with medium amplitudes in the Hammerfest Basin to clinoforms that prograded to the SW in the Nordkapp Basin (Figs. 8, 11c and Fig. 12c). The top surface of the sequence (Surface K2) which show high to medium amplitudes, is interpreted as a flooding surface (Figs. 1, 3 and Fig. 12c). An erosional unconformity is present above the flooding surface and locally cuts down into it. The unconformity are penetrated in well 7231/04-U-01 and 7321/7-1 and have traditionally defined the boundary between the Kolje and Kolmule formations (Bugge et al., 2002, Figs. 3 and 7). The clinoforms typically downlap onto the top surface of the underlying sequence (Surface K1; Fig. 12c) or onto the condensed limestones of the Klippfisk Formation, Smelror et al., 1998; Bugge et al., 2002; Fig. 3.

In the Nordkapp Basin a wedge-shaped clinoform package with a flat to descending trajectory occur on top of the low-angle clinoforms of S1. These clinoforms have reliefs of 70–60 m, oblique

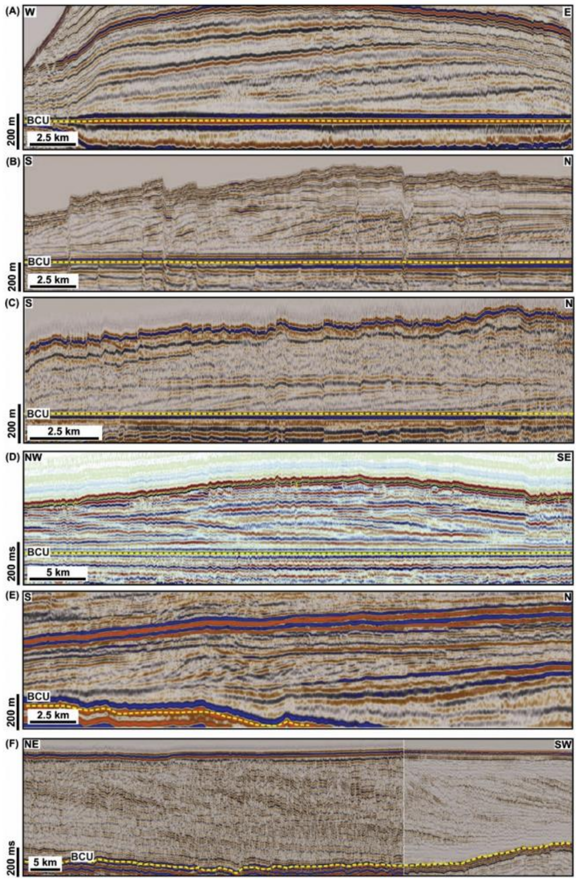

Fig. 11. Uninterpreted two-dimensional seismic profiles showing clinoform architectures in S1–S3 (based on Marin and Escalona, 2014; Marin et al., 2016a). The profiles are flattened on the BCU. For location of the profiles see Fig. 1b, and for interpretation of the profiles see Fig. 12.

parallel geometries and steep foreset angles with an average of 1.5–6°, all suggesting rapid progradation under relative sea-level fall (Figs. 11 and 12).

5.4. Age of S2

Sequence 2 was studied in core and SWC samples from five wells 7019/1-1, 7120/1-2, 7120/2-2, 7121/5-1 and 7121/5-2. The upper of the two samples from well 7019/1-1 yielded reworked Early to Middle Jurassic dinocysts (*Nannoceratopsis gracilis*, *Nannoceratopsis pellucida* and *Nannoceratopsis ridingii*). The most important Early Cretaceous age diagnostic dinocysts observed within S2 are: *Atopodinium haromense*, *Circulodinium brevispinosum*, *Dingodinium cerviculum*, *Nyktericysta vitrea*, *Odontochitina operculata*,

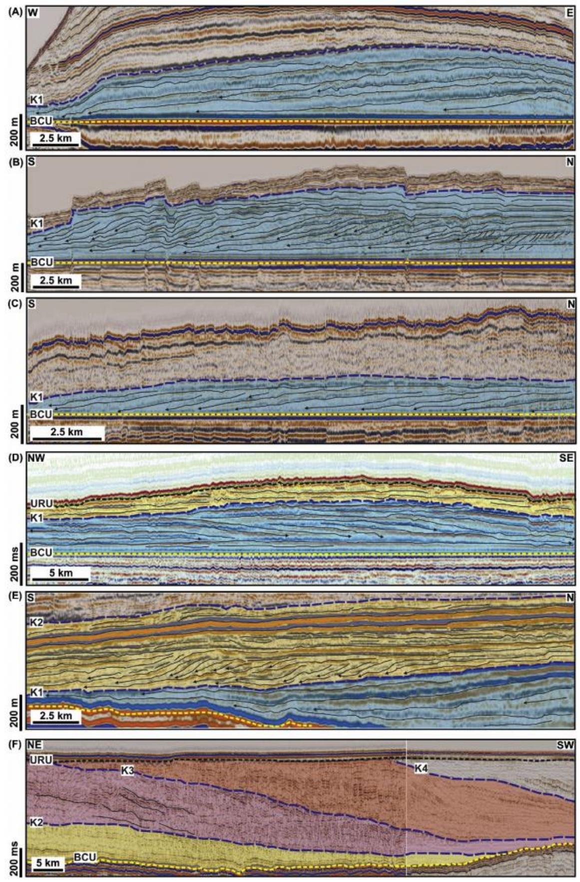

Fig. 12. Interpretation of the two-dimensional seismic profiles shown in Fig. 11. For location of the profiles see Fig. 1b. (A) Profile from the Nordkapp Basin through S1. Note the low angle (c. 1deg;) and the extensive lengths of the foresets (>30 km). (B) Profile from the western Bjarmeland Platform through S1 showing steep-angled, oblique parallel to sigmoidal clinoforms. (C) Profile from the north central Bjarmeland Platform through S1. (D) Profile from the Olga Basin showing S1 clinoforms that migrated in a SE-ward direction from the Svalbard Platform. (E) Profile from the Nordkapp Basin through S2. Note how the steep-angled S2 clinoforms downlap onto the K1 surface. (F) Composite profile from the area south of the Nordkapp Basin showing the successive southward migration of S2, S3 and S4. Because of poor seismic quality in this area, internal reflections are difficult to trace. Note the SW-ward thinning of the sequences.

Palaeoperidinium cretaceum, Pseudoceratium nudum, Pseudoceratium cf. *retusum, Vesperopsis longicornis* and *Vesperopsis mayi*. The lower part of S2 is tentatively dated from latest Barremian to early late Aptian (i.e. dinocyst Subzone I (3) to dinocyst Subzone III (1) of Nøhr-Hansen (1993), Fig. 10). The dinocyst assemblages from the 7120/2-2 well are less diverse, and the inferred age for the upper part of S2 is late early Aptian to middle late Aptian (Fig. 10).

5.5. Sequence 3 (S3)

Reflectors in S3 varies from parallel continuous with medium amplitude to chaotic. Where it is not truncated by the URU, the top surface of S3 (Surface K3) is characterized by low amplitude in some areas (e.g. the Hammerfest Basin) and is consequently difficult to map. It is, however, interpreted as a flooding surface because younger sequences clearly downlap onto Surface K3. In the western part of the Bjarmeland Platform, clinoforms with oblique parallel to tangential geometries are observed to prograde to the SE (Figs. 11 and 12). In the Fingerdjupet Subbasin, clinoforms with reliefs of 40–65 m, foreset angles up to 11° and oblique tangential geometries occur locally in association with basin bounding faults. These clinoforms are bidirectional with dip directions from SE–NW and from NW–SE.

In the Fingerdjupet Subbasin, the small-scale, steep-angled clinoforms with opposing dip-directions, suggests the presence of a deltaic system with several protuberances that prograded towards the SE and filled a local depocentre. The scale and local fault-associated occurrence suggest that this system is not related to the large-scale palaeo-drainage system investigated here. Thus, it is speculated that these clinoforms formed in response to fault activity along the northern margin of the Fingerdjupet Subbasin (Marin et al., 2016b).

5.6. Age of S3

Dinocysts from S3 were studied on three DC and one SWC samples from the 7121/5-1 well (interval between 1574.0 m and 1886.0 m). The most characteristic dinocysts for S3 are: *Odontochitina operculata, Palaeoperidinium cretaceum* and *Vesperopsis mayi*. The topmost sample (1589.0 m; DC) yields furthermore *Leptodinium cancellatum, Rhombodella paucispina* and *Chichaouadinium vestitum*. If these species are considered in situ, then the upper part of S3 may be referred to the dinocyst Subzone III (1) of Nøhr-Hansen (1993) and dated to early middle Albian (Fig. 10). The lower and middle parts of S3 yields also *Dingodinium cerviculum*. The last occurrence of the species is considered a good marker for uppermost Aptian to lowermost Albian (e.g. Nøhr-Hansen, 1993, Fig. 10). The middle part of the S3 (1775.0 m; SWC) yields *Surculosphaeridium longifurcatum*. The first occurrence of the species was dated to 111.16 Ma (Williams et al., 2004), suggesting that this part of the sequence is not older than early Albian. The base of S3 (1886.0 m; DC) yields also *Circulodinium brevispinosum*. The last occurrence of the species in NE Greenland is observed in the early Albian (Nøhr-Hansen, 1993). Based on these observations, a latest Aptian/earliest Albian to an early middle Albian age is suggested for S3 (Fig. 10).

6. Discussion

6.1. Onshore–offshore age-correlations

Based on the biostratigraphy established in this study, it is clear that the onshore system, age-vise, corresponds to Sequences 1–3 in the offshore areas (Figs. 3 and 10). Detailed one to one correlations are not possibly at present due to data limitations. However, it is suggested that the Rurikfjellet Formation (Valanginian–Hauterivian/lower Barremian) correlate to S1 (uppermost Valanginian/Hauterivian–lower Barremian), the Helvetiafjellet Formation (lower Barremian–lower Aptian) and the Dalkjegla and Innkjegla members of the Carolinefjellet Formation (lower Aptian to upper Aptian) to S2 (uppermost Barremian–upper Aptian), and the remaining part of the Carolinefjellet Formation (Langstakken, Zillerberget and Schönrockfjellet members, upper Aptian–middle Albian) to S3 (uppermost Aptian–lower/middle Albian).

The lower Aptian flooding surface that separates the Helvetiafjellet and Carolinefjellet formations onshore (Figs. 3–6) may thus not correlate to any of the sequence-bounding maximum flooding surfaces offshore (i.e. Surface K2; Figs. 3 and 6). Seismic resolution may have hampered its recognition offshore, but a minor flooding surface have been reported in the Fingerdjupet Subbasin (the stippled line that separates the Knurr and Kolje formations in well 7321/7-1 in Fig. 7). Although topset truncations occur locally within the offshore sequences, the lower Barremian subaerial unconformity at the base of the Helvetiafjellet Formation in Svalbard have not been detected in seismic or well data offshore. This may indicate that it is: 1) below seismic resolution, or 2) not present south of Svalbard but instead is time-equivalent to a marine correlative conformity surface offshore. Although a lower Barremian unconformity is recognized at the base of the Kolje Formation in large parts of the western Barents Shelf (Smelror et al., 1998; Bugge et al., 2002), its relation to the onshore unconformity is unclear. How much time the onshore unconformity represent is not known. However, based on the occurrence of Barremian dinocysts below and early Barremian dinocysts above the unconformity (Grøsfjeld, 1992, Fig. 10), it is suggested that the time of subaerial exposure must have been less than two million years. This estimate also seems likely when it is taken into consideration that the Barremian stage only lasted for about five million years (Fig. 10).

In Svalbard, the amount of incision at the base of the Helvetiafjellet Formation ranges from some few to several tens of meters (Figs. 3 and 6), generally decreasing southward (Gjelberg and Steel, 1995, 2013). The latter reflects differential uplift and southward tilting of the Svalbard Platform and the adjacent land areas (e.g. the Lomonosov High, Fig. 2). The unconformity, however, is also present in southernmost Spitsbergen (Edwards, 1976; Grundvåg and Olaussen, 2017) implying that the entire outcrop area at one stage was subaerially exposed in the early Barremian (Figs. 3 and 13). The consequence of the exposure was a significant forced regression with bypass of a considerable volume of eroded sediments towards the southeast (Gjelberg and Steel, 1995, 2013; Midtkandal and Nystuen, 2009). The offshore areas south of Spitsbergen was concurrently little affected by the uplift, and in combination with deeper water and higher rates of subsidence, subaerial exposure of the deeper shelf areas south of Svalbard was prevented. These basinal areas instead offered accommodation space and acted as depocentres for sediments eroded from the uplifted shelf. This promoted rapid southward progradation of the deltaic system (Fig. 13). Due to the lack of data between Svalbard and the Fingerdjupet Subbasin, it is difficult to estimate the rate of progradation for this large-scale system. Based on the age assignment presented here (Fig. 10), it may be speculated that the upper part of the Rurikfjellet Formation and the Barremian unconformity in Svalbard, down-dip, correlates to the clinoforms of S1 in the Fingerdjupet Subbasin.

Grab samples containing sandstones of similar petrographic character to the ones in the Helvetiafjellet and the Carolinefjellet formations have been described from the shallow banks 200 km south of Spitsbergen (Edwards, 1975, Fig. 13). The sandstones were suggested to be locally derived, and their distribution fits well with the subcrop map shown in Fig. 13. Biostratigraphic studies of shale

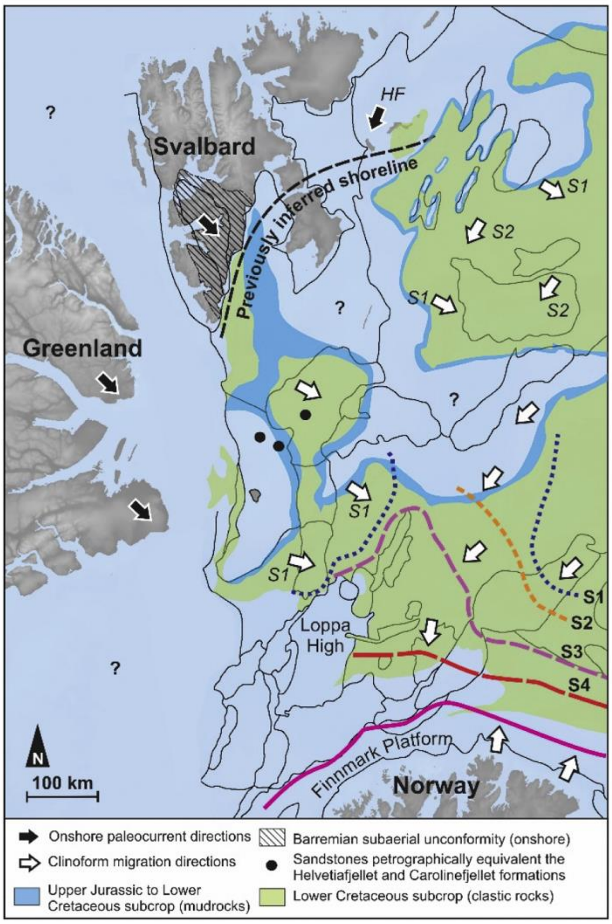

Fig. 13. Map showing minimum extent of the lower Barremian subaerial unconformity in Svalbard (hatched area) and the distribution of Upper Jurassic to Lower Cretaceous subcrops on the Barents Shelf. The map also summarizes onshore palaeocurrent directions (black arrows), offshore clinoform migration directions (white arrows), and the final shelf-break positions of S1–S3 (stippled lines annotated S1–S3). The final position of the S4 shelf-break is also shown just to illustrate the progradational nature of the Lower Cretaceous system. An adjacent shelf break is also inferred to have existed along the north sloping margin of the Finnmark Platform (pink line). The clinoform migration directions on the western Barents Shelf are based on Marín and Escalona (2014), Marín et al. (2016a), and Kairanov et al. (2015), whereas the directions on the eastern side is based on Kayukova et al. (2014). The onshore palaeo-current data from Svalbard are based on Steel et al. (1978), Nemec (1992), Gjelberg and Steel (1995, 2013), Midtkandal and Nystuen (2009) and the present study. Onshore data from Greenland are based on Dypvik et al. (2002). According to models by Gjelberg and Steel (1995) and Steel et al. (2000) a shoreline marking the regressive–transgressive turn-around point of the onshore depositional system developed just south of Svalbard in the Barremian (marked "previously inferred shoreline"). The map forms the framework for the regional palaeogeographic reconstructions shown in Fig. 14. (For interpretation of the references to colour in this figure legend, the reader is referred to the web version of this article.)

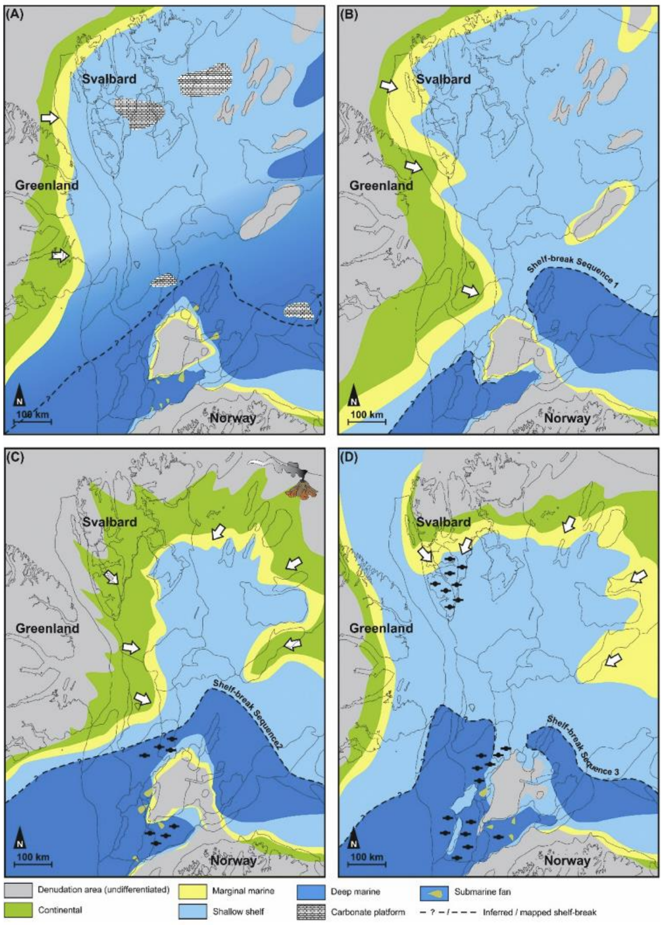

Fig. 14. Palaeogeographic reconstructions of the western Barents Shelf showing: (A) the earliest Valanginian at c. 139 Ma (Myklegardfjellet Bed and S0) characterized by sediment starvation and the formation of carbonate platforms, (B) the latest Hauterivian at c. 132 Ma (upper part of Rurikfjellet Formation and S1) with shallow marine wedges locally building out from a source area to the west (i.e. Greenland), (C) the middle to late Barremian at c. 129 Ma (the Helvetiafjellet Formation and S2) with a fluvio-deltaic system that was forced southeastward following uplift and southward tilting of the shelf (which created the subaerial unconformity in Svalbard), and (D) the latest Aptian at c. 114 Ma (the Carolinefjellet Formation and S2 to S3) when large parts of the platform was flooded. A seaway may have connected the Barents Shelf with the Canada Basin in the latest Aptian to earliest Albian, enabling cold, polar water to invade the shallow shelf.

samples from the same data set (Bjærke and Thusu, 1976) reveal a mixture of non-age diagnostic, Jurassic, Cretaceous, and Palaeogene palynomorph assemblages. According to Bjærke and Thusu (1976), *Oligosphaeridium complex* occurred in several of the investigated shale samples, partly resembling the Valanginian to Hauterivian dinocyst assemblage described in the Rurikfjellet Formation in the present study (Fig. 10).

6.2. Regional palaeogeography and depositional controls

Three primary source areas are suggested to have provided sediments to S1–S3 (Valanginian–lower middle Albian; Fig. 14). The most important one during the earliest stages of the shelf-margin accretion (S1) was located to the W and NW (Fig. 14a and b). This is indicated by the presence of the two S- and SE-ward thinning, shallow marine wedges in the upper part of the Rurikfjellet Formation (Figs. 3 and 14b). In addition, SE-ward directed clinoforms with steep foresets, descending trajectories, and high amplitude foresets occur in the Fingerdjupet Subbasin (Figs. 12 and 13). As a result of differential uplift, the NW source area became increasingly important during the earliest Barremian and deposition of S2 and the Helvetiafjellet Formation (Fig. 14c). This is indicated by the presence of SE-ward directed oblique clinoforms in the Fingerdjupet Subbasin. The progradation direction coincides with the SE-oriented palaeocurrents reported in the fluvial Festningen Member of the Helvetiafjellet Formation on Spitsbergen (Steel et al., 1978; Gjelberg and Steel, 1995; Midtkandal and Nystuen, 2009, Fig. 13). A less important source area was located NE of the Barents Shelf. In this region, including Kong Karls Land and the Olga Basin, NE–SW-striking folds controlled the sediment dispersal by funneling the fluvio-deltaic system in a SW-ward direction (Kairanov et al., 2015). The folds were the result of pre-Barremian inversion of older Palaeozoic rift basins. In the Valanginian to Hauterivian, the northeastern source area had little influence on sedimentation in Spitsbergen and the western Barents Shelf area (Fig. 14a and b). Due to increased volcanic activity (e.g. extruded basaltic lava flows in Kong Karls Land) and thermal doming in the late Barremian and Aptian, it apparently became more important (Fig. 14c). In eastern Svalbard, this change is seen by an upwards change from quartzitic sandstones in the lower part of the Helvetiafjellet Formation to volcanic arenites in its upper parts and in the overlying Carolinefjellet Formation (Edwards, 1979; Maher et al., 2004). In addition, SW-ward directed clinoforms occur in S3. Uplifted terrain on the Loppa High and the Finnmark Platform locally fed fan deltas along on the basin margins, as well as submarine fans in the adjacent basins (e.g. the Hammerfest Basin; Seldal, 2005; Sattar et al., 2017, Fig. 14). However, these localized sediment source areas played a more important role during deposition of Sequence 0 (Fig. 14a; not discussed here).

The lower Barremian subaerial unconformity at the base of the Helvetiafjellet Formation occur in all the investigated outcrops (Figs. 5, 6 and 13). Based on the present day areal extent of the unconformity in Spitsbergen (c. 14.000 km^2; Fig. 13), it becomes clear that uplift of Svalbard itself could not have contributed with enough sediments to account for the thickness and the volume of the Lower Cretaceous succession reported in the western Barents Shelf. It may therefore be speculated that the northern margin of the Barents Shelf, the Lomonsov High, NE Greenland, and other Arctic terranes such as the Chukchi Borderland and the disintegrated Crockerland of Embry (1992) together formed a large source area to the north and northwest of Svalbard prior to the opening of the Canada Basin (Fig. 2; e.g. Miller et al., 2006). Other terranes in the E and NE such as uplifted parts of the Kara Shelf, remnants of the Late Palaeozoic–Triassic Taimyr Foldbelt and the Siberian Traps (Zhang et al., 2013), and the more distant South Anyui Orogen (Nikishin et al., 2014), probably became increasingly important source areas during deposition of the younger sequences (S4–S6).

In the Nordkapp Basin, the depocentre was systematically displaced towards the SW (Fig. 14; Bugge et al., 2002), and the final shelf-break for the investigated system (S1–S3) developed just south of the Nordkapp Basin (Figs. 13 and 14). The regional-scale drowning of the shelf in late Aptian to earliest Albian times may relate to a combination of several factors including circum-Arctic plate-tectonic reconfiguration, regional sag-like subsidence related to thermal cooling of the lithosphere, abrupt shut-down of sediment supply leading to relative sea-level rise due to delta top subsidence and compaction, eustatic sea-level rise, auto-retreat mechanisms, or a combination of all these factors. However, the regional extent of the flooding as well as the switch to a more eastern to northeastern source terrain in the younger and succeeding sequences (S4–S6; Marin and Escalona, 2014) suggests that large-scale tectonics had a major influence on the sequence development and clinoform accretion. Allogenic forcing is also supported by the dramatic height increase of the clinoforms from less than 130 m in S1 to more than 500 m in S4 (not considered here, see Marin et al., 2016a). This may indicate either an increase in basin subsidence due to fault activity or salt tectonics, or that the clinoforms prograded into a deeper area of the Nordkapp Basin.

6.3. Sediment partitioning and sand distribution

The low-amplitude reflections observed in the foresets of the majority of the larger-scale clinoforms (relief >150 m) in S1–S3 may indicate that they are generally mudstone-dominated. This notion is also confirmed by the gamma ray logs from the many exploration wells that have penetrated the Lower Cretaceous succession in the SW Barents Sea. The apparent lack of sandstone in the SW therefore suggests that most of the sand was trapped in the northern and northwestern areas of the shelf. Sand-grade sediments were mostly stored in the clinoform topsets in coastal plain, regressive shoreline, and inner shelf environments, particularly during periods of relative rise of sea-level. Onshore, this is clearly demonstrated by the large amount of sandstone in the upper part of the overall transgressive Helvetiafjellet Formation (the Glitrefjellet Member, Figs. 3–6). The sediment partitioning may also reflect proximal to distal trends, which are typical for graded shelf systems (Swift and Thorne, 1991), or physiographic and hydrodynamic conditions in the basin (Helland-Hansen and Hampson, 2009). Although the successive migration of deltas and shorelines across the shelf is the main mechanism of transporting sediments to the shelf-edge, storms play a major role in offshore sediment transport on many shelves by eroding sediments that aggrade above the shelf equilibrium profile (Seilacher, 1982; Pratson et al., 2004). Storm-eroded sediments, particularly mud, may be driven across a low-gradient sloping shelf under the combined influence of gravity and storm waves (Traykovski et al., 2000; Wright et al., 2001; MacQuaker et al., 2010). In addition, storms indirectly may aid highly concentrated suspended fluid muds to escape the energy fence of the inner shelf through, storm-modified hyperpycnal flows (Myrow et al., 2002; Pattison, 2005) and offshore flushing of estuaries and prodelta environments during river floods (Neill and Allison, 2005) The combined result of these processes is a net basinward transport of mud across the shelf and onto the upper slope where instability and gravity-driven processes dominate. Thus, in some modern deltas, a mud-prone shoreline-detached subaqueous platform tend to form in front of the subaerial delta (Alexander et al., 1991; Swenson et al., 2005; Patruno et al., 2015). The rollover-point of such subaqueous deltas are in some modern cases separated from its shoreline by more than 100 km (Swenson et al., 2005; Patruno et al., 2015). It has also been reported that some modern subaqueous deltas may show higher accretion rates than its associated shoreline, which in some extreme cases experience net erosion (e.g. Nittrouer et al., 1996). Accretion rates of 12–17 m per year have been reported from the subaqueous delta of the Ganges-Brahmaputra (Michels et al., 1998). Good examples of modern subaqueous deltas include those of the western Adriatic Shelf (Cattaneo et al., 2003, 2007), the Gulf of Papua (Walsh et al., 2004), the South Yellow Sea (Yang and Liu, 2007), and the Bay of Bengal (Kuehl et al., 2005).

It may be speculated that sigmoidal-shaped, low-angle clinoforms in S1 in the Nordkapp Basin and on the Bjarmeland Platform, represent subaqueous delta-type clinforms similar to those described above. However, to our current knowledge, subaqueus deltas are more typical of relative sea-level stillstands and most Holocene examples occur in inner shelf settings at relatively shallow waters (Patruno et al., 2015). The clinoforms investigated here (see also Marin et al., 2016a), both in size and geometries (Fig. 12), more resemble prograding shelf-prism-scale clinoforms (Patruno et al., 2015). Shelf-prism-type clinoforms commonly have paralic to shallow marine topsets, and good reservoir sands may thus be expected in these segments. Although turbidite lobes and mass transport complexes occur in places, the sandstone content in the clinoform slope and toe-sets are expected to be generally low. However, given the right conditions (i.e. mode and rate of sediment supply, shelf width, relative sea-level etc.; Steel et al., 2000), good reservoir sands may also occur in the slope to basin floor region of some clinoforms. The inner shelf in the present case was most likely a zone of limited accommodation space; the eroded volume of sediments that was shed of from the uplifted Svalbard platform could not be stored on the shallow inner shelf. The large amount of bypassed sediments in combination with available lateral accommodation space ultimately gave rise to prograding clinoform successions further offshore. .

In Svalbard, tempestite deposits dominated by hummocky cross-stratification occur in both the Rurikfjellet and Carolinefjellet formations and indicate that the shelf sea frequently experienced storm activity. Apparently, strong longshore currents and tidal currents also influenced the sediment distribution on the shelf (Birkenmajer, 1966; Maher et al., 2004). Tidal deposits in estuarine and coastal plain settings occur in the overall transgressive Helvetiafjellet Formation at several locations in central Spitsbergen (Gjelberg and Steel, 1995; Midtkandal and Nystuen, 2009), including in some of the inferred most proximal outcrop sections (e.g. at the Festningen section, Fig. 1). Due to the low angle of the coastal plain, tidal currents could penetrate several tens to hundreds of kilometers upstream, similar to that reported from some modern rivers that drain low-angle coastal plains (e.g. the Mississippi River; Holle, 1951; the Orinoco River and its predecessor, Escalona and Mann, 2006). This suggests that tidal currents in combination with frequent storm activity, and strong longshore currents periodically played a major role in the sediment distribution in the Svalbard area by trapping sand-grade sediments within estuaries, deltas, and distributary channels, particularly during the long-term rise in relative sea-level that followed the forced regression in the early Barremian.

Smaller-scale (relief <70 m) clinoforms with steep-angled foresets (up to eight degrees dip), typically characterized by high amplitude reflections, occur in the proximity of faults or along the margin of some palaeo-highs (e.g. S3 in the northern part of the Fingerdjupet Subbasin). These clinoforms represent more localized, and potentially sand-rich deltaic/shallow marine systems that were not genetically or directly related to the large-scale palaeo-drainage system discussed here. The different systems did however interact in the areas were they met (Marin and Escalona, 2014). The sandstone-dominated shallow marine parasequences in the Kikutodden Member of the Rurikfjellet Formation in southernmost Spitsbergen (Edwards, 1976; Mørk, 1978, Figs. 4 and 5e) may represent an onshore facies analog to these inferred sand-rich clinoforms in the Fingerdjupet Subbasin (Grundvåg and Olaussen, 2017). Based on the onshore dip-extent of the onshore parasequences (from Kikutodden to Fotografryggen, minimum 70 km, see Fig. 1) and their limited lateral facies variation across southern Spitsbergen (c.f. Edwards, 1976; Mørk, 1978), it is suggested that they probably extended several tens of kilometers southward (offshore) before they terminated (Grundvåg and Olaussen, 2017).

6.4. *Lower Cretaceous clinoforms onshore?*

Although Steel et al. (2000) interpreted the presence of a canyon head in a shelf-edge setting at Kvalvågen in eastern Spitsbergen (later disputed by Onderdonk and Midtkandal, 2010), shelf-margin-scale clinoforms or facies indicative of such features have not been reported from the Lower Cretaceous in Svalbard. However, the low-angle nature and the large size of the clinoforms in combination with outcrop limitations may have hindered their recognition. Some of the mudstone-prone, low-angle clinforms in the offshore areas have dip-angles of less than one degree, and slope lengths of more than 30–40 km (Fig. 8). If clinoforms occur onshore, their slope segment could easily be hidden in the shale-dominated and commonly scree-covered Rurikfjellet Formation which has an average thickness of 200 m but reaches a thickness of 400 m in places (Figs. 3–5). In general, the topset of these inferred low-angle clinoforms could have been eroded during formation of the lower Barremian subaerial unconformity at the base of the Helvetiafjellet Formation, creating a subtle toplap situation, which is difficult, not say impossible to recognize in an outcrop.

A c. 150 m thick succession of gravity flow deposits which include rafted blocks of coastal plain origin has been reported from the onshore wells Dh-1 and Dh-2 (Braathen et al., 2012, Fig. 5a and Fig. 6). Recent dinocyst studies indicate an early late Hauterivian age for these sediments (Śliwińska et al., 2016, Fig. 6). Although gravity flow deposits occur in large slump scars in slightly younger strata, as reported from eastern Spitsbergen by Nemec et al. (1988) and Steel et al. (2000), similar deposits have not been encountered in any of the other investigated outcrop sections in Svalbard. The gravity flow deposits is overlain by a clearly regressive prodelta to delta front package (Fig. 5a), and the thickness of the deposits also indicates that there must have been enough relief in the area to accommodate such a succession and to allow for the initiation of turbidity currents and debris flows. An explanation for the thickness of the gravity flow deposits and their localized occurrence is that they represent lower slope to basin floor fans and mass transport complexes (MTCs) that accumulated in front of prograding and periodically unstable shelf-prism-scale clinforms. High-amplitude anomalies, probably also representing MTCs, are seen in the lower slope segment of several of the offshore sequences (e.g. Figs. 11 and 12). The late Hauterivian age of the MTC onshore, potentially highlight the inferred offlapping nature of the Lower Cretaceous system as it predates the lower Barremian unconformity and the Helvetiafjellet Formation, and thus record a hitherto unknown regression and shelf-edge development in Svalbard.

7. Conclusions

By combining new biostratigraphic data with conventional outcrop data from Svalbard and a sequence stratigraphic framework defined from well and seismic data offshore, this study shed new light on the palaegeographic development of the Lower

Cretaceous in the northwestern part of the Barents Shelf. It is suggested that three offshore sequences (S1–S3) of latest Valanginian–earliest middle Albian age correspond and correlate to the Lower Cretaceous succession onshore Svalbard, which includes the Rurikfjellet (Valanginian–Hauterivian/early Barremian), Helvetiafjellet (early Barremian–early Aptian) and Carolinefjellet formations (early Aptian in its lower part, middle Albian in its upper part). Clinoforms within the offshore sequences generally show a south to southeastward progradation-direction, a trend which coincides with palaeocurrent directions in both the Rurikfjellet and Helvetiafjellet formations onshore. This strongly indicates that the onshore and the offshore depositional systems were parts of the same large-scale palaeo-drainage system. The presence of a regionally extensive subaerial unconformity onshore Spitsbergen indicates that the entire northwestern part of the shelf were uplifted and acted as a bypass zone during the early Barremian. The presence of Barremian dinocyts in the strata above and immediately below the unconformity further suggests a minor hiatus and that the shelf was exposed for only a relatively short period of time (<2 million years). Sediments eroded from the exposed shelf were forced southeastward and deposited in basinal areas where the amount of accommodation space were higher. High rates of sediment supply in combination with the low-gradient ramp setting and the lack of vertical accommodation space on the shallow inner shelf promoted basinward clinoform accretion. The apparent lack of sand in the slope and basin floor segment of the majority of the shelf-prism-scale clinoforms (relief >150 m) may relate to the physiographic conditions in the receiving basin (storm waves, along-shore currents plus strong tidal currents) resulting in a net basinward transport of mud. Apparently, sand was mostly trapped in paralic to inner shelf environments in the clinoform topsets. . Smaller scale (relief <60 m) clinoforms with steep foresets (up to 8° dip) characterized by high amplitude reflections represent localized, and potentially sand-rich systems that interacted with the larger-scale clinoform systems. Due to outcrop limitations, clinoform geometries at the scale of shelf-prism are yet to be recognized onshore. However, based on the large scale (minimum slope lengths of 30–40 km) and low-angle geometries (foreset dips < 1deg;) of some of the offshore clinoforms, it is speculated that clinoforms may be present in the up to 400 m thick Rurikfjellet Formation (Valanginan–Hauterivian/early Barremian). This may be evident by the occurrence of a 150 m thick succession of gravity flow deposits (including rafted blocks of coastal plain origin) overlain by a regressive prodelta slope to delta front package in the Rurikfjellet Formation in some of the onshore wells. The thickness of these deposits indicate that there must have been enough relief in the basin to accommodate such a succession and to allow for the initiation of turbidity currents and debris flows. We thus interpret the gravity flow deposits to represent lower slope to basin floor fans and mass transport complexes that accreted in front of a prograding shelf-slope system. The documented late Hauterivian age of the gravity flow deposits potentially highlights the inferred offlapping nature of the Lower Cretaceous system as they predate the lower Barremian unconformity, and thus record a hitherto unknown regression in Svalbard.

Acknowledgments

The authors are grateful to all the sponsors of the LoCrA consortium whom provided us financial support to carry out field work, as well as several PhD grants. We are also grateful to Lundin Norway for their generous support of a postdoctoral research grant to the first author. HN-H and KKS acknowledge Dorthe Samuelsen, Anette Ryge and Charlotte Olsen for preparing palynological slides. Additionally, KKS thanks NPD for lending slides from wells 7121/5-1 and 7121/5-2. SAG also received funding from the ARCEx project (Research Centre for Arctic Petroleum Exploration) which is funded by the Research Council of Norway (grant number 228107).

References

Alexander, C.R., DeMaster, D.J., Nittrouer, C.A., 1991. Sediment accumulation in a modern epicontinental-shelf setting. Mar. Geol. 98, 51–72.

Antonsen, P., Elverhøi, A., Dypvik, H., Solheim, A., 1991. Shallow bedrock geology of the Olga Basin area, nortwestern Barents Sea. AAPG Bull. 75, 1178–1194.

Århus, N., 1991a. The transition from deposition of condensed carbonates to dark claystones in the Lower Cretaceous succession of the southwestern Barents Sea. Nor. J. Geol. 71, 259–263.

Århus, N., 1991b. Dinoflagellate cyst stratigraphy of some aptian and albian sections from north Greenland, southeastern spitsbergen and the Barents Sea. Cret. Res. 12, 209–225.

Århus, N., 1992. Some dinoflagellate cysts from the lower cretaceous of spitsbergen. Grana 31, 305–314.

Århus, N., Kelly, S.R.A., Collins, J.S.H., Sandy, M.R., 1990. Systematic paleontology and biostratigraphy of two Early Cretaceous condensed sections from the Barents Sea. Polar Res. 8, 165–194.

Basov, V.A., Vasilenko, L.V., Viskunova, K.G., Korago, E.A., Ko-rchinskaya, M.V., Kupriyanova, N.V., Povysheva, L.G., Preo-brazhenskaya, E.N., Pchelina, T.M., Stolbov, N.M., Suvorova, E.B., Suprunenko, O.I., Suslova, V.V., Ustinov, N.V., Ustritsky, V.I., Fefilova, L.A., 2009. Evolution of sedimentary environments of the barents-north Kara palaeobasins in the phanerozoic. Neft. Geol. Teor. Prakt. 4, 1–44.

Birkenmajer, K., 1966. Lower cretaceous tidal deposits of central vest Spitsbergen. Nor. Polarinst. Årb. 1964, 73–85.

Bjærke, T., Thusu, B., 1976. Cretaceous palynomorphs from spitsbergenbanken, NW Barents Shelf. Nor. Polarinst. Årb. 1974, 258–262.

Braathen, A., Bælum, K., Christensen, H.H., Dahl, T., Eiken, O., Elvebakk, H., Hansen, F., Hanssen, T.H., Jochmann, M., Lie, T., Johansen, T.A., Johnsen, H., Larsen, L., Mertes, J., Mørk, A., Mørk, M.B., Nemec, W.J., Olaussen, S., Oye, V., Rø, K., Titlestad, G.O., Tveranger, J., Vagle, K., 2012. The Longyearbyen CO_2 Lab of Svalbard, Norway - initial assessment of the geological conditions for CO_2 sequestration. Nor. J. Geol. 92, 353–376.

Bugge, T., Elvebakk, G., Fanavoll, S., Mangerud, G., Smelror, M., Weiss, H.M., Gjelberg, J., Kristensen, S.E., Nilsen, K., 2002. Shallow stratigraphic drilling applied in hydrocarbon exploration of the Nordkapp Basin, Barents Sea. Mar. Petrol. Geol. 19, 13–37.

Cattaneo, A., Correggiari, A., Langone, L., Trincardi, F., 2003. The late-Holocene Gargano subaqueous delta, Adriatic shelf. Mar. Geol. 193, 61–91.

Cattaneo, A., Trincardi, F., Asioli, A., Correggiari, A., 2007. The Western Adriatic shelf clinoform: energy-limited bottomset. Cont. Shelf Res. 27, 506–525.

Corfu, F., Polteau, S., Planke, S., Faleide, J.I., Svensen, H., Zayoncheck, A., Stolbov, N., 2013. U–Pb geochronology of cretaceous magmatism on svalbard and Franz Josef land, Barents sea large igneous province. Geol. Mag. 150, 1127–1135.

Dalland, A., 1981. Mesozoic sedimentary succession at Andøya, Northern Norway, and relation to structural development of the North Atlantic region. In: Gelogy of the North Atlantic Borderlands, pp. 563–584. Canadien Soc. Petrol. Geol. Mem. 7.

Dalland, A., Worsley, D., Ofstad, K., 1988. A lithostratigraphic scheme for the mesozoic and cenozoic succession offshore Norway north of 62 N. NPD Bull. 4, 67 pp.

Doré, A.G., Lundin, E.R., Jensen, L.N., Birkeland, Ø., Eliassen, P.E., Fichler, C., 1999. Principal tectonic events in the evolution of the northwest European Atlantic margin. In: Fleet, A.J., Boldy, S.A.R. (Eds.), Petroleum Geology of Northwest Europe: Proceedings of the 5th Conference, pp. 41–61. Geol. Soc., London.

Dypvik, H., Nagy, J., Eikeland, T.A., Backer-Owe, K., Johansen, H., 1991. Depositional conditions of the bathonian to hauterivian janusfjellet subgroup, spitsbergen. Sed. Geol. 72, 55–78.

Dypvik, H., Nagy, J., Krinsley, D.E., 1992. Origin of the myklegardfjellet bed, a basal cretaceous marker on spitsbergen. Polar Res. 11, 21–31.

Dypvik, H., Håkansson, E., Heinberg, C., 2002. Jurassic and Cretaceous palaeogeography and stratigraphic comparisons in the North Greenland–Svalbard region. Polar Res. 21, 91–108.

Edwards, M.B., 1975. Gravel fraction on the spitsbergen bank, NW Barents shelf. Nor. Geol. Sur. Bull. 29, 205–217.

Edwards, M.B., 1976. Depositional environments in lower cretaceous regressive sediments, kikutodden, Sørkapp land, svalbard. Nor. Polarinst. Årb. 1974, 35–50.

Edwards, M.E., 1979. Sandstone in lower cretaceous Helvetiafjellet formation, svalbard: bearing on reservoir potential of Barents shelf. AAPG Bull. 63, 2193–2203.

Embry, A.F., 1992. Crockerland - the northwest source for the sverdrup basin, canadian arctic islands. In: Vorren, T.O., Bergsager, E., Dahl-Stamnes, Æ.A., Holter, E., Johansen, B., Lie, E., Lund, T.B. (Eds.), Arctic Geology and Petroleum Potential, pp. 205–216. NPF Spec. Publ. 2.

Escalona, A., Mann, P., 2006. Sequence-stratigraphic analysis of Eocene clastic foreland basin deposits in central Lake Maracaibo using high-resolution well correlation and 3-D seismic data. AAPG Bull. 90, 581–623.

Faleide, J.I., Vågnes, E., Gudlaugsson, S.T., 1993. Late Mesozoic-Cenozoic evolution of the south-western Barents Sea in a regional rift-shear tectonic setting. Mar.

Petrol. Geol. 10, 186–214.
Faleide, J.I., Tsikalas, F., Breivik, A.J., Mjelde, R., Ritzmann, O., Engen, O., Wilson, J., Eldholm, O., 2008. Structure and evolution of the continental margin off Norway and the Barents Sea. Episodes 31, 82.
Gabrielsen, R.H., Grunnaleite, I., Rasmussen, E., 1997. Cretaceous and tertiary inversion in the bjørnøyrenna fault complex, south-western Barents Sea. Mar. Petrol. Geol. 14, 165–178.
Gjelberg, J., Steel, R.J., 1995. Helvetiafjellet formation (Barremian-Aptian), spitsbergen: characteristics of a transgressive succession. In: Steel, R.J., Felt, V.L., Johannesen, E.P., Mathieu, C. (Eds.), Sequence Stratigraphy on the Northwest European Margin. Elsevier, Amsterdam, pp. 571–593.
Gjelberg, J., Steel, R., 2013. Depositional model for the lower cretaceous Helvetiafjellet formation on svalbard - diachronous vs. layer-cake models. Nor. J. Geol. 92, 41–54.
Golonka, J., Bocharova, N.Y., Ford, D., Edrich, M.E., Bednarczyk, J., Wildharber, J., 2003. Paleogeographic reconstructions and basins development of the Arctic. In: Golonka, J. (Ed.), Thematic Set on Paleogeographic Reconstruction and Hydrocarbon Basins: Atlantic, Caribbean, South America, Middle East, Russian Far East, pp. 211–248. Arctic. Mar. Petrol. Geol. 20.
Grantz, A., Hart, P.E., Childers, V.A., 2011. Geology and tectonic development of the amerasia and Canada Basins, Arctic Ocean. In: Spencer, A.M., Gautier, D., Stoupakova, A., Embry, A., Sørensen, K. (Eds.), Arctic Petroleum Geology, pp. 771–799. Geol. Soc., London Mem. 35.
Grogan, P., Østvedt-Ghazi, A.-M., Larssen, G.B., Fotland, B., Nyberg, K., Dahlgren, S., Eidvin, T., 1999. Structural elements and petroleum geology of the Norwegian sector of the northern Barents Sea. In: Fleet, A.J., Boldy, A.R. (Eds.), Petroleum Geology of Northwest Europe. Proceedings 5th Conference, pp. 247–259.
Grogan, P., Nyberg, K., Fotland, B., Myklebust, R., Dahlgren, S., Riis, F., 2000. Cretaceous magmatism south and east of Svalbard: evidence from seismic reflection and magnetic data. Polarforschung 68, 25–34.
Grøsfjeld, K., 1992. Palynological age constraints on the base of the Helvetiafjellet formation (barremian) on spitsbergen. Polar Res. 11, 11–19.
Grundvåg, S.-A., Olaussen, S., 2017. Sedimentology of the lower cretaceous at kikutodden and keilhaufjellet, southern spitsbergen: implications for the onshore-offshore link. Polar Res. 36, 1302124. http://dx.doi.org/10.1080/17518369.2017.1302124.
Helland-Hansen, W., Hampson, G.J., 2009. Trajectory analysis: concepts and applications. Basin Res. 21, 454–483.
Henriksen, E., Ryseth, A.E., Larssen, G.B., Heide, T., Rønning, K., Sollid, K., Stoupakova, A.V., 2011. Tectonostratigraphy of the greater Barents Sea: implications for petroleum systems. In: Spencer, A.M., Embry, A.F., Gautier, D.L., Stoupakova, A.V., Sørensen, K. (Eds.), Arctic Petroleum Geology, pp. 163–195. Geol. Soc., London, Mem. 35.
Hernández-Molina, F.J., Fernández-Salas, L.M., Lobo, F., Somoza, L., Díaz-del-Rio, V., Alveirinho Dias, J.M., 2000. The infralittoral prograding wedge: a new large-scale progradational sedimentary body in shallow marine environments. Geo-Mar. Lett. 20, 109–117.
Holle, C.G., 1951. Sedimentation at the mouth of the Mississippi river. In: Johnson, J.W. (Ed.), Coastal Engineering, pp. 111–129. Coastal Engineering Proc. 2.
Houseknecht, D.W., Bird, K.J., Schenk, C.J., 2009. Seismic analysis of clinoform depositional sequences and shelf-margin trajectories in Lower Cretaceous (Albian) strata, Alaska North Slope. Basin Res. 21, 644–654.
Hurum, J.H., Roberts, A.J., Dyke, G.J., Grundvåg, S.-A., Nakrem, H.A., Midtkandal, I., Śliwińska, K.K., Olaussen, S., 2016. Bird or maniraptoran dinosaur? A femur from the Albian strata of Spitsbergen. Palaeontol. Pol. 67, 137–147.
Indrevær, K., Gabrielsen, R., Faleide, J.I., 2016. Early Cretaceous syn-rift uplift and tectonic inversion in the Loppa high area, southwestern Barents Sea, Norwegian Shelf. J. Geol. Soc. Lond. http://dx.doi.org/10.1144/jgs2016-066.
Kairanov, B., Marin, D., Escalona, A., Kayukova, A., 2015. Structural control in the progradation direction of the Lower Cretaceous clinoforms in the greater Barents Sea. In: Poster Presented at: 3P Arctic Conference & Exhibition: the Polar Petroleum Potential. Stavanger, Norway, September 29th - October 2nd, 2015.
Kayukova, A.V., Suslova, A.A., Stoupakova, A.V., Kurasov, I.A., Gilaev, R.M., 2014. Cyclicity and petroleum prospects of cretaceous in the Barents Kara sea region. In: Eriksen, S., Haflidason, H., Olesen, O., Husås, A.M. (Eds.), The Arctic Days Conference: Arctic Energy. Nor. Geo. Soc Abstracts and Proceedings, vol. 2, pp. 53–54.
Koevoets, M., Abay, T.B., Hammer, Ø., Olaussen, S., 2016. High-resolution organic carbon-isotope stratigraphy of the middle jurassic–lower cretaceous Agardhfjellet Formation of central spitsbergen, svalbard. Palaeogeogr. Palaeoclimatol. Palaeoecol. 449, 266–274.
Kuehl, S.A., Allison, M.A., Goodbred, S.L., Kudrass, H., 2005. The ganges-brahmaputra delta. In: Giosan, L., Bhattacharya, J.P. (Eds.), River Deltas: Concepts, Models and Examples, pp. 413–434. SEPM Spec. Publ. 83.
Langrock, U., Stein, R., Lipinski, M., Brumsack, H.J., 2003. Paleoenvironment and sea-level change in the early Cretaceous Barents Sea—implications from near-shore marine sapropels. Geo-Mar. Lett. 23, 34–42.
Lawver, L.A., Muller, R.D., 1994. Iceland hotspot track. Geology 22, 311–314.
Lawver, L., Grantz, A., Gahagan, L., 2002. Plate kinematic evolution of the present Arctic region since the Ordivician. In: Miller, E.L., Grantz, A., Klemperer, S.L. (Eds.), Tectonic Evolution of the Bering Shelf – Chukchi Sea – Arctic Margin and Adjacent Landmasses, pp. 337–362. GSA Bull. Spec. Papers 360.
Lundin, E.R., Doré, A.R., 1997. A tectonic model for the Norwegian passive margin with implications for the NE Atlantic: early Cretaceous to break-up. J. Geol. Soc. 154, 545–550.
MacQuaker, J.H.S., Bentley, S.J., Bohacs, K.M., 2010. Wave-enhanced sediment gravity flows and mud dispersal across continental shelves: reappraising sediment transport processes operating in ancient mudstone successions. Geology 38, 947–950.
Maher, H.D., 2001. Manifestations of the Cretaceous high arctic large igneous province in Svalbard. J. Geol. 109, 91–104.
Maher, H.D., Hays, T., Shuster, R., Mutrux, J., 2004. Petrography of the lower cretaceous sandstones of spitsbergen. Polar Res. 23, 147–165.
Marin, D., Escalona, A., 2014. Architecture and distribution analysis of the lower cretaceous clinoforms in the western Barents sea. In: EAGE 6th International Conference & Exhibition. Saint Petersburg, Russia. Extended abstract. http://dx.doi.org/10.3997/2214-4609.20140307.
Marin, D., Escalona, A., Sliwinska, K., Nøhr-Hansen, H., Mordasova, A., 2016a. Sequence stratigraphy and lateral variability of lower cretaceous clinoforms in the SW Barents sea. AAPG Bull. http://dx.doi.org/10.1306/10241616010.
Marin, D., Escalona, A., Grundvåg, S.-A., Olaussen, S., Sliwinska, K., 2016b. Depositional history of the lower cretaceous sequences in the southwestern Barents sea. In: International Arctic Geological Conference (IAGC)/Norwegian Petroleum Society (NPF): Arctic Exploration - Understanding the Barents Sea Potential. Tromsø, Norway, May 31th-June 2nd.
Michels, K.H., Kudrass, H.R., Hübscher, C., Suckow, A., Wiedicke, M., 1998. The submarine delta of the Ganges–Brahmaputra: cyclone-dominated sedimentation patterns. Mar. Geol. 149, 133–154.
Midtkandal, I., Nystuen, J.P., 2009. Depositional architecture of a low-gradient ramp shelf in an epicontinental sea: the Lower Cretaceous of Svalbard. Basin Res. 21, 655–675.
Midtkandal, I., Svensen, H., Planke, S., Corfu, F., Polteau, S., Torsvik, T., Faleide, J.I., Grundvåg, S.-A., Selnes, H., Olaussen, S., 2016. The Aptian oceanic anoxic event (OAE1a) in Svalbard and the age of the Barremian-Aptian boundary. Palaeogeogr. Palaeoclimatol. Palaeoecol. 463, 126–135.
Midtkandal, I., Nystuen, J.P., Nagy, J., 2007. Paralic sedimentation on an epicontinental ramp shelf during a full cycle of relative sea-level fluctuation; the Helvetiafjellet Formation in Nordenskiöld Land, Spitsbergen. Nor. J. Geol. 87, 343–359.
Midtkandal, I., Nystuen, J.P., Nagy, J., Mørk, A., 2008. Lower Cretaceous lithostratigraphy across a regional subaerial unconformity in Spitsbergen: the Rurikfjellet and Helvetiafjellet formations. Nor. J. Geol. 88, 287–304.
Miller, E.L., Toro, J., Gehrels, G., Amato, J.M., Prokopiev, A., Tuchkova, M.I., Akinin, V.V., Dumitru, T.A., Moore, T.E., Cecile, M.P., 2006. New insights into Arctic paleogeography and tectonics from U-Pb detrital zircon geochronology. Tectonics 25, TC3013. http://dx.doi.org/10.1029/2005TC001830.
Mitchum Jr., R., Vail, P., Sangree, J., 1977. Seismic stratigraphy and global changes of sea level: Part 6. Stratigraphic interpretation of seismic reflection patterns in depositional sequences: section 2. Application of seismic reflection configuration to stratigraphic interpretation. In: Peyton, C.E. (Ed.), Seismic Stratigraphy – Applications to Hydrocarbon Exploration, pp. 117–133. AAPG Memoir 26.
Mørk, A., 1978. Observations on the stratigraphy and structure of the inner Hornsund area. Nor. Polarinst. Årb. 1977, 61–70.
Mørk, A., Dallmann, W.K., Dypvik, H., Johannessen, E.P., Larssen, G.B., Nagy, J., Nøttvedt, A., Olaussen, S., Pčelina, T.M., Worsley, D., 1999. Mesozoic lithostratigraphy. In: Dallmann, W.K. (Ed.), Lithostratigraphic Lexicon of Svalbard, pp. 127–214. Norsk Polarinstitutt (Tromsø).
Myrow, P.M., Fischer, W., Goodge, J.W., 2002. Wave-modified turbidites: combined-flow shoreline and shelf deposits, Cambrian, Antarctica. J. Sed. Res. 72, 641–656.
Nagy, J., 1970. Ammonite faunas and stratigraphy of lower cretaceous (albian) rocks in southern spitsbergen. Nor. Polarinst. Skr. 152, 1–58.
Neill, C.F., Allison, M.A., 2005. Subaqueous deltaic Formation on the atchafalaya shelf, Louisiana. Mar. Geol. 214, 411–430.
Nemec, W., 1992. Depositional controls on plant growth and peat accumulation in a braidplain delta environment: Helvetiafjellet Formation (Barremian-Aptian), Svalbard. In: McCabe, P.J., Parish, J.T. (Eds.), Controls on the Distribution and Quality of Cretaceous Coals. Boulder Colorado, pp. 209–226. Geol. Soc. Spec. Paper 267.
Nemec, W., Steel, R.J., Gjelberg, J., Collinson, J.D., Prestholm, E., Øxnevad, I.E., 1988. Anatomy of collapsed and re-established delta front in Lower Cretaceous of Eastern Spitsbergen: gravitational sliding and sedimentation process. AAPG Bull. 72, 454–476.
Nikishin, A.M., Malyshev, N.A., Nikishin, V.A., Soloviev, A.V., Aleksandrova, G.N., Escalona, A., 2014. Aptian Paleogeography of North Kara Sea Region: Provenance Analyses Based on Detrital Zircon Ages from Vize Island Aptian Sandstones, p. 29. AAPG Search and Discovery Article #10566.
Nilsen, K.T., Vendeville, B.C., Johansen, J.-T., 1995. Influence of regional tectonics on halokinesis in the Nordkapp Basin, Barents sea. In: Jackson, M.P.A., Roberts, D.G., Snelson, S. (Eds.), Salt Tectonics: a Global Perspective, pp. 413–436. AAPG Memoir 65.
Nittrouer, C.A., Kuehl, S.A., Figueiredo, A.G., Allison, M.A., Sommerfield, C.K., Rine, E., Faria, E.C., Silveira, O.M., 1996. The geological record preserved by Amazon shelf sedimentation. Cont. Shelf Res. 16, 817–841.
Nøhr-Hansen, H., 1993. Dinoflagellate cyst stratigraphy of the barremian to albian, lower cretaceous. East Greenl. Geol. Greenl. Sur. Bull. 166, 171.
Nøhr-Hansen, H., 2012. Palynostratigraphy of the cretaceous–lower Palaeogene sedimentary succession in the kangerlussuaq basin, southern east Greenland. Rev. Palaeobot. Palynol. 178, 59–90.

Nøttvedt, A., Cecchi, M., Gjelberg, J.G., Kristensen, S.E., Lønøy, A., Rasmussen, A., Rasmussen, E., Skott, P.H., van Veen, P.M., 1992. Svalbard-Barents Sea correlation: a short review. In: Vorren, T.O., Bergsager, E., Dahl-Stamnes, Ø.A., Holter, E., Bohansen, B., Lie, E., Lund, T.B. (Eds.), Arctic Geology and Petroleum Potential. Elsevier, Amsterdarn, pp. 363–375. NPF Spec. Publ 2.

Onderdonk, N., Midtkandal, I., 2010. Mechanisms of collapse of the cretaceous Helvetiafjellet Formation at kvalvågen, eastern spitsbergen. Mar. Petrol. Geol. 27, 2118–2140.

Osmundsen, P.T., Ebbing, J., 2008. Styles of extension offshore mid-Norway and implications for mechanisms of crustal thinning at passive margins. Tectonics 27, TC6016. http://dx.doi.org/10.1029/2007TC002242.

Parker, J.R., 1967. The jurassic and cretaceous sequence in spitsbergen. Geol. Mag. 104, 487–505.

Patruno, S., Hampson, G.J., Jackson, C., A.-L, 2015. Quantitative characterisation of deltaic and subaqueous clinoforms. Earth-Sci. Rev. 142, 79–119.

Pattison, S.A.J., 2005. Storm-influenced prodelta turbidite complex in the Lower Kenilworth Member at Hatch Mesa, Book Cliffs, Utah, U.S.A.: implications for shallow marine facies models. J. Sed. Res. 75, 420–439.

Pinous, O.V., Karogodin, Y.N., Ershov, S.V., Sahagian, D.L., 1999. Sequence stratigraphy, facies and sea level change of the Hauterivian productive complex, Priobskoe oil field (West Siberia). AAPG Bull. 83, 972–989.

Pinous, O., Levchuk, M., Sahagian, D., 2001. Regional synthesis of the productive Neocomian complex of West Siberia: sequence stratigraphic framework. AAPG Bull. 85, 1713–1730.

Polteau, S., Hendriks, B.W.H., Planke, S., Ganerød, M., Corfu, F., Faleide, J.I., Midtkandal, I., Svensen, H.S., Myklebust, R., 2015. The early cretaceous Barents sea sill complex: distribution, 40Ar/39Ar geochronology, and implications for carbon gas formation. Palaeogeogr. Palaeoclimatol. Palaeoecol. http://dx.doi.org/10.1016/j.palaeo.2015.07.007.

Pratson, L., Swenson, J., Kettner, A., Fedele, J., Postma, G., Niedoroda, A., Friedrichs, C., Syvitski, J., Paola, C., Steckler, M., Hutton, E., Reed, C., Van Dijk, M., Das, H., 2004. Modelling continental shelf formation in the Adriatic and elsewhere. Oceanography 17, 118–131.

Rojo, L.A., Escalona, A., Schultze, L., Sayghe, S.A., 2015. Interpretation, modeling, and halokinetic evolution of salt diapirs in the Nordkapp Basin. In: EAGE 77th International Conference & Exhibition. http://dx.doi.org/10.3997/2214-4609.201412529. Madrid, Spain. Extended abstract.

Rokoengen, K., Mørk, A., Mørk, M.B.E., Smelror, M., 2005. The irregular base Cretaceous reflector offshore Mid Norway: a possible result of the Mjølnir impact in the Barents Sea? Nor. Geol. Sur. Bull. 443, 19–27.

Sattar, N., Juhlin, C., Koyi, H., Ahmad, N., 2017. Seismic stratigraphy and hydrocarbon prospectivity of the lower cretaceous Knurr sandstone lobes along the southern margin of Loppa high, Hammerfest Basin, Barents sea. Mar. Petrol. Geol. 85, 54–69.

Seilacher, A., 1982. General remarks about event deposits. In: Einsele, G., Seilacher, A. (Eds.), Cyclic and Event Stratification. Springer-Verlag, Berlin, pp. 161–174.

Seldal, J., 2005. Lower Cretaceous: the next target for oil exploration in the Barents Sea? In: Doré, A.G., Vining, B.A. (Eds.), Petroleum Geology: North- West Europe and Global Perspectives. Proceedings of the 6th Petroleum Geology Conference. Petroleum Geology Conferences Ltd. Published by the Geological Society, London, pp. 231–240.

Senger, K., Tveranger, J., Ogata, K., Braathen, A., Planke, S., 2014. Late mesozoic magmatism in svalbard: a review. Earth-Sci. Rev. 139, 123–144.

Śliwińska, K.K., Nøhr-Hansen, H., Jelby, M.E., Grundvåg, S.-A., Olaussen, S., 2016. Dinocyst biostratigraphy of the lower cretaceous succession of central and southeastern spitsbergen. European geosciences union (EGU) general assembly, Vienna, Austria. Geophys. Res. Abstr. 18, EGU2016–13858.

Smelror, M., Mørk, A., Monteil, E., Rutledge, D., Leereveld, H., 1998. The Klippfisk Formation - a new lithostratigraphic unit of lower cretaceous platform carbonates on the western Barents shelf. Polar Res. 17, 181–202.

Solheim, A., Kristoffersen, Y., 1984. The Physical Environment Western Barents Sea 1:1500 000, Sheet B: Sediments above the Upper Regional Unconformity: Thickness, Seismic Stratigraphy and Outline of the Glacial History, p. 26. Norsk Polarinstitutt Skrifter 179B.

Steel, R.J., Worsley, D., 1984. Svalbard's post-Caledonian strata – an atlas of sedimentational patterns and palaeogeographic evolution. In: Spencer, A.M. (Ed.), Petroleum Geology of the North European Margin. Norwegian Petroleum Society. Graham and Trotman Ltd, pp. 109–135.

Steel, R.J., Gjelberg, J., Haarr, G., 1978. Helvetiafjellet formation (barremian) at festningen, spitsbergen – a field guide. Nor. Polarinst. Årb. 1978, 111–128.

Steel, R.J., Crabaugh, J., Schellpepper, M., Mellere, D., Plink-Björklund, P., Deibert, J., Løseth, T., 2000. Deltas vs. rivers on the shelf edge: their relative contributions to the growth of shelf-margins and basin-floor fans (Barremian and Eocene, Spitsbergen). In: Weimer, P., et al. (Eds.), Deep-water Reservoirs of the World. Proceedings of the GCSSEPM Foundation 20th Annual Research Conference, pp. 981–1009.

Stewart, D.J., Berge, K., Bowlin, B., 1995. Exploration trends in the southern Barents sea. In: Hanslien, S. (Ed.), Petroleum Exploration and Exploitation in Norway. Elsevier, Amsterdam, pp. 253–276. NPF Spec. Publ. 4.

Swenson, J.B., Paola, C., Pratson, L., Voller, V.R., Murray, A.B., 2005. Fluvial and marine controls on combined subaerial and subaqueous delta progradation: morphodynamic modeling of compound-clinoform development. J. Geophys. Res. 110, 1–16.

Swift, D.J.P., Thorne, J.A., 1991. Sedimentation on continental margins, I: a general model for shelf sedimentation. In: Swift, D.J.P., Oertel, G.F., Tillman, R.W., Thorne, J.A. (Eds.), Shelf Sand and Sandstone Bodies, pp. 3–31. IAS Spec. Publ. 14.

Torsvik, T.H., Carlos, D., Mosar, J., Cocks, L.R.M., Malme, T., 2002. Global reconstructions and north atlantic palaeogeography 400 Ma to recent. In: Eide, E.A. (Ed.), BATLAS – Mid Norway Plate Reconstructions Atlas with Global and Atlantic Perspectives, pp. 18–39. Geol. Surv. Nor.

Traykovski, P., Geyer, W.R., Irish, J.D., Lynch, J.F., 2000. The role of wave induced density-driven fluid mud flows for cross-shelf transport on the Eel River continental shelf. Cont. Shelf Res. 20, 2113–2140.

Ulmishek, G.F., 2003. Petroleum geology and resources of the west Siberian Basin, Russia. USGS Bull. 1–49, 2201-G.

Van Wagoner, J.C., Mitchum, R.M., Campion, K.M., Rahmanian, V.D., 1990. Siliciclastic sequence stratigraphy in well logs, cores, and outcrops: concepts for high resolution correlation of time and facies. AAPG Methods Explor. Ser. 7, 55 p.

Vickers, M.L., Price, G.D., Jerrett, R.M., Watkinson, M., 2016. Stratigraphic and geochemical expression of Barremian–Aptian global climate change in Arctic Svalbard. Geosphere 12, 1–12. http://dx.doi.org/10.1130/GES01344.1.

Walsh, J.P., Nittrouer, C.A., Palinkas, C.M., Ogston, A.S., Sternberg, R.W., Brunskill, G.J., 2004. Clinoform mechanics in the Gulf of Papua, new Guinea. Cont. Shelf Res. 24, 2487–2510.

Wierzbowski, A., Hryniewicz, K., Hammer, Ø., Nakrem, H.A., Little, C.T.S., 2011. Ammonites from hydrocarbon seep carbonate bodies from the uppermost Jurassic–lowermost Cretaceous of Spitsbergen and their biostratigraphical importance. N. Jb. Geol. Paläont. Abh 262, 267–288.

Williams, G., Brinkhuis, H., Pearce, M., Fensome, R., Weegink, J., 2004. Southern Ocean and global dinoflagellate cyst events compared: index events for the Late Cretaceous–Neogene. In: Exon, N.F., Kennett, J.P., Malone, M.J. (Eds.), Proceedings of the Ocean Drilling Program, Scientific Results, vol. 189, pp. 1–98. Available from World Wide Web. http://www-odp.tamu.edu/publications/189_SR/VOLUME/CHAPTERS/107.PDF.

Worsley, D., Johansen, R., Kristensen, S.E., 1988. The mesozoic and cenozoic succession of tromsøflaket. In: Dalland, A., Worsley, D., Ofstad, K. (Eds.), A Lithostratigraphic Scheme for the Mesozoic and Cenozoic Succession Offshore Mid- and Northern Norway, pp. 42–65. NPD Bull. 4.

Wright, L.D., Friedrichs, C.T., Kim, S.C., Scully, M.E., 2001. Effects of ambient currents and waves on gravity-driven sediment transport on continental shelves. Mar. Geol. 175, 25–45.

Yang, Z.S., Liu, J.P., 2007. A unique Yellow River-derived distal subaqueous delta in the Yellow Sea. Mar. Geol. 240, 169–176.

Zhang, X., Omma, J., Pease, V., Scott, R., 2013. Provenance of late paleozoic-mesozoic sandstones, Taimyr peninsula, the arctic. Geosciences 3, 502–527.

Paper 5

Effects of adjacent fault systems on drainage patterns and evolution of uplifted rift shoulders: The Lower Cretaceous in the Loppa High, southwestern Barents Sea

Dora Marín, Alejandro Escalona, Sten-Andreas Grundvåg, Henrik Nøhr-Hansen, Bereke Kairanov

Marine and Petroleum Geology, 94, 2018, 212-229, ISSN 0264-8172,

https://doi.org/10.1016/j.marpetgeo.2018.04.009

Marine and Petroleum Geology 94 (2018) 212–229

Contents lists available at ScienceDirect

Marine and Petroleum Geology

journal homepage: www.elsevier.com/locate/marpetgeo

Research paper

Effects of adjacent fault systems on drainage patterns and evolution of uplifted rift shoulders: The Lower Cretaceous in the Loppa High, southwestern Barents Sea

Dora Marín[a,*], Alejandro Escalona[a], Sten-Andreas Grundvåg[b], Henrik Nøhr-Hansen[c], Bereke Kairanov[a]

[a] *Department of Petroleum Engineering, University of Stavanger, NO-4036, Stavanger, Norway*
[b] *Department of Geosciences, UiT The Arctic University of Norway, PO Box 6050, Langnes, 9037, Tromsø, Norway*
[c] *Geological Survey of Denmark and Greenland (GEUS), Øster Voldgade 10, DK-1350, Denmark*

ABSTRACT

Sedimentological models for rift shoulders have poorly documented the effect of adjacent fault systems on drainage patterns. In this study we investigate the Loppa High, an ancient tilted rift shoulder located in the southwestern Barents Sea. We use seismic and well data, sedimentological log descriptions, and biostratigraphic information to understand the drainage patterns and the Early Cretaceous geological history of the Loppa High. This study provides an example of how the drainage systems in low-gradient flanks of a rift shoulder can be modified and confined by normal faults occurring almost orthogonal to the main fault system. These orthogonal faults might have acted as preferential sediment routes. Thus, potential deposits of the main drainage systems directed to the low gradient flank are found almost exclusively associated with grabens formed due to these orthogonal faults. The Early Cretaceous evolution of the Loppa High is summarized as follow: 1) during the Boreal Berriasian/Volgian to early Barremian, the Asterias and the Bjørnøyrenna fault complexes were active. Diachronous shallow to eventually deep-marine fans and incised valleys were developed along the southern and western flanks of the Loppa High; 2) late Barremian–Aptian fault activity is interpreted along the Ringvassøy Loppa Fault Complex. A second generation of incised valleys and their related shallow-marine fans were formed in the western flank of the Loppa High; and 3) during late Aptian–early Albian the Loppa High and the Hammerfest Basin were tilted eastwards. The latter event triggered a switch in depocenter location and development of shelf-margin clinoforms downlapping in close proximity to the eastern flank of the high.

1. Introduction

Uplifted rift shoulders are a major factor controlling the filling of rift basins (Steckler and Omar, 1994; Lambiase and Bosworth, 1995; Allen and Densmore, 2000; Gawthorpe and Leeder, 2000; Withjack et al., 2002; Leppard and Gawthorpe, 2006; Armitage et al., 2011). They usually have high gradient slopes towards the master fault and low gradient slopes away from the master faults, resembling large-scale tilted blocks (Frostick and Reid, 1989; van Balen et al., 1995; Bosence, 1998). High gradient slopes are characterized by incised valleys, and back-stepping or aggradational fans (Ravnås and Steel, 1998; O'Grady et al., 2000; Densmore et al., 2007; Hadler-Jacobsen et al., 2005). In contrast, the development of incised valleys in low gradient slopes is less pronounced, and fans tend to be progradationally-stacked, indicating the development of deltas or shorelines (Ravnås and Steel, 1998; O'Grady et al., 2000; Densmore et al., 2007; Hadler-Jacobsen et al., 2005). Drainage evolution on rift shoulders and the time variation of its deposits depend on several factors including among others: climate, lithology and thickness of the bedrock, morphology and gradient of the high and its flanks, variation in fault propagation and slip rate, selective reactivation of faults, pre-existing drainage, structures, and topography (Frostick and Reid, 1989; Leeder et al., 1991; Steckler and Omar, 1994; Lambiase and Bosworth, 1995; Ravnås and Steel, 1998; Gawthorpe and Leeder, 2000; Sklar and Dietrich, 2001; Sharp et al., 2000; Leppard and Gawthorpe, 2006; Densmore et al., 2007; Mortimer and Carrapa, 2007; McArthur et al., 2013; Henstra et al., 2017; Ford et al., 2016; Gawthorpe et al., 2017). Current drainage systems in large-scale tilted rift shoulders have been studied in the Red

* Corresponding author.
E-mail addresses: doraluzmr@gmail.com (D. Marín), alejandro.escalona@uis.no (A. Escalona), sten-andreas.grundvag@uit.no (S.-A. Grundvåg), hnh@geus.dk (H. Nøhr-Hansen), bereke.kairanov@uis.no (B. Kairanov).

https://doi.org/10.1016/j.marpetgeo.2018.04.009
Received 29 November 2017; Received in revised form 27 March 2018; Accepted 11 April 2018
Available online 12 April 2018

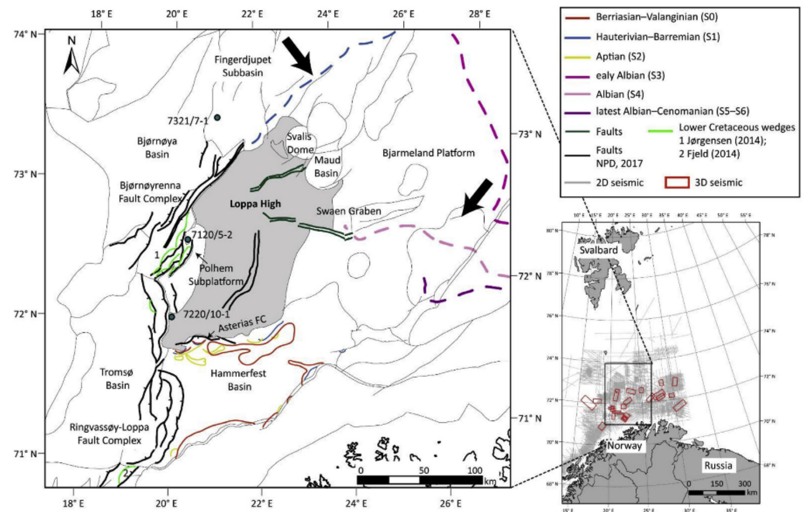

Fig. 1. Location map with the main structural elements and the dataset used in this study. The map also shows the different types of Lower Cretaceous wedges previously identified in the study area (Marín et al., 2017a, 2017b; Jørgensen, 2014; Fjeld, 2014). Dashed lines represent the clinoform rollover points and black arrows indicate their progradation direction. Continuous lines represent wedges associated with scarps. The colors of the lines represent the seven sequences used in this study (sequences 0–6). (For interpretation of the references to color in this figure legend, the reader is referred to the Web version of this article.)

Sea and Gulf of Aden (Frostick and Reid, 1989). In these areas, the main drainage system is directed towards the low gradient slope and away from the master faults (Frostick and Reid, 1989; Bosence, 1998). The drainage directed towards the rifted basin usually has a smaller length, beside some particular rivers where the rate of erosion keeps the uplift rate (Frostick and Reid, 1989; Bosence, 1998; Leppard and Gawthorpe, 2006).

Rift shoulders can be complex structures affected by two or more adjacent fault systems. These fault systems can rejuvenate the topography periodically and preferentially in certain areas of the high and affect the drainage patterns (Lambiase and Bosworth, 1995; Bosence, 1998; Marín et al., 2017a). Rift shoulders affected by adjacent fault systems are rarely preserved in the geological record. An example of an ancient uplifted rift shoulder affected by adjacent fault systems is the Loppa High, located in the southwestern Barents Sea (Fig. 1). The southern and the western flanks of the Loppa High were affected by a Late Jurassic–Early Cretaceous rift event (Sund et al., 1986; Berglund et al., 1986; Wood et al., 1989; Faleide et al., 1993). This rift event controlled the geometry of the high, which is characterized by a series of terraces and fault scarps in its western and southwestern flanks and gentle slopes in its eastern and southeastern flanks, giving the aspect of a large-scale tilted block (Fig. 2) (Wood et al., 1989; Gabrielsen et al., 1990). Lower Cretaceous syn-to post-rift clastic wedges occur in the southern and western flanks of the Loppa High and have been targeted in several petroleum exploration campaigns (Seldal, 2005; Knutsen et al., 2000; Sandvik, 2014; Jørgensen, 2014; NPD, 2017; Blaich et al., 2017; Marín et al., 2017a). Lower Barremian SE-prograding clinoforms and Aptian to ?mid-Cenomanian SW-prograding clinoforms have been described in the neighboring Fingerdjupet Subbasin and in the Bjarmeland Platform respectively (Fig. 1) (Glørstad-Clark, 2011; Dahlberg, 2014; Dimitriou, 2014; Hinna et al., 2016; Marín et al., 2017b; Serck et al., 2017). These clinoforms prograded toward the Loppa High, suggesting that the Loppa High was tilted to the north and east during the Early Cretaceous (Figs. 1 and 2).

Due to the amount of seismic and well data available, the flanks of the Loppa High are an excellent laboratory to study drainage pattern evolution in rift shoulders affected by fault systems in adjacent basins (e.g. the Hammerfest, Tromsø and Bjørnøya basins and the Swaen Graben). Additionally, the size of the Loppa High (approx. 90 km × 175 km) contributes to the understanding of the evolution of drainage systems in large uplifted rift shoulders, which can complement previous models that have been mainly created for local uplifted blocks (e.g. Allen and Densmore, 2000; Densmore et al., 2007; Armitage et al., 2011).

We study the effect of rift-related tectonic rearrangements on sedimentary systems on the flanks of the Loppa High. The main objectives are to: 1) provide an age control for the wedges deposited in the western flank of the Loppa High; 2) document and interpret the seismic facies in the western flank of the Loppa High within a sequence stratigraphic framework (the interpretations are aided by sedimentological log descriptions of well 7220/10-1); 3) describe the tectono-stratigraphic relationship of previously documented Lower Cretaceous clinoforms with the northern and eastern flanks of the Loppa High; and 4) integrate new descriptions from the western flank of the Loppa High with previous observations of the Lower Cretaceous strata in the southern flank of Loppa High (Marín et al., 2017a), in order to understand the mechanisms controlling the drainage patterns in rift shoulders affected by adjacent diachronous fault systems.

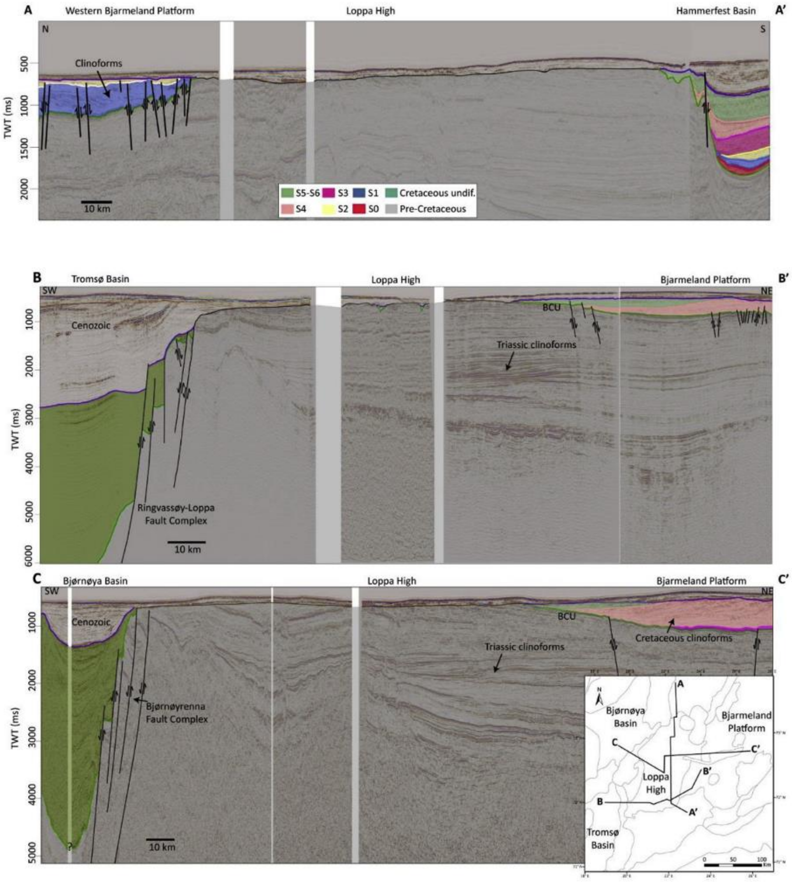

Fig. 2. Regional seismic lines showing the terraces and fault scarps of the western and southern flanks and the eastern low gradient flank of the Loppa High. S0: Berrriasian–Valanginian; S1: Hauterivian–Barremian; S2: Aptian; S3: early Albian; S4: Albian and S5–S6: latest Albian–Cenomanian. A–A′) N–S regional line showing the northwestern part of the Bjarmeland Platform, the Loppa High and the Hammerfest Basin. B–B′) Seismic line showing the deep Tromsø Basin, the Ringvassøy-Loppa Fault Complex, the Loppa High and the Bjarmeland Platform. C-C′) Seismic line showing the deep Bjørnøya Basin, the Bjørnøyrenna Fault Complex, the Loppa High and the Bjarmeland Platform.

2. Geological setting

2.1. Tectonic framework

The Loppa High is located in the southwestern Barents Sea and is bounded to the west by the NE–SW-striking Bjørnøyrenna and the N–S-striking Ringvassøy-Loppa fault complexes, and to the southwest by the E–W-striking Asterias Fault Complex (Figs. 1 and 2) (Gabrielsen et al., 1990). The southeastern and eastern Loppa High borders with the Bjarmeland Platform and with the Hammerfest Basin are gently dipping to the east and are interrupted by the Swaen Graben (Figs. 1 and 2) (Gabrielsen et al., 1990). During the Triassic to Middle Jurassic, the Loppa High area acted as a depocenter, which was later uplifted (Sund et al., 1986; Wood et al., 1989; Glørstad-Clark, 2011). Most authors have suggested a Late Jurassic–Early Cretaceous (Sund et al., 1986; Berglund et al., 1986; Wood et al., 1989) or earliest Cretaceous age for this uplift event (Glørstad-Clark, 2011; Indrevær et al., 2017).

The surrounding basins, including the Hammerfest, Tromsø and Bjørnøya basins, as well as the Fingerdjupet Subbasin and the Swaen Graben, were affected by Late Jurassic to Early Cretaceous extension (for location see Fig. 1) (Berglund et al., 1986; Sund et al., 1986; Wood et al., 1989; Gabrielsen et al., 1990; Løseth et al., 1992; Faleide et al., 1993; Clark et al., 2014; Lazarević, 2017). An earliest Cretaceous and an Aptian faulting event are well constrained for the Bjørnøya Basin and the Fingerdjupet Subbasin, both resulting in the formation of clastic wedges associated with the main fault planes (Faleide et al., 1993; Clark et al., 2014; Blaich et al., 2017; Serck et al., 2017). Early Cretaceous local inversion has been suggested along the Bjørnøyrenna, Ringvassøy-Loppa and Asterias fault complexes as a result of transpression along these faults or because of space problems related to the uplift of the Loppa High (Berglund et al., 1986; Sund et al., 1986; Gabrielsen et al., 1990; Indrevær et al., 2017). As a consequence, the inversion of seismic wedges and formation of structural highs controlling the location of the paleo shelf-edge, has been described in the Polhem Subplatform and the Hammerfest Basin (Indrevær et al., 2017; and Marín et al., 2017a).

2.2. *Stratigraphic framework*

The Lower Cretaceous succession is divided into four main formations in the Barents Sea: Knurr, Klippfisk, Kolje and Kolmule (Dalland et al., 1988; Mørk et al., 1999) and more recently, into seven genetic sequences (sequences 0–6; Marín et al., 2017b) (Fig. 3). The lower boundary of the Lower Cretaceous is known as the Base Cretaceous Unconformity (BCU), which is expressed as a high amplitude seismic reflector, but its age and stratigraphic significance is complex (Nøttvedt et al., 1995; Gabrielsen et al., 2001). In the areas of the southwestern Barents Sea affected by Late Jurassic to Early Cretaceous tectonism, the BCU represents an unconformity. The age of the succession immediately above the BCU varies from Boreal Berriasian/Volgian to Valangianian (Århus et al., 1990; Mørk et al., 1999; Marín et al., 2017a) to Barremian (e.g. 7220/10-1) (Fig. 3). The Lower Cretaceous sequences (sequences 0–6) are bounded by flooding surfaces and some of which are interpreted as potentially having regional scale (Fig. 3) (Marín et al., 2017a, 2017b; Grundvåg et al., 2017).

2.3. *The Hammerfest Basin*

A detailed Early Cretaceous filling history of the Hammerfest Basin is provided by Marín et al. (2017a). Westward deflected fan deltas sourced by incised valleys were interpreted along the southern flank of the Loppa High. The western fans have been dated as Boreal Berriasian/Volgian to early Valanginian or younger. The eastern fans have been dated as early Barremian age, but NPD (2017) also reports Valanginian ages. Aptian submarine fans are interpreted preferentially in the southwestern flank of the Loppa High and are deflected eastward. An upper Aptian to lower Albian unconformity is interpreted in the southwestern flank of the Loppa High. This unconformity coincides with a depocenter shift from the western part of the Hammerfest Basin to its central and northeastern parts which is interpreted as the result of tectonic activity in the Ringvassøy-Loppa Fault (Fig. 4) (Faleide et al., 1993; Marín et al., 2017a).

3. Data and methods

This study uses two and three dimensional seismic reflection data and well logs provided by the Norwegian DISKOS database (Fig. 1). The frequency values of the seismic data are mainly between 10 and 50 Hz. A sequence stratigraphic framework is established in the western flank of the Loppa High, based on stacking pattern analysis of wells 7220/5-2 and 7220/10-1 and mapping of reflector terminations on seismic. Sequence boundaries are defined by maximum flooding surfaces (i.e. genetic sequences; Galloway, 1989), elucidated by a spike with high gamma ray log (GR) values. The top of the sequences are tied to the seismic with synthetic seismograms. The sequences from the western flank of the Loppa High are correlated with a previously defined stratigraphic framework of seven genetic sequences established for the Hammerfest Basin, the Fingerdjupet Subbasin, the Bjarmeland and the Finnmark platforms (sequences 0–6; Fig. 3) (Marín et al., 2017b). The age of the sequences is based on palynological analysis. For well 7220/10-1, 31 ditch cutting samples have been palynological analyzed, 17 of

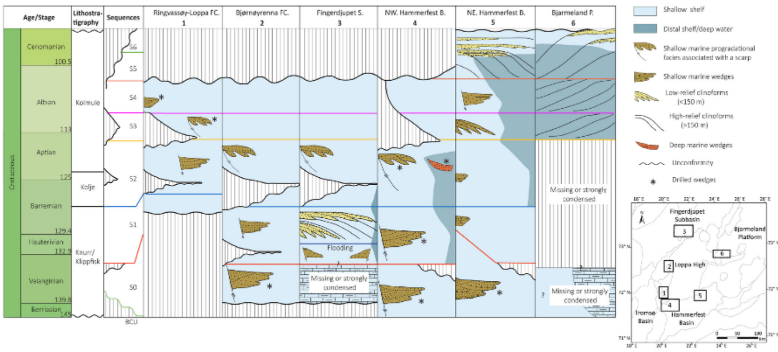

Fig. 3. Sequence correlation around the Loppa High. Note that the BCU time gap in the southwestern flank of the Loppa High is from Late Jurassic to late early Barremian. Two additional unconformities are interpreted in the western flank of the Loppa High, one during the late Barremian to earliest Aptian age and a second during the late Aptian–early Albian. Formation names and ages from Dalland et al. (1988) and Mørk et al. (1999).

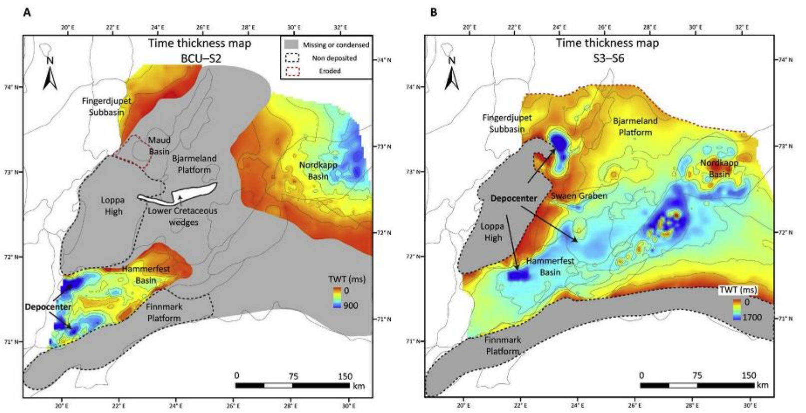

Fig. 4. A) Preserved time thickness maps between the BCU and the top of sequence 2. B) Preserved time thickness map between the top of sequence 2 and the top of sequence 6. Note the depocenter shift in the Hammerfest Basin from its western part in the BCU–sequence 2, to its eastern part in sequences 3–6. The Tromsø and the Bjørnøya basins are not included in this study. Note the differences in color scale in maps A and B. (For interpretation of the references to color in this figure legend, the reader is referred to the Web version of this article.)

these provided dinocyst assemblages of Early Cretaceous age mixed with caved Paleocene dinocyst species. The age interpretation for well 7220/5-2 is based on a StrataBugs v2.0 charts, created from DEXFile with palynomorph occurrences data from 200 samples prepared by Robertson (UK) Ltd. (from the DISKOS database), using the zonation by Nøhr-Hansen (1993).

A description and interpretation of seismic facies is provided, which is based on the geometry of the sequences and the internal reflector character following the principles of Mitchum et al. (1977). Where clinoforms are present, a time-depth conversion and a decompaction process was performed (for details see Marín et al., 2017b) to have an estimative of the original depositional geometry (Salazar et al., 2016).

A detailed sedimentological log description for two cores of well 7220/10-1 is included to aid the depositional environment interpretation. The sedimentary log includes descriptions of rock type, grain size, sorting, sedimentary structures, body and trace fossils and degree of bioturbation.

4. Lower Cretaceous sequences in the north and east of the Loppa High

During the deposition of the oldest sequences (sequences 0–2; Boreal Berriasian–Aptian) the main depocenters were located in the northwestern and the southwestern parts of the Hammerfest Basin, associated with the main bounding faults (Fig. 4a). At the top of sequence 2 (earliest Albian), a switch in the depocenter location is observed in the area (Fig. 4). During deposition of the youngest sequences (sequences 3–6; Albian–Cenomanian), the main depocenters were located in the eastern part of the Hammerfest Basin, the southwestern part of the Bjarmeland Platform and the Nordkapp Basin (Fig. 4b). Lower Cretaceous clinoforms located to the east and north of the Loppa High have previously been documented (Glørstad-Clark, 2011; Dahlberg, 2014; Dimitriou, 2014; Hinna et al., 2016; Marín et al., 2017b). However, their tectono-stratigraphic relationship with the Loppa High is not well understood. Below we provide a description of these clinoforms focusing on their relationship with the Loppa High.

4.1. Lower Cretaceous to the east of the Loppa High (the Bjarmeland Platform and the Swaen Graben)

The oldest sequences (sequences 0–1) are not properly documented in areas such as the Loppa High and the southwestern part of the Bjarmeland Platform (Figs. 3 and 4a), because they are either condensed intervals below seismic resolution (4–35 m of the time equivalent Knurr and Klippfisk formations; Smelror et al., 1998; NPD, 2017) or because there were not deposited. The BCU is tilted towards the east in the boundary of the Loppa High and the Bjarmeland Platform. Southwestward prograding clinoforms of sequences 3–4 downlap onto this tilted BCU (Fig. 5b). The clinoforms have a height of approx. 500 m and the topsets are usually eroded (Marín et al., 2017b). Sequences 5 and 6 are observed on the eastern flank of the Loppa High (Fig. 5d). The eastern flank of the Loppa High is interrupted by the Swaen Graben and by a series of NE–SW striking faults, connecting the northern part of the Loppa High with the Maud Basin (Fig. 1). Lower Cretaceous wedges are observed associated to these faults (Figs. 6 and 7d). The Swaen Graben is constituted by several segments of WNW–ESE, E–W and WSW–ENE normal faults creating a segmented graben (Gabrielsen et al., 1990) (Figs. 1 and 6b). Clastic wedges occur at several stratigraphic intervals within the Lower Cretaceous basin fill succession (Lazarević, 2017) (Fig. 6). In a seismic line oriented parallel to the strike of the graben a local unconformity is observed. There is no age control in this graben, but from regional correlations, an age older than sequence 4 (i.e. Albian) is suggested for the succession below the unconformity.

4.2. Lower Cretaceous to the north of the Loppa High (the western Bjarmeland Platform and the Fingerdjupet Subbasin)

In the southern part of the Fingerdjupet Subbasin, sequence 1 is interpreted above the BCU. Sequence 1 in this area is divided into two by a downlap surface, interpreted as local flooding surfaces (Figs. 3 and

Marine and Petroleum Geology 94 (2018) 212–229

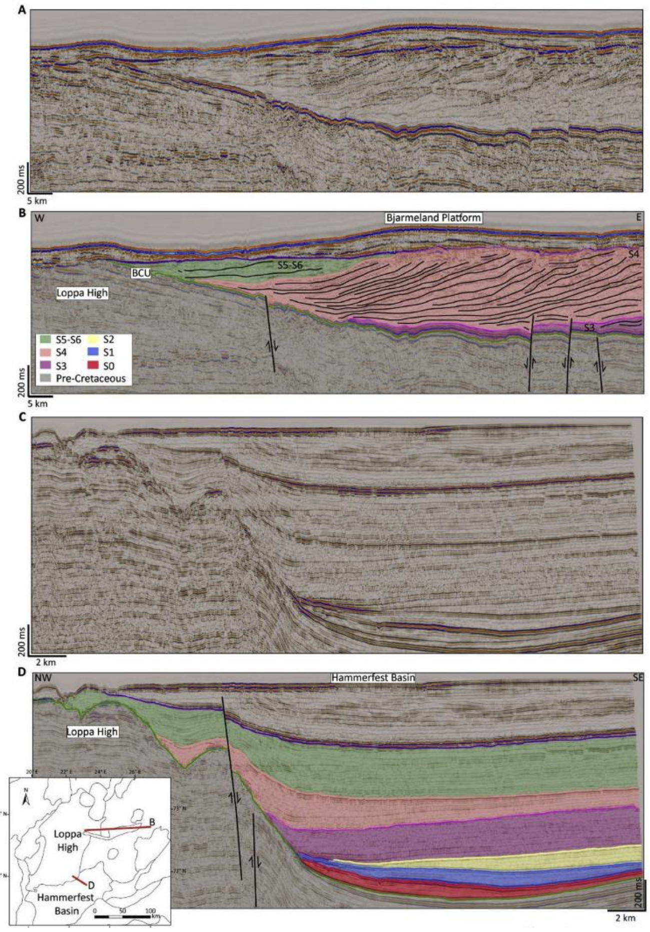

Fig. 5. Seismic lines showing the Lower Cretaceous sequences in the eastern and southeastern flanks of the Loppa High. A) Uninterpreted seismic line. B) Interpreted seismic line showing the clinoforms of sequences 3–6 downlap onto the BCU. C) Uninterpreted seismic line. D) Interpreted seismic line showing the relationship of the Lower Cretaceous sequences deposited on the northeastern Hammerfest Basin. Note that the oldest sequences (sequences 0–3) onlap onto the BCU without being faulted. The youngest sequences (sequences 4–6) are faulted and deposited on the Loppa High.

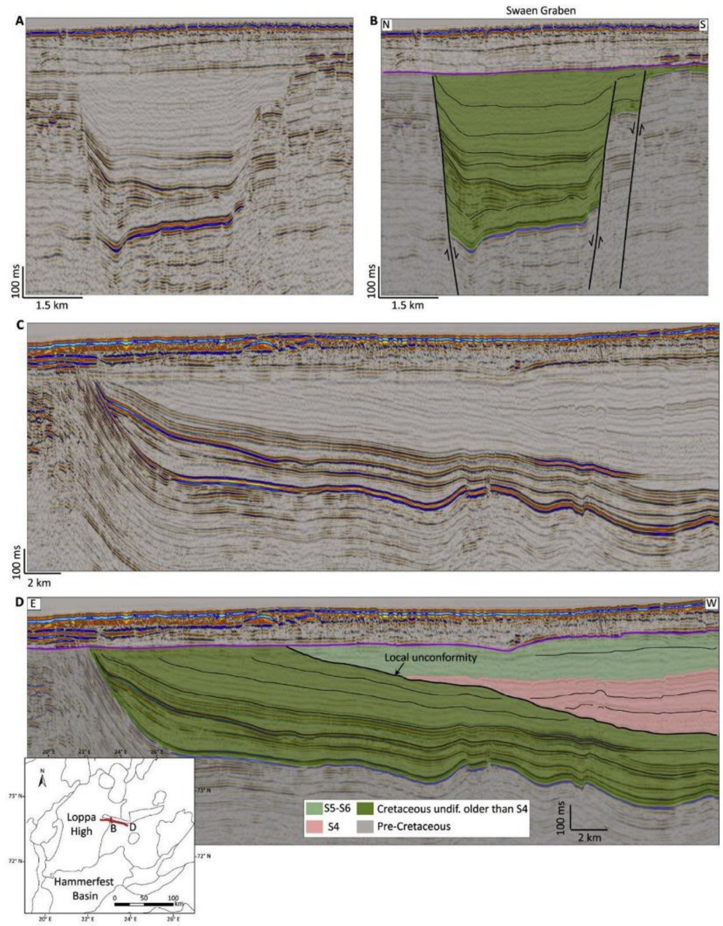

Fig. 6. Seismic lines showing the Lower Cretaceous sequences in the Swaen Graben. A) Uninterpreted seismic line. B) Interpreted seismic line showing the Lower Cretaceous clastic wedges developed along the main faults in the graben. C) Uninterpreted seismic line. D) Interpreted seismic line showing an unconformity in the area indicating a switch in the source of sediment.

7b). The lower part of sequence 1 is characterized by wedges closely associated with normal faults. Above the downlap surface, a package of clinoforms occur (Marín et al., 2017b) (Figs. 3, 7b and 7d). These clinoforms prograded to the SE in close proximity to the Loppa High, where they appear to be tilted towards the Fingerdjupet Subbasin or to the western Bjarmeland Platform (Fig. 7). The top of sequence 1 in the uplifted footwalls is truncated by an unconformity (Fig. 7b). Based on well 7321/7-1 the age of the unconformity is late Barremian–early

Marine and Petroleum Geology 94 (2018) 212–229

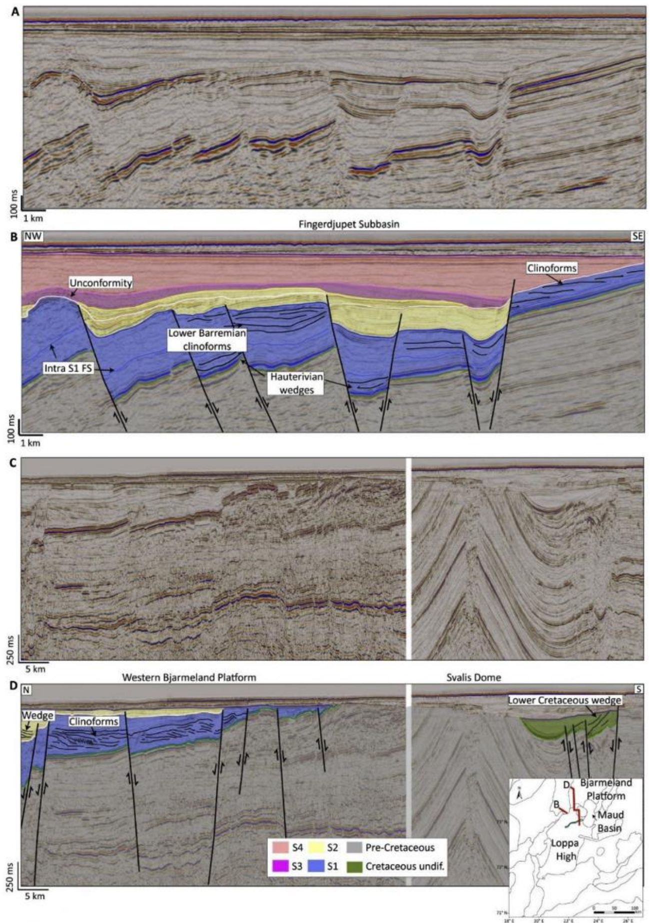

Fig. 7. A) Uninterpreted seismic line. B) Interpreted seismic line showing the Lower Cretaceous sequences in the northern flank of the Loppa High. Note the low angle wedges in the lower part of sequence 1, and clinoforms in the upper part. An intra sequence 2 unconformity is observed in the area. C) Uninterpreted seismic line. D) Interpreted seismic line shows the Barremian clinoforms in the western Bjarmeland Platform. Local wedges are identified in sequences 2–3?.

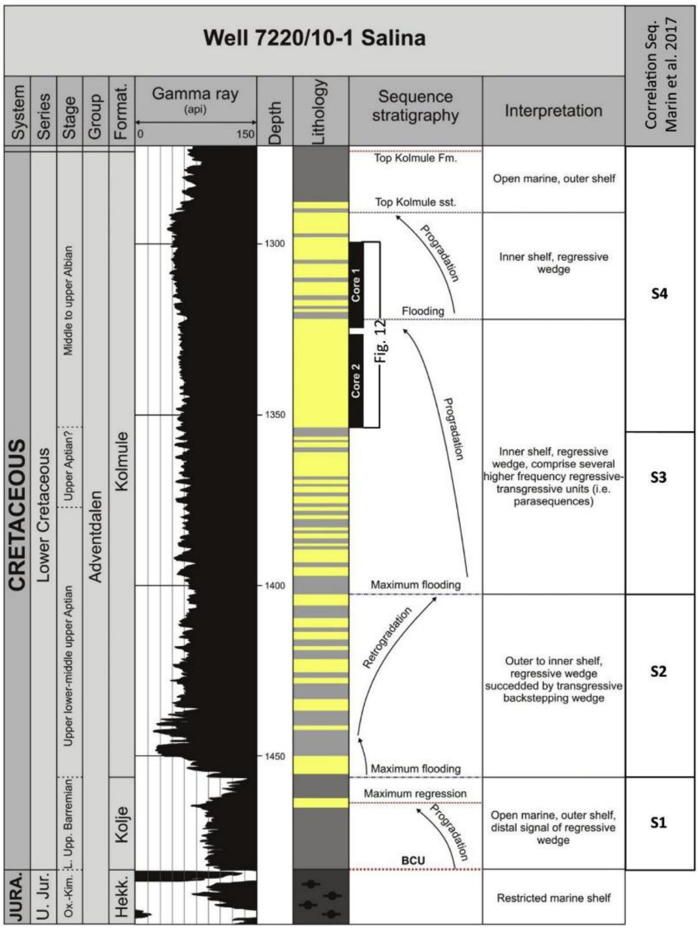

Fig. 8. Gamma ray log, lithology distribution and sequence stratigraphic interpretation of the Lower Cretaceous interval in well 7220/10-1. The sequences are correlated with the stratigraphic framework of Marín et al. (2017b).

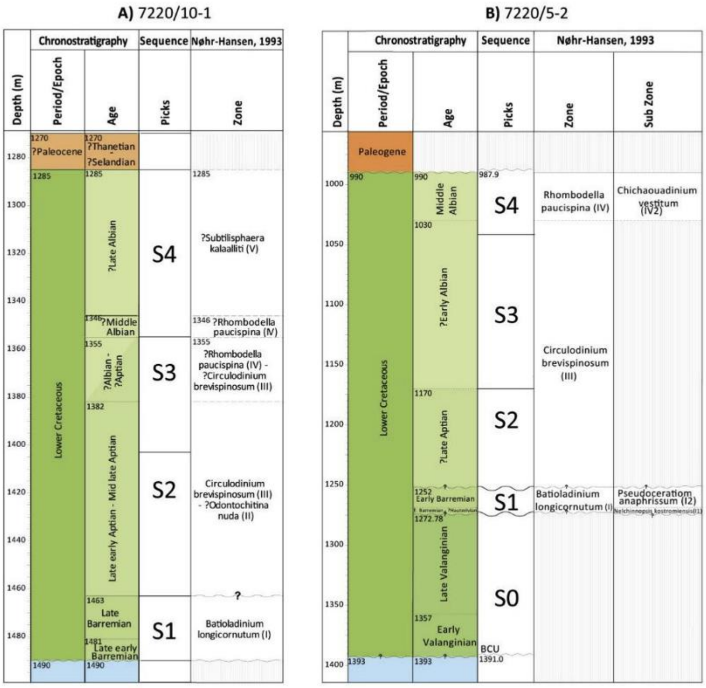

Fig. 9. A) Summary of the biostratigraphy for well 7220/10-1 located in the Ringvassøy-Loppa Fault Complex. B) Summary of the biostratigraphy for well 7220/5-2 located in the southern Bjørnøyrenna Fault Complex.

Aptian (Fig. 3) (Robertson Group plc, 1989). Thickness changes and wedges associated with faults are observed in the area within sequences 2 and 3 (Fig. 7b and d).

5. Lower Cretaceous in the western flank of the Loppa High

5.1. Sequence stratigraphy

The gamma ray log of well 7220/10-1 suggests that the Lower Cretaceous succession can be divided into three large-scale regressive-transgressive sequences that are punctuated by several higher-order regressive and transgressive pulses (Fig. 8). The oldest maximum flooding surface interpreted in well 7220/10-1 is correlated with the top of sequence 1, although it appears to be slightly younger than in the Hammerfest Basin, where an age of Hauterivian–early Barremian was assigned (Marín et al., 2017a). The second maximum flooding surface is interpreted as the top of sequence 2 with an age of late early to mid late Aptian. A flooding surface representing the top of sequence 3 is not evident in well 7220/10-1. However, the top of this sequence is interpreted in the western flank of the Loppa High based on seismic correlations. The age of this event is time equivalent with the top of sequence 3 in the Hammerfest Basin. Sequence 4 is partially identified, but its top is truncated by an unconformity at the top of the Lower Cretaceous (Fig. 9a). Sequence 0 of an age Boreal Berriasian–Valanginian, is not identified in this well. However, sequence 0 is interpreted in well 7220/5-2 located in the southern Bjørnøyrenna Fault Complex (Fig. 9b). Sequences 5 and 6 (latest Albian–mid Cenomanian age) are not observed in the western flank of the Loppa High.

5.2. Seismic facies and core description

5.2.1. Description

5.2.1.1. The Lower Cretaceous in the southern Bjørnøyrenna Fault Complex. The southern segment of the Bjørnøyrenna Fault Complex is characterized by a series of terraces and fault scarps (Fig. 2c). The Lower Cretaceous succession was drilled in one of these terraces by well 7220/5-2 (Fig. 10b). Three unconformities are interpreted in the area. The first unconformity coincides with the BCU, the second is an upper

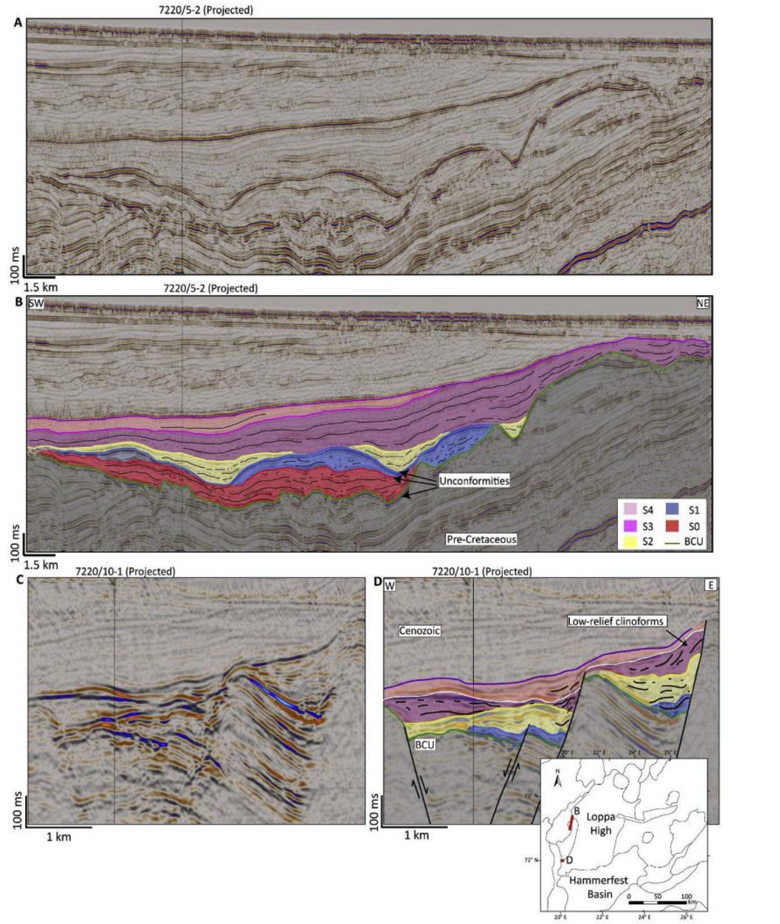

Fig. 10. Seismic lines showing the details of the sequences in the western flank of the Loppa High. A) Uninterpreted seismic line. B) Interpreted seismic line showing the details of the sequences in the southern segment of the Bjørnøyrenna Fault Complex. Note the three unconformities interpreted in the area, where incisions were developed. C) Uninterpreted seismic line. D) Interpreted seismic line showing the wedges associated with the Ringvassøy-Loppa Fault Complex.

Valanginian–Hauterivian unconformity and the youngest is an upper Barremian–lower Aptian unconformity (Figs. 9 and 10b). These unconformities are characterized by erosional features (i.e. incisions). Incisions are particularly marked in the BCU and in the youngest unconformity (Fig. 10b). The incisions are located in some of the terraces of the southern segment of the Bjørnøyrenna Fault Complex, particularly in the higher footwalls located to the east (Figs. 10b and 11). It is not easy to determine the length of these incisions in the

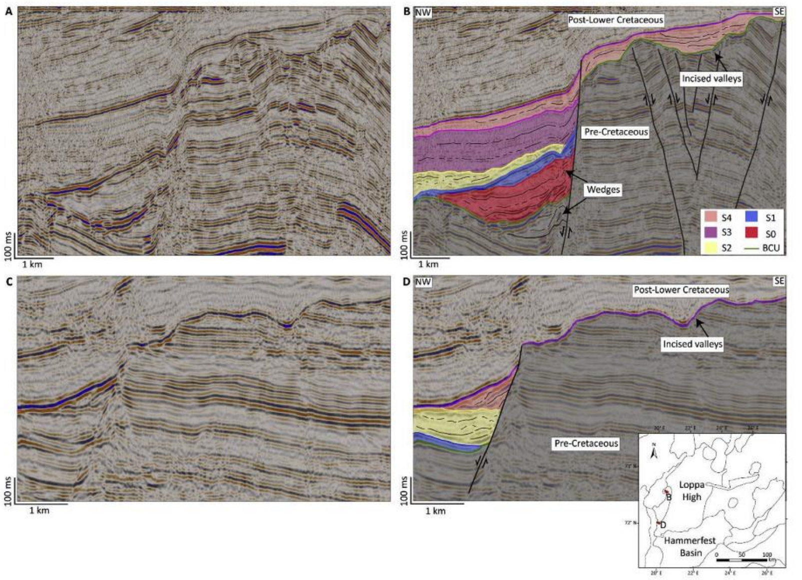

Fig. 11. Seismic lines showing the seismic facies in the western flank of the Loppa High. A) Uninterpreted seismic line. B) Interpreted seismic line showing an incised valley with narrow fans associated with the Bjørnøyrenna Fault Complex. C) Uninterpreted seismic line. D) Interpreted seismic line showing an incised valley with fans associated with the Ringvassøy-Loppa Fault Complex.

western flank of the Loppa High, since this area has experienced several post Early Cretaceous erosion events (Solheim and Kristoffersen, 1984; Henriksen et al., 2011). The incisions at the BCU level are partially filled by sequences 0 and 1 in the terraces and by sequences 3–4 in the higher footwalls (Figs. 10b and 11b). The incisions located at the top of sequence 1 are filled by sequence 2 (Fig. 10b). Sequences 0 and 1 have wedge geometries, thicker towards a fault plane. Internally, the reflectors are continuous to semi-continuous. Additionally, Upper Jurassic wedges have been previously described in the area (Blaich et al., 2017). Wedges are observed next to incisions occurring in the higher footwalls (Fig. 11b). Sequence 2 thins towards the southern segment of the Bjørnøyrenna Fault Complex and the internal reflectors are discontinuous (Fig. 11b).

5.2.1.2. The Lower Cretaceous in the Ringvassøy Loppa Fault Complex. A series of stacked Lower Cretaceous wedges are observed in the terraces of the western flank of the Loppa High, closely associated with the fault scarps of the Ringvassøy Loppa Fault Complex, (Fig. 10d).

Wedges are not observed in the Upper Jurassic succession, unlike the southern segment of the Bjørnøyrenna Fault Complex and sequence 0 is absent here (Figs. 9a, 10d; 11). The upper part of sequence 1 overlies the Upper Jurassic succession and together with sequence 2 comprise the first wedge level (Fig. 10d). Internally, the reflectors are aggradational. The age for this first wedge level is late early Barremian to mid late Aptian. The younger wedge level is interpreted as part of sequences 3–4 (Fig. 10d). Low-relief clinoforms (30–50 ms, approx. < 60 m) that prograded westward are interpreted in the eastern wedge (Fig. 10d). The age of this second wedge level is ?Aptian to ?late Albian. The wedges in the Ringvassøy Loppa Fault Complex are also observed in close proximity to the incisions present in the southwestern part of the Loppa High (Fig. 11d). The incisions in the southwestern part of the Loppa High are filled with post-Lower Cretaceous successions (Fig. 11d).

5.2.1.3. Core description 7220/10-1. Two core sections from well 7220/10-1 were described in this study from 1299.5 m to 1355 m (Fig. 12). The investigated core consists mostly of bioturbated siltstone and thin very fine to fine grained sandstones with trace fossils attributable to the *Zoophycos*, *Cruziana* and mixed *Cruziana* and *Skolithos* Ichnofacies (Table 1). Based on the core description, three facies associations (FA) are recognized: 1) FA1 is composed of poorly sorted bioturbated mudstone and laminated siltstone. Siderite concretions and horizons and shell fragments occur locally. Some of the observed trace fossils include: *Nereites missouriensis*, *Phycosiphon incertum*, *Planolites*, *Palaeophycus*, *Asterosoma*, and rare *Thalassinoides* (Fig. 12, Table 1); 2) FA2 is composed of bioturbated mudstones, siltstones, laminated siltstones and normally graded sandstones beds. Soft sediment deformation and convolute lamination occurs locally. The most common trace fossils include: *Nereites missouriensis*, *Phycosiphon incertum*, *Planolites*, *Asterosoma*, *Arenicolites* and *Teichnichnus* (Fig. 12,

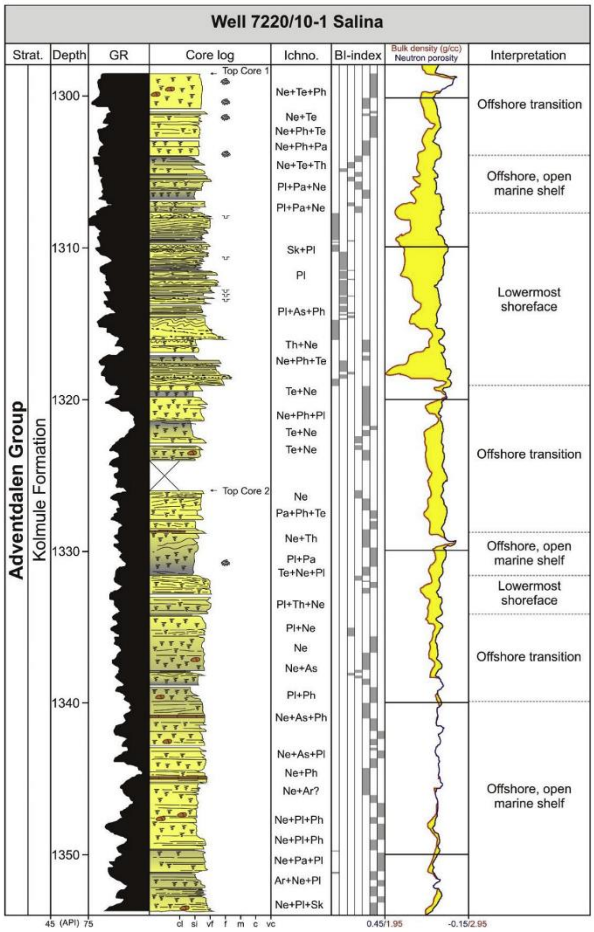

Fig. 12. Detailed sedimentary logs of core sections 1 and 2 in well 7220/10-1. The description of degree of bioturbation follows the bioturbation index (BI) of Taylor and Goldring (1993).

Table 1); and FA3 is dominated by planar and low-angle laminated sandstone beds with ripple cross-laminated or soft deformed tops. The sandstone beds are normal graded and are mainly sharp-based, with basal lags of rip-up mudstones. Loading structures are common in the sandstone and mudstone basal contacts. Some of the observed trace fossils include: *Planolites*, *Arenicolites*, *Nereites missouriensis*, *Teichnichnus* and rare *Skolithos*. *Phycosiphon Incertum* and *Thalassinoides* (Fig. 12, Table 1).

Table 1
Facies association identified for well 7220/10-1. The description of degree of bioturbation follows the bioturbation index (BI) of Taylor and Goldring (1993).

FA	Example	Description	Interpretation
FA 1 Open marine shelf deposits	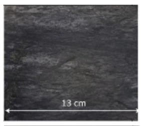 	Bioturbated mudstone, and subordinate bioturbated, or laminated siltstone. The rocks are generally poorly sorted and are rich in sand-grade grains. Siderite concretions and horizons occur in places. Shell fragments are present locally. The sediments are generally intensely bioturbated (BI 4–6), and the ichnodiversity is moderately low. Trace fossils includes *Nereites missouriensis*, *Phycosiphon incertum*, *Planolites*, *Palaeophycus*, *Asterosoma*, and rare *Thalassinoides*.	The dominance of fine-grained sediments and the high degree of bioturbation, is interpreted to represent deposition in a low-energy shelf setting, generally below storm-wave base. The sporadic occurrence of siltstones and fragmented shells suggests influence by major storms.
FA 2 Offshore transition deposits	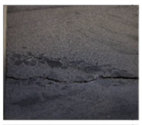 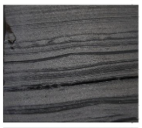	Bioturbated mudstone and siltstone beds alternating with laminated siltstone and sandstone beds. The sandstone beds are commonly sharp-based and normally graded. Soft sediment deformation in the shape of flame structures and convolute lamination occurs in some beds. Shell fragments are present locally. The finest grained sediments are generally intensely bioturbated (BI 4–6), whereas the sandstones are moderately bioturbated (BI 3–4). Trace fossils includes: *Nereites missouriensis*, *Phycosiphon incerum*, *Planolites*, *Asterosoma*, *Arenicolites* and *Teichnichnus*.	Based on its mudstone dominated nature and the sporadic occurrence of sandstone beds with storm-wave generated structures, this facies association is interpreted as offshore transition deposits.
FA 3 Lower-most shoreface deposits	 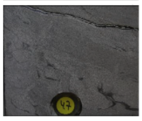	Planar and low-angle laminated sandstone beds with ripple cross-laminated or soft-sediment deformed tops. Most beds are sharp-based, contain basal lags of rip-up mudstone clasts and show normal grading. Successive sandstone beds are separated by thin beds of bioturbated mudstone or siltstone. Loading structures commonly occur at the basal contact between sandstones and mudstones. The degree of bioturbation is generally low (BI 0–2), and typical trace fossils include *Planolites*, *Arenicolites*, *Nereites missouriensis*, *Teichnichnus* and rare *Skolithos*. *Phycosiphon Incertum* and *Thalassinoides* occur in the mudstones.	The sandstone beds with storm-wave generated structures suggests a high-energetic, shallow marine setting. The preservation of storm deposits suggests that the environment was not affected by the constant reworking by fair-weather waves and is thus indicative of deposition within the lowermost shoreface.

5.2.2. *Interpretation*

Based on the dominance of fined-grained sedimentary rocks and the high degree of bioturbation, FA1 is interpreted as open marine shelf deposits. The dominance of mudstone and the presence of sandstone beds, with rip-up mudstone clasts suggest that FA2 represents offshore transition deposits. The occurrence of sandstones beds with wave and storm-wave generated structures and the preservation of the storm deposits suggest that FA3 represents lowermost shoreface deposits (Table 1). The interpretation of the sedimentary log is consistent with the height of the clinoforms identified in one of the wedges (< 60 m), which indicates relatively shallow shelfal waters (for details of clinoforms classification, see Helland-Hansen and Hampson, 2009). Thus, based on the configuration of the seismic reflectors in combination with the sedimentological log description (Fig. 12, Table 1), we attribute the wedges in the terraces of the Ringvassøy Loppa Fault Complex and southern segment of the Bjørnøyrenna Fault Complex to deposition in shallow marine to shelfal environments. Shallower deposits like upper shoreface, foreshore or marginal marine facies have not been detected in the core sections. This indicates that the investigated sediment were deposited at a certain water depth and distance from the actual shoreline.

5.3. *Biostratigraphy*

5.3.1. *Age of sequences in the Ringvassøy-Loppa Fault Complex (well 7220/10-1)*

Well 7220/10-1 recorded sequences 1–4 (Fig. 9a). The palynological assemblage of three ditch-cutting samples from the interval 1463–1481 m contains Barremian dinocysts, representing sequence 1 (Fig. 9a). The lower sample is dated as late early Barremian (dinocyst subzone I (2), Nøhr-Hansen, 1993) based on the presence of *Batioladinium longicornutum, Odontochitina nuda, Pseudoceratium anaphrissum,* and *P. toveae* (Fig. 9a). The two upper samples are dated as late Barremian, (dinocyst subzone I (3), Nøhr-Hansen, 1993) based on the presence of *Batioladinium longicornutum,* and *Pseudoceratium toveae*. The interval 1382–1463 m representing sequence 2 and lower part of sequence 3, is dated as late early to middle late Aptian (?zone II to lower part of dinocyst zone III, Nøhr-Hansen, 1993) based on the presence of *Aptopodinium haromense, Circulodinium, brevispinosum, Dingodinium albertii, Pseudoceratium* cf. *retusum* and *Stephodinium dianneae*. However, the dinocyst content of the upper part of sequence 3 do not exclude an early middle Albian age (Fig. 9a). A hiatus of latest Barremian and/or earliest Aptian age is suggested for the sequences 1–2 boundary, based on the missing record of marker species for that time interval. Sequence 4 is tentatively dated middle to late Albian (dinocyst zone IV, and zone V, Nøhr-Hansen, 1993) based on the study of two samples from 1285 m and −1346 m. The palynological assemblages in these samples consist of caved Selandian, Paleocene dinocysts, together with the few (presumably *in situ*) middle to late Albian, Early Cretaceous dinocyst indicators: *Chichaouadinium* cf. *vestitum, Ovodinium* sp. 3 of Nøhr-Hansen (1993), *Luxadinium propatulum* and *Pseudoceratium* aff. *expolitum* (Fig. 9a).

5.3.2. *Age of sequences in the southern Bjørnøyrenna Fault Complex (well 7220/5-2)*

Well 7220/5-2 recorded sequences 0–4 (Fig. 9b). The lower part of sequence 0 (1391–1357 m) is dated as early Valanginian age based on the last occurrence (LO) of *Circulodinium compta* (Costa and Davey, 1992), *Tubotuberella apatela, Perisseiasphaeridium insolitum* and *Palaecysta palmula* (Duxbury, 2001). The top of sequence 0 is dated as late Valanginian based on *Gochteodinia villosa* subsp. *multifurcata* and *Isthmocystis disticta* at 1272 m. Sequence 1 is dated as early Barremian to ?Hauterivian age based on the LO of *Nelchinopsis kostromiensis* and *Stanfordella ordocava* at 1270 m and by the LO of *Batioladinium longicornutum* and *Pseudoceratium anaphrissum* at 1252 m, correlating with the dinocyst subzones 1 (1) and 1 (2) (of Nøhr-Hansen, 1993). Sequences 2 and 3 are interpreted as having an age of ?late Aptian ?early Albian respectively, based on the LO of *Aptea polymorpha* and *Psedoceratium retusum* consistent with Duxbury (2001) and Brideaux (1977) and tentatively assigned to the *Circulodinium brevispinosum* III Zone (of Nøhr-Hansen, 1993). An age of middle Albian dinocyst zone IV is suggested for sequence 4 based on the LO of *Chichaouadinium vestitum* at 990 m (Fig. 9b).

6. Discussion

6.1. *Tectonic events controlling the formation of Lower Cretaceous shallow to deep-marine fans*

6.1.1. *The Loppa High uplift and activity of the Asterias and the Bjørnøyrenna fault complexes*

Clastic wedges suggest that Boreal Berriasian/Volgian to lower Valanginian–lower Barremian syn-rift fans were deposited in the southern flank of the Loppa High and along the southern Bjørnøyrenna Fault Complex. The fans are observed next to incisions interpreted as multiple incised valleys. These incised valleys are interpreted to be formed during the Valanginian or before, since some of them are filled with sequence 0 (Valanginian) (Fig. 10b). The age and location of the incised valley indicate that they fed the fans along the western and southern flanks of the Loppa High (Figs. 10b, 11 and 13a). Upper Jurassic wedges suggest that these incisions on the Loppa High probably started from the Late Jurassic (Fig. 11b). For the southern flank of the Loppa High, the formation of incised valleys is interpreted as diachronous, since their associated fans have been dated as Boreal Berriasian/Volgian to early Valanginian or younger in the western part and as ?Valanginian–early Barremian age in the eastern part (Marín et al., 2017a). Indrevær et al. (2017) proposed that the Loppa High was differentially uplifted, because its western flank experienced higher fault activity. We suggest that this factor together with diachronous movement of faults explain the diachronism of the clastic wedges deposition. The southwestern flank of the Loppa High was faulted at the time of the deposition of sequences 0–1 (Fig. 13a). However the southeastern part of the high is less faulted (Fig. 13a) (Gabrielsen et al., 1990). This suggests that the faulting was propagating laterally eastwards (as described for the Suez rift by Sharp et al., 2000), indicating that the uplift of the high was progressively younger in that direction. The non-homogeneous uplift event resulted in eastwards younger sediment input points. The older age of the fans (Late Jurassic and Boreal Berriasian/Volgian to early Valanginian) is constraining the time of initial erosion of the Loppa High and coincides with previous works, suggesting an age of Late Jurassic–earliest Cretaceous for the uplift event (Sund et al., 1986; Berglund et al., 1986; Wood et al., 1989; Glørstad-Clark, 2011).

On the western Bjarmeland Platform, Serck et al. (2017) described NW-prograding Barremian clinoforms (which correlate with the lower part of sequence 1) sourced from the Loppa High (Fig. 3). The upper part of sequence 1 (early Barremian age) was deposited after an intra sequence 1 flooding event (marked by the downlap surface) (Fig. 3). This local flooding event affected the Fingerdjupet Subbasin and the western Bjarmeland Platform, where it flooded the NW-prograding clinoforms described by Serck et al. (2017). In addition, the SE-prograding clinoforms observed in close proximity to the Loppa High (Glørstad-Clark, 2011; Marín et al., 2017b) suggest that the northernmost part of the this high was also flooded (Fig. 7b and d).

6.1.2. *Faulting of the Ringvassøy-Loppa Fault Complex*

Wedges associated with the Ringvassøy-Loppa Fault Complex suggest that faulting occurred along this fault complex during the late Barremian–Aptian (sequence 2). These wedges are interpreted as shallow marine fans (Fig. 12). Incised valleys are observed next to these fans in the uplifted footwall of the Ringvassøy-Loppa Fault Complex (Fig. 11d) and along the southern segment of the Bjørnøyrenna Fault Complex eroding the fans of sequences 0–1 (Figs. 10b, 11b and 13b). We interpret these incised valleys as another potential episode of sediment bypass to the Tromsø and Bjørnøya basins (outside of our study area). Furthermore, it reveals that new fairways of sediment (incisions) and their related diachronous fans are being formed, as a consequence of a non-homogenous uplift of the Loppa High, diachronous fault movement and that its topography was renewed in the western part. Besides, a Barremian–Aptian (sequence 2) unconformity is observed in the Fingerdjupet Subbasin formed as a response of footwall uplift (as described by Kusznir et al., 1991; Ravnås and Steel, 1998 for other settings).

An Aptian faulting event is well known in the Fingerdjupet Subbasin (Faleide et al., 1993; Clark et al., 2014; Blaich et al., 2017; Serck et al., 2017). This activity formed localized wedges, compartmentalized the clinoforms in the Fingerdjupet Subbasin (Fig. 7b and d) and contributed to the uplift of the northernmost part of the Loppa High. In addition, the Svalis Dome and the faults located close to it (Fig. 7d), have been described as active during the Late Jurassic–Early Cretaceous (Berglund et al., 1986), but the fault activity continued until the mid-Cretaceous (Løseth et al., 1992). We suggest that the activity of the Svalis Dome and the faults in that area could have locally influenced the uplift of the northernmost part of the Loppa High. However, the ages are not well constrained and more detailed studies are therefore necessary.

6.1.3. *Tilting of the Loppa High and Hammerfest Basin*

The unconformity observed at the top of sequence 2 (upper Aptian–lower Albian) in the southwestern flank of the Loppa High coincides with the eastwards tilting event of the Hammerfest Basin suggested Marín et al. (2017a) (Fig. 13c). This tilting event indicates that the northwestern part of the Hammerfest Basin was shallow to

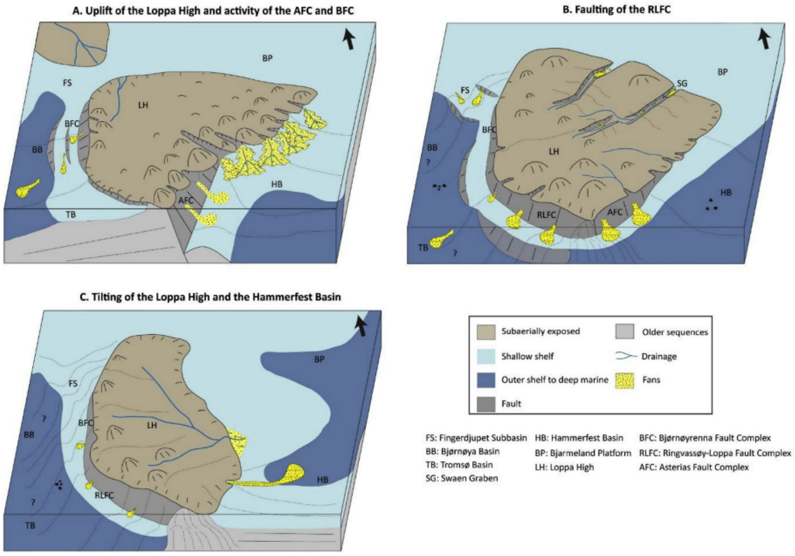

Fig. 13. Three-dimensional cartoons illustrating the three main events controlling the deposition of the clastic wedges around the Loppa High. A) The activity of the Asterias and the Bjørnøyrenna fault complexes and the uplift event of the Loppa High during the Late Jurassic–earliest Cretaceous controlled the deposition of progressively younger wedges toward the east; B) a late Barremian–Aptian faulting episode affected the western flank of the Loppa High, depositing shallow and deep marine wedges; C) A late Aptian–early Albian renewed uplift and eastwards tilting event affected the Loppa High and the Hammerfest Basin, forming subaerial to shallow marine conditions in the southwestern part of the study area and progressively deeper conditions to the east.

subaerially exposed in the early Albian. In contrast, clinoforms with a height of 80–200 m and 500 m have been described for sequences 3–4 in the eastern part of the Hammerfest Basin and in the Bjarmeland Platform (Marín et al., 2017a). (Fig. 5b). This shows progressively deeper conditions toward the east. The southwestward prograding clinoforms in the northeastern part of the Hammerfest Basin are interpreted to have been sourced by the Loppa High. This depositional arrangement could be the result of the tilting of the Loppa High eastwards. The tilting of the Loppa High is additionally supported by Albian shelf-margin clinoforms (sequences 3–4; Marín et al., 2017b) downlapping on the BCU in the boundary between the Loppa High and the Bjarmeland Platform (Fig. 5b).

Marín et al. (2017a) interpreted the unconformity in the northwestern part of the Hammerfest Basin as the response of a period of activity of the Ringvassøy-Loppa Fault Complex, which locally uplifted the western part of the Loppa High and Hammerfest Basin. However, the gradual deepening of the Hammerfest Basin to the east, the height of the clinoforms (> 500 m) in the Bjarmeland Platform and their relationship with the Loppa High and the switch of the depocenter location during sequences 3–4, indicate that this tilting was not a local event. Finally, due to the eastwards tilting, the eastern part of the Loppa High became flooded in the latest Albian–Cenomanian where sequences 5–6 were deposited (Fig. 5d) (Marín et al., 2017a).

6.2. Drainage evolution on uplifted rift shoulders affected by adjacent fault systems

Based on the evidence of fault activity in the western and southern flanks of the Loppa High and the presence of incised valleys, we suggest that the western and southern flanks of the Loppa High were characterized by topographic highs. By contrast, the eastern flank of the Loppa High was not affected by N–S or NE–SW faults and there is an absence of incised valleys and its related wedges (except where E–W and NE–SW Grabens are presented) (Fig. 13b). Thus, the eastern flank of the Loppa High is interpreted as having a relative low gradient slope for most of the Early Cretaceous, giving the aspect of an ancient large scale tilted fault block (Fig. 2b and c). The morphology of the Loppa High provide a lot of insights about the evolution of drainage systems in uplifted rift shoulders (Fig. 13). The western flank face the basins where Late Jurassic–Early Cretaceous rifting was concentrated (Figs. 2 and 11). Sediment eroded through the incised valleys fed the fans developed along the terraces in this margin. Most of the incised valleys in the western flank of the Loppa High are interpreted as short length drainage systems to the deep Tromsø and Bjørnøya basins (Figs. 11 and 13). The fans in the area tend to show a progressive change from aggradational to progradational stacking, reflecting changes in the available accommodation space as described by amongst others Densmore et al. (2007) and Gawthorpe and Leeder (2000) (Fig. 10d).

If the eastern flank of the Loppa High was a low gradient slope for most of the Early Cretaceous, it can be expected that a longer drainage system was developed towards the east sourced by the topographic high from the western flank. In the eastern flank, clinoforms prograding from the Loppa High have been identified only in narrow areas in the southeastern flank (NE Hammerfest Basin; Marín et al., 2017a) and in the northern part, where Serck et al. (2017) described NW-prograding clinoforms. However, most of the eastern flank of the Loppa High is characterized by a lack of clinoform geometries that could indicate the development of a shoreline or delta, conversely to the uplifted footwall models (e.g. Ravnås and Steel, 1998; Gawthorpe and Leeder, 2000) or as in other uplifted rift shoulders such as the Red Sea and Gulf of Aden (Frostick and Reid, 1989). From this, two questions arise: 1) how were the drainage patterns configured in the Loppa High? And 2) why is there an apparent lack of drainage systems running from the western uplifted flank of the Loppa High to its low gradient eastern flank? One possibility is that the deposits of these drainage systems (e.g. clinoforms) are below the seismic resolution.

A second option is the role that adjacent fault systems could have played on the drainage system development on the Loppa High. During the Early Cretaceous, the eastern flank of the Loppa High was further affected by different E–W, ESE–WNW and NE–SW-striking faults. For instance, the Swaen Graben and the northern faults that connected the Loppa High to the Maud Basin (Figs. 6 and 7d). This faulting is interpreted to have happened before Albian, almost simultaneously to the faulting in the western flank of the Loppa High. Seismic wedges were only observed within these grabens. We suggest that the E–W, ESE–WNW and NE–SW faults controlled the drainage patterns on the Loppa High, acted as sediment routes, and thus their related deposits were confined within the grabens (Fig. 13b). Marín et al. (2017a) suggested that rifting in adjacent basins could renew the topography in the post-rift stages and preferentially control the development of fans within a basin. In this paper, we propose another implication of faulting happening in adjacent basins, which is related to the routing of sediment. Although the western flank of the Loppa High behaves as the models for high gradient slopes predict (O'Grady et al., 2000; Densmore et al., 2007; Hadler-Jacobsen et al., 2005), the eastern low gradient flank of the Loppa High does not completely follow the previous models, since the deposits of the long river systems are apparently missing (Frostick and Reid, 1989; Ravnås and Steel, 1998; O'Grady et al., 2000; Densmore et al., 2007; Hadler-Jacobsen et al., 2005). In the last case, the normal faulting occurring almost orthogonal to the main fault system, acted as pathways of sediment to grabens located in the lower gradient flank of a regional scale tilted rift shoulder (Fig. 13b).

When faulting occurs almost simultaneous in two or more adjacent basins, it is important to consider how fault activity can affect the drainage patterns and the sedimentation in an area, for example by acting as preferential pathway routes. The existing models of sedimentation in rift basins are a useful guideline. However, in order to make more realistic predictions we need to be able to challenge these models when they do not fulfill our observations and consider other key variables that could have affected a specific area.

7. Conclusions

The ancient Loppa High is an example of an uplifted rift shoulder that was affected by several adjacent fault systems during the Early Cretaceous. The flank that faces the master fault complexes is characterized by incised valleys and shallow to eventually deep marine fans. In the gently tilted flank the main drainage systems were confined and deflected to a series of E–W, ESE–WNW and NE–SW graben structures occurring almost simultaneous with the main fault system. In this study we propose that three main events controlled the deposition of fans in the flanks of the high: 1) the activity of the Asterias and the Bjørnøyrenna fault complexes, interpreted to have happened during the Boreal Berriasian/Volgian to early Valanginian – early Barremian. Associated with this event, incised valleys and fans were formed. Fans in the area are diachronous, indicating that new entry points of the sediment were differentially formed as a consequence of diachronous fault movement in the Loppa High flanks. 2) Faulting along the Ringvassøy Loppa Fault Complex during the late Barremian–Aptian. Related to this event, incised valleys were formed in the southwestern flank of the Loppa High and shallow marine fans were formed in the terraces of the Ringvassøy Loppa Fault Complex. 3) Tilting of the Loppa High and the Hammerfest Basin during late Aptian–early Albian. A depocenter switching is suggested as a result of this last event.

Acknowledgements

This study is part of industry-sponsored LoCrA consortium. We are grateful with all the sponsors for the financial support. We acknowledge Francisco José José Lobo, John Armitage and an anonymous reviewer for their constructive comments. Thanks to Halliburton-Landmark and to the Norwegian DISKOS database for the software and dataset provided.

References

Allen, P.A., Densmore, A., 2000. Sediment flux from an uplifting fault block. Basin Res. 12, 367–380.
Århus, N., Kelly, S.R., Collins, J.S., Sandy, M.R., 1990. Systematic palaeontology and biostratigraphy of two Early Cretaceous condensed sections from the Barents Sea. Polar Res. 8, 165–194.
Armitage, J.J., Duller, R.A., Whittaker, A.C., Allen, P.A., 2011. Transformation of tectonic and climatic signals from source to sedimentary archive. Nat. Geosci. 4, 231–235.
Berglund, L., Augustson, J., Færseth, R., Gjelberg, J., Ramberg-Moe, H., 1986. The evolution of the Hammerfest Basin. In: Spencer, A.M. (Ed.), Habitat of Hydrocarbons on the Norwegian Continental Shelf, pp. 319–338 Norwegian Pet. Soc. Graham Trotman.
Blaich, O.A., Tsikalas, F., Faleide, J.I., 2017. New insights into the tectono-stratigraphic evolution of the southern stappen high and its transition to Bjørnøya basin, SW Barents Sea. Mar. Petrol. Geol. 85, 89–105.
Bosence, D.W.J., 1998. Stratigraphic and sedimentological models of rift basins. In: Purser, B.H., Bosence, D.W.J. (Eds.), Sedimentation and Tectonics in Rift Basins Red Sea:- Gulf of Aden. Springer, Netherlands, Dordrecht, pp. 9–25.
Brideaux, W.W., 1977. In: Taxonomy of Upper Jurassic–lower Cretaceous Microplankton from the Richardson Mountains, District of Mackenzie, Canada, vol. 281. pp. 1–89 Printing and Publishing, Supply and Services Canada, Ottawa, Canada.
Clark, S., Glorstad-Clark, E., Faleide, J., Schmid, D., Hartz, E., Fjeldskaar, W., 2014. Southwest Barents Sea rift basin evolution: comparing results from backstripping and time-forward modelling. Basin Res. 26, 550–566.
Costa, L.I., Davey, R.J., 1992. Dinoflagellate cysts of the cretaceous system. In: Powell, A.J. (Ed.), A Stratigraphic Index of Dinoflagellate Cysts. British Micropaleontological Society Publication Series. Chapman & Hall, London, pp. 99–153.
Dahlberg, M.E., 2014. Structural and Stratigraphical Evolution of the Fingerdjupet Subbasin, SW Barents Sea. Master thesis. University of Oslo, pp. 102.
Dalland, A., Worsley, D., Ofstad, K., 1988. A lithostratigraphic scheme for the Mesozoic and Cenozoic succession offshore Norway north of 62 N. Nor. Pet. Dir. Bull. 4, 67.
Densmore, A.L., Allen, P.A., Simpson, G., 2007. Development and response of a coupled catchment fan system under changing tectonic and climatic forcing. J. Geophys. Res. Earth Surf. 112 F01002.
Dimitriou, M., 2014. Lower Cretaceous Prograding Units in the Eastern Part of the SW Barents Sea. Master thesis. University of Oslo, pp. 88.
Duxbury, S., 2001. A palynological zonation scheme for the lower cretaceous-United Kingdom Sector, Central North Sea. Neues Jahrbuch fur Geologie und Palaontologie-Abhandlungen 219, 95–137.
Faleide, J.I., Vågnes, E., Gudlaugsson, S.T., 1993. Late Mesozoic-Cenozoic evolution of the south-western Barents Sea in a regional rift-shear tectonic setting. Mar. Petrol. Geol. 10, 186–214.
Fjeld, T.L., 2014. Seismic Characterization of Lower Cretaceous Clastic Wedges in the Tromsø Basin. Master thesis. University of Stavanger, pp. 71.
Ford, M., Hemelsdaël, R., Mancini, M., Palyvos, N., 2016. Rift Migration and Lateral Propagation: Evolution of Normal Faults and Sediment-routing Systems of the Western Corinth Rift (Greece). Geological Society, London Special Publications 439.
Frostick, L., Reid, I., 1989. Is structure the main control of river drainage and sedimentation in rifts? J. Afr. Earth Sci. (and the Middle East) 8, 165–182.
Gabrielsen, R.H., Faerseth, R.B., Jensen, L.N., 1990. Structural elements of the Norwegian continental shelf. Pt. 1. The Barents Sea region. Nor. Pet. Dir. 6, 47.
Gabrielsen, R.H., Kyrkjebø, R., Faleide, J.I., Fjeldskaar, W., Kjennerud, T., 2001. The cretaceous post-rift basin configuration of the northern north Sea. Petrol. Geosci. 7, 137–154.
Galloway, W.E., 1989. Genetic stratigraphic sequences in basin analysis I: architecture and genesis of flooding-surface bounded depositional units. AAPG Bull. 73, 125–142.
Gawthorpe, R., Leeder, M., 2000. Tectono-sedimentary evolution of active extensional basins. Basin Res. 12, 195–218.
Gawthorpe, R.L., Leeder, M.R., Kranis, H., Skourtsos, E., Andrews, J.E., Henstra, G.A., Mack, G.H., Muravchik, M., Turner, J.A., Stamatakis, M., 2017. Tectono-sedimentary

evolution of the plio-pleistocene Corinth rift, Greece. Basin Res. http://dx.doi.org/10.1111/bre.12260.

Glørstad-Clark, E., 2011. Basin analysis in the Western Barents Sea Area: the Interplay between Accommodation Space and Depositional Systems. PhD thesis. University of Oslo, pp. 212.

Grundvåg, S.A., Marin, D., Kairanov, B., Śliwińska, K.K., Nøhr-Hansen, H., Jelby, M.E., Escalona, A., Olaussen, S., 2017. The lower cretaceous succession of the northwestern Barents shelf: onshore and offshore correlations. Mar. Petrol. Geol. 86, 834–857.

Hadler-Jacobsen, F., Johannessen, E., Ashton, N., Henriksen, S., Johnson, S., Kristensen, J., 2005. Submarine fan morphology and lithology distribution: a predictable function of sediment delivery, gross shelf-to-basin relief, slope gradient and basin topography, Geological Society, London. In: Petroleum Geology Conference Series. Geological Society of London, pp. 1121–1145.

Helland-Hansen, W., Hampson, G.J., 2009. Trajectory analysis: concepts and applications. Basin Res. 21, 454–483.

Henriksen, E., Bjørnseth, H.M., Hals, T.K., Heide, T., Kiryukhina, T., Kløvjan, O.S., Larssen, G.B., Ryseth, A.E., Rønning, K., Sollid, K., Stoupakova, A., 2011. Chapter 17: uplift and erosion of the greater Barents Sea: impact on prospectivity and petroleum systems. Geol. Soc. Mem. 35, 271–281.

Henstra, G.A., Gawthorpe, R.L., Helland-Hansen, W., Ravnås, R., Rotevatn, A., 2017. Depositional systems in multiphase rifts: seismic case study from the Lofoten margin, Norway. Basin Res. 29, 447–469.

Hinna, C.H., Escalona, A., Bryn, B., Haaland, S., 2016. Seismic characterization of lower cretaceous clinoform packages in the Fingerdjupet sub-basin, southwestern Barents Sea. In: 78th EAGE Conference and Exhibition 2016, Vienna.

Indrevær, K., Gabrielsen, R.H., Faleide, J.I., 2017. Early Cretaceous synrift uplift and tectonic inversion in the Loppa High area, southwestern Barents Sea, Norwegian shelf. J. Geol. Soc. 174, 242–254.

Jørgensen, K., 2014. Development of Fault Complexes in Time and Space at Loppa High-sw Barents Sea. Master thesis. The Arctic University of Norway, pp. 108.

Knutsen, S.-M., Augustson, J.H., Haremo, P., 2000. Exploring the Norwegian part of the Barents Sea—Norsk Hydro's lessons from nearly 20 years of experience. In: Ofstad, K., Kittilsen, J.E., Alexander-Marrack, P. (Eds.), Improving the Exploration Process by Learning from the Past, Proceedings of the Norwegian Petroleum Society Conference, pp. 99–112 Norwegian Petroleum Society Special Publications 9.

Kusznir, N., Marsden, G., Egan, S., 1991. A flexural-cantilever simple-shear/pure-shear model of continental lithosphere extension: applications to the Jeanne d'Arc Basin, Grand Banks and Viking Graben, North Sea. In: Roberts, A.M., Yielding, G., Freeman, B. (Eds.), The Geometry of Normal Faults, pp. 41–60 Geological Society Special Publication 56.

Lambiase, J., Bosworth, W., 1995. Structural Controls on Sedimentation in Continental Rifts. Geological Society, London, pp. 117–144 Special Publications 80.

Lazarević, S., 2017. Lower Cretaceous Clastic Wedges in the Swaen Graben, the Barents Sea, Norway. Bachelor thesis. University of Stavanger, pp. 65.

Leeder, M.R., Seger, M.J., Stark, C.P., 1991. Sedimentation and tectonic geomorphology adjacent to major active and inactive normal faults, southern Greece. J. Geol. Soc. 148, 331–343.

Leppard, C.W., Gawthorpe, R.L., 2006. Sedimentology of rift climax deep water systems; lower rudeis formation, hammam faraun fault block, Suez Rift, Egypt. Sediment. Geol. 191, 67–87.

Løseth, H., Lippard, S., Sættem, J., Fanavoll, S., Fjerdingstad, V., Leith, T., Ritter, U., Smelror, M., 1992. Cenozoic uplift and erosion of the Barents Sea—evidence from the Svalis Dome area. In: Vorren, T.O., Bergsager, E., Dahl-Stamnes, Ø.A., Holter, E., Johansen, B., Lie, E., Lund, T.B. (Eds.), Arctic Geology and Petroleum Potential, Norwegian Petroleum Society Special Publications 2, pp. 643–664.

Marín, D., Escalona, A., Grundvåg, S.-A., Olaussen, S., Sandvik, S., Śliwińska, K.K., 2017a. Unraveling key controls on the rift-climax to post-rift fill of marine rift basins: insights from 3D seismic analysis of the Lower Cretaceous of the Hammerfest Basin, SW Barents Sea. Basin Res. http://dx.doi.org/10.1111/bre.12266.

Marín, D., Escalona, A., Śliwińska, K.K., Nøhr-Hansen, H., Mordasova, A., 2017b. Sequence stratigraphy and lateral variability of Lower Cretaceous clinoforms in the southwestern Barents Sea. AAPG Bull. 101, 1487–1517.

McArthur, A.D., Hartley, A.J., Jolley, D.W., 2013. Stratigraphic development of an upper jurassic deep marine syn-rift succession, inner moray firth basin, Scotland. Basin Res. 25, 285–309.

Mitchum Jr., R., Vail, P., Sangree, J., 1977. Seismic Stratigraphy and Global Changes of Sea Level: Part 6. Stratigraphic Interpretation of Seismic Reflection Patterns in Depositional Sequences: Section 2. Application of Seismic Reflection Configuration to Stratigraphic Interpretation.

Mørk, A., Dallmann, W., Dypvik, H., Johannessen, E., Larssen, G., Nagy, J., Nøttvedt, A., Olaussen, S., Pchelina, T., Worsley, D., 1999. Mesozoic lithostratigraphy. In: Dallmann, W.K. (Ed.), Lithostratigraphic Lexicon of Svalbard. Upper Palaeozoic to Quaternary Bedrock. Review and Recommendations for Nomenclature Use. Norwegian Polar Institute, pp. 127–214.

Mortimer, E., Carrapa, B., 2007. Footwall drainage evolution and scarp retreat in response to increasing fault displacement: Loreto fault, Baja California Sur, Mexico. Geology 35, 651–654.

Nøhr-Hansen, H., 1993. Dinoflagellate cyst stratigraphy of the Barremian to Albian, lower cretaceous, east Greenland. Bulletin Grønlands Geologiske Undersøgelse 166, 171.

Nøttvedt, A., Gabrielsen, R., Steel, R., 1995. Tectonostratigraphy and sedimentary architecture of rift basins, with reference to the northern North Sea. Mar. Petrol. Geol. 12, 881–901.

NPD, 2017. Norwegian Petroleum Directorate Factpages. (Accessed April 2017). http://factpages.npd.no/factpages/Default.aspx?culture = en.

O'Grady, D.B., Syvitski, J.P., Pratson, L.F., Sarg, J., 2000. Categorizing the morphologic variability of siliciclastic passive continental margins. Geology 28, 207–210.

Ravnås, R., Steel, R.J., 1998. Architecture of marine rift-basin successions. Am. Assoc. Pet. Geol. Bull. 82, 110–146.

Robertson Group plc, 1989. Mobil 7321/7-1 Norwegian Barents Sea Well: Biostratigraphy of the Interval 613m (SWC)-3552mTD, 80.

Salazar, M., Moscardelli, L., Wood, L., 2016. Utilising clinoform architecture to understand the drivers of basin margin evolution: a case study in the Taranaki Basin, New Zealand. Basin Res. 28, 840–865.

Sandvik, S., 2014. Description and Comparison of Lower Cretaceous Deposits from Svalbard and the Southern Loppa High. Master thesis. University of Bergen, pp. 135.

Seldal, J., 2005. Lower Cretaceous: the Next Target for Oil Exploration in the Barents Sea? pp. 231–240.

Serck, C.S., Faleide, J.I., Braathen, A., Kjølhamar, B., Escalona, A., 2017. Jurassic to early Cretaceous basin configuration(s) in the Fingerdjupet Subbasin, SW Barents Sea. Mar. Petrol. Geol. 86, 874–891.

Sharp, I.R., Gawthorpe, R.L., Underhill, J.R., Gupta, S., 2000. Fault-propagation folding in extensional settings: examples of structural style and synrift sedimentary response from the Suez rift, Sinai, Egypt. Geol. Soc. Am. Bull. 112, 1877–1899.

Sklar, L.S., Dietrich, W.E., 2001. Sediment and rock strength controls on river incision into bedrock. Geology 29, 1087–1090.

Smelror, M., Mørk, A., Monteil, E., Rutledge, D., Leereveld, H.A.N., 1998. The Klippfisk formation—a new lithostratigraphic unit of lower cretaceous platform carbonates on the western Barents shelf. Polar Res. 17, 181–202.

Solheim, A., Kristoffersen, Y., 1984. Sediments above the Upper Regional Unconformity: Thickness, Seismic Stratigraphy and Outline of the Glacial History. Norwegian Polar Institute 179B, 26.

Steckler, M.S., Omar, G.I., 1994. Controls on erosional retreat of the uplifted rift flanks at the Gulf of Suez and northern Red Sea. J. Geophys. Res. 99 (12) 12,159–12,173.

Sund, T., Skarpnes, O., Jensen, L.N., Larsen, R.M., 1986. Tectonic development and hydrocarbon potential offshore Troms, northern Norway. In: Halbouty, M.T. (Ed.), Future Petroleum Provinces of the World, 40. AAPG Mem, pp. 615–627.

Taylor, A.M., Goldring, R., 1993. Description and analysis of bioturbation and ichnofabric. J. Geol. Soc. 150, 141–148.

van Balen, R.T., van der Beek, P.A., Cloetingh, S.A.P.L., 1995. The effect of rift shoulder erosion on stratal patterns at passive margins: implications for sequence stratigraphy. Earth Planet Sci. Lett. 134, 527–544.

Withjack, M.O., Schlische, R.E., Olsen, P.E., 2002. Rift-basin structure and its influence on sedimentary systems. In: Renault, R.W., Ashley, G. (Eds.), Sedimentation in Continental Rifts, 73. Society for Sedimentary Geology Special Publication, pp. 57–81.

Wood, R., Edrich, S., Hutchison, I., 1989. Influence of north Atlantic tectonics on the large-scale uplift of the stappen high and Loppa high, western Barents shelf: chapter 36: north Sea and Barents shelf. In: Tankard, A.J., Balkwill, H.R. (Eds.), Extensional Tectonics and Stratigraphy of the North Atlantic Margins, 46. AAPG Mem pp. 559–556.

Appendices

Kairanov, B., A. Escalona, and P. Abrahamson, 2016, Lower Cretaceous evolution of the Tromsø basin: NPF Arctic Exploration. Tromsø, Norway, 31 May to 2 June.

Kairanov, B., A. Escalona, A. Kayukova, and D. Marin, 2015, Overview and timing of main structural elements in the North Central Barents Sea and impact on the Lower Cretaceous deposition: 3P Arctic. Stavanger, Norway, 11-14 April.

Kairanov, B., A. Escalona, A. Kayukova, and D. Marin, 2016, Overview and timing of main structural elements in the North Central Barents Sea and impact on the Lower Cretaceous deposition: EAGE. Saint Petersburg, Russia, 11-14 April.

Kairanov, B., A. Escalona, I. Norton, L. Lawver, and P. Abrahamson, 2017, The Early Cretaceous structural evolution of the Tromsø Basin, SW Barents Sea: EAGE Annual Conference. Paris, France, 12-15 June.

Kairanov, B., A. Escalona, I. Norton, P. Nadeau, and L. Lawver, 2016, Early Cretaceous-Cenozoic relation between the Tromsø Basin and NE Greenland; implications for margin evolution: NPF Onshore-Offshore relationships on the North Atlantic Margins. Trondheim, Norway, 18-19 October.

Kairanov, B., D. Marin, and A. Escalona, 2015, Structural controls in progradation direction of Lower Cretaceous clinoforms in the Barents Sea: 3P Arctic. Stavanger, Norway, 11-14 April.